

**Naučnom veću Instituta za fiziku Beograd**

Beograd, 21. maj 2019.

**Predmet:**

**Molba za pokretanje postupka za reizbor u zvanje istraživač saradnik**

Molim Naučno veće Instituta za fiziku da pokrene postupak za moj reizbor u zvanje istraživač saradnik.

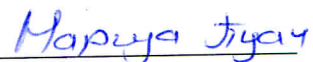
U prilogu dostavljam:

- Potpisan zahtev za pokretanje reizbora
- Mišljenje rukovodioca
- Biografiju
- Kratak pregled naučne aktivnosti kandidata
- Spisak objavljenih naučnih radova
- Fotokopije objavljenih naučnih radova
- Potvrdu o upisanim doktorskim studijama
- Potvrdu o proseku na osnovnim i master studijama
- Potvrdu o prihvaćenoj temi za izradu doktorske disertacije

U Beogradu,

21.05.2019.

Sa poštovanjem,

  
Marija Puač

## Naučnom veću Instituta za fiziku Beograd

Beograd, 21. maj 2019.

### Predmet:

### Mišljenje rukovodioca projekta o reizboru Marije Puač u zvanje istraživač saradnik

Molim Vas da pokrenete postupak reizbora u zvanje *istraživač saradnik* za Mariju Puač, istraživača saradnika Instituta za fiziku u Beogradu. Kandidat Marija Puač je angažovana na projektu ON171037 – Fundamentalni procesi i primena transporta čestica u neravnotežnim plazmama, trapovima i nanostrukturama. 2009-te godine upisala je doktorske studije na Elektrotehničkom fakultetu Univerziteta u Beogradu - smer Nanoelektronika i fotonika. Univerzitet u Beogradu, Veće naučnih oblasti tehničkih nauka dalo je saglasnost na predlog teme doktorske disertacije Marije Puač pod nazivom „**Modelovanje proboja u gasovima Monte Karlo tehnikom**“, na sednici održanoj 24.09.2018. godine. U junu 2019. godine se očekuje i zakazivanje datuma odbrane doktorske disertacije.

Kandidat Marija Puač je, do sada, publikovala jedanaest radova od kojih su neki u vrhunskim časopisima kategorije M21, dok su rezultati njenih istraživanja prezentovani na velikom broju međunarodnih konferencija.

Sa realizacijom obaveza na fakultetu se kasni usled problema sa kašnjenjem uplata Elektrotehničkom fakultetu na ime školarine. Treba napomenuti da je kandidat Marija Puač zbog bolesti uzela dve godine mirovanja, školska 2014/2015 i 2015/2016, kada nije bila u mogućnosti da izlazi na ispite i ispunjava obaveze na fakultetu.

Na osnovu svega navedenog, mišljenja sam da je, kandidat Marija Puač, zadovoljila sve formalne i suštinske uslove koji su potrebni za reizbor u zvanje *istraživač saradnik*, kako od strane Ministarstva prosvete, nauke i tehnološkog razvoja, tako i od strane Instituta za fiziku u Beogradu.

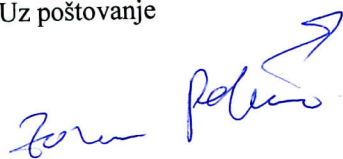
Predlažem komisiju u sastavu:

Dr Zoran Lj Petrović, naučni savetnik Instituta za fiziku Univerziteta u Beogradu

Prof. Antonije Đorđević, redovni profesor Elektrotehničkog fakulteta Univerziteta u Beogradu

Dr Dragana Marić naučni savetnik Institut za fiziku Univerziteta u Beogradu

Uz poštovanje



dr Zoran Lj. Petrović, rukovodilac projekta ON171037 MPNTR

Beograd, 21.05.2019.

## Biografija kandidata

Marija Puač (rođena Savić) je rođena u Paraćinu 10.06.1985. godine. Pohađala je Paraćinsku gimnaziju, koju je završila kao đak generacije. Tokom srednje škole je učestvovala na brojnim takmičenjima iz fizike gde je ostvarila značajne rezultate.

Elektrotehnički fakultet Univerziteta u Beogradu - smer Nanoelektronika, optoelektronika i laserska tehnika završila je 2008. godine. Iste godine, upisala je master studije na Elektrotehničkom fakultetu Univerziteta u Beogradu - smer Nanoelektronika, optoelektronika i laserska tehnika koje je kompletirala 2009. godine, odbranom master rada, pod nazivom, "Monte Karlo simulacije proboja u gasovima" urađenim u Laboratoriji za gasnu elektroniku Instituta za fiziku, pod rukovodstvom prof. dr Zorana Lj. Petrovića i dr Marije Radmilović-Rađenović. Doktorske studije na Elektrotehničkom fakultetu Univerziteta u Beogradu - smer Nanoelektronika i fotonika upisala je 2009. godine. Naučno veće Instituta za fiziku na sednici održanoj 07.06.2016. godine donelo je odluku o reizboru u zvanje Istraživač saradnik za saradnika Instituta za fiziku Mariju Puač. Univerzitet u Beogradu, Veće naučnih oblasti tehničkih nauka dalo je saglasnost na predlog teme doktorske disertacije Marije Puač pod nazivom „**Modelovanje proboja u gasovima Monte Karlo tehnikom**“, na sednici održanoj 24.09.2018. godine.

U svojoj karijeri kandidat Marija Puač je publikovala 11 radova u međunarodnim časopisima, bila je koautor na 10 predavanja po pozivu na međunarodnim konferencijama (od čega je održala jedno predavanje). Pored navedenog kandidat ima 13 radova publikovanih na konferencijama u obliku rezimea i 12 u kompletnom obliku. Broj citata kandidatkinje je 78 a H faktor 5 (prema bazi Google scholar).

## **Naučnom veću Instituta za fiziku Beograd**

Beograd, 21. maj 2019.

### Naučna aktivnost kandidata

Marija Puač se bavi numeričkim simulacijama proboja u gasovima, primenom Monte Karlo tehnike. Njen zadatak je izgradnja koda koji će verno opisati fizičke procese koji su odgovorni za formiranje plazme. U toku izrade master rada bavila se probojima u jednosmernim poljima (DC). Na primeru argona ispitivan je uticaj različitih tipova čestica na proboj, ali i uticaji materijala od kog su izrađene elektrode i rastojanja između njih.

Znanje stečeno tom prilikom u nastavku svog rada primenjuje na proboje u radiofrekvencijskim (RF) poljima, frekvencije reda MHz. Na primeru argona kao pozadinskog gasa i sa elektronima kao česticama koje su odgovorne za proboj, izgrađen je model kojim se može modelovati naponska probojna kriva, za date uslove, koja kvalitativno odgovara dostupnim eksperimentalnim rezultatima. Analiziran je i zakon skaliranja RF naponskih probojnih krivih koji mora uključivati još jedna uslov (u odnosu na skaliranje DC krivih), a to je da proizvod frekvencije i rastojanja između elektroda mora ostati konstantan.

Sledeći korak u istraživanju RF proboja jeste razmatranje uticaja površina elektroda na naponske probojne krive. Razmatrani su efekti na površinama kao što su elastična i neelastična refleksija i emisija sekundarnih elektrona sa površine. Njihov uticaj na naponsku probojnu krivu je analiziran. Pored efekata površina, ispitan je i uticaj promene frekvencije na oblik naponske probojne krive, kao i uticaj napajanja čiji signal predstavlja zbir dva sinusoidna signala, od kojih je jedan napajan nižom a drugi višom frekvencijom. Ovo je jako bitno ukoliko za primenu RF plazmi, jer industrijske RF plazme su najčešće napajane dvofrekvencijskim izvorima.

Poslednji razvojni korak jeste uticaj teških čestica na RF proboj. Njihov uticaj se ogleda u izbacivanju sekundarnih elektrona sa površina elektroda u trenucima udara čestice u elektrodu. Razvijeni kod je testiran na primerima smeša gasova kao što su sintetički vazduh i atmosfera Marsa i dao je odlično slaganje sa dostupnim eksperimentalnim rezultatima za sintetički vazduh.



Veoma važno je napomenuti da je u laboratoriji izgrađen uređaj koji treba da da eksperimentalne podatke za RF proboj te će proračuni Marije Puač biti osnova za proveru uređaja i podataka i mogućnost da se iz eksperimenta izvuku podaci.

U svojoj karijeri kandidat Marija Puač je publikovala 11 radova u međunarodnim časopisima, bila je koautor na 10 predavanja po pozivu na međunarodnim konferencijama (od čega je održala jedno predavanje). Pored navedenog kandidat ima 13 radova publikovanih na konferencijama u obliku rezimea i 12 u kompletnom obliku. Broj citata kandidatkinje je 78 a H faktor 5 (prema bazi Google scholar).

## Списак радова Марије Пуач

### Рад у тематском зборнику међународног значаја (M14):

1. Zoran Lj Petrović, Jelena Sivoš, Marija Savić, Nikola Škoro, Marija Radmilović-Radjenović, Saša Gocić, Dragana Marić: New phenomenology of gas breakdown in DC and RF fields – *Journal of Physics: Conference Series* (2014), Vol. 514, pp. 012043.

DOI: 10.1088/1742-6596/514/1/012043

ISBN 978-86-7025-782-5

### Рад у међународним часописима изузетних вредности (M21a):

1. Marija Puač, Dragana Marić, Marija Radmilović-Radjenović, Milovan Šuvakov and Zoran Lj Petrović: Monte Carlo modeling of radio-frequency breakdown in argon – *Plasma Sources Sci. Technol.* (2018), Vol. 27, pp. 075013.

ИФ 3.939 DOI: 10.1088/1361-6595/aacc0c

ISSN 0963-0252

### Рад у врхунским међународним часописима (M21):

1. Zoran Lj Petrović, Dragana Marić, Marija Savić, Srđan Marjanović, Saša Dujko, Gordana Malović: Using swarm models as an exact representation of ionized gases – *Plasma Process Polymers* (2016), Vol. 14, pp. 1600124, број хетероцитата 6.

ИФ 2.846 DOI: 10.1002/ppap.201600124

ISSN 1612-8850

### Рад у истакнутим међународним часописима (M22):

1. Dragana Marić, Marija Savić, Jelena Sivoš, Nikola Škoro, Marija Radmilović-Radjenović, Gordana Malović and Zoran Lj. Petrović: Gas breakdown and secondary electron yields: – *Eur. Phys. J. D* (2014), Vol. 68, pp. 155, број хетероцитата 32.

ИФ 1.240 DOI: 10.1140/epjd/e2014-50090-x

ISSN 1434-6060

2. M. Savić, M. Radmilović-Radjenović, M. Šuvakov, S. Marjanović, D. Marić and Z. Lj. Petrović: On Explanation of the Double-Valued Paschen-Like Curve for RF Breakdown in argon – *IEEE Trans. Plasma Sci.* (2011), Vol. 39, pp. 2556-2557, број хетероцитата 10.

ИФ 1.174 DOI: 10.1109/TPS.2011.2159244

ISSN 0093-3813

3. Srđan Marjanović, Milovan Šuvakov, Ana Banković, Marija Savić, Gordana Malović, Stephen J. Buckman, and Zoran Lj. Petrović: Numerical Modeling of Thermalization of Positrons in Gas-Filled Surko Traps – *IEEE Trans. Plasma Sci.* (2011), Vol. 39, pp. 2614-2615, број хетероцитата 10.

ИФ 1.174 DOI: 10.1109/TPS.2011.2159129

ISSN 0093-3813

### **Рад у међународним часописима (M23):**

1. Marija Radmilović-Radjenović, Branislav Radjenović, Marija Savić: Microwave field strength computing for the resonator designs and filters – *Acta Physica Polonica A* (2016), Vol 129, pp. 289-292.

ИФ 0.469 DOI: 10.12693/AphysPolA.129.289

ISSN 0587-4246

2. Š. Matejčik, M. Klas, B. Radjenović, M. Durian, M. Savić and M. Radmilović-Radjenović: The Role of the Field Emission Effect in the Breakdown Mechanism of Direct-Current Helium Discharges in Micrometer Gaps – *Contrib. Plasma Phys.* (2013), Vol. 53, pp. 573-579, број хетероцитата 4.

ИФ 0.983 DOI: 10.1002/ctpp.201300032

ISSN 0863-1042

3. M. Radmilović-Radjenović, B. Radjenović and M. Savić: The surface charging effects in three-dimensional simulation of the profiles of plasma-etched nanostructures – *International Journal of Numerical Modelling: Electronic Networks, Devices and Fields* (2011), Vol. 24, pp. 535-544, број хетероцитата 5.

ИФ 0.600 DOI: 10.1002/jnm.798

ISSN 0894-3370

4. A. Bojarov, M. Radmilović-Radjenović and M. Savić: Influence of the secondary electron emission on the characteristics of radio frequency plasmas – *Hemijska Industrija* (2011), Vol. 65, pp. 1-8.

ИФ 0.205 DOI: 10.2298/HEMIND100810063B

ISSN 0367-598X

5. Marija B. Savić, Marija Radmilović-Radenović: Modelovanje proboja u gasovima na niskim pritiscima Monte Karlo tehnikom (Gas discharges modeling by Monte Carlo technique) – *Hemijska Industrija* (2010), Vol. 64, pp. 171-175.

ИФ 0.137 DOI: 10.2298/HEMIND091221022S

ISSN 0367-598X

6. Marija Radmilović-Radjenović, Branislav Radjenović, Marija Savić: Breakdown phenomena in water vapor microdischarges – *Acta Physica Polonica A* (2010), Vol. 117, pp. 752-755.

ИФ 0.467 DOI: 10.12693/APhysPolA.117.752

ISSN 0587-4246

### **Предавање по позиву са међународног скупа штампано у целини (M31):**

1. Marija Puač, Zoran Lj Petrović: Modeling of radio-frequency breakdown by Monte Carlo technique, 22nd International Conference on Gas Discharges and their Applications, 2nd to 7th September 2018. Novi Sad, Serbian Academy of Science and Arts, pp. 335-338.

### **Предавање по позиву са међународног скупа штампано у изводу (M32):**

1. Zoran Lj Petrović, Antonije Djordjević, Marija Puač, Jana Petrović, Jelena Sivoš, Gordana Malović, Dragana Marić: Measurements and simulations of RF breakdown in gases – 7th

International Conference on Advanced Plasma Technologies, Plasmadis Ltd, Teslova ulica 30, 1000 Ljubljana, Slovenia, 24th February – 1st March 2019. Hue, Vietnam  
ISBN 978-961-290-061-8

2. Z. Lj Petrović, A. Djordjević, J. Petrović, J. Sivoš, M. Puač, G. Malović, D. Marić: RF breakdown as a swarm experiment – 82nd IUVSTA Workshop, Osaka University, Japan, 04.-07. Decembre 2017.

3. Z. LJ Petrović, S. Marjanović, M. Puač, S. Dujko, I. Simonović, D. Marić: Transport theory as a foundation of nonequilibrium plasma models – 81st IUVSTA Workshop on Response of Biological Materials to Plasma Treated Medium, Rogla, Slovenia, 12th to 16th March 2017.  
ISBN 978-961-285-628-1

4. Saša Dujko, Gordana Malović, Dragana Marić, Srdjan Marjanović, Zoran Lj Petrović, Marija Radmilović-Radjenović, Marija Savić, Ilija Adžić, Antonije Djordjević: Avalanches of electrons and positrons in Atmospheres of Planets and Satellites of the Solar System: Basic Phenomenology and Application to Gas Breakdown in DC and RF Fields, National Symposium on Plasma Science and Technology & International Conference on Plasma Science and Technology (PLASMA 2014), Mahatma Gandhi University, 8th to 11th December 2014.

5. Zoran Lj Petrović, Saša Dujko, Jasmina Mirić, Danko Bošnjaković, Ana Banković, Srdjan Marjanović, Dragana Marić, Jelena Sivoš, Nikola Škoro, Marija Savić, Olivera Šašić, Gordana Malović: Cross Sections for Scattering of Electrons and Positrons in Modeling of Ionized Gases and Non-Equilibrium Plasmas, International Symposium on Non-equilibrium Plasma and Complex-System Sciences (IS-NPCS), Osaka University, 26th to 28th February 2014.

6. Marija Radmilović-Radjenović, Zoran Lj Petrović, Marija Savić, Milovan Šuvakov: Modelling of a breakdown phenomena in radio-frequency discharges in micro gaps, 6th International Workshop on Microplasmas – 6th International Workshop on Microplasmas, CNRS and Universite Parys-Sud, Orsay, France, 3. - 6. Apr. 2011, pp. 33.

7. Branislav Radjenović, Marija Radmilović-Radjenović, Marija Savić: Two-dimensional simulations of the microhollow cathode discharges in argon at atmospheric pressures – VI International Workshop on Microplasmas, Laboratoire de Physique des Gaz et des Plasmas CNRS& University of Paris-Sud, Orsay, France, 3. - 6. Apr, 2011, pp. 94-94

8. Zoran Lj Petrović, Jelena Sivoš, Marija Savić, Nikola Škoro, Marija Radmilović-Radjenović, Dragana Marić: New phenomenology in description of Townsend discharges and gas breakdown: from standard size to micro discharges – The 4th International Conference on Plasma Nanotechnology and Science (IC-PLANTS), Plasma Nanotechnology Research Center, Nagoya University, Gifu, Japan, 10. - 12. Mar, 2011, pp. I-07\_1 - I-07\_2.

9. D. Marić, M. Savić, S. Marjanović, N. Škoro, M. Šuvakov, M. Radmilović-Radjenović, G. Malović and Zoran Lj. Petrović: Plasma breakdown: Experiments and simulation – 38th EPS Conference on Plasma Physics, European Physical Society & Institute for Magnetic Fusion Research, 27. 06. - 01. 07. 2011. Strasbourg, France, pp. I4.316

**Саопштење са међународног скупа штампано у целини (М33):**

1. Marija Puač, Dragana Marić, Zoran Lj Petrović: Electron energy distribution functions in a radio-frequency argon discharge - Monte Carlo simulations -29th Summer School and International Symposium on the Physics of Ionized Gases, University of Belgrade, Faculty of Physics, Serbia  
Belgrade, Serbia, 22. Aug - 1. Sep, 2018, pp. 218-221.  
ISSN 978-86-7306-146-7
2. Marija Savić, Dragana Marić, Zoran Lj Petrović: Monte Carlo simulation of radio-frequency breakdown in air and oxygen – 28th Summer School and International Symposium on the Physics of Ionized Gases, University of Belgrade, Faculty of Physics, Serbia  
Belgrade, Serbia, 29. Aug - 2. Sep, 2016, pp. 312-315.  
ISSN 978-86-84539-14-6
3. Marija Savić, Marija Radmilović-Radjenović, Milovan Šuvakov, Zoran Lj Petrović: Modeling of the radio frequency breakdown Paschen like curves by Monte Carlo technique – 27th Summer School and International Symposium on the Physics of Ionized Gases (SPIG 2014), Institute of Physics, Belgrade, 26.-29. Aug. 2014. Serbia, pp. 411-414  
ISSN 978-86-7762-600-6
4. Marija Savić, Marija Radmilović-Radjenović, Milovan Šuvakov, Dragana Marić, Zoran Lj Petrović: Monte Carlo simulation of radio-frequency breakdown in argon – 20th International Conference on Gas Discharges and their Applications, Orleans, France, 6.-11. Jul 2014, pp. 28511, sciencesconf.org:gd2014:28511
5. Marija Savić, Marija Radmilović-Radjenović, Milovan Šuvakov, Zoran Lj Petrović: The influence of the surface effects on argon radio-frequency discharge characteristics –3rd National Conference on Electronic, Atomic, Molecular and Photonic Physics, University of Belgrade, Faculty of Physics, Serbia, 25. - 25. Aug, 2013, pp. 25-28  
ISBN 978-86-84539-10-8
6. Marija Savić, Marija Radmilović-Radjenović, Branislav Radjenović: Theoretical Predictions of the Microwave Breakdown Field – 26th Summer School and International Symposium on the Physics of Ionized Gases, University of Novi Sad, Zrenjanin, Serbia, 27. - 31. Aug, 2012, pp. 325-328
7. Marija Savić, Marija Radmilović-Radjenović, Dragana Marić, Milovan Šuvakov, Zoran Lj Petrović: Monte Carlo simulations of RF breakdown – 26th Summer School and International Symposium on the Physics of Ionized Gases, University of Novi Sad, Zrenjanin, Serbia, 27. - 31. Aug, 2012, pp. 329-332
8. Marija Savić, Marija Radmilović-Radjenović, Milovan Šuvakov, Zoran Lj Petrović: Modeling of breakdown behavior in radio-frequency argon discharges – International Conference on Advanced Plasma, Slovenian Society for Vacuum Technique, Strunjan, Slovenia, 9. - 13. Sep, 2011, pp. 144-147
9. Marija Savić, Marija Radmilović-Radjenović, Milovan Šuvakov, Zoran Lj Petrović: The breakdown voltage curves and spatial profiles of ionization rates in argon rf discharges – 30th International Conference on Phenomena in Ionized Gases, Queen's University Belfast

Belfast, Northern Ireland, UK, 28. Aug - 2. Sep, 2011, pp. C9-149-1 – C9-149-3

10. Marija Radmilović-Radjenović, Marija Savić, Milovan Šuvakov, Branislav Radjenović, Stefan Matejček, M. Klas: The breakdown voltage curves in argon dc and rf discharges from large to small gap sizes – 18th Symposium on Application of Plasma Processes Workshop on Plasmas as a Planetary Atmosphere Mimics, Comenius University in Bratislava; Society for Plasma Research and Applications, Vratna, Mala Fatra, Slovakia, 15. - 20. Jan, 2011, invited lecture, pp. 70-74.

11. Marija Savić, Marija Radmilović-Radjenović: Modelovanje interakcija plazme sa površinama – Naučni skup Physics 2010 BL, Prirodno-matematički fakultet, Banja Luka, Republika Srpska, Bosna i Hercegovina, 22. - 24. Sep, 2010, str. 101-110.  
ISSN: 978-99955-21-21-9

12. Marija Savić, Marija Radmilović-Radjenović, Zoran Lj Petrović: The effect of metastable atoms on the secondary electron production in argon – 25th Summer School and International Symposium on the Physics of Ionized Gases, Astronomical Observatory of Belgrade, Donji Milanovac, Serbia, 30. Aug - 3. Sep, 2010, No 89, pp. 269-272.  
ISSN 0373-3742

#### **Саопштење са међународног скупа штампано у изводу (M34):**

1. Marija Puač, Antonije Djordjević, Zoran Lj Petrović: The role of electron-electrode collisions and secondary electrons in radio-frequency breakdown – 71st Annual Gaseous Electronics Conference, American Physical Society, Portland, Oregon, USA, 5 - 9. Nov. 2018, poster ID: GT1.00071.  
[http://www.apsgec.org/gec2018/all\\_GEC18.pdf](http://www.apsgec.org/gec2018/all_GEC18.pdf)

2. Zoran Petrović, Antonije Djordjević, Jana Petrović, Jelena Sivoš, Marija Puač, Gordana Malović, Dragana Marić: RF Breakdown as a Swarm Experiment – 82nd IUVESTA Workshop, Osaka University, Japan, Bankoku Shinryokan, Okinawa, Japan, 4. - 7. Dec, 2017, pp. O2

3. Zoran Lj Petrović, Srdjan Marjanović, Marija Savić, Saša Dujko, Ilija Simonović, Dragana Marić: Transport theory as a foundation of nonequilibrium plasma models – 81st IUVESTA Workshop on Response of Biological Materials to Plasma Treated Medium, 12-16. March 2017, Slovenia, pp. 22-23

4. Marija Savić, Dragana Marić, Marija Radmilović-Radjenović, Zoran Lj Petrović: Monte Carlo simulation of radio-frequency breakdown in oxygen and air – 69th Annual Gaseous Electronics Conference, American Physical Society, Bochum, Germany, 10. - 14. Oct, 2016, poster ID: BAPS.2016.GEC.MW6.74.  
<http://meetings.aps.org/link/BAPS.2016.GEC.MW6.74>

5. Saša Dujko, Gordana Malović, Dragana Marić, Srdjan Marjanović, Zoran Lj Petrović, Marija Radmilović-Radjenović, Marija Savić, Ilija Adžić, Antonije Djordjević: Avalanches of electrons and positrons in Atmospheres of Planets and Satellites of the Solar System: Basic Phenomenology and Application to Gas Breakdown in DC and RF Fields – National Symposium on Plasma Science and Technology & International Conference on Plasma

Science and Technology (PLASMA 2014), Mahatma Gandhi University, 8-11. Dec.2014. India, pp. 18.

6. Zoran Lj Petrović, Saša Dujko, Jasmina Mirić, Danko Bošnjaković, Ana Banković, Srdjan Marjanović, Dragana Marić, Jelena Sivoš, Nikola Škoro, Marija Savić, Olivera Šaić, Gordana Malović: Cross Sections for Scattering of Electrons and Positrons in Modeling of Ionized Gases and Non-Equilibrium Plasmas – International Symposium on Non-equilibrium Plasma and Complex-System Sciences (IS-NPCS), Osaka University, Icho Kaikan, Osaka, Japan, 26. - 28. Feb, 2014.

7. Zoran Lj Petrović, Jelena Sivoš, Marija Savić, Nikola Škoro, Marija Radmilović-Radjenović, Dragana Marić: New Phenomenology of Gas Breakdown In DC And RF Fields – 18th International Summer School on Vacuum, Electron and Ion Technologies (VEIT 2013) Sozopol, Bulgaria, 7. - 11. Oct, 2013, PP. 37-38.

8. Marija Savić, Marija Radmilović-Radjenović, Zoran Lj Petrović: The rf breakdown voltage curves-similarity law – 66th Annual Gaseous Electronics Conference, American Physical Society, USA, 30. Sep - 4. Oct, 2013, pp. CT1.23  
ISSN 0003-0503

9. Marija Savić, Marija Radmilović-Radjenović, Milovan Šuvakov, Zoran Lj Petrović: First steps in obtaining Monte Carlo model of RF breakdown – ESCAMPIG XXI, Instituto de Plasmas e Fusão Nuclear from Instituto Superior Técnico, Universidade Técnica de Lisboa, Universidade do Porto, Universidade do Minho and Universidade da Madeira Portugal, 10. - 14. Jul, 2012, pp. T6-296-1 – T6-296-2

10. Marija Savić, Marija Radmilović-Radjenović, Zoran Lj Petrović: Monte Carlo simulations of breakdown in radio-frequency discharges – 64th Annual Gaseous Electronics Conference, Bulletin of the American Physical Society, Salt Lake City, Utah, 14. - 18. Nov, 2011, pp. 36-36

11. Marija Savić, Marija Radmilović-Radjenović, Milovan Šuvakov, Zoran Lj Petrović: Monte Carlo simulation of RF discharges – 2nd National Conference on Electronic, Atomic, Molecular and Photonic Physics, Institute of Physics, Belgrade, Serbia, 21. - 25. Jun, 2011, pp. 134-134

12. Z. Lj. Petrović, M. Radmilović-Radjenović, M. Savić, D. Marić, M. Šuvakov, N. Škoro and S. Dujko: Basic phenomenology and experimental techniques for gas breakdown from DC to RF and from few cm to micrometers – High Frequency Gas Breakdown Workshop Laboratoire de Physique des Plasmas, Ecole Polytechnique, 91128 Palaiseau, France, 4. Oct. 2010 France, pp. 4

13. Marija Savić, Marija Radmilović-Radjenović, Zoran Lj Petrović: Modeling of low pressure breakdown by Monte Carlo technique – 20th European Conference on the Atomic and Molecular Physics of Ionized Gases, European Physical Society, Novi Sad, Serbia, 13. - 17. Jul, 2010, pp P2.58  
ISSN 2-914771-63-0



## New phenomenology of gas breakdown in DC and RF fields

Zoran Lj Petrović<sup>1,3,4</sup>, Jelena Sivoš<sup>1</sup>, Marija Savić<sup>1</sup>, Nikola Škoro<sup>1</sup>, Marija Radmilović Rađenović<sup>1</sup>, Gordana Malović<sup>1</sup>, Saša Gocić<sup>2</sup> and Dragana Marić<sup>1</sup>

<sup>1</sup>Institute of Physics, University of Belgrade, POB 68, 11080 Zemun, Serbia

<sup>2</sup>Faculty of Natural Sciences, University of Niš, 33 Višegradska, 18000 Niš, Serbia

E-mail: Zoran@ipb.ac.rs

**Abstract.** This paper follows a review lecture on the new developments in the field of gas breakdown and low current discharges, usually covered by a form of Townsend's theory and phenomenology. It gives an overview of a new approach to identifying which feedback agents provide breakdown, how to model gas discharge conditions and reconcile the results with binary experiments and how to employ that knowledge in modelling gas discharges. The next step is an illustration on how to record volt-ampere characteristics and use them on one hand to obtain the breakdown voltage and, on the other, to identify the regime of operation and model the secondary electron yields. The second aspect of this section concerns understanding the different regimes, their anatomy, how those are generated and how free running oscillations occur. While temporal development is the most useful and interesting part of the new developments, the difficulty of presenting the data in a written form precludes an easy publication and discussion. Thus, we shall only mention some of the results that stem from these measurements. Most micro discharges operate in DC albeit with complex geometries. Thus, parallel plate micro discharge measurements were needed to establish that Townsend's theory, with all its recent extensions, is still valid until some very small gaps. We have shown, for example, how a long-path breakdown puts in jeopardy many experimental observations and why a flat left-hand side of the Paschen curve often does not represent good physics. We will also summarize a kinetic representation of the RF breakdown revealing a somewhat more complex picture than the standard model. Finally, we will address briefly the breakdown in radially inhomogeneous conditions and how that affects the measured properties of the discharge. This review has the goal of summarizing (rather than developing details of) the current status of the low-current DC discharges formation and operation as a discipline which, in spite of its very long history, is developing rapidly.

### 1. Introduction: Townsend's theory and low-current DC discharges - 100 years ago and now

With the development of basic phenomenology and theory of gas breakdown, Townsend's theory was forged some 100 years ago [1-3]. In this paper we shall give a review of how in the past 20 years the basic Townsend's theory and phenomenology have been revived, extended, revitalized and put in perspective of modelling higher current technological discharges and plasmas. This was primarily done by the groups of Art Phelps and the Gaseous Electronics Laboratory in Belgrade.

<sup>3</sup> Author affiliation: also at Serbian Academy of Sciences and Arts, Belgrade, Serbia.

<sup>4</sup> To whom any correspondence should be addressed.



Recent advances in diagnostics and modelling of complex plasma systems opened an opportunity to revisit the breakdown in gases both in DC and RF fields and also for micro gaps. We shall first discuss the experimental techniques to determine the breakdown voltage. Typical errors, such as neglecting the long-path breakdown on the left-hand side of the Paschen minimum, conditioning of the electrode and measuring properties within an unstable (oscillating) regime, will be covered briefly. In addition, we shall describe a proper methodology to establish volt-ampere ( $V$ - $I$ ) characteristics and how to use those with the goal of determining the breakdown voltage and the secondary electron yields.

Time-resolved imaging [4] provides us with information on the development of the anatomy of the discharge and its different modes. Using the spatial profile one may decide which of the mechanisms dominate the discharge. The Townsend regime is the low-current diffuse discharge with exponential growth towards the anode [5]. It is necessary to observe such a profile to ascertain that the discharge operates in the Townsend regime where Townsend's theory may be used to establish the condition for breakdown and effective secondary electron yield. The temporal development of the normal glow or abnormal glow following the breakdown reveals transient multi-regime operation that requires a new paradigm.

When considering volt-ampere characteristics, one may first observe the negative differential resistance in the Townsend regime which may be explained by a combination of space-charge effects and an energy-dependent secondary electrons yield. Thus,  $V$ - $I$  characteristics should be used in addition to the Paschen curve to determine the secondary electrons yields. With the newly found field of discharges in and above liquids, we have also analyzed breakdown in water vapor and ethanol [6,7].

RF and microwave breakdowns have a different phenomenology as the secondary ions production of electrons at the cathode may not be necessary. Yet the RF breakdown is prone to phenomena not often observed in DC breakdowns, like S shaped (double valued) Paschen-like curves, frequency/gas number density scaling and additional mechanisms like multipactors. The principal experimental problem with the RF breakdown is the magnitude of the displacement current that thwarts the measurement of the conduction current making it difficult to ascertain the initiation of the discharge.

## 2. Gas breakdown, feedback mechanism, secondary electron yields and how to use them

Traditionally, the gas breakdown is characterized by Paschen curves. In figure 1 we show one such example of Paschen curves for the topical water vapor and ethanol vapor [6,7].

While most people will argue (including the present authors) that the Paschen law itself is developed with limiting assumptions

$$V_b = \frac{Bpd}{\ln(Apd) - \ln\left[\ln\left(1 + \frac{1}{\gamma}\right)\right]}, \quad (1)$$

the breakdown equation from the Townsend's law is in principle exact if the assumptions of the primary feedback through ions are correct:

$$\gamma(E/N)\left(e^{\alpha(E/N)d} - 1\right) = 1. \quad (2)$$

Different forms of analytical laws have been employed for the DC breakdown in order to provide some insight [8,9], but one needs to be aware of the approximate nature of some of the basic formulae. Still, the same limitations that enter the analytical form of Paschen law may enter the implementation

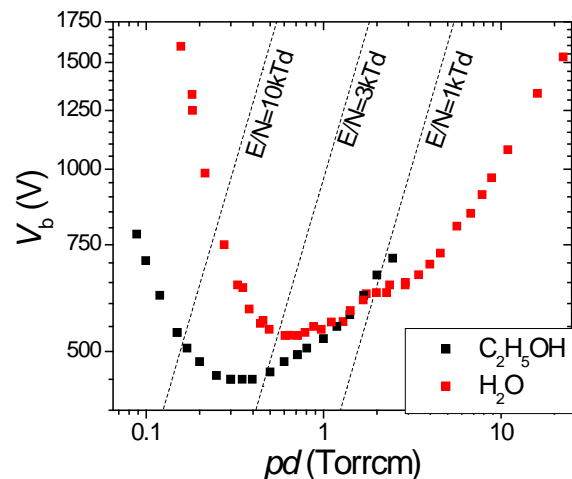


**Figure 1.** Paschen curves for water [6] and ethanol vapor [7].

of equation (2). Over the years, a large amount of data on  $\gamma$  have been accumulated, yet seldom those have been compared and systematically collected. Even more importantly, comparisons to binary collision (beam-surface) experiments [10] have been almost avoided in the literature presumably due to poor agreement (both qualitative and quantitative). One example where both systematic collection of data and comparisons to binary experiments have been made is the paper of Phelps and Petrović [3].

In figure 2 we show a comparison of the secondary electron yields obtained from Paschen curves in argon for a range of experiments [3]. These should be compared with a constant yield of 0.08 obtained by beam experiments with an atomically clean surface [10] or to the dot-dash line obtained for the same conditions of the cathode as found in discharge experiments. Discharge results are one order of magnitude too high at higher  $E/N$ , one order of magnitude lower at moderate  $E/N$  and two orders of magnitude higher at the lowest  $E/N$ . Phelps and Petrović managed to reconcile the binary collision data and the discharge results by including the following:

- ionization coefficient fitted in a wide range of  $E/N$ ;
- a region close to the cathode where electrons gain energy and become in equilibrium with the local field, the simplest way of representing this being using a delay distance  $d_0$ ;
- ion-induced yields at the cathode, modified to represent surfaces that are not atomically clean;
- back-diffusion, i.e. the return of newly emitted electrons back to the cathode;
- secondary electron production by metastables;
- secondary electron production by fast neutrals;
- secondary electron production by resonant radiation – the photo effect;
- trapping of resonant radiation;
- secondary electron production by fast neutrals;
- secondary production due to molecular emission.

The solid and dashed lines in figure 2 indicate the model predictions based on binary collision data (for two limits of possible contributions by molecular radiation). These two lines encompass most of the available experimental data. The good agreement with the experiments shows that all pertinent processes have been included. It also shows that the process of secondary yields modelling may be quite complex and quite challenging due to the need for a wide range of data.

The fact that Townsend's theory could associate all the yields with the flux of ions is because all fluxes are proportional to the electron flux and the system is linear in the breakdown-Townsend discharge phase. On the other hand, one cannot expect linearity to hold for higher current modes, such as glow discharges. For those, one is left with fitting the experimental data. Thus, we compared the fitting procedure with one based on the breakdown data from Phelps and Petrović [3]. We found [11] that fitting of the glow discharge is well represented by the procedure recommended for the breakdown data [3], except when  $pd$  is quite low and fast neutral effects become dominant. Yet, for RF discharges, for example, or for some more complex geometries, one needs to provide a clear guidance as to how the secondary electron yield may be modelled. Also, we need a considerable effort to provide the data for a number of relevant gases, as argon is the only gas covered so far by the detailed analysis.

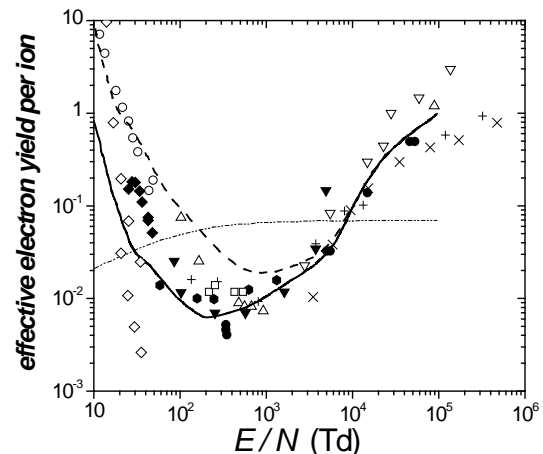


**Figure 2.** Effective secondary electron yield  $\gamma$  for argon obtained from breakdown data [3]. The different types of points indicate different experiments - see [3]. The dot-dash curve shows binary collision experiment data.

### 3. Volt-ampere characteristics and spatial emission profiles

There are two ways to determine the breakdown voltage. The first option is very accurate albeit very difficult – one can extrapolate pre-breakdown currents. The second one, favored by our group, is to establish a self-sustained discharge in the low-current diffuse, i.e. Townsend, discharge and then extrapolate the measurements to zero current. All other techniques suffer from arbitrariness, either induced by the long statistical time lags or by a direct transition to the glow regime. The Townsend's regime is recognized by an exponential growth peaking at the anode and a normally broad diffusion-determined profile over the entire surface [5,12], as can be seen in figure 3.

In conducting such measurements, we (re)established that in the Townsend regime one has a negative differential resistance. As the effective resistance of the discharge is negative, sometimes, coupled with the external circuit, the overall loop resistance may become negative and oscillations may occur [13,14]. As it turns out, the space charge due to ions increases the field in front of the cathode, which increases the electron production allowing a lower field elsewhere and thus the overall voltage is reduced [14,15]. Thus, the dependence of  $\gamma$  on the mean energy is the reason for the negative differential resistivity, brought about by space charge induced electric field and represented as a current dependence of  $\gamma$ . As the discharge approaches constriction, non-linearities become important [16] and a sudden transition eventually takes place. It has also been shown that if  $\gamma$  were constant, the slope of the  $V$ - $I$  characteristics in Townsend's regime could become positive [16]. Thus one may conclude that for the full representation of the secondary electron yield one needs to fit not only the Paschen curve but also the  $V$ - $I$  characteristics. The realm of oscillations often precludes us from achieving stable operation in Townsend's regime but it is also a source of information on important processes. Thus, fitting of the induced damped or free running oscillations may reveal identity of the dominant ionic species, multiplication and may be related to basic transport properties of relevant particles.

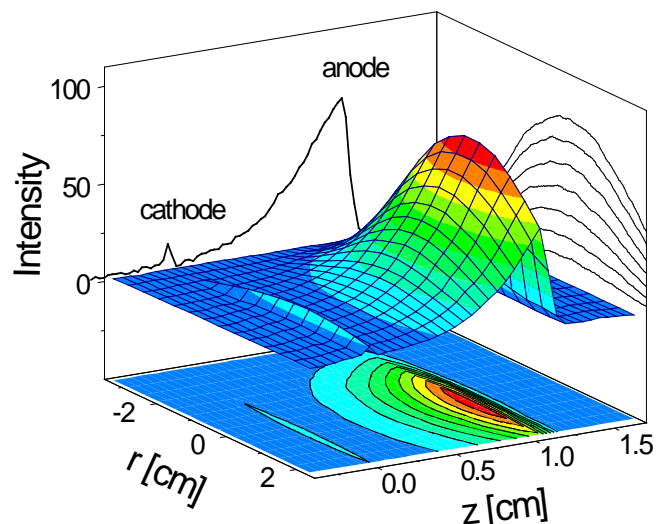


**Figure 3.** Spatial profile of the Townsend's regime low-current diffuse discharge [12].

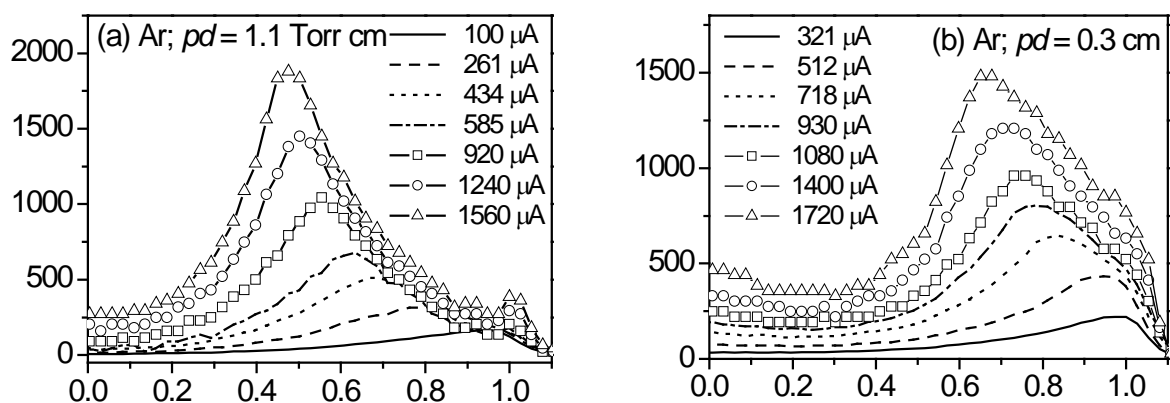


**Figure 4.** Axial profiles of higher current discharge regimes in argon, at (a)  $pd = 1.1$  Torr cm (close to the Paschen minimum); (b)  $pd = 0.3$  Torr cm (in the left-hand branch of the Paschen curve).

Another important aspect that stems from figure 3 is that spatial profiles not only give us information on the regime of operation (see figure 4 – the peak in front of the anode is for Townsend’s low current discharges, the peak in the bulk corresponds to the glow discharge) but also (if put on an absolute scale) a basis to establish absolute cross sections and even profile of the field. It also shows whether and to what extent is equilibrium (with the field) developed or whether fast neutral excitation is important as recognized by the peak right in front of the cathode.

#### 4. Scaling of the basic properties of micro discharges

Micro discharges were basically developed to take advantage of the non-equilibrium plasma that is formed around the Paschen minimum, but at a much higher pressure. Atmospheric pressure would require a 10  $\mu\text{m}$  gap. On the other hand, to achieve a stable operation at high pressures one needs to use complex geometries as it proved very difficult to operate parallel plate micro discharges. Yet, many authors have assumed parallel plate geometries with narrow strips crossing at small distances and assumed that the breakdown occurs at the shortest distances. This has led to a number of papers where the left hand side of the Paschen curve showed no or little variation that could be erroneously interpreted as the onset of field emission (that was predicted to occur only for  $d < 10 \mu\text{m}$  [9]). We have made an effort to perform measurements in well defined and contained parallel plate discharges, to test the applicability of Townsend’s phenomenology at small gaps [17].

Before proceeding to any modelling, we needed to test the laws of scaling, which for low pressure collision dominated discharges are  $E/N$ ,  $pd$  and  $jd^2$  (and also  $\omega/N$  and  $B/N$  for time varying fields and for magnetic fields). The critical scaling is due to the current density  $j$ . Rarely are the  $V-I$  characteristics represented through  $j$  (as it should be) and even then it is not stated that  $j$  is actually determined by dividing the current by the entire area of the electrodes. In reality, however, constriction dominates in the glow regime. Even in the Townsend’s and in the abnormal glow regimes the radial profile is quite different and so is the effective area. Taking advantage of transparent yet conducting materials for electrodes and also of ICCD cameras, we were able to record  $V-I$  characteristics and scale them to the real current density even in cases of complex constricted modes. First, we established that in the normal size discharges, when the current density is properly determined, it remains constant throughout the glow regime (so it is represented by a single point in  $V-I$  characteristics [18]).

Secondly, we have been able to show that for discharges bordering on micro discharges (0.5 and 1 mm gaps) the  $jd^2$  scaling works and finally we have extrapolated those findings (by using  $pD$  scaling where  $D$  is the diameter of the constricted region) to smaller gaps where we could not easily record the current profiles [17]. It was found, as can be seen in figure 5, that a Townsend type of scaling holds at those gaps until perhaps some smaller geometries where field emission really comes into play [19]. We have even shown that the spatial profiles scale well so that the ionization coefficient could be determined rather accurately from the axial emission profile of micro discharges [20].

It was also shown that the Paschen curves obtained for micro discharges (and sometimes even for the standard size discharges) that do not show a change of voltage on the left hand side beyond the minimum are due to an incorrectly assumed shortest distance for the gap when long path breakdown was allowed [21]. Reducing the chances for the long path breakdown brings back the Paschen curve to agreement with that obtained for standard dimensions/pressures.

The fact that we proved scaling and also were able to obtain accurate readings of ionization coefficients proves that it is possible to apply Townsend’s phenomenology and even to some degree theory to micro discharges. The  $jd^2$  scaling allows Townsend regime to operate at considerably higher current densities.

#### 5. Time resolved measurements

A preliminary publication of our results on time dependent recordings of the development of the breakdown and DC discharge regimes was given in [9,22], while the majority of the data remain unpublished. The results may be summarized as follows. During the initial stage, the discharge passes through the Townsend regime and, as the current increases, glow and abnormal glow regimes are visited. During the minimum of oscillations, the discharge almost immediately returns to the

Townsend regime and then changes occur again and again following oscillations in current. Studies such as this one performed for a parallel plate geometry are needed to provide the background for understanding developments in more complex geometries [23] and different scales.

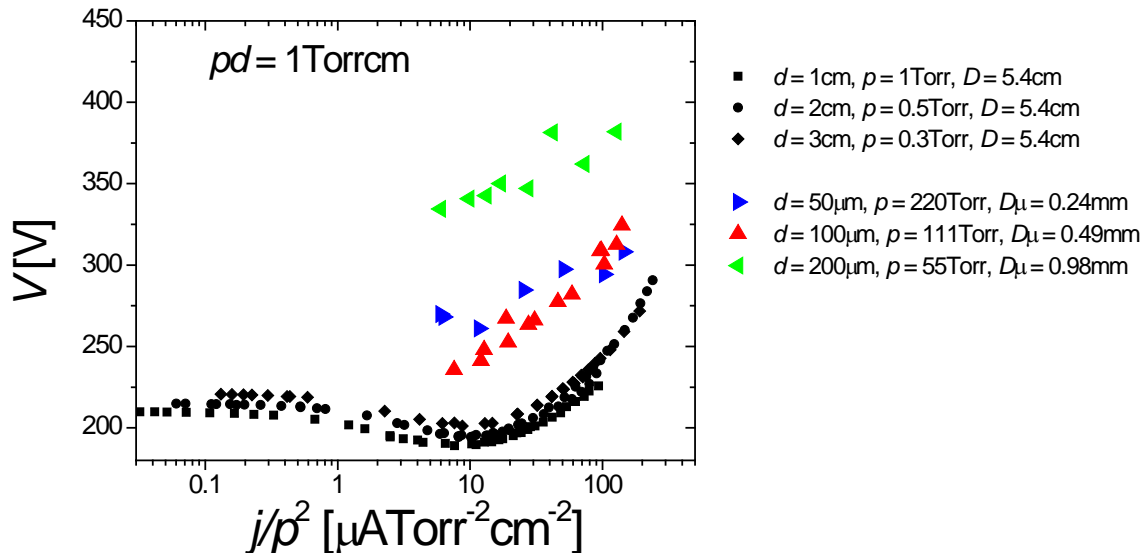


**Figure 5.**  $V$ - $I$  characteristics for standard size and micro discharges obtained by using the  $jd^2$  scaling and  $pD$  scaling for the size of the constricted regions. One should not pay attention to the actual vertical scale, normally it is taken care of by subtracting the breakdown voltages in each case, but in the case of micro discharges we could not make accurate measurements as it was not possible to achieve stable operation in the Townsend regime. The vertical scale variations are due to different conditions on the electrodes surface [17].

## 6. Discharges with inhomogeneous cathodes

The usual assumption in the low current limit is that the discharge is uniform over the entire surface and the radial profile is the solution to the diffusion equation. Only in the higher current (glow) regime a constriction develops and only when the field ceases to be constant along the axis. This has been questioned recently for micro discharges when it was found that the scaling laws are maintained only when an assumption of localized modes is made, the modes that have a dimension proportional to the diffusion length for the given pressure [17]. The problem is hindered further by the high pressure that reduces the diffusion length and by the fact that the ratio of gap to radius becomes very small in practical experiments [17].

We have, however, observed localized discharges in Townsend regime for standard size discharges (1 cm) and moderately low pressures [24]. In figure 6 we show one such example in nitrogen where the discharge is limited in the radial direction by the region of deposited material due to numerous pulses in the high current mode. It is clear that the deposited region has a lower secondary electron yield  $\gamma$  and thus the discharge cannot be self-sustained over that area for the given voltage. In order to overcome this region of reduced  $\gamma$ , the volt-ampere characteristics have to be quite different as compared to the one with pristine cathode. Even a positive differential resistance is observed [24].

The characteristics of such a discharge may be a prototype for the breakdown in pulsed DC discharges where numerous discharges change the properties of the cathode considerably. In addition, one may construct cathodes of different materials and design desired characteristics. For example, cathodes coated by a semiconductor [25, 26] have been often used for achieving some properties that are not easily accessible by conducting electrodes. The high resistance of the semiconductor which is in the innermost circuit assures a broader range of stable operation [14]. Combining conducting and semiconductor materials may help reduce the breakdown potential while achieving a  $V$ - $I$  characteristic that is less prone to oscillations.



### 7. RF breakdown

When rate of change of the field is such that ions cannot complete their trajectories, then it is possible to operate in conditions when electrons may be the only particles sustaining the discharge. The feedback is provided by returning electrons in the second half of the period and thus a full circle is achieved. It has been assumed in old textbooks and papers [27] and in more recent papers [28, 29] that an optimum breakdown condition is achieved when the average electron can cross the gap in one half period. In fact, the breakdown condition has been used to obtain experimental values of the drift velocities for RF fields and convert them to DC values by assuming that in RF fields the drift velocity is a sinus function peaking with the DC drift velocity and having no delay [29]. We modelled the RF breakdown using a detailed Monte Carlo

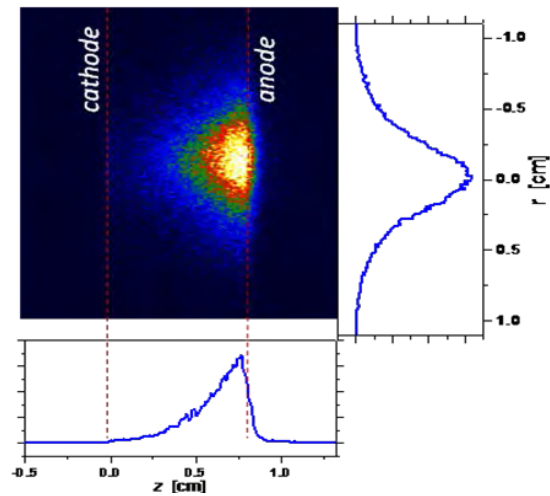


**Figure 6.** Townsend regime discharge in  $N_2$  with Cu cathode and for  $d = 0.8$  cm,  $D = 2$  cm,  $p = 2$  Torr and  $V_b = 310$  V. The axial profile shows exponential growth peaking at the anode while the radial profile is very narrow covering only a small part of the diameter ( $D$ ).

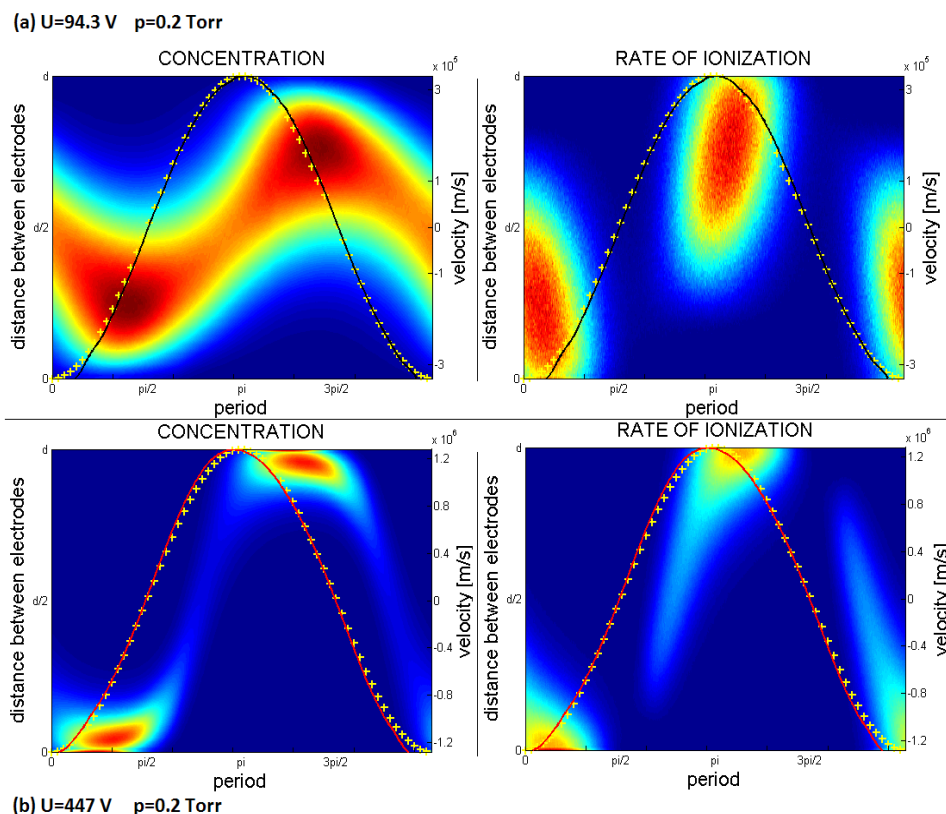


**Figure 7.** Development of density and ionization rate for the breakdown of RF swarms. Solid curves represent mean velocity (different colours are for better contrast), while the dotted sinusoidal lines represent inversed AC field. Both curves are for 0.2 Torr; the top curves are for the minimum breakdown voltage (93 V) while the bottom curves are for the maximum breakdown voltage (447 V) [30].



representation of all the collisions and field dependence on time. Figure 7 shows the temporal development of the concentration of electrons and of the ionization rate [30]. As the quasi-Paschen curve for the RF breakdown has double values for breakdown voltage at the same  $pd$  (for a range of  $pd$ ) we show results at the lower and at the higher breakdown point. Outside these borders the discharge cannot be ignited. At the lower point, the breakdown condition is achieved by merely matching the production without much of the electrodes overlapping with the swarm. At the higher end, however, the swarm overlaps considerably with the electrodes thus representing significant losses to the electrodes. At the same time, the peaking ionization must compensate for all the losses.

We found that, while the standard explanation of the RF breakdown is very good, still some fine tuning needs to be done by a full kinetic representation (such as a Monte Carlo simulation) to be able to describe all the intricacies. In addition, one needs to extend our model by the contribution of ions and fast neutrals as well as photons. These will modify the Paschen like curve and hopefully make it more realistic but for a wide range of conditions one may find that electrons dominate in sustaining the plasma. We also have to include the secondary electrons formed by the electron impact on electrodes. This effect will lead to the so-called multipacting modes.

One should also note that numerous attempts to use analytical and semi analytical models based on simplified expressions for the basic properties have migrated from DC discharges to the RF breakdown. These results provide insight into pertinent processes [31-34] but require some form of fitting to provide quantitative agreements.

## 8. Conclusions

The oldest chapter in the book on plasma physics, the breakdown and low current discharges, has been changed tremendously in the past twenty years. The main agent facilitating the feedback needed to achieve DC breakdown, the ions colliding with surfaces, have been changed to include photons, fast neutrals, metastables as well as ions. By including all these processes, as well as back-diffusion [3,35] one was able to predict effective yields and Paschen curves based on the binary collision data [3].

The field of low pressure DC discharges proved to be a fertile ground for both fundamental studies and for obtaining and testing the applicability of the fundamental data that would eventually be used for modelling of more complex systems. Extensions to micro discharges and RF breakdown have been made, together with first attempts to model RF plasmas with secondary electron yields [36] as obtained in a more detailed and recent analysis.

With the new drive for benchmarking plasma modelling systems [37], we believe that the best strategy would be to start from the swarm benchmarks and then use the negative differential resistance of a DC Townsend discharge as a benchmark for space charge effects and also use some additional breakdown properties. This would provide clear and simple experimental observables that may be modelled exactly and independently and provide the next step for more complex plasma benchmarks.

## Acknowledgement

This paper has been completed under the overall support of projects 171037 and III41011 of the Ministry of Education and Science of Serbia, and project 155 of the Serbian Academy of Sciences and Arts. Numerous discussion, shared research and data and ideas from the late Art V. Phelps are gratefully acknowledged.

## References

- [1] Townsend J S 1910 *The Theory of Ionization of Gases by Collision* (Constable, London)
- [2] Townsend J S 1915 *Electricity in Gases* (Oxford: Clarendon) 313
- [3] Phelps A V and Petrović Z Lj 1999 *Plasma Sources Sci. Technol.* **8** R21
- [4] Marić D, Malović G and Petrović Z Lj 2009 *Plasma Sources Sci. Technol.* **18** 034009
- [5] Petrović Z.Lj. and Phelps A.V. 2009 *Phys. Rev.E* **80** 016408
- [6] Škoro N, Marić D, Malović G, Graham W G and Petrović Z Lj 2011 *Phys. Rev. E* **84** 055401R
- [7] Petrović Z Lj, Sivoš J, Škoro N, Malović G and Marić D 2013 *Bul. Am. Phys. Soc. Ser. II* **58/8**

## HW1 35

- [8] Kihara T 1952 *Rev. Modern Phys.* **24** 45
- [9] Radmilović-Radjenović M and Lee J K 2005 *Phys. Plasmas* **12** 063501
- [10] Hagstrum H D 1954 *Phys. Rev.* **96** 336
- [11] Marić D, Hartmann P, Malović G, Donko Z and Petrović Z Lj 2003 *J. Phys. D: Appl. Phys.* **36** 2639
- [12] Petrović Z Lj, Donko Z, Marić D, Malović G and Živanov S 2002 *IEEE Trans. Plasma Sci.* **30** 136-7
- [13] Petrović Z Lj and Phelps A V 1993 *Phys. Rev. E* **47** 2806
- [14] Phelps A V, Petrović Z Lj and Jelenković B M 1993 *Phys. Rev. E* **47** 2825
- [15] Živanov S, Živković J, Stefanović I, Vrhovac S and Petrović Z Lj 2000 *Eur. Phys. J. AP* **11** 59
- [16] Nikolić M, Đorđević A, Stefanović I, Vrhovac S and Petrović Z Lj 2003 *IEEE Trans. Plasma Sci. PS* **31** 717
- [17] Petrović Z Lj, Škoro N, Marić D, Mahony C M O, Maguire P D, Radmilović-Radenović M and Malović G 2008 *J. Phys. D: Appl. Phys.* **41** 194002
- [18] Škoro N, Marić D and Petrović Z Lj 2008 *IEEE Trans. Plasma Sci.* **36** 994
- [19] Radmilović-Radjenović M, Matejčik Š, Klas M and Radjenović B 20013 *J. Phys. D:-Appl. Phys.* **46** 015302
- [20] Kuschel T, Stefanović I, Malović G, Marić D and Petrović Z Lj 2013 *Plasma Sources Sci. Technol.* **22** 045001
- [21] Marić D, Škoro N, Maguire P D, Mahony C M O, Malović G and Petrović Z Lj 2012 *Plasma Sources Sci. Technol.* **21** 035016
- [22] Marić D, Malović G and Petrović Z Lj 2007 *J. Phys.: Conf. Series* **86** 012009
- [23] Wagenaars E, Bowden M D and Kroesen G M W 2005 *IEEE Trans. Plasma Sci.* **33** 254
- [24] Gocić S R, Škoro N, Marić D and Petrović Z Lj 2010 *20<sup>th</sup> ESCAMPIG* (Novi Sad Serbia July 2010) P3.17
- [25] Kurt H, Četin S, and Salamov B G 2011 *IEEE Trans. Plasma Sci.* **39** 1086
- [26] Portsel L M, Lodygin A N and Astrov Yu A 2009 *J. Phys. D: Appl. Phys.* **42** 235208
- [27] Gill E B and von Engel A 1949 *Proc. R. Soc. A* **197** 107
- [28] Lisovskiy V A and Yegorenkov V D 1994 *J. Phys. D: Appl. Phys.* **27** 2340
- [29] Lisovskiy V, Booth J-P, Landry K, Douai D, Cassagne V and Yegorenkov V 2006 *J. Phys. D: Appl. Phys.* **39** 660
- [30] Savić M, Radmilović-Radjenović M, Šuvakov M, Marjanović S, Marić D and Petrović Z Lj 2011 *IEEE Trans. Plasma Sci.* **39** 2556
- [31] Sato M and Shoji M 1997 *Jpn. J. Appl. Phys.* **36** 5729
- [32] Iliev I, Gocheva-Ilieva S and Sabotinov N 2004 *Proc. SPIE* **5449** 131
- [33] Iliev I, Gocheva-Ilieva S and Sabotinov N 2009 *J. Optoelectr. Adv. Mater.* **11** 1392
- [34] Smith H B, Charles C and Boswell R W 2003 *Phys. Plasmas* **10** 875
- [35] Radmilović M and Petrović Z Lj 2000 *Eur. J. Appl. Phys.* **11** 35
- [36] Radmilović-Radjenović M and Petrović Z Lj 2009 *Eur. Phys. J. D* **54** 445
- [37] Turner M M, Derzsi A, Donkó Z, Eremin D, Kelly S J, Lafleur T and Mussenbroc T 2013 *Phys. Plasmas* **20** 013507

# Monte Carlo modeling of radio-frequency breakdown in argon

Marija Puač<sup>1,2,4</sup> , Dragana Marić<sup>2</sup> , Marija Radmilović-Radjenović<sup>2</sup>,  
Milovan Švakov<sup>2</sup> and Zoran Lj Petrović<sup>2,3</sup>

<sup>1</sup> School of Electrical Engineering, University of Belgrade, 11120 Belgrade, Serbia

<sup>2</sup> Institute of Physics, University of Belgrade, Pregrevica 118, 11080 Zemun, Serbia

<sup>3</sup> Serbian Academy of Sciences and Arts, Knez Mihailova 35, 11001 Belgrade, Serbia

E-mail: [smarija@ipb.ac.rs](mailto:smarija@ipb.ac.rs)

Received 29 March 2018, revised 29 May 2018

Accepted for publication 12 June 2018

Published 13 July 2018



CrossMark

## Abstract

This paper contains results of the detailed simulation study of the breakdown in low-pressure radio-frequency (RF) argon discharges. Calculations were performed by using a Monte Carlo code including electrons only, with the assumption that the influence of heavy particles was negligible. The obtained results are in a good qualitative agreement with the available experimental data and clearly show the multivalued nature of the left-hand branches of the breakdown voltage curves. The physical processes defining the breakdown conditions were analyzed based on the spatial profiles of electron density, local mean energy and the number of elastic and ionization collisions. Under the conditions where two breakdown values existed one could identify two regimes and two different balances between the electron losses and production. Using the dependence of the breakdown voltage on the product of the pressure and the interelectrode distance, and the product of the frequency and the interelectrode distance, similarity laws for RF breakdown have been reexamined.

Keywords: plasma modeling, Monte Carlo simulation, radio-frequency breakdown, similarity law

## 1. Introduction

Capacitively coupled radio-frequency (RF) discharges are attracting increasing attention due to their wide applications in many technological processes [1] such as plasma etching for semiconductor materials, thin film deposition, plasma cleaning [2] and increasingly popular biomedical applications [3–5]. One of the crucial issues is understanding the pertinent processes that drive the breakdown and transition to RF plasma and how those could be modeled. In that respect a wealth of information can be obtained from the breakdown voltage curves. Gas breakdown represents the first step in plasma generation. A specific characteristic of RF plasmas is that the self-sustained discharge may be maintained merely through ionization by electrons. There the feedback process is the return of electrons when the field changes direction, as a replacement of the ion drifts towards the cathode, which is the feedback in DC discharges [6–9].

Although gas breakdown has been studied for more than 100 years, many aspects are poorly understood. A simplified explanation dating back to an early version of the textbook by von Engel [8] (and perhaps dating back even further) is that only the group of electrons that completes the transition in one half period from one electrode to the other has a chance of being multiplied. Basically, the drift velocity that is integrated and averaged over the half period has to be equal to the gap between two electrodes [6, 7]. Most certainly the points that need clarification are the mechanism of the double-valued breakdown curve, the validity of the proposed mechanism of the relationship between drift in one half period and the gap, and also the role of non-locality on the development of the breakdown. All of these processes are properly accounted for in the simulation presented here.

In the first half of the 20th century there has been a major development of techniques to solve the time dependent Boltzmann equation [10–16] continued by Wilhelm and Winkler in the '70s and Makabe in the '80s [17, 18]. First exact solutions for the time dependent transport were obtained by using Monte

<sup>4</sup> Author to whom any correspondence should be addressed.

Carlo (MC) simulations [19] and numerical solutions to the time dependent Boltzmann equation [20, 21]. Numerous approximate experimental and theoretical papers have been published on the breakdown in RF using simplified semi-analytic forms [22–26]. At the same time fluid, hybrid and particle-in-cell (PIC) models of RF plasmas include early stages of the growth of ionization [18, 27, 28]. In recent years, computer modeling and simulation has emerged as an effective tool that complements laboratory experiments and analytic models. PIC/MC simulations have been used extensively to study fundamental processes in capacitively coupled RF discharges [29–32].

In this paper calculations were performed for argon discharges by using an MC code under the condition of a low degree of ionization so that the transport of particles could take place in the externally defined uniform field. In doing so we tried to use the advantage of the well tested MC codes that may provide very accurate time dependent transport data [33, 34]. At the same time the development of the plasma through weakly ionized phases was studied in order to test the applicability of the transport coefficients and fluid models in representing such a breakdown. Thus, we have used a fully tested and benchmarked code for electrons (that also has the facility to include heavy particles, ions and neutrals) with a full range of sampling and treatment of the cross-section data. The logic is that during the breakdown the swarm physics exactly describes the charged particle ensemble and only a much higher density particle needs to include the space-charge effects. As it has been mentioned earlier, that electrons alone may maintain discharge through ionization and described the main features of the breakdown curves, we start with electrons as the only agents precipitating the breakdown. Only after we start comparing with the experiment do we add other effects (ion induced secondaries, metastable induced secondaries, fast neutrals and their effect, photon induced secondaries and finally electron induced secondary-multipactors). But those are not in the scope of this paper. This paper represents one of the first steps in obtaining a more complete description of the low-pressure RF argon discharge, which provides us with an insight into the basic physics of the breakdown (preliminary results are presented in [35]).

## 2. Methods

For this study an MC code, which was developed and tested (tested both for DC and RF benchmarks [33, 34, 36]) is used. Since MC technique have been explained elsewhere [37, 38], only a brief description of the code will be given here. We developed an MC code that traced electrons only. Heavy particles and the effect of photons were also added, but those results are not included in this paper. The code was tested for electron (and ion) transport and was shown to give accurate electron energy distribution functions (EEDFs) and transport coefficients in model gases and in argon [33, 37].

The calculations were carried out for argon discharges generated between infinite plane-parallel electrodes at a frequency of 13.56 MHz (unless specified otherwise). Argon was chosen for many reasons: first of all, it is an atomic gas with a simple energy transition spectrum and it is easy to operate with.

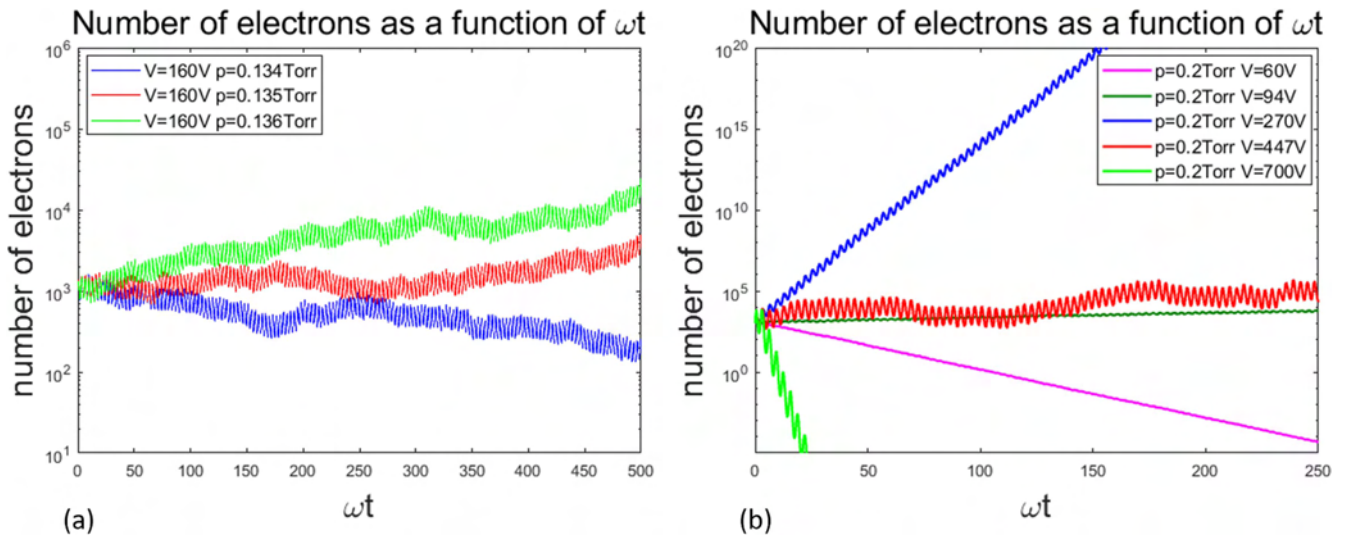
At the same time, its cross-section data and other necessary input data are available and well tested, thus are reliable. One can refer to argon as a ‘benchmark’ gas in discharge studies. We included a set of cross-sections that were shown to provide excellent agreement with the measured transport data and which included: elastic scattering of electrons, excitation to the effective triplet state levels, excitation to the effective singlet state levels and ionization. The two excitation cross-sections had been well tested for argon swarms [39, 40]. This paper includes a complete set of the electron–argon interactions included in the modeling representing all the processes that we needed to produce the basic breakdown curves and explain their features.

At the beginning, the electrons were released from the middle of the gap between the two electrodes with no initial energy. Any further electron motion and different interactions depended on the applied alternating current (AC) field, random number generator and the solutions of the kinetic and balance equations. At this point, the surface effects of the electrodes were not included. When an electron reached the boundary, it was assumed to be removed and had no influence on the discharge kinetics. We had a facility to add reflection or other surface processes easily based on the available experimental data.

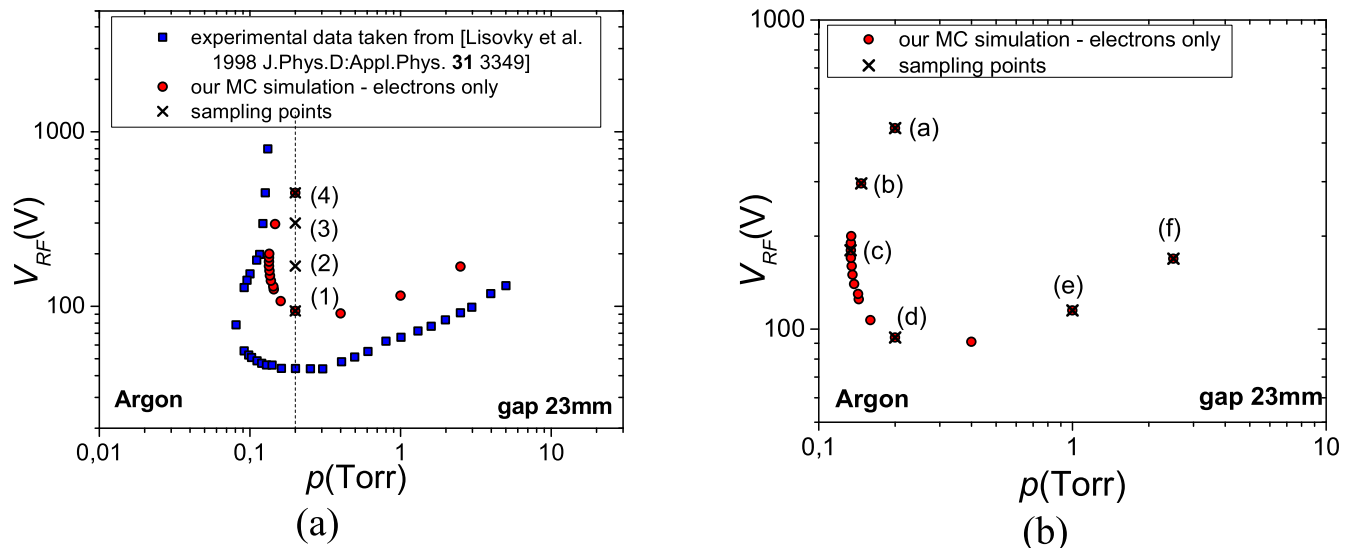
In our simulations the breakdown voltage curves were recorded in accordance with the procedure described in [6, 41, 42]. On the right-hand side of the breakdown voltage curve, the breakdown voltage was determined by fixing a pressure and increasing the applied voltage. For the left-hand side of the curve, the voltage was fixed while the pressure was varied. In the MC simulations these two procedures were equally simple while the case of experiments with variations of pressure may be more complex.

Figure 1 shows the changes in the number of electrons over time for: (a) the fixed maximum voltage of  $V = 160$  V and at three different pressures ( $p_1 = 0.134$  Torr,  $p_2 = 0.135$  Torr and  $p_3 = 0.136$  Torr) and (b) the fixed pressure of 0.2 Torr and five different voltages (60, 94, 270, 447 and 700 V). As can be seen from figure 1(a), at the pressure  $p_1 = 0.134$  Torr there was no electron amplification in the required quantity that could compensate the electron losses at the electrode, so the total number of electrons decreased over time and the slope is negative. At the pressure  $p_2 = 0.135$  Torr, however, there was a notable increase in the total number of electrons over time, which can be interpreted as an increased number of ionizations due to the higher density (as compared to  $p_1$ ) of the background atoms and consequently a larger number of collisions. The breakdown occurred somewhere between  $p_1 = 0.134$  Torr and  $p_2 = 0.135$  Torr. The pressure resolution was 0.001 Torr. A more accurate pressure can be obtained by interpolation between the nearest two values of pressure, in this case  $p_1$  and  $p_2$ .

Figure 1(b) is presented to depict how the number of electrons changed over time with large variations in the voltage. The pressure (0.2 Torr) and voltages that were chosen correspond to the vertical line in figure 2(a). When the pressure was fixed (see figure 1(b)), there were two values where the mean number of electrons was barely maintained, which means that those are the boundaries of the breakdown (94 and 447 V). In-between the two breakdown values one has excessive growth in the density (in a real circuit this would push the operating point to either of the



**Figure 1.** The time dependence of the simulated number of electrons for: (a) the fixed voltage of 160 V and various pressures and (b) constant pressure of 0.2 Torr and various voltages.



**Figure 2.** The breakdown voltage curves for argon RF discharges at 13.56 MHz and the gap size of 23 mm. The Monte Carlo Simulation (MCS) includes electrons only. (a) Comparison of the breakdown voltage curve obtained by MCS (red circles) and experimental available data [6] (blue squares). Vertical line for  $p = 0.2$  Torr and different voltages indicates sampling points presented in figures 3 and 4. (b) MCS obtained curve indicating sampling points of spatial profiles presented in figure 5. Sampling points are marked by numbers and letters.

two breakdown voltages). Results within that range are on a positive slope, whereas results outside that range showed decay advancing towards termination (e.g. data for 60 and 700 V). Outside the breakdown region (above 447 V and below 94 V) the density of the electrons rapidly diminished (60 and 700 V).

In both figures 1(a) and (b), there are periodic oscillations of the electron number. In figure 1(a), with a fixed voltage, these oscillations are the same in the sense of period and amplitude. In figure 1(b) the period of the oscillations is the same while the amplitudes are different depending on the applied voltage. With changes in voltage the effective rates that define the speed of relaxation may change and affect the undulations of the properties such as the number of electrons. This is because the high voltage electrons reached the ionization energies more easily and in larger numbers so the

number of electrons changed more rapidly within one period of time. The losses at the electrodes may have balanced the increased production, they increased because more of the electrons were being pushed to the electrodes by a strong AC field. As the voltage decreased less energy was transferred from the field to the electrons and the number of ionizations reduced (the increasing number of electrons within one period was smaller). For a lower voltage both the loss and production were smaller as the electrons did not reach the electrodes (oscillations were barely noticeable for a voltage of 60 V). One can conclude that the period of oscillation of the electron number was determined by the frequency of the external AC field while the amplitude of the oscillation of the electron number depended on the amplitude of the applied AC field (energy transfer from the field to the electrons).



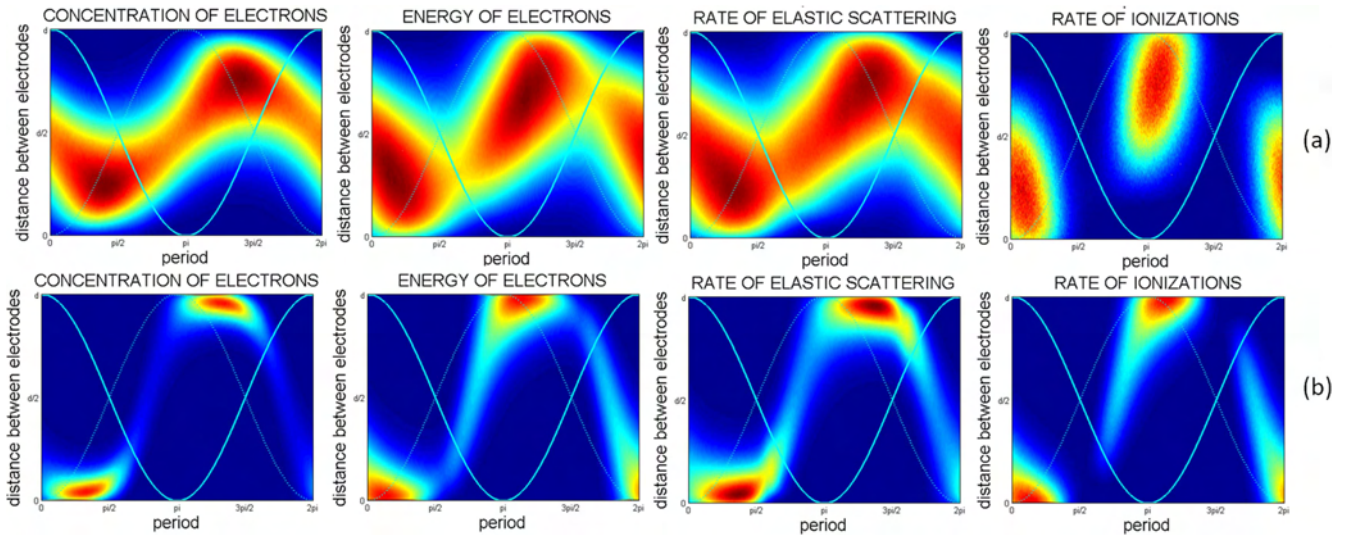


**Figure 3.** Spatial distributions of: electron concentration, mean energy and rates of elastic scattering and ionization for the pressure of 0.2 Torr and two breakdown points: (a)  $V = 94$  V and (b)  $V = 447$  V (points are marked in figure 2(a), (a) corresponds to (1) and (b) corresponds to (4)). The light blue line represents the AC field, while the dashed light blue line corresponds to the field dependence inverted to represent the force affecting the electrons. Interelectrode gap is 23 mm and frequency is 13.56 MHz. Number of electrons in the simulation was selected to have a similar statistical quality of the results with the smallest rate (i.e. ionization). Thus the color scales are not representing any quantitative data that may be compared for different conditions only the indication of the profile of the ensemble.

### 3. Results and discussion

#### 3.1. Spatial profiles of electron density and ionization rate as a representation of the potential for achieving breakdown

The dependence of the RF breakdown voltage on the pressure is presented in figure 2. The results of our MC simulations (red circles) are compared with the experimental data taken from [6] (blue squares) in figure 2(a). As can be seen on the left-hand side of the simulated curve, for a fixed pressure there are two values for the breakdown voltage. The discharge may start between these two values, while above and below it quenches rapidly (as indicated in figure 1). This observation is in agreement with the previously published experimental data [6], at least qualitatively. The crosses correspond to the sampling points on a vertical line  $p = 0.2$  Torr. Two points are on the breakdown curve (94 and 447 V) and two points are in-between (170 and 300 V). In principle, in a simulation operation above the breakdown conditions the growth of electrons is allowed. In experiments, however, the operating point will move towards either of the two breakdown curves. The development of the spatial profiles (see figures 3, 4) along the vertical line provides an insight into the pertinent physical processes. On the other hand in figure 2(b) the sampling points marked by letters are on the breakdown curve. The spatial profiles associated with these points and shown in figure 5 indicate a difference in the physical processes with a variation of  $p$  ( $pd$ ).

The spatio-temporal development of the profiles of: electron density, mean energy, elastic collisions and ionization are shown in figure 3. The calculations were performed for a frequency of 13.56 MHz, a gap size of 23 mm, a pressure of 0.2 Torr and two breakdown points: (a) 94 V and (b) 447 V (as indicated in figure 2(a)). As the voltage increased,

the low voltage breakdown point was reached, but most of the electrons did not reach the electrodes. The profile of the electron cloud is broad, not really sinusoidal, but generally follows a sinusoidal shape. There were maxima in density, elastic scattering and in mean energy when the cloud was closest to the electrodes. The peaks were delayed by a large phase delay to the voltage waveform. In fact, the peak started moving towards the center of the gap only at the phase when the field changed direction and not for the maximum of the field. This can be easily understood because for ionization only two regions close to the maximum of the applied voltage (field) were abundant in the collisions while still following a similar temporal and spatial dependence.

At the higher breakdown point the spatial profiles were much narrower and there was a strong overlap with the electrode. While the electron density peaks were slightly away from the electrode the highest energy/the most likely to ionize the electrons' peak was right at the edge of the electrode.

It is important to note that our MC code obtained a double-valued voltage on the breakdown curve by treating electrons only. For some gases [43] even 'S' shaped curves with three points may be observed. The explanation of this phenomenon is as follows: for the lower voltage one needs to compensate losses at electrodes by increasing ionization, and any increase in voltage leads to a higher ionization. If we move to higher voltages, ionization is increased but so are the losses at the instantaneous anode. This is a consequence of pushing electrons closer to the electrodes with an increasing AC field. The losses may be represented by imagining the remaining electron ensemble spatial distributions that extend over the electrode edge into its bulk and this distribution increases with the applied voltage. At a certain point this part of the ensemble that passes past the electrode will increase so

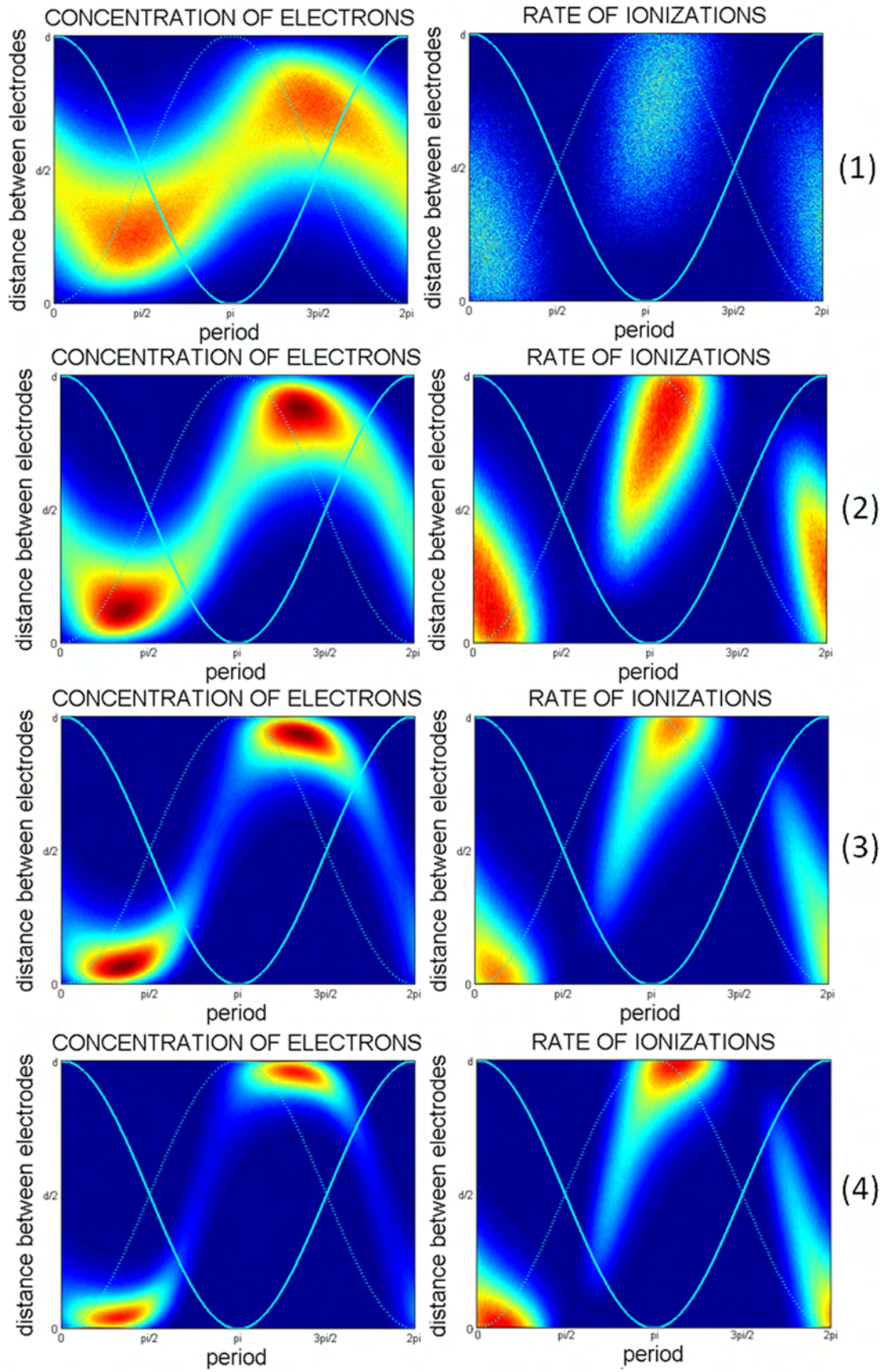


**Figure 4.** Spatial profiles of the electron concentration and ionization rates for the pressure of 0.2 Torr and voltages of (1) 94 V, (2) 170 V, (3) 300 V and (4) 447 V. Points are marked in figure 2(a). Interelectrode gap is 23 mm and frequency is 13.56 MHz. All figures are obtained with the same initial number of electrons so the relative magnitudes of the same coefficient are indicated by the colors scale.



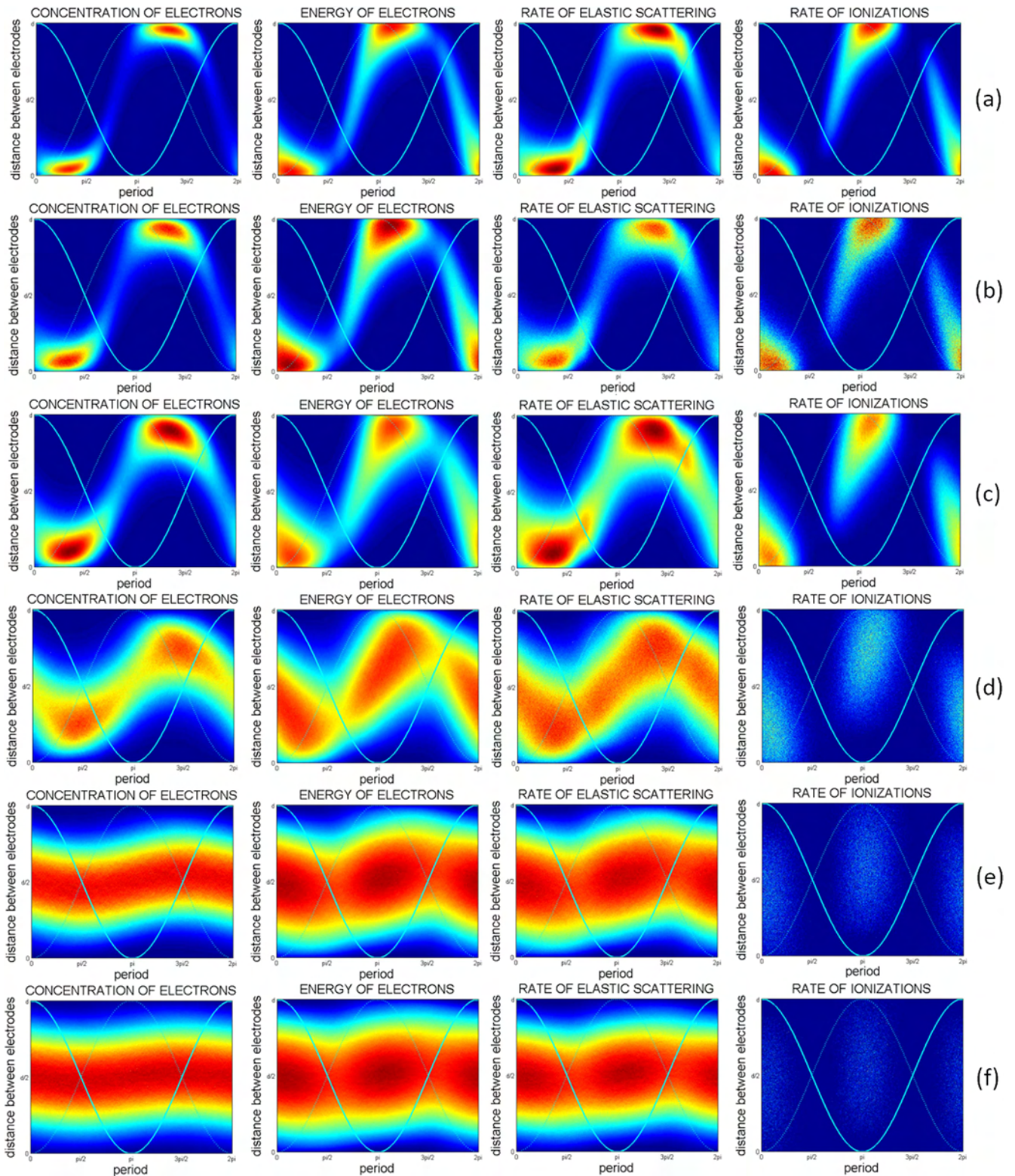


**Figure 5.** Spatial distributions of concentration of electrons, electron energy and rates of elastic scattering and ionization: (a) 447 V 0.2 Torr, (b) 296 V 0.147 Torr, (c) 180 V 0.1335 Torr, (d) 94 V 0.2 Torr, (e) 115 V 1 Torr and (f) 169 V 2.5 Torr. Points are marked in figure 2(b). Interelectrode gap is 23 mm and frequency is 13.56 MHz. All figures are obtained with the same initial number of electrons so the relative magnitudes of the same coefficient are indicated by the colors scale.

much that ionization in the gas (in front of the electrode) cannot compensate the losses and the discharge will switch itself off. In figure 3 this is represented by the spatial profile of the electron concentration and mean energy, which indicates the potential for ionization.

The profile of the increasing ionization rate of the group closest to the anode is shown in figure 4 along the fixed  $p = 0.2$  Torr for four points marked in figure 2(a). With an increasing voltage more and more of the ionization-capable electrons would be lost at the surface. At the lower applied voltage (94 V) though, the swarm oscillates between two electrodes without reaching them and the majority of ionization-capable electrons have no difficulty ionizing.

### 3.2. Variation of the spatial profiles with $pd$ along the breakdown curve

Having presented results that indicate the changes in the spatial profiles of all the discharge parameters along a vertical line ( $p = \text{const.}$ ), figure 5 exhibits the spatial profiles along the Paschen-like breakdown potential curve. Stating that the curve is Paschen-like does not imply in any way that the Paschen mechanism is relevant here in its entirety. The points on the  $V$ - $p$  plane that have been selected to show the spatial profiles of the various properties of the electron swarm ensemble are marked on the breakdown curve shown in figure 2(b).

Plots (a) and (d) in figure 5 are repeated from the previous figures. The first represents the higher point on the breakdown curve, the second the lower point on the breakdown curve for  $p = 0.2$  Torr. Plots (b) and (c) on the left are the rapidly rising branch of the breakdown curve. It is clear that under those conditions the magnitude of the field manages to bring all of the electrons close (within one mean free path) to the electrodes during one half period. Those points have all the characteristics of the operation well above the lower breakdown points and close to the upper branch. The principal issue here is whether the losses at the electrode may be balanced by the production of electrons in its proximity, the production that is made more and more difficult by the reduced number of collisions in a similar fashion to the left-hand branch of the DC–Paschen curve. As a result of this balancing between losses and gains the peak of the mean energy and the number of ionizing collisions clearly occur right before reaching the electrode and after the maximum in the field. At the same time the peak in density occurs a little later as a consequence of the ensuing burst of ionization. The number of elastic collisions follows the profile of the density better, while, as stated, the number of ionizations follows the profile of the mean energy.

The spatial profiles in figure 5(c) also become somewhat closer to the lower branch profiles of figure 5(d), where the majority of ionizations occur in the bulk of the discharge, and the whole ensemble merely brushes against the electrodes. The balance between losses and gains, as displayed in figure 5(d), seems optimal as there are minimal losses while the number of collisions provides ample opportunities to compensate for them. As the pressure increases (for a fixed  $d$ ) the number of collisions increases further and thus it is more difficult to achieve higher energies so the breakdown voltage

increases but slowly. More importantly, the density profile of the electrons loses sharp peaks and becomes more sinusoidal in the center of the gap with vanishing density due to losses close to the walls. The mean energy is still modulated following the field dependence albeit with a delay. A similar modulation is observed in the elastic collisions mainly due to the energy dependence of the cross-section. It is important to note that collisions occur on both halves of the gap, as the density profile, while modulated, does not show complete migration of electrons towards the instantaneous anode and away from the cathode. As a result of the ensemble overlapping from one to the other electrode, the highest energy electrons responsible for ionization will be generated throughout the gap and under those conditions, ionization, however weak, spreads on both halves almost equally (figures 5(e), (f)). The difference between ionization profiles in figures 3(a) and 5(d) is that in the former one we have enhanced the number of events by the accumulation of events through releasing more electrons for the same set of conditions to make the simulation conditions the same for all figures in the cluster of figure 5.

Furthermore, we employed an MC code to provide a more detailed picture of the physical processes by observing the energy distribution function that has to be related to the processes occurring in the region of active ionization (i.e. near the electrode). As can be seen in figure 6, the overlap of the distribution function with the relevant cross-sections (both excitation of metastable and ionization) is of essential importance for the maintenance of the discharge. For high voltages (figure 6(a)) there is a significant overlap of the EEDF and cross-section for ionization. A great deal of high energy electrons that can ionize were being absorbed by the electrodes and lost. Under these conditions ( $V = 447$  V and  $p = 0.2$  Torr) there was a fine balance between the losses and production of electrons. A significant increase in the EEDF right in front of the electrode at higher voltages (i.e. lower pressures) is also observed. The increase means energy (and the mean free path) for lower pressures was the result of a reduced number of collisions as the electrons crossed the gap so ionization was to become more efficient. As for high pressures (figure 6(b)) only the tail of the EEDF at the electrodes is overlapping with the cross-section for ionization. There is no significant loss of ionization-capable electrons and discharge is easier to maintain which can be observed as smaller increase of voltage in right branch of breakdown voltage curve as compared to the left branch.

### 3.3. Scaling of RF breakdown profiles: breakdown voltage depending on the gap length and frequency

RF breakdown has a different nature compared to DC breakdown. Therefore,  $pd$  scaling that is applicable in DC breakdown voltage curves needs to be extended to include frequency dependence. Figure 7 shows the breakdown voltage curves for various: (a) gaps and (b) frequencies. The curves have a similar shape with a large variation of parameters. For a fixed frequency one cannot maintain the scaling, as in addition to  $pd$  scaling there is also  $fd$  (interelectrode distance times frequency) scaling

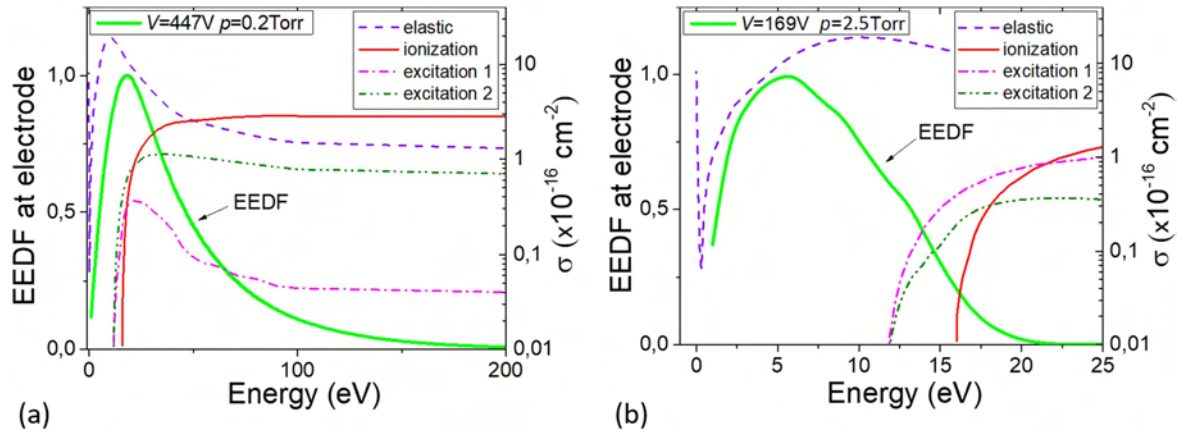


**Figure 6.** Electron energy distribution function at the electrodes separated by 23 mm at the frequency of 13.56 MHz for: (a)  $V = 447$  V,  $p = 0.2$  Torr and (b)  $V = 169$  V,  $p = 2.5$  Torr. Right-hand side y-axes shows set of cross-sections for argon.

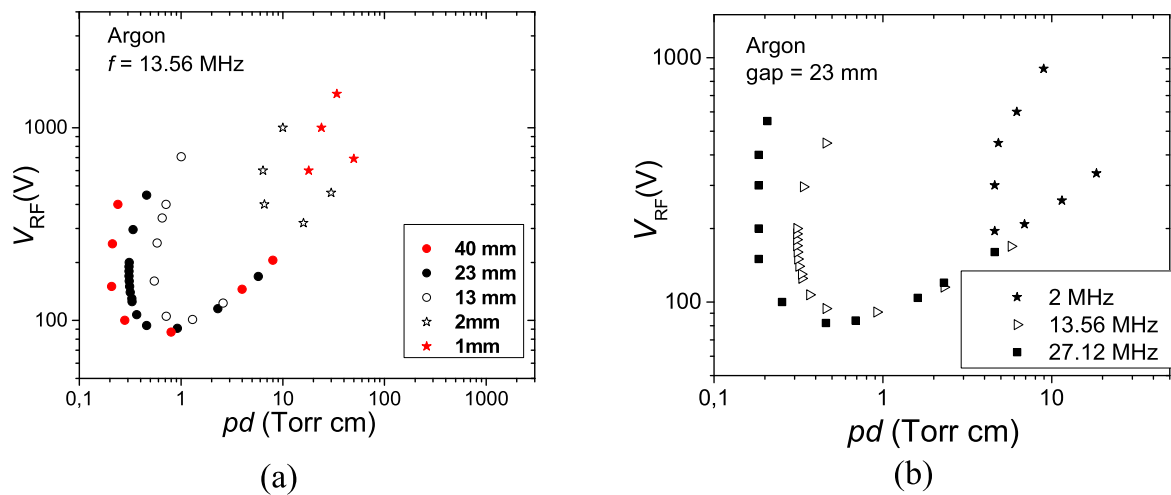


**Figure 7.** (a) Simulated breakdown voltage curves for: (a) a fixed frequency of 13.56 MHz and various gaps sizes and (b) a fixed gap of 23 mm and various frequencies.

that needs to be satisfied [44–46]. The same is valid for a fixed gap. Scaling with proper variation of both the frequency and the gap is shown in figure 8.

Both the frequency and gap are varied while keeping the  $fd$  constant and observing the  $pd$  dependence. We can see a very good overlap that is excellent at higher values of  $pd$  while at lower values of  $pd$  and higher breakdown voltages there is more of a difference, presumably due to the non-linearities brought about by the overlap of the electron cloud with the electrode. While presenting breakdown curve scaling is important and indeed points out the validity of the scaling. The critical test of the scaling would be the observation of the spatial profiles depicted in figure 9 for  $pd$  around 0.34 Torr cm and a number of frequencies with the corresponding gaps. It is clear that for a narrow range of  $fd$  and  $pd$  all the spatial profiles coincide. That is the physical foundation of the scaling laws, which basically scales the number of collisions per length and time.

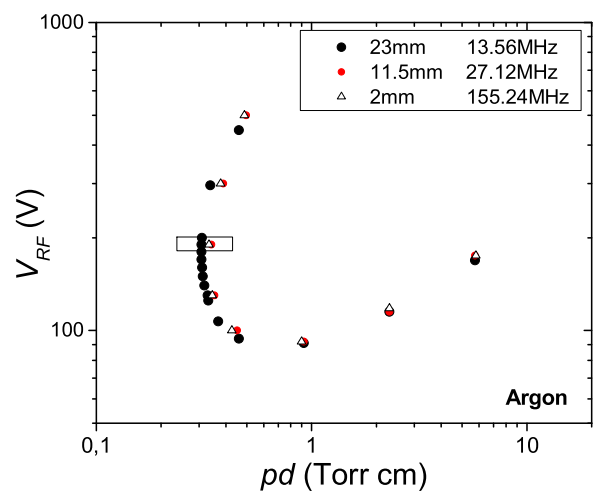


**Figure 8.** Scaling according to  $pd$  and  $fd$  scaling laws of RF voltage breakdown curves. Box indicates region with points for which the spatial profiles are plotted in figure 9.



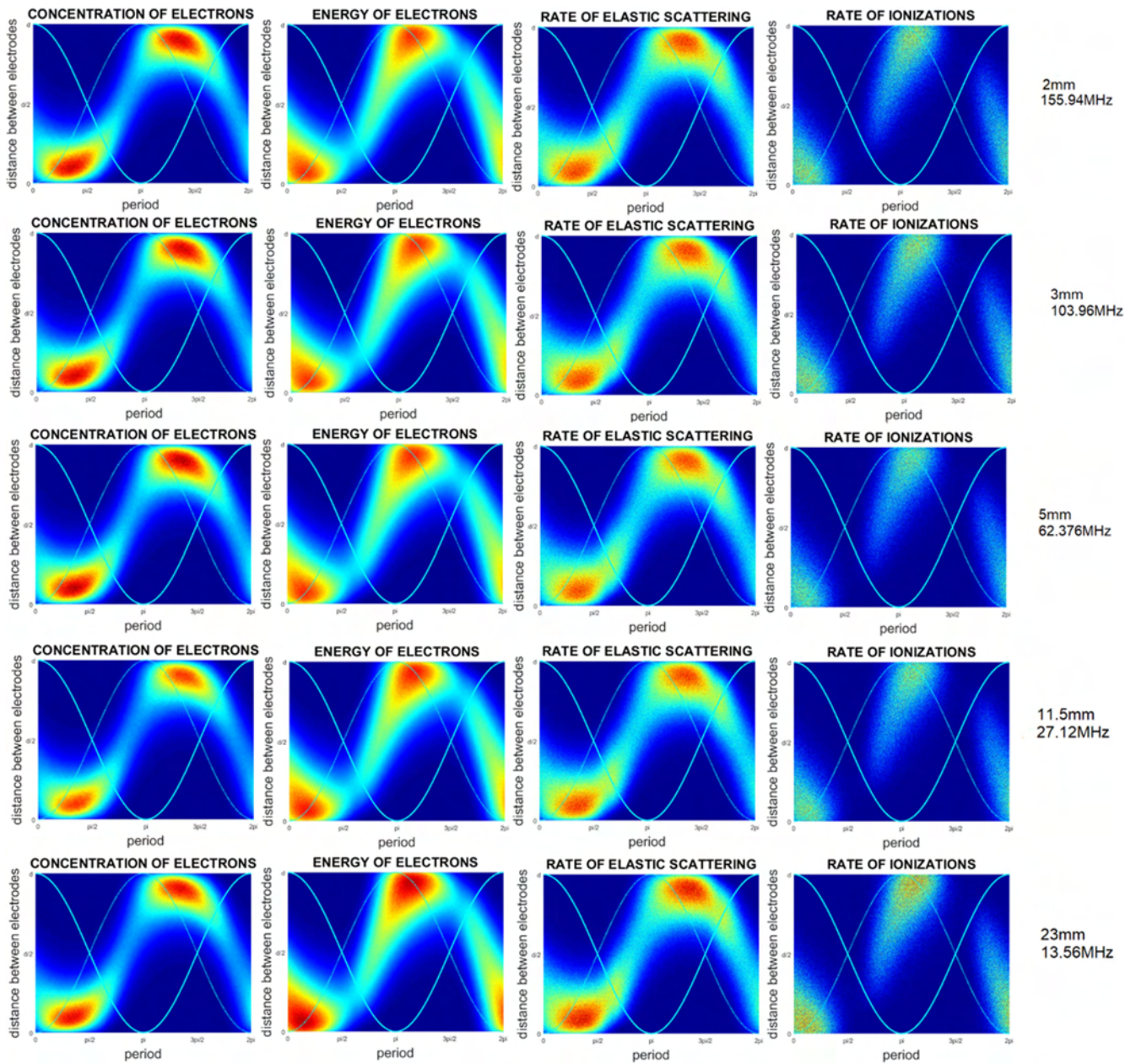


**Figure 9.** Spatial distributions for a number of points that have the same product of frequency and distance between electrodes ( $fd = \text{constant}$ ) and also for a fixed  $pd = 0.34$  Torr cm. All figures are obtained with the same initial number of electrons so the relative magnitudes of the same coefficient are indicated by the colors scale.

#### 4. Conclusion

In this paper the physical background of low-pressure RF argon discharges is studied. It is found that the simplified phenomenology of transfers from one electrode to the other is often not met especially at higher pressures where electrons may produce sufficient ionization while crossing shorter distances. At lower pressures, conditions to reach the electrodes are acquired at the cost of an increased breakdown voltage. Under those conditions the balance between new electrons being produced and the increase in mean energy determines the breakdown. Thus it is possible to have two breakdown points (and the region of the double-valued breakdown curve coincides with the region where electrons reach electrodes in

one half period) for one  $pd$  value. The higher point is where the balance is encountered due to the losses of high energy electrons hitting the anode and being absorbed by it.

Another issue of scaling is illustrated well with the obtained results. The breakdown follows the standard  $pd$  scaling very well but it has to adjust itself to the  $fd$  scaling as well. The  $fd$  scaling has been discussed within the terms of breakdown physics by Lisovsky *et al* [45] and it addressed [44]. However both scalings have been established in the earlier electron transport (swarm) studies [14–16, 46] basically as a condition to maintain the number of collisions per certain distance or in certain time. The spatial profiles of the electron properties shown in figure 9 give an indication of how scaling involves identical spatial distributions and other properties thus supporting the predicted scaling.

Results, presented and discussed here, confirm that the modeling of RF breakdown by using a detailed MC code provides an excellent and relatively easy entrance into the pertinent physical processes. In the later stages plasma properties become important and one has to follow the space-charge development, which makes the situation much more complex. Yet the onset of the breakdown is purely a swarm phenomenon and the beginning of the development of the plasma may be clearly envisioned and explained even quantitatively by a swarm model.

## Acknowledgments

This paper was completely finalized at the Institute of Physics University of Belgrade under basic funding from projects OI 171037 and III 41011 of the Serbian Ministry of Education, Science and Technological development of Serbia. ZLjP is grateful to the Serbian Academy of Sciences and Arts and its project F155 for its partial support. Authors are grateful to Dr Srđan Marjanović for help in several stages of the development of the code.

## ORCID iDs

Marija Puač  <https://orcid.org/0000-0002-6011-0434>

Dragana Marić  <https://orcid.org/0000-0002-1728-5458>

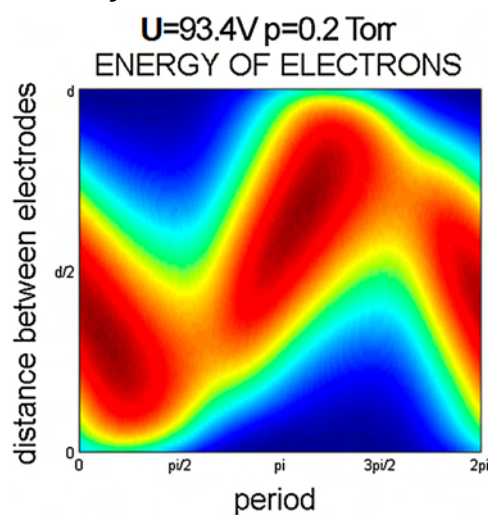
## References

- [1] Adamovich I et al 2017 *J. Phys. D: Appl. Phys.* **50** 323001
- [2] Makabe T and Petrović Z Lj 2006 *Plasma Electronics: Applications in Microelectronic Device Fabrication* (London: Taylor and Francis)
- [3] Puač N, Škoro N, Spasić K, Živković S, Milutinović M, Malović G and Petrović Z Lj 2017 *Plasma Process Polym.* **15** e1700082
- [4] Lazović S et al 2010 *New J. Phys.* **12** 083037
- [5] Puač N, Gherardi M and Shiratani M 2018 *Plasma Process Polym.* **15** e1700174
- [6] Lisovskiy V A and Yegorenkov V D 1998 *J. Phys. D: Appl. Phys.* **31** 3349
- [7] Gill E B W and von Engel A 1949 *Proc. R. Soc. A* **197** 107
- [8] von Engel A 1965 *Ionized Gases* (Oxford: Clarendon Press)
- [9] Phelps A V and Petrović Z Lj 1999 *Plasma Sources Sci. Technol.* **8** R21
- [10] Allis W P 1956 Motions of ions and electrons *Electron-Emission Gas Discharges I Encyclopedia of Physics* ed S Flugge vol 21 (Berlin: Springer) pp 383–444
- [11] Allis W P and Brown C 1952 *Phys. Rev.* **87** 419
- [12] MacDonald A D 1966 *Microwave Breakdown in Gases* (New York: Wiley)
- [13] Morse P M, Allis W P and Lamar E S 1935 *Phys. Rev.* **48** 412
- [14] Margenau H and Hartman L M 1948 *Phys. Rev.* **73** 309
- [15] Holstein T 1946 *Phys. Rev.* **70** 367
- [16] Ginzburg V L and Gurevich A V 1960 *Sov. Phys. Usp.* **70** 393
- [17] Wilhelm J and Winkler R 1969 *Ann. Der Physik* **23** 28
- [18] Goto N and Makabe T 1990 *J. Phys. D* **23** 686
- [19] Bzenic S, Petrović Z Lj, Raspopovic Z and Makabe T 1999 *Jpn. J. Appl. Phys.* **38** 6077
- [20] Dujko S, White R D and Petrović Z Lj 2011 *IEEE Trans. Plasma Sciences* **39** 2560
- [21] White R D, Ness K F and Robson R E 2002 *Appl. Surf. Sci.* **192** 26
- [22] Kihara T 1952 *Rev. Mod. Phys.* **24** 45
- [23] Raizer Y P 1991 *Gas Discharge Physics* (Berlin: Springer)
- [24] Makabe T, Nakano N and Yamaguchi Y 1992 *Phys. Rev. A* **45** 2520
- [25] Klas M, Moravsky L, Matejček Š, Radjenović B and Radmilović-Radjenović M 2015 *J. Phys. D: Appl. Phys.* **48** 405204
- [26] Klas M, Matejček Š, Moravsky L, Radjenović B and Radmilović-Radjenović M 2017 *EPL* **120** 25002
- [27] Lee I, Graves D B and Lieberman 2008 *Plasma Sources Sci. Technol.* **17** 015018
- [28] Kushner M J 2009 *J. Phys. D: Appl. Phys.* **42** 194013
- [29] Donko Z 2011 *Plasma Sources Sci. Technol.* **20** 024001
- [30] Verboncoeur J P 2005 *Plasma Phys. Control. Fusion* **47** A231
- [31] Birdsall C K and Langdon A B 1985 *Plasma Physics via Computer Simulation* (New York: McGraw-Hill)
- [32] Birdsall C K 1991 *IEEE Trans. Plasma Sci.* **19** 65
- [33] Raspopovic Z M, Sakadzic S, Bzenic S A and Petrović Z Lj 1999 *IEEE Trans. Plasma Sci.* **27** 1241
- [34] Petrović Z Lj, Raspopovic Z M, Dujko S and Makabe T 2002 *Appl. Surf. Sci.* **192** 1–25
- [35] Savić M, Radmilovic-Radjenovic M, Šuvakov M, Marjanović S, Marić D and Petrović Z Lj 2011 *IEEE Trans. Plasma Sci.* **39** 2556
- [36] Šuvakov M, Ristivojević Z, Lj P Z, Dujko S, Raspopović Z M, Dyatko N A and Napartovich A P 2005 *IEEE Trans. Plasma Sci.* **33** 532
- [37] Ristivojevic Z and Petrović Z Lj 2012 *Plasma Sources Sci. Technol.* **21** 035001
- [38] Petrović Z Lj, Bzenic S, Jovanovic J and Đurovic S 1995 *J. Phys. D: Appl. Phys.* **28** 2287
- [39] Petrović Z Lj, Šuvakov M, Nikitović Ž, Dujko S, Šašić O, Jovanović J, Malović G and Stojanović V 2007 *Plasma Sources Sci. Technol.* **16** S1–12
- [40] Phelps A V [https://fr.lxcat.net/data/set\\_specA.php](https://fr.lxcat.net/data/set_specA.php)
- [41] Korolov I, Derzsi A and Donko Z 2014 *J. Phys. D: Appl. Phys.* **47** 475202
- [42] Korolov I and Donko Z 2015 *Phys. of Plasmas* **22** 093501
- [43] Lisovskiy V, Booth J-P, Landry K, Douai D, Cassagne V and Yegorenkov V 2006 *J. Phys. D: Appl. Phys.* **39** 660
- [44] Francis G 1956 Gas discharges II *Encyclopedia of Physics* ed By ed S Flugge **XXII** (Berlin: Springer)
- [45] Lisovskiy V, Booth J-P, Landry K, Douai D, Cassagne V and Yegorenkov V 2008 *Europhys. Lett.* **82** 15001
- [46] Margenau H 1948 *Phys. Rev.* **73** 326

# Using Swarm Models as an Exact Representation of Ionized Gases

Zoran Lj. Petrović,\* Dragana Marić, Marija Savić, Srdan Marjanović, Saša Dujko, Gordana Malović

In this review, several examples of ionized gases are presented where swarm models may be employed to provide full description. Those situations include low space charge pre-breakdown, Townsend region breakdown where space charge effects may be calculated from the swarm model and used as the first order perturbation to describe oscillations and transient signal and afterglows. In addition, implications are considered for microdischarges, discharges in and close to liquids, gas-filled particle traps, thermalization of particles in living tissue, and many more. In all those situations, swarm models provide full description of the discharge, while for most other collision dominated non-equilibrium plasmas swarm physics (transport-related phenomena) provides a part of the foundation of modeling.



## 1. Introduction

Swarm data and the basic transport equations have been the foundation of the modeling of low temperature (i.e., non-equilibrium) plasmas.<sup>[1–4]</sup> In doing so, it is often assumed that the transport data obtained under such conditions fit well the fluid or other equations used to model plasmas. Without going into discussion of whether that is the case or not, we need to stress that the use of swarm data or of the swarm derived cross-section sets<sup>[5–7]</sup> is a prerequisite in achieving proper energy, momentum, and number balances in plasma models and in having properly calculated non-equilibrium distribution functions. Even

though in RF fields and in the presence of strong variations of the distribution function, the use of swarm parameters may become complex due to non-locality<sup>[8–10]</sup> these data have been used successfully and with little evidence of inadequacy. That is presumably due to a robust nature of plasma models (physics) dictated primarily by the space charge adjustment that provides a field distribution necessary to maintain the existence of the plasma itself.

In this paper, we shall, however, focus on the ionized gases where the swarm models are an exact representation of the system, as exact as the available data allow it and as exact as small perturbations of the external field do not constitute a major source of the relevant particles. Usually it is assumed that by cornering yourself into the low current limit and favoring situations where ionized gas does not use its ability to self adjust the field profile, will lead to very few, if any (with exception of swarm experiments of course), examples where such physical models is adequate. That, luckily, is not true and we have a number of examples where swarm models provide sufficient and even complete description. This paper attempts to provide a review of such examples and also to

Prof. Z. Lj. Petrović, Dr. D. Marić, M. Savić, S. Marjanović,  
Dr. S. Dujko, Dr. G. Malović  
Institute of Physics Belgrade, University of Belgrade, POB 68 11080  
Zemun, Belgrade, Serbia  
E-mail: zoran@ipb.ac.rs  
Prof. Z. Lj. Petrović  
Serbian Academy of Sciences and Arts, Knez Mihajlova 35, 11000  
Belgrade, Serbia



provide an insight on how swarm models may be used as plasma models. This work is naturally primarily focused on the results of our group.

### 1.1. What Are Swarms?

Swarms have been defined as ensembles of charged (although the paradigm may be extended beyond charge) ensembles of particles freely moving through the background gas, gaining energy from the external electric field, being under the influence of the external magnetic field, and dissipating energy and momentum in collisions with the gas molecules. It is assumed that all collisions are with the pristine, unperturbed gas and also that space charge effects and Coulomb coupling are both negligible. In other words, it is the zero ionization limit of plasmas where collisions reign supreme and where the field is “known,” i.e., defined by the external voltage. The behavior of charged particles is defined by collisions and also by the energy gain and the field configuration. Thus, this is the end where atomic and molecular physics, integrated into the transport theory, and overall kinetic calculations dominate.

An additional condition is also often introduced that boundaries (such as metallic walls, sometimes grounded, sometimes at some potential) are not felt throughout most of the volume of the discharge. That, however, is not absolutely necessary, it is merely there to provide the basis for the so called hydrodynamic expansion that allows us to separate the distribution function into a velocity space distribution ( $f$ ) multiplied by the real space particle density profile ( $n(\mathbf{r}, t)$ ) by using spatial gradients of the density:

$$f(\mathbf{r}, v, t) = \sum_{k=0}^{\infty} f^{(k)}(v) \otimes (-\nabla)^k n(\mathbf{r}, t) \quad (1)$$

and spherical harmonics:

$$f(v) = \sum_{l=0}^{\infty} f_{lm}(v) P_l^m(\cos \theta) e^{-im\varphi}, \quad (2)$$

where  $P_l^m(\cos \theta)$  are Legendre polynomials and  $\theta$  and  $\varphi$  are polar angles.

Very important aspect of this expansion, that allows us a much easier numerical solution to the Boltzmann equation, is the fact that if it is satisfied we effectively assume the distribution function to be uniform throughout the entire volume of the discharge. The standard swarm experiments, and swarm physics have always been strongly associated with well-defined experiments, that are able to achieve such conditions throughout most of the volume of the discharge. To do so, a combination of the use of high pressure and control of the current density is required. In any case, substituting Equation (1) and (2) into Boltzmann

equation:

$$\frac{\partial f}{\partial t} + \mathbf{c} \cdot \frac{\partial f}{\partial \mathbf{r}} + \frac{q}{m} (\mathbf{E} + \mathbf{c} \times \mathbf{B}) \cdot \frac{\partial f}{\partial \mathbf{c}} = -J(f, F_0) \quad (3)$$

where  $J(f, F_0)$  is the collision operator, provides the means to define and calculate the transport (swarm) coefficients.

On the other hand, most low temperature plasmas operate under conditions where hydrodynamic approximation may not be appropriate. Those include low pressure discharges, where mean free path may be comparable to the size of the vessel, sheaths, and electrode regions and also high gradient areas, like those found in the front of the streamers, thermalization from the initial distribution, or the very high  $E/N$  conditions, when charged particles may achieve a runaway. Thus we shall apply swarm models in both sets of circumstances allowing for non-hydrodynamic conditions when required.

### 1.2. Swarm Models

A swarm model would be a model based on a Boltzmann equation (BE),<sup>[11–14]</sup> Monte Carlo simulation (MCS),<sup>[15–18]</sup> or some of the simplified equations such as the Momentum transfer theory (MTT).<sup>[19–21]</sup> More than actual modeling, one may use transport data to directly calculate properties in hydrodynamic region. If, however, it is not hydrodynamic then the ionized gas should perhaps be modeled by MCS.

An important feature of swarm models is that those are often approximate, like MTT in general, or BE if only two terms are maintained (in expansion given by Equation (2)) or some model collisional operator is employed. Verifying exact nature of the model is thus an important issue and for that purpose, swarm benchmarks are often employed.<sup>[15,18,22–25]</sup> We will not spend more time on this issue as it has been well covered by a number of papers.<sup>[26]</sup>

We will, however, define conditions where swarm models are expected to be appropriate and then proceed to illustrate some, such as:

- Low space charge density ionized gas in general like the charges in the atmospheric gas.
- Pre-breakdown avalanches requiring external field but not quite making it to the self-sustained regime.
- Breakdown where the initial phase and the transition to the self-sustained regime are in swarm regime while the final stage may be a fully developed plasma, and thus the conditions for the breakdown are defined by the swarm regime.
- Gaseous dielectrics are also defined by the operation in the swarm regime as their use is to prevent development of the plasma in the first place.
- Gas-filled traps such as Penning Malmberg Surko trap for positrons.

- Detectors of elementary particles starting from Willson's chamber and Geiger counter, through drift and avalanche chambers and finally including the most frequently used resistive plate chambers (RPC) detectors.
- Low current diffuse discharge (Townsend discharge) that operates in the low space charge limit, although even when space charge starts making the entrance it is usually as a perturbation to the swarm model.<sup>[27–29]</sup>
- Afterglows, after the collapse of the ambipolar field.
- Thermalization of elementary particles emitted from radioactive sources or of cosmic rays and of their secondary products, and many more.

## 2. Pre-Breakdown, Free Electrons in Ionized Gases

Pre-breakdown, or transport of charged particles in field free conditions or in fields too weak to achieve self-sustained operation have been studied for many years. For obvious reasons, the primary target of such studies has always been modeling of swarm experiments that have been designed to provide high accuracy without uncertainties in interpretation so that the measured transport coefficients may be used to normalize the sets of cross-sections. It is important to say that modeling may be done in the real space and thus provide the connection between observables and actual transport coefficients under the study. Modeling may also be in the velocity space where calculating data is easier and then one comes to the point when it is possible that due to differences between the real space (bulk) and velocity space (flux) transport coefficients one needs to actually model non-conservative aspects of the complete transport in the experiment in order to fit the measured observables and the resulting transport data.<sup>[8,9]</sup> In a basic swarm model in weakly ionized gas, would be the use of an equation:

$$j = e n v_{dr} \quad (4)$$

where  $j$  is the current density,  $v_{dr}$  the electron drift velocity, and  $n$  is the charged particle density together with the swarm data for the drift velocity. The spatial and temporal profiles of swarms are usually described in hydrodynamic approximation by using the so called continuity equation<sup>[30]</sup>:

$$-\frac{\partial n}{\partial t} + (v_i - v_{att})n - v_{dr} \frac{\partial n}{\partial z} + D_T \left( \frac{\partial^2 n}{\partial x^2} + \frac{\partial^2 n}{\partial y^2} \right) + D_L \left( \frac{\partial^2 n}{\partial z^2} \right) = 0 \quad (5)$$

where  $D$  is the diffusion coefficient (which may be either transverse ( $T$ ) or longitudinal ( $L$ )) and non-conservative rate coefficients are  $\nu$  (ionization –  $i$  and attachment –  $att$ ).

Equations such as 4 and 5 have been used successfully to model a number of experiments<sup>[30–32]</sup> provided that hydrodynamic approximation holds. Best examples of the validity of this approach and the use of continuity equation may be observed in photon emission profiles of time of flight experiments of Blevin and Fletcher.<sup>[31,33]</sup> In some way, these profiles are akin to the detected profiles of avalanches by Raether<sup>[34]</sup> in gaseous elementary particle detectors (see also ref.<sup>[35]</sup> and discussion of detectors later on in the paper).

When, however, assumptions going into the hydrodynamic approximation are not valid,<sup>[9]</sup> then a door is opened for kinetic effects such as diffusion or attachment heating or cooling,<sup>[36–40]</sup> transient negative mobility,<sup>[41–43]</sup> negative absolute mobility,<sup>[43–47]</sup> anomalous time varying diffusion,<sup>[48,49]</sup> negative transient diffusion,<sup>[50]</sup> Holst Oosterhuis (Frank Hertz) luminous layers,<sup>[51–53]</sup> negative differential conductivity (NDC),<sup>[20,54]</sup> and many more. A group of kinetic phenomena may occur even when hydrodynamic conditions are not met and transport is not local.

As an example of how we may use swarm physics to get an insight about the functioning of a device, we may use a display of NDC to discuss its role in gas-filled (diffuse discharge) switches. In Figure 1, we show drift velocity of electrons in pure  $\text{CF}_4$  where the most prominent feature is a peak around 20 Td. The region beyond the peak where drift velocity counter intuitively decreases is the NDC.

One class of devices, the so called diffuse discharge switches, were developed to control inductive storage of energy. Apparently, the power density in inductive discharges is two orders of magnitude greater than the power density of capacitive storage, which proved to be essential for applications in space. Unlike capacitive storage switch, the switch for inductive storage requires a high conductivity at low  $E/N$  and low conductivity at high. Thus it has been possible just to use the calculated drift

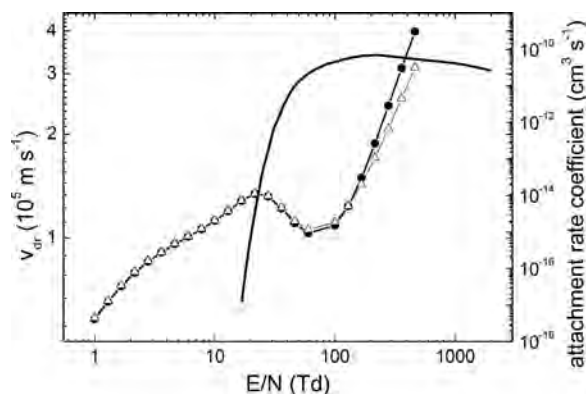


**Figure 1.** Drift velocity  $v_{dr}$  (points triangles flux, solid circles bulk) and attachment rate (line) for electrons in pure  $\text{CF}_4$ .<sup>[55]</sup> The drift velocity shows NDC from 20 to 60 Td while the attachment rate peaks at around 120 Td.

velocity versus  $E/N$  to select the best candidates for practical devices.<sup>[56,57]</sup>

## 2.1. DC Breakdown

In studies of the breakdown, the self-sustained discharge is achieved when production exceeds the losses. For electro-positive gases, losses are difficult to calculate and depend strongly on the geometry of the discharge. In case of electronegative gases attachment dominates the losses and as it is a gas phase process, it is easily established in general terms. Thus, one could claim that the breakdown  $E/N$  (which defines the breakdown voltage for a specific geometry) is that where ionization rate becomes greater than the attachment rate; or when the effective multiplication coefficient ( $\nu_i - \nu_{att}$ ) (or represented in spatial Townsend rate coefficients ( $\alpha - \eta$ )) becomes zero. Actually it has to be larger than zero to compensate other geometry

dependent losses, but zero point is a good indicator of the dielectric strength of the gas (mixture). In Figure 2, we also show effective multiplication rate coefficient for tetrafluoroethane mixtures with argon.<sup>[58,59]</sup>

One can see in Figure 2 that for a low content of the electronegative gas (5%), the breakdown  $E/N$  is smaller, around 25 Td. For 50%, it is more than 70 Td and for pure tetrafluoroethane it is more than 110 Td. Thus, having in mind a cross-section set for a good gaseous dielectric, it is required that there is an attachment process (dissociative presumably) peaking at high energies just below the threshold for ionization in order to postpone to higher  $E/N$  the predominance of production over losses. Good dielectrics, however, also have an attachment (scavenging process) that would peak at the lowest energies and thus remove low energy electrons before they have a chance of accelerating to higher energies.  $SF_6$  is such a gas with several non-dissociative and dissociative attachment processes covering continuously energies from zero to just

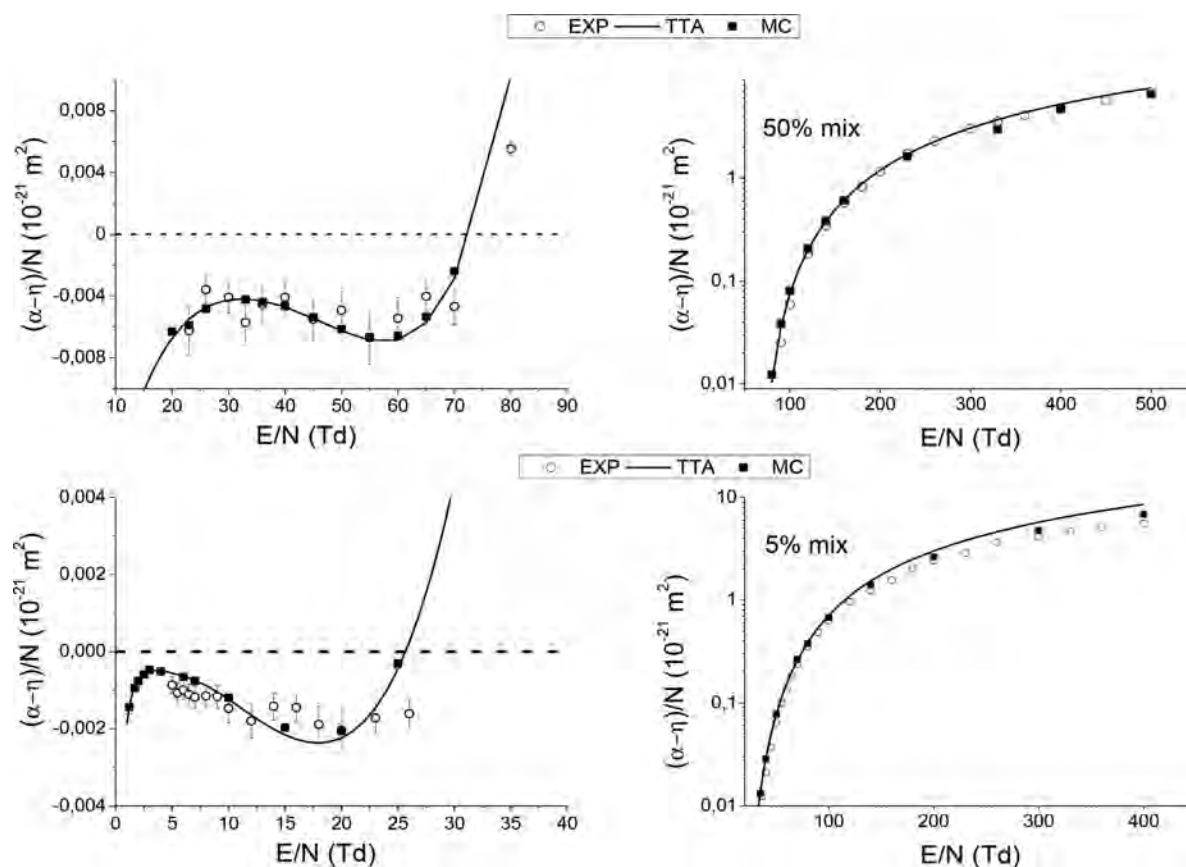


**Figure 2.** Effective multiplication rate for the mixture of tetrafluoroethane (5 and 50%) and argon. As we had to show the ionization rate (denoted by  $\alpha$ ) in a logarithmic plot, the negative part due to the attachment rate (denoted by  $\eta$ ) is shown separately on a linear scale.<sup>[58,59]</sup> MC denotes results of a Monte Carlo simulation, while TTA is an abbreviation for the two term approximation theory. Both sets of calculated results are compared to experiment. The cross-sections were obtained by employing a standard swarm procedure to the available experimental transport data.<sup>[58,59]</sup> The principal thing that should be observed here is that for gases with large attachment, the breakdown  $E/N$  may be easily established from the calculated ionization and attachment rates as a crossover point. For many application, such analysis is sufficient for making engineering decisions.

below the ionization. Other issues in developing a good dielectric would certainly include plasma chemistry that ensues after a possible breakdown. It is preferable that the original molecule is re-formed to ascertain the longevity of the dielectric, and should the gas from the dielectric be released to the atmosphere, toxicity of products of a discharge may become an issue. Except for the plasma chemistry calculations of the dissociative effects, all other aspects of gaseous dielectrics may be modeled by a swarm model or related zero dimensional chemical kinetics models.

Similar issues need to be resolved in gas discharge switches except that the conducting phase involves high conductivity plasma that may (or may not) require a full plasma model. Yet the breakdown itself, a critical feature of the switch, is established easily through swarm modeling. Returning to the diffuse discharge opening switch, the basic principle involving NDC in gaseous mixture may be improved upon by adding a gas with a high threshold attachment that would reduce further the conductivity at the high (off phase)  $E/N$ , but in this case without the low energy attachment (as that would be a hindrance).  $CF_4$  would be excellent for this purpose (as shown in Figure 1).

The issue of breakdown in general terms is also related purely to swarm modeling and it has been covered in some detail by Phelps and Petrović.<sup>[60]</sup> The standard Townsend model of breakdown consists of an electron-induced avalanche and ion feedback producing new electrons at the cathode by secondary emission. It turned out<sup>[60]</sup> that actually photo emission at low  $E/N$ , fast neutrals at high, and metastables at all  $E/N$  contribute significantly to the breakdown, sometimes even dominating. Adding to this the loss processes not accounted for in the Townsend model, such as back-diffusion, we may actually have an effective secondary electron yield obtained from the breakdown curves (according to the Paschen's theory) one order of magnitude lower or up to two orders of magnitude higher than the secondary electron yield measured in a binary beam experiment.<sup>[60]</sup> Townsend's theory worked basically because in the SWARM regime, all fluxes are proportional (linearly) and thus the effective production could be associated with the flux of only one particle. However, in real plasmas with non-linearities and especially temporal developments the basic Townsend theory may not be adequate and thus analysis akin to that of Phelps and Petrović (that is still a swarm-type modeling) may be in order.

## 2.2. RF Breakdown

Basic data for radio-frequency plasma applications can be acquired from simulations and experimental results, and from recorded breakdown voltage curves. DC breakdown

voltages versus  $pd$  ( $p$ -pressure,  $d$ -gap between two parallel electrodes) are known as Paschen curves. For RF breakdown,  $pd$  scaling may be expected to work again but the curves, although similar in shape, are not determined by the Paschen law. Nevertheless, these curves are often called Paschen curves in the literature while it is better to call them RF breakdown curves or sometimes even Paschen-like RF breakdown curves.

One should never attempt to determine secondary electron yields from RF breakdown curves in a direct manner, at least for the following reason. A necessary condition for a self-sustained discharge is to have feedback between the electron growth toward instantaneous anode and their initialization at the cathode. In DC breakdown, it is the drift of ions toward the cathode coupled with a secondary electron production that provides the feedback. In RF fields, however, electrons go in both directions, depending on the phase, so a discharge may be supported purely by electrons. We have performed calculations with only electrons and also with added heavy particles, ions, and fast neutrals.

Initially, electrons were released from the middle of the gap. Cross-section sets have been compiled and tested (argon, oxygen – Itikawa<sup>[61]</sup>; synthetic air – Phelps<sup>[62]</sup>). In our previous paper, we have examined radio-frequency breakdown in argon under conditions when ion-induced secondary emission is negligible (electron-dominated regime).<sup>[63]</sup> In this paper, we move further by including ions and their contribution to secondary electrons emitted from electrodes surfaces. Breakdown points are determined by slowly increasing the voltage to approach the breakdown from below the curve (right hand side and lower branch of the curve) and by increasing pressure to approach higher breakdown voltage branch (left hand side). Breakdown point is established as the one where the number of electrons begins to increase over extended time of many periods (detailed discussion is given in ref.<sup>[63]</sup>).

At first, we examine MC simulation that includes only electrons with distance between electrodes of 1 cm. Figure 3 shows RF breakdown curves for synthetic air. Furthermore, we adjust two parameters to try to fit the experimental data, the first being the reflection coefficient for electrons on the surface of electrodes ( $R$ ) and also the secondary electron yield  $\gamma$  (gamma) due to ion bombardment. One can observe deformation of Paschen-like curve pushing breakdown point toward lower voltages when reflection coefficient is increased arbitrarily. However the "second minimum," as Korolov et al.<sup>[65]</sup> obtained in their experiment (also shown in Figure 3), is only achieved through an addition of the effect of secondary electron emission due to ions. Multipacting effects are observed only at much lower pressures and higher voltages. A good agreement with Korolov et al. was achieved by an assumption that secondary electron yield for ions is 0.002.

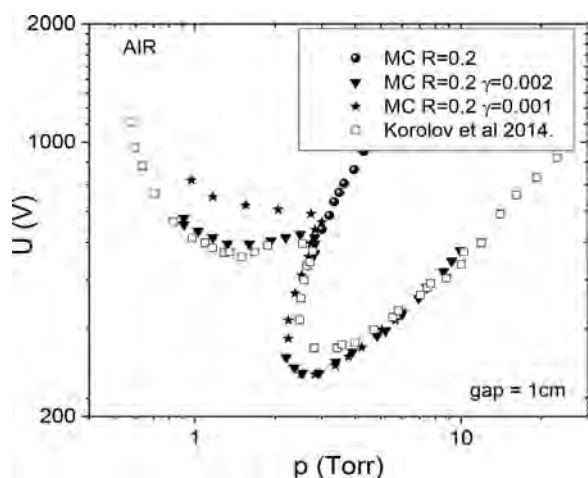


**Figure 3.** Paschen-like RF breakdown curves in synthetic air.<sup>[64]</sup> Gap is 1 cm, frequency 13.56 MHz. Open points are the available experimental results in the literature.<sup>[65]</sup> At first, only reflection of electrons ( $R$ ) was adjusted but it failed to reproduce the shape of the experimental data. Furthermore, a secondary electron yield due to ion bombardment ( $\gamma$ ) was added and a good fit of the left side branches has been achieved for  $\gamma = 0.2\%$ . It must be noted that Korolev et al. managed to fit their experimental points equally well by using a particle in the cell (PIC) code. While technically their code is a plasma code and thus more complex and perhaps less detailed than our Monte Carlo code. Their code has all the ingredients of a swarm model but it was not certain to what degree in their modeling the plasma-related features were necessary to fit and explain the experiments.

In Figure 4, we show space time resolved development of electron swarm properties in an RF breakdown in argon. Results are presented for both conditions where a self-sustained mode (lower (a) and higher (b) peak voltages) is operational (i.e., this is done in the region of the breakdown curves where for a fixed  $pd$  there are two values of the curve). For argon, we have used data from ref.<sup>[60]</sup> At the lower branch of the breakdown curve, majority of electrons does not make a translation from one electrode to another as assumed in simple models<sup>[66,67]</sup> and the discharge is maintained by a small group of higher energy particles some of which reach the electrodes. At higher branch, most electrons make the excursion along the entire gap. Remaining and newly produced electrons stay by the electrode until direction of the field changes and thus some phase shift between the positions and the field waveforms are observed together with a skewness for some properties. In both situations, the critical issue is in achieving high energies and consequently ionization to compensate the losses at the surface.

### 3. Low Current Discharges

In the low current limit of DC discharges, the space charge effects are either negligible or small enough to be treated as a perturbation to the external field.<sup>[27,28,68,69]</sup> In particular, the diffuse low current regime known as

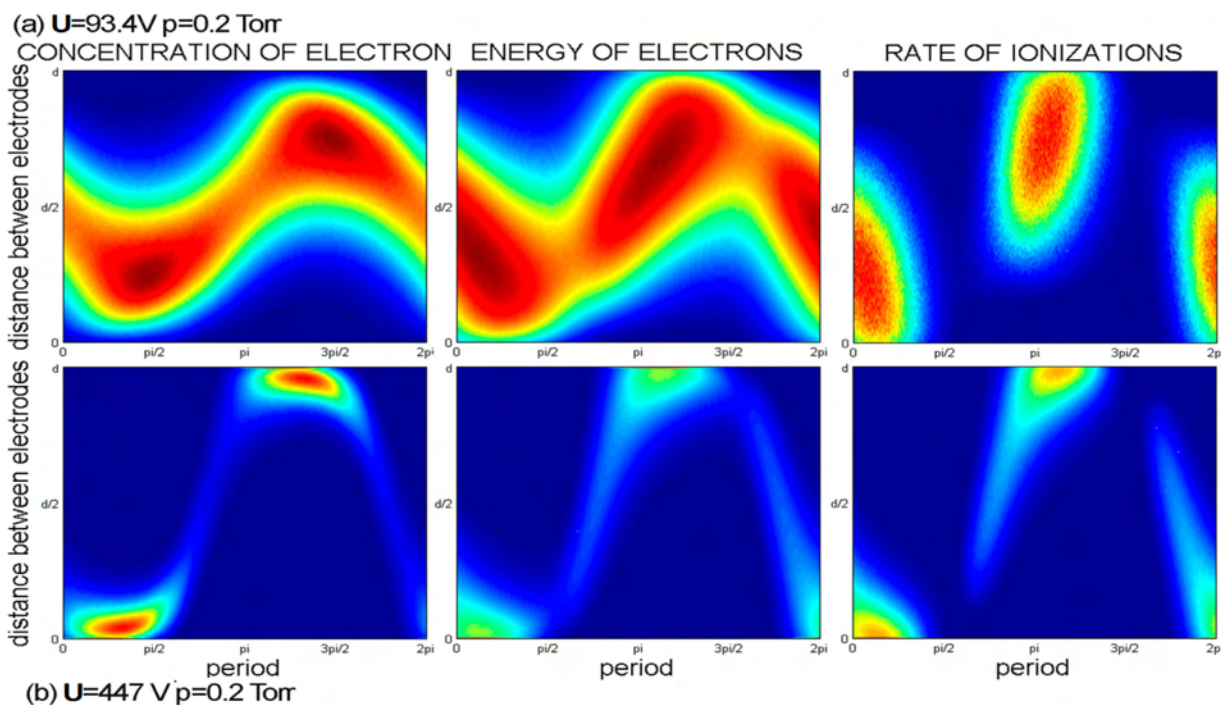


**Figure 4.** Spatial profiles of electron density, energy, and electron-induced ionization under conditions of an RF breakdown.<sup>[63]</sup>



Townsend regime of DC discharges is often taken as a representation of swarm conditions<sup>[70,71]</sup> (steady state Townsend experiment<sup>[32,72]</sup>).

### 3.1. Townsend Regime/DC Discharges

If one records axial and radial profiles of emission along the Volt–Ampere ( $V$ – $A$ ) characteristics (Figure 5) of the low current DC discharges, it is clear that for the lowest of currents the profile is diffusion defined and centered<sup>[73]</sup> while electron density exponentially increases all the way to the anode. That is the sign of the space charge free conditions and the swarm-based models will suffice or in other terms the regime is the so called Townsend discharge. The profiles in the two other regimes (Figure 5 – normal and abnormal glow) reveal a strong effect of the space charge, one in the radial the other in the axial direction. Nevertheless, even under those circumstances, charged particles may not be strongly coupled and for the purposes of theoretical description may behave like swarms, within the limitations of the modified local electric field, thus allowing the swarm physics and transport theory to be the foundation for the description of plasma.

In spite of being supposedly free of space charge effects and any strong coupling, the  $V$ – $A$  characteristics shows

negative slope even in the low current limit (according to the basic Townsend theory, it should be constant) and as a result of the overall  $V$ – $A$  characteristics and external circuit the discharge may slip into oscillations of different kinds.<sup>[73,74]</sup>

The model developed to explain these oscillations due to the negative slope (and thus to extend Townsend's theory) is an example of swarm-based models where space charge effect is calculated based on swarm calculations and added as a perturbation. The basic assumption is that the field right next to the cathode is affected by the space charge and is affecting the energy of ions. The feedback coefficient – the secondary electron yield – cannot be assumed to be constant, as it has been well established that it is dependent on the energy of ions hitting the surface.<sup>[60]</sup> During oscillations, the voltage and the field will change and affect secondary electron yield (the development from Equation (6) to (11) follows the theory in Phelps et al.<sup>[27]</sup>):

$$\gamma - \gamma_p + k_U U + k_I I, \quad (6)$$

The term  $k_U$  describes the linear component of the voltage dependence. However, the critical assumption in the model is the term proportional to the current. It is actually representation of the space charge which is proportional to the current which then provides additional effect due to the slightly skewed electric field right next to the cathode. It is possible to use the density profiles of electrons and ions (ions being much slower have a much higher density and predominantly define the field perturbation) obtained by swarm physics considerations (drift and free diffusion). Using a Poisson equation we get:

$$E_{Sz}(z) - E_S^C = \frac{1}{\epsilon_0} \frac{j_z}{W_{+z}} \frac{1}{[\alpha_0 z - \exp(\alpha_0(z-d)) + \exp(-\alpha_0 d)]}, \quad (7)$$

where  $n_+$  and  $n_e$  are concentrations of ions and electrons,  $j_z$  electrical current density in  $z$ -direction,  $W_{+z}$  drift velocity of ions,  $e$  elementary charge of electrons. The corresponding voltage drop is thus equal to:

$$\begin{aligned} \delta U_S &= - \int_0^d (E_{Sz}(z) - E_S^C) dz \\ &= - \frac{1}{\epsilon_0} \frac{j_z}{W_{+z}} f(\alpha_0, d), \end{aligned} \quad (8)$$

where  $f$  is:

$$f(\alpha_0, d) = d^2 \left[ \frac{1}{2} + \frac{\exp(-\alpha_0 d)}{\alpha_0 d} - \frac{(1 - \exp(-\alpha_0 d))}{(\alpha_0 d)^2} \right], \quad (9)$$

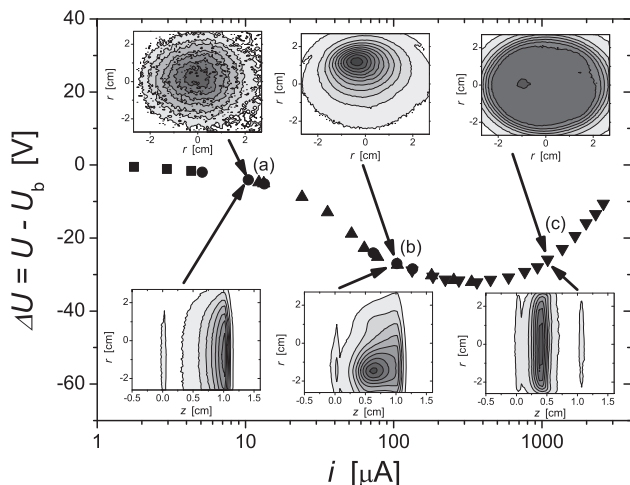


**Figure 5.** Spatial profiles of emission in low current DC discharges, covering the three regimes with three characteristic profiles: (a) Townsend regime or diffuse low current discharge-falling well under the realm of swarm models; (b) glow discharge-constricted low current discharge; and (c) abnormal glow-diffuse high current discharge<sup>[73]</sup> (© IOP Publishing. Reproduced with permission. All rights reserved – doi: 10.1088/0963-0252/18/3/034009). Anode is at 1.1 cm and cathode at 0 cm and some small amount of scattered light indicates the positions of electrodes.



with round the loop multiplication being

$$g(t) = \gamma[\exp(\alpha(t)d) - 1] = 1. \quad (10)$$

The effective normalized discharge resistance is

$$R_N = \frac{A}{d^2} R_D = \frac{A}{d^2} \frac{\delta U}{I} = - \frac{\hat{\gamma}}{\epsilon_0 W_{+z} \hat{g}} \frac{f(\alpha d)}{d^2}, \quad (11)$$

where  $A$  is the area of the electrode and  $\hat{g}$  is the logarithmic derivative of the multiplication factor  $g$  ( $\hat{g} = \hat{\gamma} + \gamma \alpha d \exp(\alpha d) \hat{\alpha}$ ).

Experimental tests have confirmed the theory both in the field distribution and in the scaling of the effective resistance.<sup>[75]</sup>  $R_N$  depends on variation with the field (and current) of the secondary electron yield but the theory also provides a foundation for the standard scaling of discharge parameters  $E/N$ ,  $pd$  ( $Nd$ ), and even  $jd^2$ . This bit of theory is added here as an example of how swarm-type considerations are weaved into the plasma theory as its fundamental aspect and also how swarm data enter such calculations as the basic input on atomic and molecular collisions.

### 3.2. High $E/N$ -Runaway Swarms

If one extends the range of measurements to the left hand branch of the Paschen curve, two things become obvious. The first is that the voltage drop between the Townsend regime and the glow discharge diminishes (see Figure 2 in ref.<sup>[76]</sup>) and sometimes it is even a continuous transition. The reason is simply in the large mean free paths and then the effect of the space charge become less obvious (spread over a larger area). Another effect is observed if energy distribution function (EDF) is sampled, whereby the EDF has a strong peak at maximum available energy thus indicating a runaway.<sup>[77]</sup> This is a situation where the initial conditions (energy distribution) is maintained (augmented by the energy drop in during the travel through the discharge) and thus properties vary from one point to the next. The low energy tail of secondary electrons also develops, which varies according to the position. Thus a hydrodynamic model is not appropriate, but a MCS may produce excellent results. It may also allow for exact inclusion of the boundary conditions, such as energy-dependent yields due to ions and electrons, energy-dependent angular distribution of secondary or reflected particles, energy-dependent energy loss, and energy-dependent electron reflection. The procedure allows for exact, experimental data to be included for any other possible boundary effect related to electrons, ions, neutrals, reactive species, metastables, and photons. At high  $E/N$  that corresponds to the left hand side of the Paschen curve, electrons are not very efficient in ionization (requiring a rapid increase in the voltage necessary for the breakdown

as  $pd$  is reduced) and even then the multiplication coefficients are only slightly higher than 1.

Due to the low pressure, mean free paths become large for both electrons and ions and they gain much larger energy than in standard discharges. This is particularly critical for ions, allowing them to extend much beyond the standard low energies (below 1 eV) all the way up to the maximum available energy. This opens the door for charge transfer collisions producing fast neutrals. It turns out that fast neutrals are at those conditions more efficient in excitation than either electrons or ions and this all leads to a peak of emission close to the cathode, that is the signature of fast neutral excitation.<sup>[78,79]</sup> Under those circumstances, momentum transfer in heavy particle collisions leads to a transfer of kinetic energy producing Doppler profiles with excessively high energy wings.<sup>[79–81]</sup> As a result, one could predict a possible application for fast neutral etching that would reduce the charging problems<sup>[82,83]</sup> in treating dielectrics in nanoelectronics and allow even higher aspect ratios of nanostructures with an increased spatial resolution.

While being mostly non-hydrodynamic, the high  $E/N$  discharges are best described by swarm physics. They also open the need for similar models of ions and fast neutrals.

### 3.3. Microdischarges, Atmospheric Pressure Discharges, Discharges in Liquids

By the virtue of the  $jd^2$  scaling (that has been tested), the Townsend regime may be extended to higher currents at very small gaps. While being counterintuitive, this is a well established fact at least as long as the standard gas discharge physics operates (i.e., below the onset of field emission).<sup>[84]</sup> Extension of the Townsend regime into higher currents allows for applications of microdischarges that take advantage of the flexibility and ability to directly adjust and achieve a high efficiency of excitation and dissociation (by merely changing the  $E/N$ ) while still having a high enough total output of photons and/or chemically active species<sup>[85]</sup> for possible applications.

Microdischarges are one way to produce non-equilibrium plasma at high pressures. They simply operate close to the Paschen minimum and thus allow for much higher pressure for the given reduction in the discharge gap. In the atmosphere, the kinetics of charges is defined by swarm physics, yet if a field is added, the increase of charge density is quite large and a quick transition to highly conductive thermal plasma ensues. Atmospheric pressure discharges often have a high charge density, but in general, the whole atmosphere is an ionized gas that may be described by the physics of swarms. Of the plasmas, the corona discharge consists of streamers and diffuse discharge, which falls under the swarms jurisdiction.<sup>[86]</sup> Calculation of transport of

electrons, ions, and other particles may proceed mainly by using free electron and ion diffusion, but one needs to take into account clusters formed by water vapor molecules and other issues.

One of the lines of the fastest development and new applications are the discharges in water (liquids in general), at the interface between liquid and gas phase, and in gas phase of vapors.<sup>[87,88]</sup> In liquids one needs to re-establish both cross-sections, transport theory, and transport coefficients. More data are needed for low pressure transport (in gas or vapor).<sup>[89,90]</sup> In addition, we need to establish techniques to determine and apply data at high pressures and in liquid, i.e., and multiple collision conditions,<sup>[91]</sup> and under the influence of hydration and breakdown<sup>[92]</sup> of clusters. In addition, even the low pressure collision and transport data for the most important ions in water vapor are missing.<sup>[93]</sup> The liquid-related discharges<sup>[94]</sup> provide a number of challenges and in many circumstances swarm modeling (albeit adjusted to the needs of very high densities) is required. A comprehensive review on discharges associated with liquids may be found in a forthcoming article, containing most importantly list of open issues.<sup>[92]</sup>

### 3.4. Afterglow

Upon switching off of the discharge, the space charge may remain for a while as long as the charged particle densities are sufficient to produce a modified field profile. At some moment, the ambipolar field will collapse and free diffusion will ensue that is modeled by swarm physics. In that period, electrons are supposed to continuously lose energy and diminish in numbers. Under some circumstances (depending on the gas, impurities, initial energy, and distribution function and electron and ion densities), an increase of the mean energy occurs during the afterglow leading to a transient peak in the decay of the mean electron energy. Sometimes that peak may be even greater than the initial mean energy, again depending on the gas and on the initial conditions. This phenomenon has often been explained by evoking atomic and molecular physics, including processes such as Penning ionization, Rydberg states, superelastic collisions and recombination.<sup>[95,96]</sup>

However, a very important process is often overlooked. It is the above-mentioned diffusion heating or cooling<sup>[37]</sup> (also there is a possibility of an attachment cooling or heating<sup>[40]</sup>). While the aforementioned processes depend on the initial densities of excited states, this process is universal as it depends only on the ground state momentum transfer cross-section. The presence of the Ramsauer–Townsend minimum in some gases allows very large mean free paths and escape of electrons to the wall of the vessel, thus increasing losses (speeding up thermalization as this could be regarded as evaporative cooling).

Results of a MCS are shown in Figure 6 where we present the development of the mean energy in a limited size discharge vessels and also for an infinite plasma in argon. In an infinite case, thermalization is slow while in the parallel plate geometry decay is much faster (Figure 6a). We also show the decay of the number density of electrons (Figure 6b). In Figure 7, we show energy distribution functions in the parallel plate and in infinite cases. In the latter case, the high energy tail disappears quickly, while the rest of the distribution is close to the Maxwell Boltzmann (MB) distribution with the same energy. This graph also shows as a very general conclusion that, even when the bulk of the distribution function is a Maxwellian, the extrapolation to the high energy tail by a Maxwellian may lead to errors of many orders of magnitude. The reason is that the high energy loss processes such as ionization

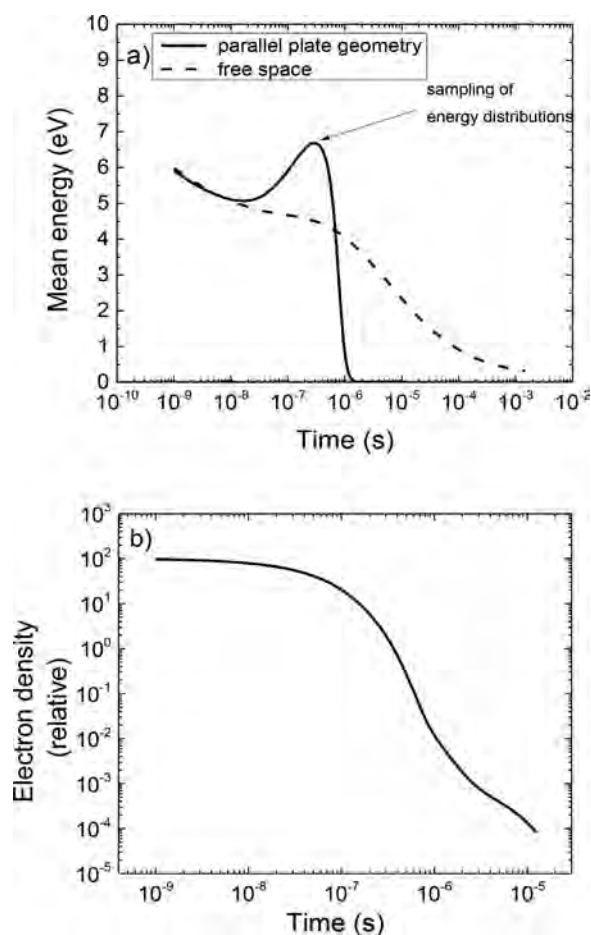


**Figure 6.** Thermalization (a) and decay of the number (b) of electrons in Ar from the initial MB distribution at 7 eV (argon at 1 Torr and a gap of 1 cm) in plane-parallel geometry and in free space. Arrow marks the point in time where the energy distributions that are shown in Figure 7 are sampled. Two Maxwell Boltzmann distributions are shown for comparison, each at a mean energy equal to that in the decayed measured distribution (6.5 and 4.4 eV).

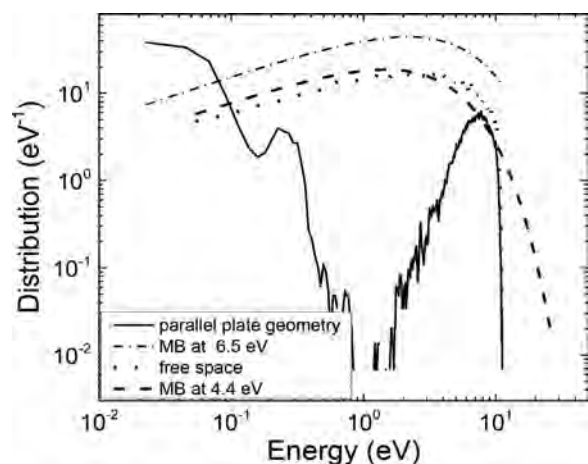


**Figure 7.** Energy distribution functions at the point marked in Figure 6 for the parallel plate geometry (solid) and infinite geometry (dashed). Two Maxwell Boltzmann distributions for the mean energies corresponding to the two distributions are shown.

deplete the high energy tail of the EDF especially in the low pressure discharges. The bulk of the distribution, and therefore the mean energy, slowly head toward the room temperature thermal equilibrium energy.

For the parallel plate system, due to the long mean free paths as compared to the size of the discharge (even for 1 Torr of argon and 1 cm dimension), a hole is rapidly burned in the Ramsauer–Townsend energy range. At higher energies, the distribution is similar to that of the corresponding Maxwellian, albeit with the high energy tails removed by high energy loss collisions. With the peak of the mean energy greater than the initial energy, the diffusion cooling should be taken into account by including a complete calculation of thermalization (with all the cross-sections and atomic and molecular processes). Diffusion cooling will invariably take place depending on the cross-section shapes; in case of resonant attachment a similar heating/cooling situation may arise and these processes may affect strongly non-local (non-hydrodynamic) systems such as plasma sheaths, Langmuir probe at low pressures<sup>[97]</sup> and distribution function at the beginning of thermalization or close to the walls.

#### 4. Data Bases for Pristine Gases and Gases with a Large Density of Excited States and Radicals

It is often discussed that the main basis of the plasma modeling is in a set of fluid equations supplied by the swarm data. It is truly important to set up the data bases with a well-prescribed procedures for evaluation in order to be able to appraise different calculations with seemingly

same gas mixtures. In addition, coherence between the cross-sections and transport data should be achieved and maintained. The fluid models that use swarm coefficients must be compared to the kinetic and hybrid codes that are based on the cross-sections. Consistency between the two sets should be achieved and it is the task of the atomic, molecular collision physics and necessarily also the swarm physics. A number of data bases has been developed for the purpose of providing low temperature plasma physics with data starting with the JILA data Center (Joint Institute for Laboratory Astrophysics of the Colorado University at Boulder and National Institute for Science and Technology),<sup>[98]</sup> the data base of Art Phelps at JILA,<sup>[62]</sup> NIST Data reviews,<sup>[99]</sup> the data base of Prof. Hayashi,<sup>[99]</sup> our data base,<sup>[100]</sup> and many more. The most focused and certainly the largest in number of participants and quantity of data is the currently active LxCAT data base.<sup>[101,102]</sup> One needs to include the data for ions<sup>[100,103]</sup> including the most comprehensive data base of Prof. L. Viehland as included in LxCAT<sup>[101]</sup> and fast neutrals.<sup>[104]</sup> If the system is a candidate for being described by swarm models sometime it suffices just to observe the available data for some of the transport coefficients to at least appreciate qualitatively the feasibility of the particular system. However, if some kinetic phenomena and in particular non-hydrodynamic kinetic phenomena are involved a full-fledged kinetic simulation is necessary. In that case, however, in order to have proper balances of number, momentum, and energy a swarm normalized cross-sections are necessary to obtain the quantitative comparisons with experiments.

A separate issue is the modeling of plasmas when the background gas may not be regarded as pristine (unperturbed). This issue may be introduced to plasma modeling by making a self-consistent (coupled) calculations of the excited state populations and then of the energy distribution functions and effective rates and other coefficients. While the very presence of the excited states breaks the principal definition of swarms as developed for swarm experiments<sup>[105]</sup> this, self-consistent modeling extends the applicability of swarm physics to the realm of higher currents/densities of electrons and elevated temperatures. Under these circumstances, a whole new realm of transport data opens, that involves the cross-sections for excited states (stepwise excitation, stepwise ionization, etc.). Not surprisingly first important applications involved modeling of CO<sub>2</sub> lasers,<sup>[106]</sup> but also hydrogen discharges<sup>[107,108]</sup> and nitrogen containing discharges.<sup>[109,110]</sup> Perhaps the widest and the simplest similar modeling is that involving properties of discharges in rare gases with a large abundance of metastables in particular in argon.<sup>[111–113]</sup> Interest in CO<sub>2</sub> has been reactivated recently due to the activity in energy conversion and storage.<sup>[114]</sup> In a similar fashion, swarm models may be applied to discharges where fragments of the molecules that may have certain

properties abound. For example, the issue of attachment in  $\text{CF}_4$  when a significant part of the molecules has been dissociated has been considered in ref.<sup>[115]</sup> In this section, we did not attempt to make a comprehensive review, we only show few examples and we apologize to those whose work was not included in the list. There are many better sources for detailed bibliography and many much more comprehensive reviews. We only wanted to stress the importance of data when swarm modeling is attempted and also that this approach may be used in the realm of strongly perturbed gases by a large degree of excitation or dissociation thus extending the domain of applicability of swarm physics but requesting a wide range of new data.

## 5. Conclusion

In addition to all the examples covered here, we have recently made swarm-type modeling in a number of cases involving ionized gases but outside the realm of standard low temperature plasmas. These applications will be the subject of a separate publication<sup>[116]</sup>:

- 1) Studies of swarms of positrons may be modeled in the same manner as electrons (without the comfort of production in collisions through ionization, although ionization produces a lot of secondary electrons).<sup>[117]</sup> With real swarm experiments lacking, the models cannot be used to get quantitative scaling of the cross-sections, but the results provide an insight into processes and new kinetic phenomena, such as Positronium (Ps) formation fueled negative differential conductivity of the bulk component of the drift velocity.<sup>[118]</sup>
- 2) In the absence of swarm data measurements, one may define averaged properties that may be used in the same fashion as the swarm data, for example thermalization times (or full thermalization development), ranges of particles, density of deposited energy, and more.<sup>[119]</sup>
- 3) Trajectories of particles have been used to describe the properties, although each individual particle does not have enough distinction to give a full insight on the pertinent processes. Still, overall image, obtained by a large set of particles or individual trajectories that are selected, provide sufficient information to make important conclusions.<sup>[120,121]</sup>
- 4) Thermalization of positronium in gases.<sup>[122,123]</sup>
- 5) Modeling of PET like environment and modeling of chemistry induced by the initial positrons in living tissue/liquid.<sup>[91]</sup>
- 6) Modeling of gas-filled positron (and electron) traps, such as Penning Malmberg Surko traps<sup>[124,125]</sup> or other gas-filled traps.
- 7) Avalanches and current pulses in gas-filled RPC frequently used detectors in elementary particle

detection and the corresponding properties of the gases used in the mixture.<sup>[126]</sup>

- 8) Streamer breakdown conditions.<sup>[127,128]</sup>
- 9) Modeling of ionization fronts in streamers.<sup>[129,130]</sup>

The list does not end here and in all those cases swarm studies provide models or an insight into the most salient properties of the discharge. At the same time, one should pay more attention to understanding plasma modeling (from the global to the complex hybrid and PIC codes), the role of plasma models in crossed electric and magnetic fields (e.g., for propulsion studies) and the description of some atmospheric and astrophysical systems (elves, blue jays, clouds of electrons and positrons formed in the vicinity of neutron stars, etc.).

Swarm physics is one of the building blocks of the physics of non-equilibrium plasmas. Another important building block is the swarm data which originate from swarm studies. In addition to being sufficient for some systems, learning how to deal with those will improve our knowledge on applying swarm-based transport equations and data in plasma models. In the meantime, each of the problems mentioned here is interesting, even fun to pursue and a worthwhile contribution.

**Acknowledgements:** This work is partly supported by Ministry of Education, Science and Technology of Republic Serbia projects ON171037 and III410011. Z. Lj. P. is also grateful to the SASA project F155. Authors are grateful to J. de Urquijo, O. Šašić, and S. Dupljanin for collaboration in obtaining results shown in Figure 2 and to M. Radmilović Radenović for collaboration in obtaining some of the results shown in Figure 4.

Received: July 3, 2016; Revised: August 12, 2016; Accepted: August 25, 2016; DOI: 10.1002/ppap.201600124

**Keywords:** breakdown; plasma modeling; swarm; Townsend discharge

- [1] M. A. Lieberman, A. J. Lichtenberg, "Principles of Plasma Discharges and Material Processing", Wiley, Hoboken, NJ, USA 2005.
- [2] T. Makabe, Z. Petrović, "Plasma Electronics: Applications in Microelectronic Device Fabrication", Taylor and Francis, CRC Press, New York 2006.
- [3] M. J. Kushner, *J. Phys. D: Appl. Phys.* **2009**, *42*, 194013.
- [4] S. Samukawa, M. Hori, S. Rauf, K. Tachibana, P. Bruggeman, G. Kroesen, J. Ch. Whitehead, A. B. Murphy, A. F. Gutsol, S. Starikovskaia, U. Kortshagen, J. P. Boeuf, T. J. Sommerer, M. J. Kushner, U. Czarnetzki, N. Mason, *J. Phys. D: Appl. Phys.* **2012**, *45*, 253001.

- [5] S. Pancheshnyi, S. Biagi, M. C. Bordage, G. J. M. Hagelaar, W. L. Morgan, A. V. Phelps, L. C. Pitchford, *Chem. Phys.* **2012**, *398*, 148. UBCdatabase, www.lxcat.net, June 30, 2016.
- [6] R. W. Crompton, *Adv. At. Mol. Opt. Phys.* **1994**, *33*, 97.
- [7] A. V. Phelps, *Rev. Mod. Phys.* **1968**, *40*, 399.
- [8] Z. Lj. Petrović, M. Šuvakov, Ž. Nikitović, S. Dujko, O. Šašić, J. Jovanović, G. Malović, V. Stojanović, *Plasma Sources Sci. Technol.* **2007**, *16*, S1.
- [9] Z. Lj. Petrović, S. Dujko, D. Marić, G. Malović, Ž. Nikitović, O. Šašić, J. Jovanović, V. Stojanović, M. Radmilović-Radenović, *J. Phys. D: Appl. Phys.* **2009**, *42*, 194002.
- [10] R. E. Robson, R. D. White, Z. Lj. Petrović, *Rev. Modern Phys.* **2005**, *77*, 41303.
- [11] K. Kumar, H. R. Skullerud, R. E. Robson, *Aust. J. Phys.* **1980**, *33*, 343.
- [12] S. Dujko, R. D. White, Z. Lj. Petrović, *J. Phys. D: Appl. Phys.* **2008**, *41*, 245205.
- [13] R. D. White, R. E. Robson, *Phys. Rev. E* **2011**, *84*, 031125.
- [14] R. E. Robson, "Introductory Transport Theory for Charged Particles in Gases", World Scientific Publishing Company, Singapore 2006.
- [15] I. D. Reid, *Aust. J. Phys.* **1979**, *32*, 231.
- [16] V. D. Stojanović, Z. Lj. Petrović, *J. Phys. D* **1998**, *31*, 834.
- [17] Z. M. Raspopović, S. Sakadžić, S. Bzenić, Z. Lj. Petrović, *IEEE Trans. Plasma Sci.* **1999**, *27*, 1241.
- [18] Z. Ristivojević, Z. Lj. Petrović, *Plasma Sources Sci. Technol.* **2012**, *21*, 035001.
- [19] R. E. Robson, *Aust. J. Phys.* **1984**, *37*, 35.
- [20] S. B. Vrhovac, Z. Lj. Petrović, *Phys. Rev. E* **1996**, *53*, 4012.
- [21] R. D. White, R. E. Robson, P. Nicoletopoulos, S. Dujko, *Eur. Phys. J. D* **2012**, *66*, 117.
- [22] L. C. Pitchford, A. V. Phelps, *Phys. Rev. A* **1982**, *25*, 540.
- [23] P. Segur, M. Bordage, J. Balaguer, M. Yousfi, *J. Comp. Phys.* **1983**, *50*, 116.
- [24] R. D. White, M. J. Brennan, K. F. Ness, *J. Phys. D: Appl. Phys.* **1997**, *30*, 810.
- [25] S. Dujko, Z. M. Raspopović, Z. Lj. Petrović, *J. Phys. D: Appl. Phys.* **2005**, *38*, 2952.
- [26] R. D. White, R. E. Robson, B. Schmidt, M. A. Morrison, *J. Phys. D: Appl. Phys.* **2003**, *36*, 3125.
- [27] A. V. Phelps, Z. Lj. Petrović, B. M. Jelenković, *Phys. Rev. E* **1993**, *47*, 2825.
- [28] Z. Lj. Petrović, I. Stefanović, S. Vrhovac, J. Živković, *J. Phys. IV France* **1997**, *C4*, 3412.
- [29] S. Živanov, J. Živković, I. Stefanović, S. Vrhovac, Z. Lj. Petrović, *Eur. Phys. J. AP* **2000**, *11*, 59.
- [30] L. G. H. Huxley, R. W. Crompton, "Diffusion and Drift of Electrons in Gases", Wiley-Interscience, New York 1974.
- [31] H. A. Blevin, J. Fletcher, S. R. Hunter, *J. Phys. D* **1976**, *9*, 471.
- [32] Z. Lj. Petrović, *PhD Thesis*, Australian National University (Canberra), February 1985.
- [33] H. A. Blevin, J. Fletcher, *Aust. J. Phys.* **1984**, *37*, 593.
- [34] H. Raether, *Electron avalanches and breakdown in gases (Butterworths advanced physics series)*, Butterworths, 1964.
- [35] S. Dujko, D. Bošnjaković, R. D. White, Z. Lj. Petrović, *Plasma Sources Sci. Technol.* **2015**, *24*, 054006.
- [36] T. Rhymes, R. W. Crompton, *Aust. J. Phys.* **1975**, *28*, 675.
- [37] R. E. Robson, *Phys. Rev. A* **1976**, *13*, 1536.
- [38] H. I. Leemon, K. Kumar, *Aust. J. Phys.* **1975**, *28*, 25.
- [39] K. Koura, *J. Chem. Phys.* **1982**, *76*, 390.
- [40] D. R. A. McMahon, R. W. Crompton, *J. Chem. Phys.* **1983**, *78*, 603.
- [41] B. Shizgal, D. R. A. Mc Mahon, *Phys. Rev. A* **1985**, *31*, 1894.
- [42] J. M. Warman, U. Sowada, M. P. De Haas, *Phys. Rev. A* **1985**, *31*, 1974.
- [43] Z. Donko, N. Dyatko, *Eur. Phys. J. D* **2016**, *70*, 135.
- [44] N. A. Dyatko, A. P. Napartovich, S. Sakadžić, Z. Lj. Petrović, Z. Raspopović, *J. Phys. D* **2000**, *33*, 375.
- [45] R. E. Robson, Z. Lj. Petrović, Z. M. Raspopović, D. Loffhagen, *J. Chem. Phys.* **2003**, *119*, 11249.
- [46] M. Šuvakov, Z. Ristivojević, Z. Lj. Petrović, S. Dujko, Z. M. Raspopović, N. A. Dyatko, A. P. Napartovich, *IEEE Trans. Plasma Sci.* **2005**, *33*, 532.
- [47] S. Dujko, Z. M. Raspopović, T. Makabe, Z. Lj. Petrović, *IEEE Trans. Plasma Sci.* **2003**, *31*, 711.
- [48] R. D. White, R. E. Robson, K. F. Ness, *Aust. J. Phys.* **1995**, *48*, 925.
- [49] K. Maeda, T. Makabe, N. Nakano, S. Bzenić, Z. Lj. Petrović, *Phys. Rev. E* **1997**, *55*, 5901.
- [50] R. D. White, S. Dujko, K. F. Ness, R. E. Robson, Z. Raspopović, Z. Lj. Petrović, *J. Phys. D: Appl. Phys.* **2008**, *41*, 025206.
- [51] M. Hayashi, *J. Phys. D* **1982**, *15*, 1411.
- [52] R. E. Robson, B. Li, R. D. White, *J. Phys. B: At. Mol. Opt. Phys.* **2000**, *33*, 507.
- [53] S. Dujko, Z. M. Raspopović, R. D. White, T. Makabe, Z. Lj. Petrović, *Eur. Phys. J. D* **2014**, *68*, 166.
- [54] Z. Lj. Petrović, R. W. Crompton, G. N. Haddad, *Aust. J. Phys.* **1984**, *37*, 23.
- [55] M. Kurihara, Z. Lj. Petrović, T. Makabe, *J. Phys. D* **2000**, *33*, 2146.
- [56] L. G. Christophorou, S. R. Hunter, "Electron Molecule Interactions", Academic Press, New York 1984.
- [57] K. H. Schoenbach, G. Schaefer, E. E. Kunhardt, M. Kristianson, L. L. Hatfield, A. H. Guenther, *IEEE Trans. Plasma Sci.* **1982**, *PS-10*, 246.
- [58] O. Šašić, S. Dupljanin, J. de Urquijo, Z. Lj. Petrović, *J. Phys. D: Appl. Phys.* **2013**, *46*, 325201.
- [59] O. Šašić, S. Dupljanin, S. Dujko, D. Bošnjaković, A. Banković, J. de Urquijo, Z. Lj. Petrović, **2017**, unpublished.
- [60] A. V. Phelps, Z. Lj. Petrović, *Plasma Sources Sci. Tech.* **1999**, *8*, R21.
- [61] Y. Itikawa, *J. Phys. Chem. Ref. Data* **2009**, *38*, 1.
- [62] A. V. Phelps, [http://jila.colorado.edu/~avp/collision\\_data/electronneutral/ELECTRON.TXT](http://jila.colorado.edu/~avp/collision_data/electronneutral/ELECTRON.TXT), 2016.
- [63] M. Savić, M. Radmilović-Radjenović, M. Šuvakov, S. Marjanović, Z. Lj. Petrović, *IEEE Trans. Plasma Sci.* **2011**, *39*, 2556.
- [64] M. Savić, J. Sivoš, D. Marić, G. Malović, Z. Lj. Petrović, **2017**, unpublished.
- [65] I. Korolov, A. Derzsi, Z. Donko, *J. Phys. D: Appl. Phys.* **2014**, *47*, 475202.
- [66] A. von Engel, "Ionized Gases", Clarendon Press, Oxford 1955.
- [67] V. A. Lisovskiy, V. D. Yegorenkov, *J. Phys. D: Appl. Phys.* **1998**, *31*, 3349.
- [68] V. I. Kolobov, A. Fiala, *Phys. Rev. E* **1994**, *50*, 3018.
- [69] R. R. Arslanbekov, V. I. Kolobov, *J. Phys. D: Appl. Phys.* **2003**, *36*, 2986.
- [70] K. Tachibana, A. V. Phelps, *J. Chem. Phys.* **1981**, *75*, 3315.
- [71] S. A. Lawton, A. V. Phelps, *J. Chem. Phys.* **1978**, *69*, 1055.
- [72] Y. Sakai, H. Tagashira, S. Sakamoto, *J. Phys. D* **1977**, *10*, 1035.
- [73] D. Marić, G. Malović, Z. Lj. Petrović, *Plasma Sources Sci. Technol.* **2009**, *18*, 034009.
- [74] Z. Lj. Petrović, A. V. Phelps, *Phys. Rev. E* **1993**, *47*, 2806.
- [75] I. Stefanović, Z. Lj. Petrović, *Jpn. J. Appl. Phys.* **1997**, *36*, 4728.
- [76] D. Marić, M. Savić, J. Sivoš, N. Škoro, M. Radmilović-Radjenović, G. Malović, Z. Lj. Petrović, *Eur. Phys. J. D* **2014**, *68*, 155.



- [77] S. B. Vrhovac, V. D. Stojanović, B. M. Jelenković, Z. Lj. Petrović, *J. Appl. Phys.* **2001**, *90*, 5871.
- [78] D. A. Scott, A. V. Phelps, *Phys. Rev. A* **1991**, *43*, 3043.
- [79] Z. Lj. Petrović, A. V. Phelps, *Phys. Rev. E* **2009**, *80*, 016408.
- [80] E. Li Ayers, W. Benesch, *Phys. Rev. A* **1988**, *37*, 194.
- [81] A. V. Phelps, B. Jelenkovic, L. C. Pitchford, *Phys. Rev. A* **1987**, *36*, 5327.
- [82] Z. Lj. Petrović, V. D. Stojanović, *J. Vac. Sci. Technol. A* **1998**, *16*, 329.
- [83] S. Samukawa, K. Sakamoto, K. Ichiki, *J. Vac. Sci. Technol.* **2002**, *A20*, 1.
- [84] Z. Lj. Petrović, N. Škoro, D. Marić, C. M. O. Mahony, P. D. Maguire, M. Radmilović-Radenović, G. Malović, *J. Phys. D: Appl. Phys.* **2008**, *41*, 194002.
- [85] J. G. Eden, S.-J. Park, *Plasma Phys. Control. Fusion* **2005**, *47*, B83.
- [86] N. Hasan, D. S. A. Farouk, *Plasma Sources Sci. Technol.* **2014**, *23*, 035013.
- [87] N. Škoro, D. Marić, G. Malović, W. G. Graham, Z. Lj. Petrović, *Phys. Rev. E* **2011**, *84*, 055401(R).
- [88] J. Sivoš, N. Škoro, D. Marić, G. Malović, Z. Lj. Petrović, *J. Phys. D: Appl. Phys.* **2015**, *48*, 424011.
- [89] R. D. White, M. J. Brunger, N. A. Garland, R. E. Robson, K. F. Ness, G. Garcia, J. de Urquijo, S. Dujko, Z. Lj. Petrović, *Eur. Phys. J. D* **2014**, *68*, 125.
- [90] F. Blanco, A. M. Roldán, K. Krupa, R. P. McEachran, R. D. White, S. Marjanović, Z. Lj. Petrović, M. J. Brunger, J. R. Machacek, S. J. Buckman, J. P. Sullivan, L. Chiari, P. Limão-Vieira, G. Garcia, *J. Phys. B: At. Mol. Opt. Phys.* **2016**, *49*, 145001.
- [91] R. E. Robson, M. J. Brunger, S. J. Buckman, G. Garcia, Z. Lj. Petrović, R. D. White, *Sci. Rep.* **2015**, *5*, 12674.
- [92] P. Bruggeman, M. Kushner, B. Locke, H. Gardeniers, B. Graham, D. Graves, R. Hofman-Caris, D. Maric, J. Reid, E. Ceriani, D. Fernandez Rivas, J. Foster, S. Garrick, Y. Gorbanev, S. Hamaguchi, F. Iza, H. Jablonowski, E. Klimova, F. Krcma, J. Kolb, P. Lukes, Z. Machala, I. Marinov, D. Mariotti, S. Mededovic Thagard, D. Minakata, E. Neyts, J. Pawlat, Z. Petrovic, R. Pflieger, S. Reuter, D. Schram, S. Schroeter, M. Shiraiwa, B. Tarabova, P. Tsai, J. Verlet, T. von Woedtke, K. Wilson, K. Yasui, G. Zvereva, *Plasma Sources Sci. Technol.* **2016**.
- [93] V. Stojanović, Z. Raspopović, D. Marić, Z. Lj. Petrović, *Eur. Phys. J. D* **2015**, *69*, 63.
- [94] P. Bruggeman, C. Leys, *J. Phys. D: Appl. Phys.* **2009**, *42*, 053001.
- [95] A. B. Blagoev, Tc. K. Popov, *Phys. Lett. A* **1979**, *70*, 416.
- [96] Y. Celik, T. V. Tsankov, M. Aramaki, S. Yoshimura, D. Luggenhölscher, U. Czarnetzki, *Phys. Rev. E* **2012**, *85*, 046407.
- [97] V. Godyak, B. Alexandrovich, *Plasma Sources Sci. Technol.* **2015**, *24*, 052001.
- [98] L. J. Kieffer, *A Compilation of Electron Collision Cross. Section Data for Modeling Gas Discharge Lasers*, JILA Report #13 **1973**.
- [99] M. Hayashi, "Electron Collision Cross Sections Determined from Beam and Swarm Data by Boltzmann Analysis", in *Nonequilibrium Processes in Partially Ionized Gases*, Plenum Press, New York **1990**, or LXcat database: <http://fr.lxcat.net>
- [100] Institute of Physics University of Belgrade, Center for non-equilibrium processes database: <http://mail.ipb.ac.rs/~cep/ipb-cnp/ionsweb/database.htm> **2016**.
- [101] LXCAT database: [http://fr.lxcat.net/data/set\\_type.php](http://fr.lxcat.net/data/set_type.php) **2016**.
- [102] L. C. Pitchford, L. L. Alves, K. Bartschat, S. F. Biagi, M. C. Bordage, A. V. Phelps, C. M. Ferreira, G. J. M. Hagelaar, W. L. Morgan, S. Pancheshnyi, V. Puech, A. Stauffer, O. Zatsarinny *J. Phys. D: Appl. Phys.* **2013**, *46*, 334001.
- [103] Z. Lj. Petrović, Z. M. Raspopović, V. D. Stojanović, J. V. Jovanović, G. Malović, T. Makabe, J. de Urquijo, *Appl. Surf. Sci.* **2007**, *253*, 6619.
- [104] A. V. Phelps, *J. Phys. Chem. Ref. Data* **1991**, *20*, 557.
- [105] L. G. Huxley, R. W. Crompton, "The Drift and Diffusion of Electrons in Gases", Wiley Interscience, New York **1974**.
- [106] J. J. Lowke, A. V. Phelps, B. W. Irwin *J. Appl. Phys.* **1973**, *44*, 4664.
- [107] C. Gorse, M. Capitelli, J. Bretagne, M. Bacal, *Chem. Phys.* **1985**, *93*, 1.
- [108] R. Celiberto, R. K. Janev, A. Laricchiuta, M. Capitelli, J. M. Wadehra, D. E. Atems, *Atomic Data Nucl. Data* **2001**, *77*, 161.
- [109] P. A. Sá, V. Guerra, J. Loureiro, N. Sadeghi, *J. Phys. D: Appl. Phys.* **2004**, *37*, 221.
- [110] G. M. Petrov, J. P. Matte, I. Pères, J. Margot, T. Sadi, J. Hubert, K. C. Tran, L. L. Alves, J. Loureiro, C. M. Ferreira, V. Guerra, G. Goussset, *Plasma Chem. Plasma Process.* **2000**, *20*, 183.
- [111] F. Tochikubo, Z. Lj. Petrović, S. Kakuta, N. Nakano, T. Makabe, *Jpn. J. Appl. Phys.* **1994**, *33*, 4271.
- [112] S. Wang, A. E. Wendt, J. B. Boffard, C. C. Lin, S. Radovanov, H. Persing, *J. Vac. Sci. Technol. A* **2013**, *31*, 021303.
- [113] D. P. Lymberopoulos, D. J. Economou, *J. Appl. Phys.* **1993**, *73*, 3668.
- [114] L. D. Pietanza, G. Colonna, V. Laporta, R. Celiberto, G. D'Ammando, A. Laricchiuta, M. Capitelli, *J. Phys. Chem. A* **2016**, *120*, 2614.
- [115] Ž. D. Nikitović, V. D. Stojanović, J. Paul Booth, Z. Lj. Petrović, *Plasma Sources Sci. Technol.* **2009**, *18*, 035008.
- [116] Z. Lj. Petrović, I. Simonovic, S. Marjanović, D. Bošnjaković, D. Maric, G. Malovic, S. Dujko, *Plasma Phys. Control. Fusion* **2016**, submitted.
- [117] A. Banković, S. Dujko, S. Marjanović, R. D. White, Z. Lj. Petrović, *Eur. Phys. J. D* **2014**, *68*, 127.
- [118] A. Banković, S. Dujko, R. D. White, J. P. Marler, S. J. Buckman, S. Marjanović, G. Malović, G. Garcia, Z. Lj. Petrović, *New J. Phys.* **2012**, *14*, 035003.
- [119] Z. Lj. Petrović, S. Marjanović, S. Dujko, A. Banković, G. Malović, S. Buckman, G. Garcia, R. White, M. Brunger, *Appl. Radiat. Isotopes* **2014**, *83*, 148.
- [120] S. Marjanović, A. Banković, R. D. White, S. J. Buckman, G. Garcia, G. Malović, S. Dujko, Z. Lj. Petrović, *Plasma Sources Sci. Technol.* **2015**, *24*, 025016.
- [121] G. Garcia, Z. Lj. Petrović, R. White, S. Buckman, *IEEE Trans. Plasma Sci.* **2011**, *39*, 2962.
- [122] S. Marjanović, M. Šuvakov, J. J. Engbrecht, Z. Lj. Petrović, *Nucl. Instrum. Methods Phys. Res. B* **2012**, *279*, 80.
- [123] M. R. Natisin, J. R. Danielson, C. M. Surko, *J. Phys. B: At. Mol. Opt. Phys. B* **2014**, *47*, 225209.
- [124] J. R. Danielson, D. H. E. Dubin, R. G. Greaves, C. M. Surko, *Rev. Mod. Phys.* **2015**, *87*, 247.
- [125] S. Marjanović, M. Šuvakov, A. Banković, M. Savić, G. Malović, S. J. Buckman, Z. Lj. Petrović, *IEEE Trans. Plasma Sci.* **2011**, *39*, 2614.
- [126] D. Bošnjaković, Z. Lj. Petrović, S. Dujko, *J. Instrum.* **2014**, *9*, P09012.
- [127] J. Teunissen, U. Ebert, *Plasma Sources Sci. Technol.* **2016**, *25*, 044005.
- [128] S. Nijdam, J. Teunissen, E. Takahashi, U. Ebert, *Plasma Sources Sci. Technol.* **2016**, *25*, 044001.
- [129] A. H. Markosyan, J. Teunissen, S. Dujko, U. Ebert, *Plasma Sources Sci. Technol.* **2015**, *24*, 065002.
- [130] S. Dujko, A. H. Markosyan, R. D. White, U. Ebert, *J. Phys. D: Appl. Phys.* **2013**, *46*, 475202.

# Gas breakdown and secondary electron yields<sup>\*</sup>

Dragana Marić<sup>a</sup>, Marija Savić, Jelena Sivoš, Nikola Škoro, Marija Radmilović-Radjenović, Gordana Malović, and Zoran Lj. Petrović

Institute of Physics Belgrade, University of Belgrade, Pregrevica 118, 11080 Belgrade, Serbia

Received 31 January 2014 / Received in final form 8 April 2014

Published online 23 June 2014 – © EDP Sciences, Società Italiana di Fisica, Springer-Verlag 2014

**Abstract.** In this paper we present a systematic study of the gas breakdown potentials. An analysis of the key elementary processes in low-current low-pressure discharges is given, with an aim to illustrate how such discharges are used to determine swarm parameters and how such data may be applied to modeling discharges. Breakdown data obtained in simple parallel-plate geometry are presented for a number of atomic and molecular gases. Ionization coefficients, secondary electron yields and their influence on breakdown are analyzed, with special attention devoted to non-hydrodynamic conditions near cathode.

## 1 Introduction

It is often said that atomic and molecular collisions define the physics of non-equilibrium (so-called low-temperature) plasma. However, in plasma modeling, where space charge and field profile effects intervene with atomic and molecular collisions, often it is claimed that the collisional cross sections, rate coefficients and swarm transport data do not need to be very accurate as the processes are so complicated that high accuracy is not required. Gas breakdown, on the other hand, is the point where inaccuracies of the atomic collision and swarm data are amplified and at the same time the conditions for the breakdown often define the operating conditions for the plasma. To illustrate this we may give an example that ionization rate enters the breakdown condition in exponent and also that rate is often exponentially dependent on the gas density normalized electric field  $E/N$ . The mean energy and the shape of the distribution function that define the rate (together with the cross section for ionization) are on the other hand strongly dependent on all relevant inelastic processes. Breakdown under DC fields and slowly varying AC fields also depends on surface collisions of ions and atoms. Thus, breakdown condition is a very sensitive projection of atomic and molecular collision and swarm transport physics onto the realm of plasma physics.

Gas breakdown has been studied over 100 years and yet many open issues still remain. In DC discharges, the breakdown is usually described by the standard Townsend's theory [1]. Within the past 20 years, with development of experimental and modeling techniques, it

became clear that the standard (basic Townsend's theory as depicted in the textbooks) theory of breakdown and low-current discharges (the so-called Townsend's regime) requires improvement. Phelps and coworkers [2–5] initiated a comprehensive revision of the theory in all its aspects.

This revision in the lowest current limit (breakdown) included taking into account the contribution of all feedback mechanisms and space-charge effects in breakdown and low-current discharges [5]. These authors only covered one gas (argon) with detailed analysis. This is why we felt that a survey of the existing well documented breakdown data would be of value as the basis for further study on the data and elucidation of the issues in use of secondary electron yields in plasma modeling. All of the presented results were obtained in our laboratory and an utmost care has been invested to avoid the usual problems in determining the breakdown data (often depicted as Paschen curves). Those include variable surface conditions, jumping straight into the glow discharge mode, recording the operating conditions for the glow discharge and also the uncertainties that arise from the long statistical delays in initiation of gas discharges.

For many years swarm experiments have represented the primary source of data for gas discharge modeling, which, on the other hand, was based on the transport theory for swarms. With only very few exceptions, the models are based on the hydrodynamic (in equilibrium with the electric field and spatially uniform) transport data. This is however not applicable in most breakdown experiments as the early stages of the breakdown occur before equilibration of the electron swarm. Thus we present also an analysis of electron excitation cross sections and studies of spatial profiles of emission to separate excitation by electrons and fast neutrals [6]. Our results also allow us to determine the width of the non-hydrodynamic region close to the cathode and the effective multiplication as

<sup>\*</sup> Contribution to the Topical Issue "Electron and Positron Induced Processes", edited by Michael Brunger, Radu Campeanu, Masamitsu Hoshino, Oddur Ingólfsson, Paulo Limão-Vieira, Nigel Mason, Yasuyuki Nagashima and Hajime Tanuma.

<sup>a</sup> e-mail: draganam@ipb.ac.rs

well as the approximate determination of the field distribution in dark Townsend discharges. These data all need to be applied to determine the secondary electron yields and in modeling of plasmas.

Over the past two decades determination of the secondary electron yields [6,7] has had renewed interests, for two reasons. First, a systematic survey [5] has been made of all the processes that participate to secondary electron production and it was shown that the basic assumption of Townsend's theory that ions produce the secondary electrons is correct only in a very narrow range of conditions, while photons and gas phase ionization by neutrals contribute to the secondary electron production in a much wider range of  $E/N$ . Most importantly, it became possible to model the observed secondary electron yields in the breakdown by using binary collision (beam to surface) data.

It was shown that it is not possible to use directly the binary collision (beam-surface) data for the analysis of gas discharges and low temperature plasmas as those would have specific distributions of all the relevant fluxes that otherwise might be connected through nonlinear relations. The analysis performed for the breakdown (where all fluxes are in linear relation to the initial flux of electrons) proved to be quite robust and still fit most of the data for the glow discharges [8,9]. Nevertheless, it is possible that for some gases or some plasmas, nonlinearities may prevail and the required model may depart from the breakdown model.

In this paper we present the data on breakdown voltages (shown as Paschen curves) for a large number of gases, we show some examples on how these data are coupled with Volt-Ampere ( $V$ - $A$ ) characteristics, and we proceed to determine secondary electron yields for rare gases (assuming ions to be the primary agent producing secondary electrons) with the inclusion of the effects of equilibration and proper determination of the ionization growth coefficient.

## 2 Breakdown voltages and Paschen curves

Breakdown is usually represented by a Paschen curve i.e. dependence of the breakdown  $V_b$  voltage on the  $pd$  (pressure  $p \times$  gap  $d$ ). Parameter  $pd$  is a scaling parameter proportional to the number of collisions over a unit distance. In this respect, a typical sharp increase of the breakdown voltage at low  $pd$ -s can be explained by the need to compensate for a small number of collisions. On the other hand, at high  $pd$ -s, due to a large number of collisions, breakdown voltage is increased in order to enhance energy gain between collisions, when mean free path is getting shorter and the energy gained between two collisions becomes smaller. In the range of the Paschen minimum, production of charges by ionization and secondary electron emission and losses by attachment, diffusion and drift are well balanced.

In Figure 1 Paschen curves for several atomic and molecular gases are presented. Measurements with  $H_2$ ,  $SF_6$ ,  $CF_4$ ,  $H_2O$  and  $C_2H_5OH$  vapours are taken with the

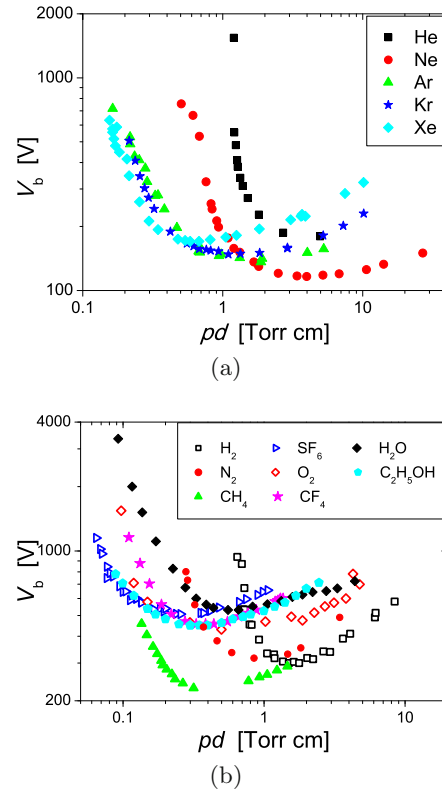


**Fig. 1.** Paschen curves for (a) atomic gases: Ar, He, Ne, Xe, Kr [6] and (b) molecular gases  $H_2$ ,  $SF_6$ ,  $O_2$ ,  $CH_4$ ,  $N_2$  [12],  $CF_4$  [10], and  $H_2O$  [11] and  $C_2H_5OH$  vapours. Measurements with  $H_2$ ,  $SF_6$ ,  $CF_4$ ,  $H_2O$  and  $C_2H_5OH$  vapours were obtained with copper cathode, for other gases stainless steel cathode was used.

copper cathode, with 1 cm electrode gap and 5.4 cm diameter [10,11]. For all other gases, stainless steel cathode was used in measurements in 2.9 cm gap and 8 cm electrode diameter [6,12]. Some of the data had preliminary presentation in the second edition of the textbook by Lieberman and Lichtenberg [13].

For most of the gases Paschen minimum is situated at  $pd$  of the order of 1 Torr cm and breakdown voltages are of the order of several hundred volts. In the case of electronegative gases, it is usually shifted towards smaller  $pd$ -s and higher voltages. This can be understood from the point of view of the balance of production and losses of charged particles. In electronegative gases, at low  $E/N$  i.e. high  $pd$ , attachment becomes important. As a loss mechanism for electrons, it will increase the breakdown voltage and shift the Paschen minimum to lower pressures as an even higher  $E/N$  is required to provide sufficient ionization.

There are several issues that one has to be aware of in breakdown measurements. Breakdown voltage depends on the gas mixture through identities of ions and on the cathode material. Even more important than the cathode material is the state of the cathode surface – roughness or possible oxide layers and other impurities deposited on its surface either by exposing the cathode to the laboratory environment or during the discharge operation. Sometimes

the state of the cathode surface has larger influence on the Paschen curve than the material of the cathode itself. For this reason, in our experiments cathode surfaces are treated in low-current ( $\sim 30 \mu\text{A}$ ) hydrogen discharge prior to the breakdown measurements. This procedure proved to give stable conditions during measurements and reproducible results over large periods of time. Even when basic breakdown voltage varies due to surface conditions, the Paschen curve (and also the  $V$ - $A$  characteristics) maintain their shape and so normalization onto the breakdown voltage is a good way to analyze the data [5,14].

Another issue that has to be taken into account in experiments is the regime in which the discharge ignites. Breakdown voltage should not be confused with the operating voltage. The point where the discharge operates is at the crossing of the circuit load-line and the Volt-Ampere characteristics. Quite often, especially with a small series resistance and sufficiently large overvoltages, this is in the regime of a glow discharge, where voltage can be significantly smaller than the breakdown voltage. Actual breakdown voltage, in the sense that is represented by the Paschen law, can only be found by extrapolating Volt-Ampere characteristics to zero current in the dark Townsend discharge mode. An alternative technique is to study the pre-breakdown currents [15,16]. Sometimes it is even necessary to record the spatial profile of the discharge in order to confirm the exponential increase of emission from the cathode all the way to the anode, which is typical for low-current Townsend discharge.

It is important to emphasize that, besides the Paschen curves, Volt-Ampere characteristics are essential in understanding the process of breakdown. These data are needed to establish the electric field/energy dependence of the secondary electron yields and as a consequence the slope of the  $V$ - $A$  characteristics in the Townsend regime is defined. The slope of the characteristics is typically negative in the low-current region and it reveals the ion energy dependence of the secondary electron yield and field distortion due to the initial growth of space charge [2,3,17]. In practice, for a full description of the discharge a 3D plot should be constructed [18], such as the one shown in Figure 2, with discharge voltage ( $V$ ), pressure  $\times$  electrode gap product ( $pd$ ) and discharge current ( $i$ ) presented at the axes.

Low-current limit represents Paschen curve and in this case it is projected onto  $1 \mu\text{A}$  as further changes of voltage at even lower currents would be negligible. Measurements are taken in a parallel-plate electrode system, with 1 cm gap, 5.4 cm electrode diameter and copper cathode. Considerable difference between the glow regime and Townsend regime voltages is clearly seen from the characteristics.

### 3 Model of the gas breakdown and secondary electron yields

Secondary electron emission is one of the key mechanisms of DC breakdown and operation of discharges. Still, there

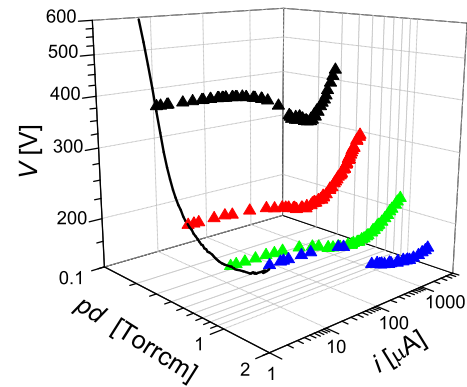


Fig. 2. Experimental  $V$ - $A$ - $pd$  characteristics for argon.

is a great confusion in literature in respect to the meaning of the data entering the breakdown condition. In fact, the secondary electron yield data obtained from the gas breakdown have always failed to match the direct measurements in the binary beam-surface experiments. As Phelps and Petrović [5] confirmed in the case of argon, the basic phenomenology of Townsend's theory required extension. Almost constant secondary yield of around 8% for argon ions that has been obtained by ion beams on surfaces cannot be applied to model even the basic low pressure breakdown. While one could justify a greater secondary yield due to additional processes, in the main section of mean energies the yield is actually ten times smaller than that from beam measurements. Phelps and Petrović developed a comprehensive model for argon that included all possible feedback mechanisms – secondary emission by ions, metastables, fast neutrals and photons. They also included back-diffusion of electrons and discussed conditions at the surface where standard gas discharge experiments cannot reach the conditions defined for atomically clean surfaces in ultra-high vacuum. Their study showed that one has to take into account energy dependent yields for each of the species from binary experiments in order to be in accordance with results of direct breakdown measurements. Here, we shall follow the standard procedure to determine secondary yields from the breakdown data and we shall also try to correct some of the problems and provide the data required for such corrections.

Under the conditions of the breakdown and low-current Townsend discharges, the effective secondary emission yield ( $\gamma$ ) is related to the ionization coefficient ( $\alpha$ ) in accordance with the Townsends self-sustaining condition:

$$\gamma = \frac{1}{e^{(\alpha/N) \times Nd} - 1} \quad (1)$$

where  $N$  represents the gas number density and  $d$  is the gap between the electrodes.  $\gamma(E/N)$  may be deduced from Paschen curves by using  $\alpha/N(E/N)$  data from the literature [19] as was done in [6]. One may also use an analytic form of  $\alpha/N(E/N)$ , e.g. Marić et al. [20], as it was shown in [21]. This procedure is the standard one. Perhaps the most important problem in the procedure is that

the non-hydrodynamic region close to the cathode ( $d_0$ ) affects the total multiplication, and therefore the secondary electron yield obtained from the Paschen curve. The second problem is that the ionization rate taken from the literature may give quite different multiplication as compared with the actual experiment. Even small errors in ionization coefficient result in large discrepancies of the secondary electron yield.

#### 4 Determination of the equilibration distance

It is well-known that hydrodynamic conditions are characterized by transport coefficients that are constant in space and time [22]. However, in low-current electrical discharges at low pressures electrons do not reach the equilibrium state immediately after leaving the cathode. Only at a certain distance from the cathode electrons establish equilibrium with the gas and parameters of electron transport become spatially independent [23,24]. In a simplified approach the width of the non-hydrodynamic region may be used to separate discharge into two regions: one that can be referred to as the non-equilibrium region, with no ionization and the other where ionization behaves as if electrons are in hydrodynamic equilibrium. The problem is then how to determine the delay distance from independent measurements, by using semi-empirical formula such as the one suggested by Phelps and Petrović [5] or by kinetic calculations.

It was shown that inclusion of the effect of equilibration causes a large difference in secondary electron yield data [5], but most authors in the available literature obtain the secondary electron yields from the breakdown data without paying attention to this correction. The role of the equilibration length in determination of the secondary electron yield was studied by Folkard and Haydon [24]. A more detailed discussion of the application of the delay distance and correct determination of the effective electron yield have already been published for the case of argon [6] and for nitrogen [21].

The appropriate form of multiplication factor under Townsend's breakdown conditions is [5]:

$$\gamma = \frac{1}{e^{\alpha(d-d_0)} - 1} \quad (2)$$

where  $d$  is the gap between electrodes, and  $d_0$  is the delay distance which has to be passed before electrons reach hydrodynamic equilibrium allowing avalanching characterized by the equilibrium ionization coefficient  $\alpha$ . As there is a great need to determine accurate yield coefficients for plasma modeling, there is also a need to establish procedures to determine the equilibration distance.

In our experiments it is possible to obtain equilibration distances from spatial scans of emission. The width of the non-hydrodynamic region  $d_0$  may be used to separate the discharge into two regions. Figure 3 shows two examples of spatial profiles of emission which illustrate the procedure for determination of the equilibration distance and ionization coefficients. In the case of xenon, the non-hydrodynamic width is exhibited as a flat region close to

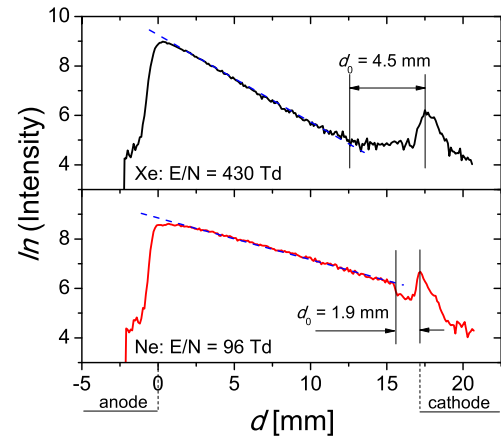


**Fig. 3.** Examples of the spatial emission profiles in xenon (upper plot) and neon (lower plot), with non-hydrodynamic regions indicated.

the cathode followed by exponential growth of emission. In the case of neon, there is even a sudden jump of emission just after the equilibration distance. It is still not clear what is the origin of emission in the region next to the cathode [25], as one would expect that there is no emission in non-equilibrium region. Growth of emission in hydrodynamic region is determined by a single exponential that is in excellent agreement with the equilibrium ionization coefficient [26]. While this is not the most accurate method to determine ionization coefficients, it is useful in some situations when the data are lacking and also to indicate the realistic conditions in a particular system which may be affected strongly by the contamination of the gas. Finally, this is the only direct way to obtain total multiplication as required by the breakdown theory.

When the spatial scans of emission are not available in the experiment that is being analyzed but were available for other experiments, the delay distance  $d_0$  can also be determined by using semi-empirical formulas such as that given in [5] through the expression for the effective value of the electrode potential difference before the exponential growth of the current:

$$V_0 = 16 \sqrt{1 + \left( \frac{E/N}{1000} \right)^2}. \quad (3)$$

Probably the best method to produce delay distances is by using Monte Carlo simulations. In this paper we apply a Monte Carlo code that has been well documented in previous publications (details can be found in [27,28]), so only a brief description will be given here. The code is based on generalized null-collision technique [29]. In the code we follow electrons released at the cathode until they reach the anode. The set of cross sections that is used involves inelastic (excitation) processes, ionization and elastic scattering. Each of these processes has associated differential cross sections that are necessary only to establish the angle of scattering. The probability of scattering is determined on the basis of the total cross section. From the simulation of the spatial profile of excitation, one may observe a region



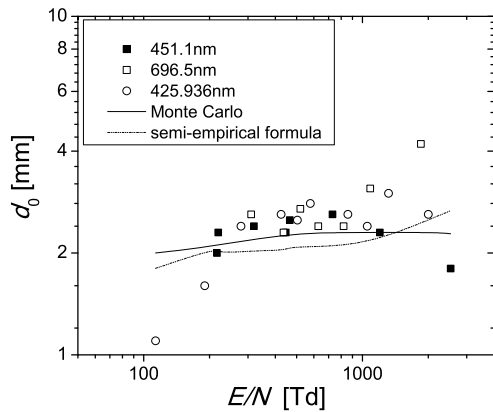


**Fig. 4.** The dependence of the delay distance  $d_0$  on the reduced field  $E/N$  for argon. The delay distances were obtained by three different techniques. Calculations were performed assuming isotropic angular distribution of electrons, the gap between the electrodes of 1.72 cm.

next to the cathode where excitation is zero, followed by an exponential growth of emission and finally a growth with the hydrodynamic ionization coefficient. The hydrodynamic region is extrapolated to the zero value and that point determines the distance as applied in equation (2).

In Figure 4 we compare results for the equilibration distance as a function of the reduced field  $E/N$  in argon obtained by experiment (symbols), Monte Carlo simulation (solid line) and semi-empirical formula (dashed line). The results obtained by using three different techniques show good agreement, except for the lowest and highest values of the reduced field. It is necessary to consider here the accuracy of experimental determination of the distance  $d_0$  at those values of  $E/N$ . At low values of  $E/N$  multiplication is very high and it is not so sensitive on the accuracy of determination of  $d_0$  which is small anyway. On the contrary, at high  $E/N$  i.e. low pressures, overall multiplication is small, so inclusion of  $d_0$  does not make significant difference. We may say that the agreement between the experimental data, semi-empirical formula and Monte Carlo simulations is excellent for the purpose of determining the secondary yield coefficients. Still, in experiment, due to reflection from the cathode and scatter of light, the results can be significantly scattered, as it is shown in Figure 4, so for the purpose of determination of secondary electron yields, we use results of Monte Carlo simulations when possible.

While Figure 4 shows results for equilibration distance along the Paschen curve, further on, we explore  $d_0$  behavior for the general non-self-sustained conditions. Pressure dependence of  $d_0$  at a fixed  $E/N$  is shown in Figure 5a and the  $E/N$  dependence at a fixed pressure in Figure 5b. In both cases, we present the results obtained using our Monte Carlo simulation code (curve) and semi-empirical formula (symbols). For a fixed reduced field, the delay continuously decreases as the gas number density (pressure) increases. On the other hand, the  $E/N$  dependence of the equilibration distance for a fixed gas number density (pressure) shows that the equilibration distance becomes

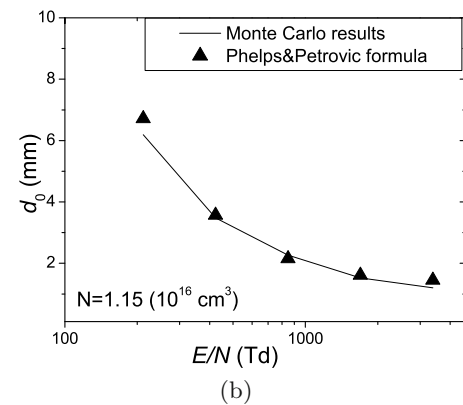
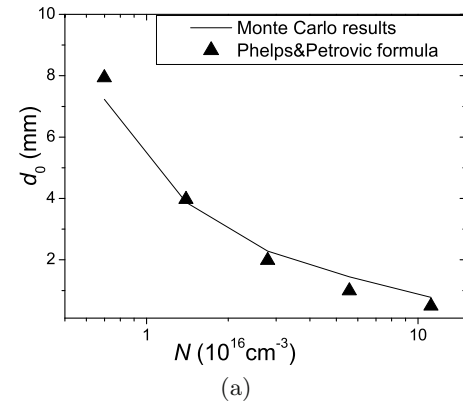


**Fig. 5.** The dependence of the delay distance on: (a) the gas number density for a fixed reduced field for argon; (b) the reduced field for a fixed gas number density for argon.

smaller as the reduced field increases (for a fixed gas number density). In both cases, the results obtained by semi-empirical formula and the Monte Carlo simulations are in satisfactory agreement. The experimental measurements are in fact less reliable than the simulation due to limited spatial resolution and possible scattering of light. Thus we really seek a general agreement and put our confidence in simulations. On the contrary, the measured exponential growth, if defined well and if not overlapping with the contribution of fast neutrals, provides better representation of multiplication in the actual experiment. Agreement between results proves that scaling for the equilibration employed in the development of the semi-empirical formula is appropriate.

In Figure 6 we show calculated equilibration distances for different gasses. We have performed analysis mainly for the rare gases and in a limited sense as compared to Phelps and Petrović [5]. Partly, the reason is that experimental determination of the delay distance in molecular gases is very difficult due to several sources of emission and complex quenching. In those gases we recommend Monte Carlo simulation of the whole system both the delay gap and the exponential growth. In Figure 6 it can be seen that the equilibration distance increases with the atomic mass; however it does not change much for a specific gas in the range of  $E/N$ -s investigated here.

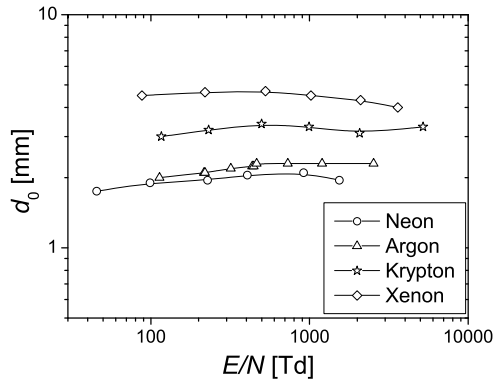


**Fig. 6.** Equilibration distances for different gases.

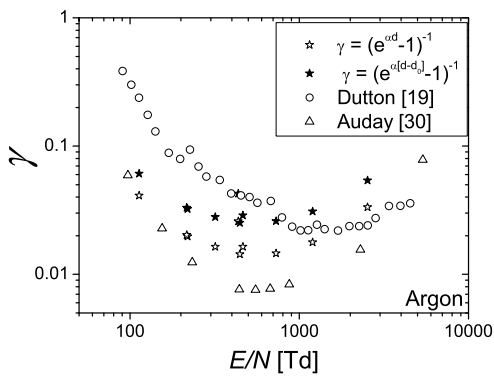


**Fig. 7.** Comparison of secondary electron yields for argon obtained with different data for ionization coefficients. The first three sets of data were obtained using our Paschen curve, the first two (stars) with our multiplication coefficient without and with the inclusion of the delay distance  $d_0$  in the analysis. The third set (circles) was obtained by using the ionization coefficients from [19] to determine the multiplication. The same ionization coefficients were used in the fourth set [30] but the basis for the results was their measurements of the Paschen curve.

## 5 Determination of the secondary electron yields and the role of ionization rate

As discussed in previous subsection, the non-hydrodynamic region near the cathode does not necessarily have a significant influence at very low and very high  $E/N$ . However, not taking into account the existence of non-equilibrium region can significantly change results for secondary electron yields in medium range of reduced electric fields. In Figure 7 we compare the secondary electron yields in argon obtained by taking into account and not taking into account the equilibration length  $d_0$  (solid and open stars respectively).  $\alpha/N(E/N)$  data obtained directly from the experiment are used here to determine  $\gamma$ . As expected, taking equilibration length into account has the largest effect close to the minimum and in the right branch as compared to the left branch. Yet, towards both ends the differences induced by including  $d_0$  diminish. The largest difference between the secondary yields with and without  $d_0$  is a factor of

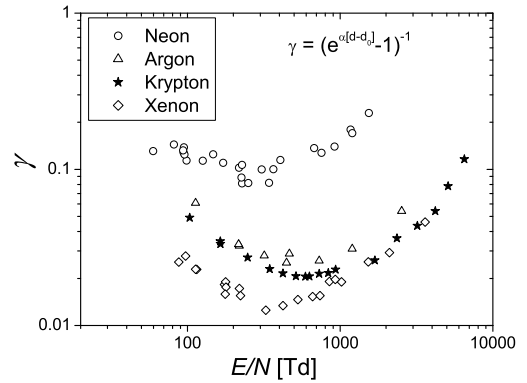


**Fig. 8.** Secondary electron yields for several different gases, with the same cathode surface (stainless steel).

two and it coincides with the minimum of the Paschen curve.

Taking the ionization rate from the literature may give a quite different multiplication as compared with the actual experiment and even small errors in the ionization coefficient result in large discrepancies of the secondary electron yield. In Figure 7 we also show secondary electron yields obtained from our Paschen curves by using ionization coefficients from the review [19] which are mostly based on experiments of Kruthiof (circles). These results are up to a factor of 10 different from our data mostly at high  $E/N$ .

We also show results of Auday et al. [30] who have analyzed their Paschen curve with the ionization rates from Dutton (triangles). Although those two sets of Paschen curves are apparently quite similar, the differences of yields are considerable, as large as a factor of 10.

For the low values of  $E/N$ ,  $\gamma$  in our experiment rises more strongly than those obtained by using values of  $\alpha/N$  from the literature. This can be explained by the fact that secondary emission of electrons can be due to any combination of numerous mechanisms of varying importance depending on the value of  $E/N$ . In the case of small values of  $E/N$ , dominant mechanism is the photoelectron emission.

Finally, a similar analysis for the secondary electron yields has been carried out for several other gases. In Figure 8 we show only final results obtained by using the most complete (correct) procedure. As expected the yield increases presumably proportional to potentials of the ion and the metastable states.

## 6 Conclusions

Measurements of properties of low-current discharges which include Paschen curves, Volt-Ampere characteristics and spatial profiles of emission proved to be a fertile basis for modeling of plasmas and discharges. In this paper we gave a short overview of the results of our breakdown studies covering five rare gases and eight molecular gases. We pointed out the most important issues in deducing secondary electron yields from the breakdown and swarm

experiments, compared results obtained by employing different procedures and we presented results for secondary yields for several rare gases obtained by a proper procedure. One should bear in mind that in this analysis the effective coefficients are attached to ion fluxes and a more thorough analysis along the same lines as done by Phelps and Petrović [5] should be performed for all gases together with an analysis of the applicability of the data in higher current discharges.

In conclusion, we may say that the treatment of electron non-equilibrium motion near the cathode includes determination of the delay in reaching the hydrodynamic rates of electron excitation and ionization. The results obtained when the equilibration distance is accounted for allow us to conclude that not taking into account the non-equilibrium region and correct values of ionization coefficients one may make quite large errors in obtaining secondary yields for the relevant particles in the discharge. These differences between the  $\gamma$  coefficients may result in some of the discrepancies between the swarm and the binary collision technique data for  $\gamma$  coefficients, which remains yet to be analyzed.

Monte Carlo simulation provides complete representation of non-equilibrium effect and influence of the electrodes and it is exact representation of breakdown itself, so it should be employed for modeling. A satisfactory agreement between the experimental data and the results obtained using Monte Carlo simulation code and semi-empirical formula proves that our treatment of the electron non-equilibrium behavior close to the cathode is accurate. It also became possible to make more direct comparisons between the secondary electron yields obtained from Paschen's law and from experiments consisting of a beam of ions hitting the surface under high vacuum conditions and separate detailed analyses should be made for all gases that are of interest.

This work was supported by MESTD ON171037 and III41011 projects.

## References

1. J.S. Townsend, *The Theory of Ionization of Gases by Collision* (Constable, London, 1910)
2. Z.Lj. Petrović, A.V. Phelps, Phys. Rev. E **47**, 2806 (1993)
3. A.V. Phelps, Z.Lj. Petrović, B.M. Jelenković, Phys. Rev. E **47**, 2825 (1993)
4. Z.Lj. Petrović, A.V. Phelps, Phys. Rev. E **56**, 5920 (1997)
5. A.V. Phelps, Z.Lj. Petrović, Plasma Sources Sci. Technol. **8**, R21 (1999)
6. G. Malović, A. Strinić, S. Živanov, D. Marić, Z.Lj. Petrović, Plasma Sources Sci. Technol. **12**, S1 (2003)
7. L.C. Pitchford, C. Pedoussat, Z. Donko, Plasma Sources Sci. Technol. **8**, B1 (1999)
8. D. Marić, K. Kutasi, G. Malović, Z. Donkó, Z.Lj. Petrović, Eur. Phys. J. D **21**, 73 (2002)
9. D. Marić, P. Hartmann, G. Malović, Z. Donko, Z.Lj. Petrović, J. Phys. D **36**, 2639 (2003)
10. N. Škoro, J. Phys.: Conf. Ser. **399**, 012017 (2012)
11. N. Škoro, D. Marić, G. Malović, W.G. Graham, Z.Lj. Petrović, Phys. Rev. E **84**, 055401(R) (2011)
12. V. Stojanović, J. Božin, Z.Lj. Petrović, B.M. Jelenković, Phys. Rev. A **42**, 4983 (1990)
13. M.A. Lieberman, A.J. Lichtenberg, *Principles of plasma discharges and materials processing*, 2nd edn. (John Wiley & Sons Inc., Hoboken, 2005)
14. I. Stefanović, J. Berndt, D. Marić, V. Šamara, M. Radmilović-Radjenović, Z.Lj. Petrović, E. Kovačević, J. Winter, Phys. Rev. E **74**, 026406 (2006)
15. R.W. Crompton, J. Dutton, S.C. Haydon, Nature **176**, 1079 (1955)
16. A.N. Prasad, J.D. Craggs, Proc. Phys. Soc. **76**, 223 (1960)
17. M. Nikolić, A. Djordjević, I. Stefanović, S. Vrhovac, Z.Lj. Petrović, IEEE Trans. Plasma Sci. **31**, 717 (2003)
18. V.I. Kolobov, A. Fiala, Phys. Rev. E **50**, 3018 (1994)
19. J. Dutton, J. Phys. Chem. Ref. Data **4**, 727 (1975)
20. D. Marić, M. Radmilović-Radenović, Z.Lj. Petrović, Eur. Phys. J. D **35**, 313 (2005)
21. V.Lj. Marković, S.R. Gocić, S.N. Stamenković, Z.Lj. Petrović, Eur. Phys. J. Appl. Phys. **30**, 51 (2005)
22. Z.Lj. Petrović, S. Dujko, D. Marić, G. Malović, Ž. Nikitović, O. Šašić, J. Jovanović, V. Stojanović, M. Radmilović-Radjenović, J. Phys. D **42**, 194002 (2009)
23. J. Fletcher, J. Phys. D **18**, 221 (1985)
24. M.A. Folkard, S.C. Haydon, J. Phys. B **6**, 214 (1973)
25. A.V. Phelps, B.M. Jelenković, Phys. Rev. A **38**, 2975 (1988)
26. Z.M. Jelenak, Z.B. Velikić, Z.Lj. Petrović, B.M. Jelenković, Phys. Rev. E **47**, 3566 (1993)
27. V.D. Stojanović, Z.Lj. Petrović, J. Phys. D **31**, 834 (1998)
28. M. Radmilović, Z.Lj. Petrović, Eur. Phys. J. Appl. Phys. **11**, 35 (2000)
29. H.R. Skullerud, J. Phys. D **1**, 1567 (1968)
30. G. Auday, P. Guillot, J. Galy, H. Brunet, J. Appl. Phys. **83**, 5917 (1998)

# On Explanation of the Double-Valued Paschen-Like Curve for RF Breakdown in Argon

Marija Savić, Marija Radmilović-Radjenović, Milovan Šuvakov, Srdjan Marjanović, Dragana Marić, and Zoran Lj. Petrović

**Abstract**—This paper represents an investigation of the dependence of the breakdown voltage on the gas pressure in radio-frequency argon discharges under conditions when ion-induced secondary electron production is negligible. Calculations were performed by using a Monte Carlo collision code including electrons only. Our simulation results clearly show a region, occurring at low pressure, where multiple values of the breakdown voltage exist at a given pressure, in agreement with previous experimental observations. The two different regimes of operation, each satisfying the breakdown condition, may be best analyzed in contour plots of electron density, ionization rate, and mean energy.

**Index Terms**—Breakdown, Monte Carlo (MC) simulations, radio frequency (RF) discharges.

**G**AS breakdown is the first step in the generation of plasma and therefore is one of the most fundamental processes [1]. In studies of the breakdown characteristics of gas discharges, the usual observable that is modeled is the Paschen curve. This breakdown voltage curve represents a balance between the number of electrons lost by diffusion and drift in the interelectrode gap and the number of secondary electrons generated at the cathode.

In the case of radio frequency (RF) discharges, it is actually possible to achieve self-sustained operation with electrons only, as the field changes direction. The Paschen-like breakdown voltage dependence is similar in shape to that of the dc discharges. The breakdown voltage generally forms a curve with unique values for each  $pd$ . Under certain circumstances, the left-hand branch of the curve exhibits a multivalued nature, i.e., a single  $pd$  corresponds to two different breakdown voltages [2]. In other words, on lowering the pressure, the breakdown voltage first decreases, passing through a minimum on the breakdown curve, before increasing to approach a turning point on the breakdown curve [2]. Lisovski and Yegorenkov [2] assert that, at this turning point, the electrons will drift exactly one-half of the gap in a one-half period of the field and are therefore all going to be swept to the electrodes. At a pressure lower than the turning point, it becomes impossible to achieve breakdown for any value of the applied voltage (ignoring multipactor effect) period.

Manuscript received November 30, 2010; revised May 30, 2011; accepted May 30, 2011. Date of publication July 22, 2011; date of current version November 9, 2011. This work was supported by the MNTRS Project 171037.

The authors are with the Institute of Physics, University of Belgrade, 11080 Belgrade, Serbia (e-mail: smarija@ipb.ac.rs; marija@ipb.ac.rs; suki@ipb.ac.rs; msrdjan@ipb.ac.rs; draganam@ipb.ac.rs; zoran@ipb.ac.rs).

Color versions of one or more of the figures in this paper are available online at <http://ieeexplore.ieee.org>.

Digital Object Identifier 10.1109/TPS.2011.2159244

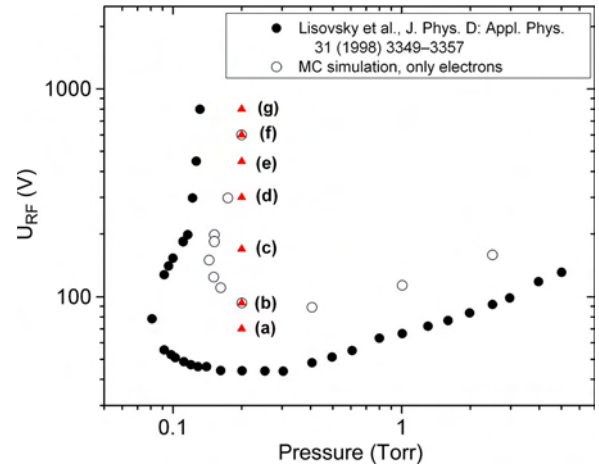


Fig. 1. Breakdown voltage versus the gas pressure in argon RF discharges at 13.56 MHz and the gap size of 2.3 cm. The (solid circles) experimental data taken from [2] are compared with (open circles) our MC simulation results taking into account electrons only. Calculations were performed for the pressure of 0.2 torr and five different voltages (red symbols).

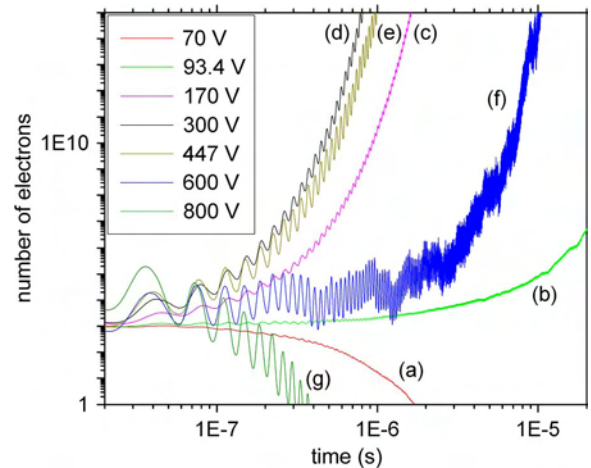


Fig. 2. Time dependence of the number of electrons for the conditions shown by red symbols in Fig. 1.

The purpose of this paper is to model the RF breakdown in an electron-dominated regime (with negligible effects of ions and multipacting) and try to understand the basic phenomenology by employing kinetic representation.

A Monte Carlo (MC) code used for the studies of RF breakdown is developed and tested in our group. The code follows the transport of electrons across the gap between electrodes. The cross-sectional set consisting of momentum transfer, two excitation, and ionization cross sections has been well tested



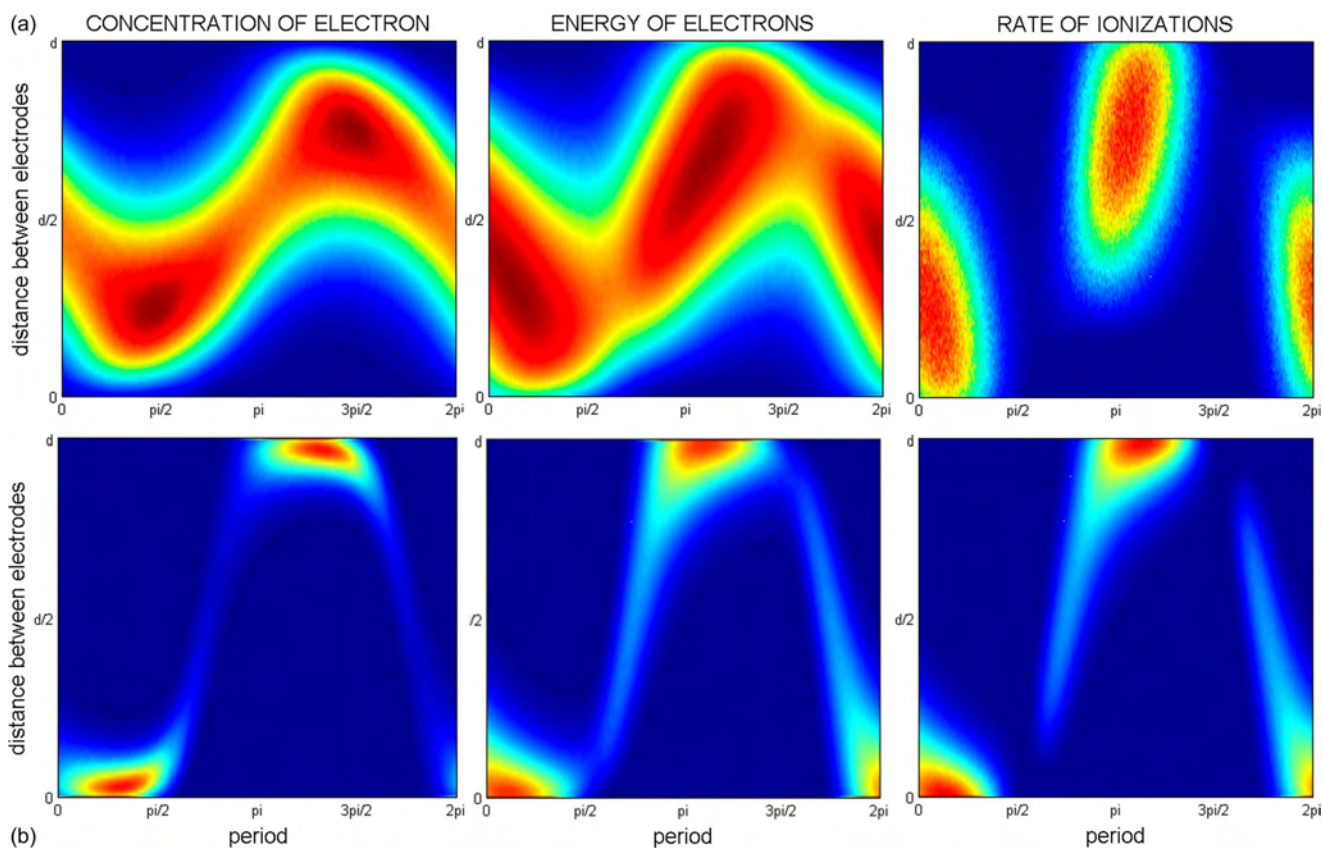


Fig. 3. Changes of various characteristics (the electron concentration, the electron energy, rates of elastic scattering and ionizations, respectively) during one period along the vertical  $pd = \text{const}$  line. Calculations were carried out in argon at 13.56 MHz, 0.2 torr, and voltages of (a) 93.4 V and (b) 600 V both satisfying the breakdown criterion as seen in Fig. 2.

for argon swarms [3]. We start the simulation with 100 000 electrons and follow the development. In the case of fast ionization or losses, we rescale the numbers but weight the number density.

Breakdown is essentially determined in the same way as that in experiment, i.e., by slowly increasing the voltage to approach from below the curve and by increasing the pressure to approach higher voltage values in the double-value region. We set out to establish the differences between two points satisfying breakdown for the same  $pd$ . The voltage or pressure steps close to the breakdown are very slow, and the uncertainty of the breakdown voltage is on the order of 0.1 V. Simulations are performed for the experimental conditions in [2].

In Fig. 1, we show the simulated Paschen curve; in shape, we get agreement with the experiment, but apparently, our turning point occurs at higher pressure. Slight differences may be explained by the fact that we neglected ion motion and secondary electron production, as well as electron reflection and secondary electron production by energetic electrons. Also, some possible experimental uncertainties could lead to the differences. In any case, the two-value behavior of the Paschen curve is confirmed, and agreement with experiment in that respect is reasonable. In Fig. 2, we show the curves representing the time dependence of electron density, and curves (b) and (f) are the first curves with the positive growth in their own conditions (93.4 and 600 V). In between these points, growth is extreme, and outside, the curve electron density decays.

The spatial profiles (see Fig. 3) of the swarm properties are shown for two stable breakdown points (b and f), and the profiles are quite different. For the lower voltage, one needs to achieve sufficient ionization to compensate for the losses, and therefore, any increase in voltage leads to a higher ionization. In both cases, most of the electrons are produced in proximity of the electrodes. For the higher breakdown voltage, one can see that most of electrons are pushed to the electrode by the strong field, and therefore, losses have increased sufficiently to compensate excessive production by ionization. Any further increase of voltage will make losses greater than production by ionization. It also becomes critical to observe where ionization occurs and the degree of multiplication that is allowed to develop before electrons are lost.

Kinetic representation of RF breakdown not only reveals details of phenomenology but also provides tools to convert experimental breakdown data into relevant coefficients.

## REFERENCES

- [1] A. V. Phelps and Z. L. Petrović, "Cold-cathode discharges and breakdown in argon: Surface and gas phase production of secondary electrons," *Plasma Sourc. Sci. Technol.*, vol. 8, no. 3, pp. R21–R44, Aug. 1999.
- [2] A. V. Lisovskiy and V. D. Yegorenkov, "RF breakdown of low-pressure gas and a novel method for determination of electron-drift velocities in gases," *J. Phys. D, Appl. Phys.*, vol. 31, no. 23, pp. 3349–3357, Dec. 1998.
- [3] Z. L. Petrović, M. Šuvakov, Ž. Nikitović, S. Dujko, O. Šašić, J. Jovanović, G. Malović, and V. Stojanović, "Kinetic phenomena in charged particle transport in gases, swarm parameters and cross section data," *Plasma Sources Sci. Technol.*, vol. 16, no. 1, pp. S1–S12, Feb. 2007.



# Numerical Modeling of Thermalization of Positrons in Gas-Filled Surko Traps

Srdjan Marjanović, Milovan Šuvakov, Ana Banković, Marija Savić, Gordana Malović, Stephen J. Buckman, and Zoran Lj. Petrović

**Abstract**—In this paper, we present the results of our Monte Carlo-based numerical simulation of a Penning–Malmberg–Surko positron trap. The results of simulations show the effect that various processes (such as positronium (Ps) formation, annihilation, losses on walls, etc.) have on trapping efficiency. The thermalization profile is shown, along with the evolution of the energy distribution that morphs from a particle beam to a broad swarm-type distribution.

**Index Terms**—Buffer gas trap, numerical simulation, particle beams, positrons.

**B**UFFER GAS traps are a general prerequisite for the study of cold positrons and their interaction with matter. Penning–Malmberg–Surko traps [1] and their variations [2] have shown excellent performance and are widely accepted as an ideal tool for atomic and molecular collision physics and material science diagnostics. The gas most commonly used for trapping is  $N_2$  because its electronic excitation cross sections are comparable to or larger than those for positronium formation in the near-threshold region. A small portion of  $CF_4$  is used in the last stage of the trap in order to speed up the thermalization at lower energies through vibrational scattering.

Our model consists of three cylindrical stages with varying radii to achieve different pressures. Positrons are moving through them, accelerating, and decelerating along the axis as they fall in, and climb out of, potential wells. An axial magnetic field is applied for beam confinement.

The Monte Carlo method, tested on numerous electron benchmarks, is used for simulating the collisions with the buffer gas. The potential of the electrodes was set so that each stage of the trap (I, II, and III) had the well depths of 10, 11, and 12 eV and pressures of  $10^{-3}$ ,  $10^{-4}$ , and  $10^{-6}$  torr, respectively. The buffer gas is  $N_2$  with 10% of  $CF_4$  in the third stage. These traps have strong axial magnetic field and cylindrical symmetry

Manuscript received November 30, 2010; revised May 26, 2011; accepted May 28, 2011. Date of publication July 5, 2011; date of current version November 9, 2011. This work was supported by the MNTR, Serbia, under Contracts ON171037 and III41011.

S. Marjanović, M. Šuvakov, A. Banković, M. Savić, G. Malović, and Z. Lj. Petrović are with the Institute of Physics, University of Belgrade, 11080 Belgrade, Serbia (e-mail: msrdjan@ipb.ac.rs; suki@ipb.ac.rs; anchuga@ipb.ac.rs; smarija@ipb.ac.rs; malovic@ipb.ac.rs; zoran@ipb.ac.rs).

S. J. Buckman is with CAMS, ANU, Canberra, A.C.T. 0200, Australia (e-mail: stephen.buckman@anu.edu.au).

Color versions of one or more of the figures in this paper are available online at <http://ieeexplore.ieee.org>.

Digital Object Identifier 10.1109/TPS.2011.2159129

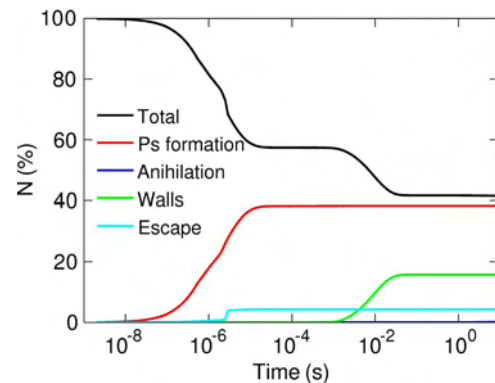


Fig. 1. Number of particles in the trap and loss processes. The process of annihilation is negligible on this timescale.

with three stages at different potentials and gas pressures [1], [2] which were selected to be similar with the setup in [1]. Cross sections for  $e^+ - N_2$  may be found in [3]. We normally release between 10 000 and 100 000 particles, and the simulations last several hours.

The positrons enter the first stage with an energy width of 1 eV and are accelerated to an energy of 10 eV in the first potential well. Particles that make the trip through the well, bounce off the potential wall, return, and still have energy over 10 eV are lost and are represented in Fig. 1 as *escaped*. The most important loss process, as shown in Fig. 1, is *positronium formation*. *Escape* and *losses to walls* can be diminished by changing the geometry of the trap and the combination of gas pressures and magnetic field. As the positrons suffer more and more collisions, their mean energy drops down (see Fig. 2).

In order to understand the performance of the trap, one needs to visualize the positron energy distribution development (see Fig. 2) which starts as a 10-eV beam. As particles enter stages II and III, they gain energy, but meanwhile, around 8 eV is lost due to electronic excitation of the  $N_2$  molecule. This leads to the splitting of the original beam into several beams (see Fig. 2) that combine together as they cool down and become a particle swarm with a broad energy distribution and a mean energy that eventually becomes close to thermal (see Fig. 2), and the distribution becomes a Maxwell–Boltzmann distribution.

The initial width of the beam is 1 mm, and it expands up to 6 mm. The particles on the front, leading the expansion, are those that scatter and transfer most of their energy to the transverse plane. These results are shown in Fig. 3 where a 3-D plot gives the magnitude of the perpendicular energy as

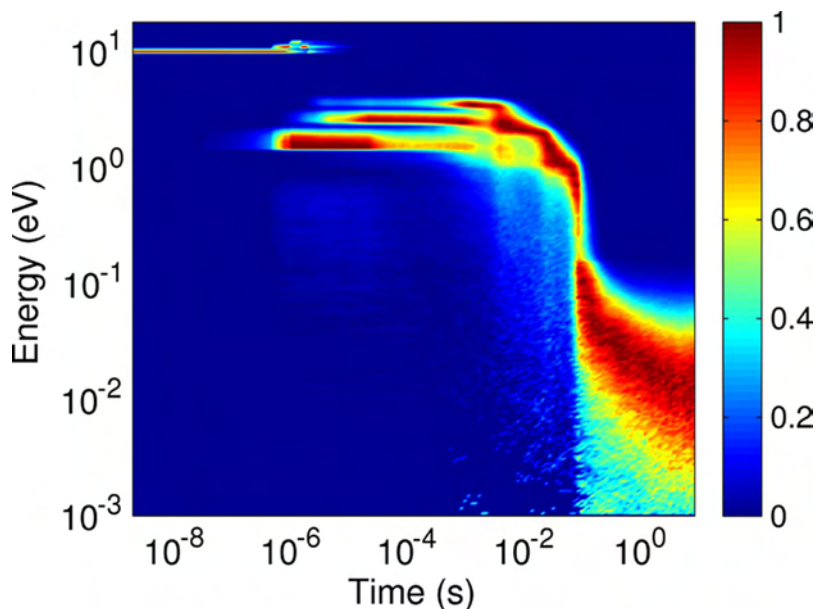


Fig. 2. Evolution of the positron kinetic energy distribution over time. Distributions are normalized for better presentation over a wide dynamic range.

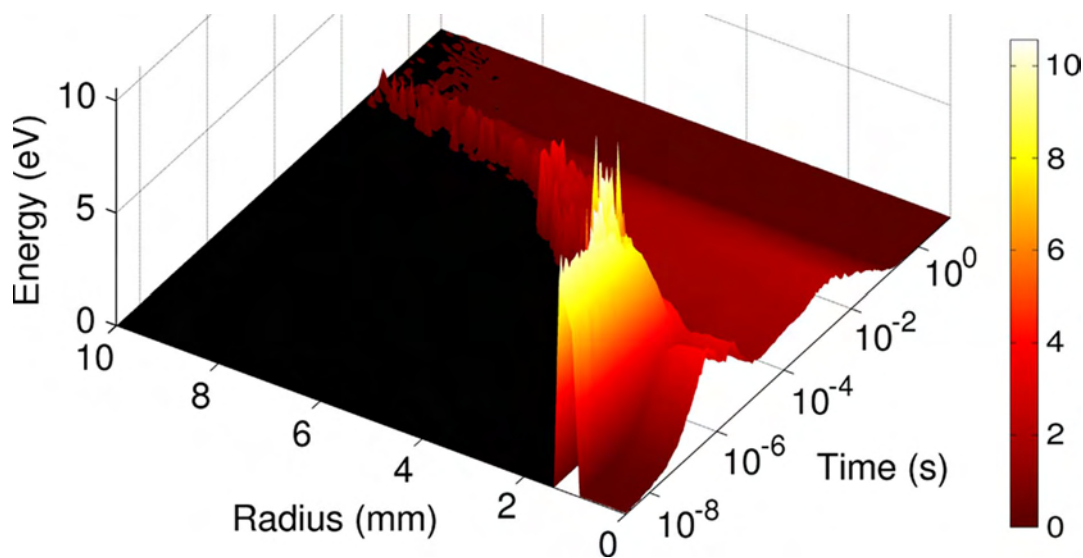


Fig. 3. Radial distribution of the transversal kinetic energy, impacting the rate of the widening of the beam and the amount of loss to the walls.

a function of spatial position. The leakage to the side walls is generated mainly by the particles with high perpendicular scattering in the last stage, in spite of the fact that higher perpendicular energies may be found in the initial stages when the beam still has mostly the original radius. The losses are mainly due to the very long time that positrons spend in the last stage due to the need to employ rotational excitation and elastic scattering to achieve the last stages of thermalization below 100 meV.

Modeling of the Surko trap by the electron-swarm-related Monte Carlo code works well because of the similar nature of the electron-molecule and positron-molecule scattering. The functioning of the trap may be best visualized with temporally resolved results for positron positions, energy distributions

of the particles, and losses. Thus, the code becomes a tool that may provide means to optimize the trap further. This may be accomplished, to a large degree, by observing visual information.

#### REFERENCES

- [1] C. M. Surko and R. G. Greaves, "Emerging science and technology of antimatter plasmas and trap-based beams," *Phys. Plasmas*, vol. 11, no. 5, pp. 2333–2348, May 2004.
- [2] J. P. Sullivan, A. Jones, P. Caradonna, C. Makochekanwa, and S. J. Buckman, "A positron trap and beam apparatus for atomic and molecular scattering experiments," *Rev. Sci. Instrum.*, vol. 79, no. 11, p. 113 105, Nov. 2008.
- [3] A. Banković, J. P. Marler, M. Šuvakov, G. Malović, and Z. L. Petrović, "Transport coefficients for positron swarms in nitrogen," *Nucl. Instrum. Methods Phys. Res. B*, vol. 266, no. 3, pp. 462–465, Feb. 2008.

# Microwave Field Strength Computing for the Resonator Designs and Filters

M. RADMILOVIĆ-RADJENović\*, B. RADJENović AND M. SAVIĆ  
Institute of Physics, University of Belgrade, Pregrevica 118, 11080 Zemun, Serbia

(Received March 29, 2013)

Recent development of microwave pulse generators, which are now capable of delivering very short and very intensive pulses requires properly generalized classical breakdown theory. On the other hand, the trend to design microwave devices as small and compact as possible, leads to a concern about the concomitant breakdown strength of the construction, involving more complicated geometries, such as in microwave resonators and filters. In this paper, several aspects of microwave field strength in commercially available resonator designs and filters are presented and analyzed. The numerical predictions based on the Slater theorem are compared with the analytical results and predictions of the fluid approach, demonstrating very good agreement.

DOI: [10.12693/APhysPolA.129.289](https://doi.org/10.12693/APhysPolA.129.289)

PACS/topics: 52.80.-s, 52.90.+z

## 1. Introduction

Microwave breakdown in gases under various physical and technical conditions is well-known and intensively studied problem from early days of gaseous electronics [1–3]. More recent, interest in microwave-induced breakdown is shifted to studies of microwave breakdown at atmospheric pressures due to its relevance both for industrial applications [4–6] and for a deeper understanding of fundamental plasma behavior [7–9]. The microwave breakdown strength of the gas is useful information for high power filter and antenna engineering [10], for determination of the conductivity and dielectric constant of a plasma [11], for modification the ionosphere for long range radio propagation [12], etc. The microwave breakdown phenomenon provides both problems and opportunities reflected in the applications of the microwave breakdown theory. The application can be divided into two main categories: the so-called no-breakdown devices — where breakdown should be avoided for proper operation of the device and breakdown devices — where breakdown is an intrinsic feature of operation.

In numerous microwave devices, the geometrical configuration contributes to local strongly enhanced microwave fields. Such regions are potentially dangerous from the point-of-view of breakdown since the field here may be much stronger than the globally predicted breakdown field. On the other hand, a locally overcritical field does not necessarily imply global breakdown. In that case, the influence of local field enhancement on the global breakdown condition has to be included.

This paper contains result of our studies of the microwave induced dielectric breakdown of gases in a uniform electric field. Cavity resonators have often been used [13, 14], but field distributions are inhomogeneous,

resulting in a spatially dependent ionization rate and breakdown which is strongly influenced by the diffusion of charged particles out of the high electric field region.

## 2. Models

Several different models of the microwave breakdown criteria exist, with varying degree of accuracy in the description. Fluid models provide description with enough details that can be used in large classes of research becoming very important for technical applications [15]. On the other hand, the kinetic approach has potential to offer a very detailed description of the mechanism and represents the basis on which other models rely. The great details in descriptions, however, make the kinetic approach very complex and more useful in pure physical research with simplified geometry.

### 2.1. The Slater theorem for computing the electric field in the gap

The electric field inside a microwave resonator can be determined analytically based on an analytic solution to the Maxwell equations. The electric and magnetic fields inside a resonator have a complicated spatial variation, which nevertheless satisfies the Helmholtz wave equation under the constraints of the conductive boundary conditions. Analytic solutions of the electric and the magnetic fields exist only for a few simple cavity geometries. It is not usually possible to analytically find the magnitude of the fields inside most resonators, let alone their geometric distribution. The field strength can be determined numerically using full-wave electromagnetic field simulation [14].

The perturbation theory of Slater is used here to obtain the local electric field. Only a small fraction of the empty space inside an electromagnetic resonator is filled with the dielectric material with relative permittivity  $\epsilon_r$ , and relative permeability  $\mu_r$ . The interaction between the magnetic permeability of the material and the magnetic field of the resonator will cause the reactance to increase

\*corresponding author; e-mail: [marija@ipb.ac.rs](mailto:marija@ipb.ac.rs)

and thus raise the resonant frequency by the inductive loading. Likewise, the interaction between the electric permittivity of the material and the electric field of the resonator will cause the reactance to decrease and thus lower the resonant frequency by the capacitive loading. This frequency shift,  $f_0 - f$  can be expressed via the Slater theorem [14]:

$$\omega^2 = (2\pi f)^2 = \omega_0^2 \left[ 1 + \frac{\int_{\text{dielectric}} (\mu_0 \mu_r H^2 - \varepsilon_0 \varepsilon_r E^2) dV}{\int_{\text{cavity}} (\frac{1}{2} \mu_0 H^2 + \frac{1}{2} \varepsilon_0 E^2) dV} \right], \quad (1)$$

where  $H$  and  $E$  represent the magnetic and electric fields, respectively, while  $\omega_0 = 2\pi f_0$  is the original, unperturbed angular frequency. The top integral is evaluated over the dielectric perturbation, and gives the energy stored in the perturbation. The bottom integral is evaluated over the entire empty cavity and is equal to the peak energy stored per cycle in the resonator —  $U_0$ .

### 2.2. An analytical-experimental approach

There is also a simple complementary approach obtained by combination of an analytical and experimental investigations suggested in [13]. Actually, the method is based on experimental data of the breakdown voltages at low pressures and their extrapolation over a wide range of pressures. The expression for the breakdown voltage is written in the form [13]:

$$E_b = 3.75p \left[ 1 + \left( \frac{2\pi f}{\nu_c} \right)^2 \right]^{1/2} \left( \frac{D}{pL_D^2} + 6.4 \times 10^4 \right)^{3/16}, \quad (2)$$

where  $E_b$  represents the real rms electric field and the characteristic length  $L_D$  determines the curvature of the breakdown voltage curve.

### 2.3. Fluid approach

In the case of microwave electric fields, the continuity equation describes the time evolution of the electron density  $n_e$  which is

$$\frac{\partial n_e}{\partial t} = \nabla \cdot (D_e \nabla n_e) + \nu n_e, \quad (3)$$

where  $D_e$  is the electron diffusion coefficient and  $\nu$  is the net production rate of electrons per electron. The microwave breakdown can be determined as a balance between the ionization rate and the loss rate of electrons by diffusion mathematically formulated by relation [15]:

$$\nu_i = \frac{D_e}{\Lambda^2}, \quad (4)$$

with the characteristic diffusion length  $\Lambda$  depending on the geometry of the discharge vessel, i.e. radius  $R$  and height  $L$  in accordance with the expression

$$\frac{1}{\Lambda^2} = \left( \frac{2.4}{R} \right)^2 + \left( \frac{\pi}{L} \right)^2, \quad (5)$$

where the diffusion to the end plates is given by the first on the right, while the second term describes the diffusion to the cylindrical walls.

In general, the electron diffusion is anisotropic, but at very high frequencies the transverse and longitudinal diffusions become almost isotropic with the values nearly equal to the transverse one  $D_\tau$  at  $\omega \rightarrow 0$ . Therefore, in Eq. (3), the electron diffusion coefficient  $D_e$  can be replaced by the transverse diffusion coefficient  $D_\tau$  that corresponds to the dc field. Combining Eq. (3) with  $\nu_i = \alpha \mu E$ :

$$\frac{\varepsilon}{\Lambda^2} = \frac{\alpha E_r}{\sqrt{1 + \left( \frac{\omega}{\nu_c} \right)^2}}, \quad (6)$$

where  $\varepsilon = D_\tau/\mu$  represents the characteristic energy, while  $\mu$  is the electron mobility. When an ac electric field  $E_r \cos \omega t$  is applied in a weakly ionized gas, a dominant collision processes are electron-neutral collisions characterized by the collision frequency  $\nu_c$ . The frequency effect can be comprehended by introducing the effective field strength

$$E_{\text{eff}} = \frac{\nu_c}{\sqrt{\nu_c^2 + \omega^2}} E_r. \quad (7)$$

Finally, substituting expression for the first Townsend coefficient  $\alpha = Ap \exp(Bp/E_{\text{dc}})$  [15] and replacing  $E_{\text{dc}}$  by  $E_{\text{eff}}$  given by Eq. (6), we obtain expression for the electric field  $E_r$  as a function of the pressure  $p$ :

$$E_r = \frac{\varepsilon \sqrt{\omega^2 + \nu_c^2} \exp\left(Bp \sqrt{\omega^2 + \nu_c^2} / (\nu_c E_r)\right)}{\nu_c \Lambda^2 Ap}, \quad (8)$$

where  $\omega$  represents angular frequency of the applied field.

## 3. Results

Atmospheric plasma source based on a microstrip splitting resonator (MSSR) is depicted in Fig. 1 with a schematic view given in Fig. 2. We have modelled the

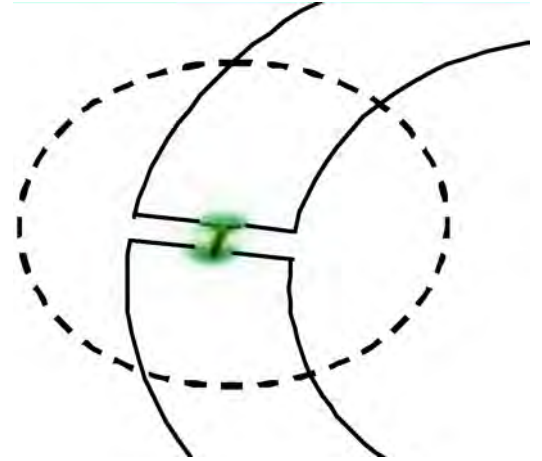


Fig. 1. Microstrip split-ring resonator.

electric field inside a microwave resonator numerically based on evaluation integrals in the Slater theorem. Coupling between electric and magnetic fields inside an electromagnetic resonator is demonstrated in Fig. 3. For the microwave threshold field of the gas which fills the resonator volume, however, the magnetic field is very low



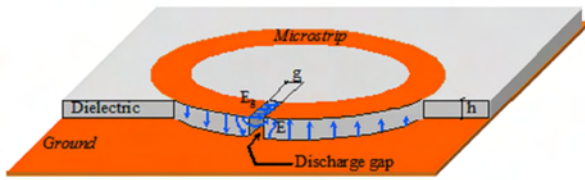


Fig. 2. Schematic view of microstrip split-ring resonator.

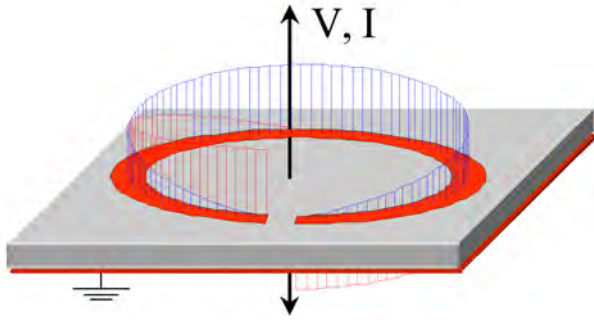


Fig. 3. Schematic view of split-ring resonator.

and can be neglected. Electric field can be treated as uniform over the volume of the dielectric. Calculated values of the magnitude of the electric field are shown in Fig. 4.

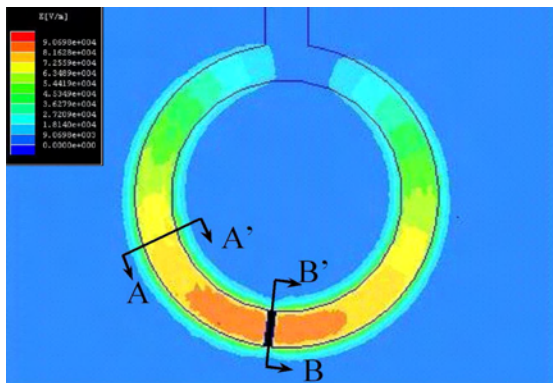


Fig. 4. Magnitude of the electric field.

The breakdown field strength as a function of pressure in nitrogen at microwave frequency of 1.85 GHz is shown in Fig. 5. Our numerical results are presented by solid line, while dot and dash lines correspond to the predictions obtained by using Eqs. (2) and (8), respectively. Theoretical predictions based on both analytical and fluid approaches provide relatively good results at lower pressures. Our numerical results, however, are in a good agreement with the data taken from [14] at all pressure values.

A good agreement between our numerical results (solid line) and results published in [14] (solid symbols) is also achieved for the pressure dependence of the breakdown field strength in nitrogen at 2.76 GHz at the temperature

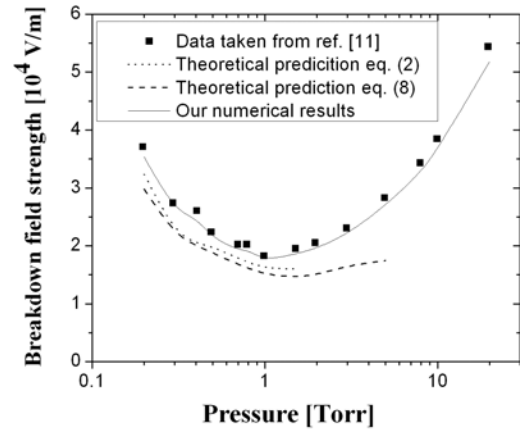


Fig. 5. The breakdown field strength versus the pressure in nitrogen at frequency of 1.85 GHz.

of 230 K (as can be seen from Fig. 6). Finally, how the pressure at the minimum breakdown voltage curve depends on frequency is illustrated in Fig. 7. As expected, there is a linear dependence indicating that the pressure at the minimum increases as the frequency is increased.

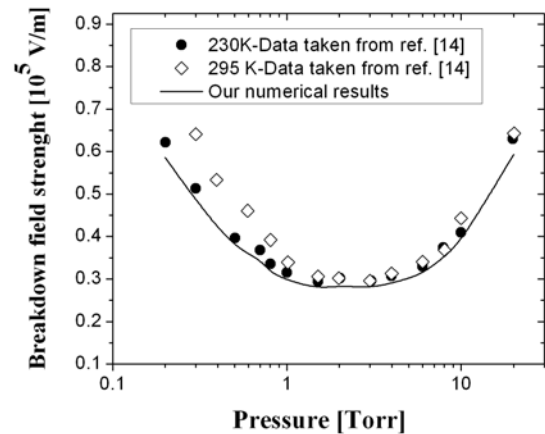


Fig. 6. The pressure dependence of the breakdown field strength in nitrogen at frequency of 2.76 GHz.

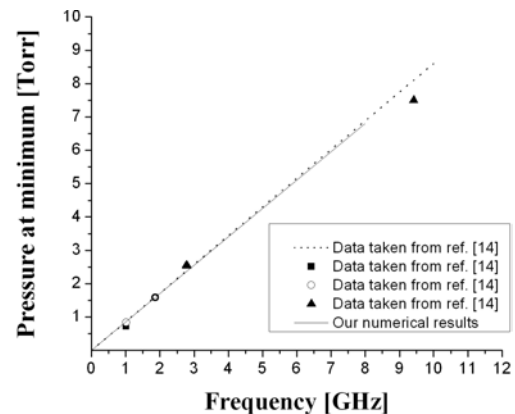


Fig. 7. The pressure at the minimum as a function of frequency in nitrogen.



#### 4. Conclusion

Nowadays, there is a growing interest in microplasma sources due to their economics, portability, less operation costs, and small sizes. The utility derived from macroscale plasmas combined with current microfabrication techniques has allowed for the development of microscale devices which use microdischarges for operation. Having in mind that relatively complicated geometrical configurations in microwave devices enhance the strong local microwave fields and such fields may be much stronger than the globally predicted breakdown field. This paper is devoted to our numerical studies of the microwave field strength computing in commercially available resonator designs and filters. Numerical method is based on Slater's theorem. Our numerical results satisfactorily agree with the available data [14] indicating their applicability for a wide range of parameters.

The results presented here, except for resonator and filters, can be also useful in localized diagnostics of ICs during their manufacture, in choosing appropriate conditions for electro mechanical micro systems which may eventually lead to nanomachining, in localized treatment of materials and assembly of nanostructures and in micro and nanobiological processing and diagnostics.

#### Acknowledgments

The work has also been carried out under by Ministry of Education and Science Republic of Serbia O171037 and III41011 projects.

#### References

- [1] M.J. Druyvestayn, F.M. Penning, *Rev. Mod. Phys.* **12**, 87 (1940).
- [2] D.Q. Posin, *Phys. Rev.* **73**, 496 (1948).
- [3] S. Krasik, D. Alpert, A.O. McCoubrey, *Phys. Rev.* **76**, 722 (1949).
- [4] F.C. Fehsenfeld, K.M. Evenson, H.P. Broida, *Rev. Sci. Instrum.* **36**, 294 (1965).
- [5] M. Radmilović-Radjenović, B. Radjenović, *Central Europ. J. Phys.* **9**, 265 (2011).
- [6] B. Radjenović, M. Milanović, M. Radmilović-Radjenović, *Phys. Scr. T* **149**, 014026 (2012).
- [7] W.P. Allis, S.C. Brown, *Phys. Rev.* **87**, 419 (1952).
- [8] H.J. Oskam, *J. Appl. Phys.* **27**, 848 (1956).
- [9] A.D. MacDonald, D.U. Gaskell, H.N. Gitterman, *Phys. Rev.* **130**, 1841 (1963).
- [10] F. Werner, D. Korzec, J. Engemann, *Plasma Sources Sci. Technol.* **3**, 473 (1994).
- [11] T. Fleisch, Y. Kabouzi, J. Pollack, E. Castañón-Martínez, H. Nowakowska, M. Moisan, *Plasma Sourc. Sci. Technol.* **16**, 173 (2007).
- [12] D. Anderson, U. Jordan, M. Lisak, T. Olsson, M. Ahlander, *IEEE Trans. Microwave Theory Techn.* **47**, 2547 (1999).
- [13] S.K. Remillard, A. Hardaway, B. Jork, J. Gilliland, J. Gibbs, *Progr. Electromagn. Res. B* **15**, 175 (2009).
- [14] M. Radmilovic-Radjenovic, J.K. Lee, F. Iza and G.Y. Park, *J. Phys. D: Appl. Phys* **38**, 950 (2005).
- [15] R. Tomala, U. Jordan, D. Anderson, M. Lisak, *Contr. Plasma Phys.* **46**, 287 (2006).

# The Role of the Field Emission Effect in the Breakdown Mechanism of Direct-Current Helium Discharges in Micrometer Gaps

Š. Matejčík<sup>1</sup>, M. Klas<sup>1</sup>, B. Radjenović<sup>2</sup>, M. Durian<sup>1</sup>, M. Savić<sup>2</sup>, and M. Radmilović-Radjenović<sup>2\*</sup>

<sup>1</sup> Department of Experimental Physics, Comenius University, Mlynski dolina F2, 84248 Bratislava, Slovakia

<sup>2</sup> Institute of Physics, University of Belgrade, Pregrevica 118, 11080 Zemun, Serbia

Received 24 May 2013, revised 11 June 2013, accepted 11 June 2013

Published online XXX 2013

**Key words** Field emission, microdischarges, breakdown mechanism.

This paper presents results of experimental studies of the direct current breakdown voltage curves and volt-ampere characteristics of discharges generated in a system consisting of two plane-parallel electrodes tungsten and molybdenum electrodes at separations from 100  $\mu\text{m}$  to 1  $\mu\text{m}$ . The measurements were performed in the pressure range from 22.5 Torr to 738 Torr. The results are presented in the form of Paschen curves. Based on the measured breakdown voltage curves, the effective yields have been estimated in the case of different cathode materials. Differences between them are attributed to the influence of the work function of the cathode material on the current-voltage characteristics due to field emission effect in small gaps and high pressures. At low-pressures, however, vaporation of impurities from electrodes material becomes significant. The present paper delivers new data on DC breakdown under these experimental conditions and conditions on the validity of the Paschen law in helium and provides better insight into the role of the field emission and the electrode materials on the breakdown voltage.

© 2013 WILEY-VCH Verlag GmbH & Co. KGaA, Weinheim

## 1 Introduction

Studies of low-temperature helium plasmas that exist in various astrophysical and laboratory environments are relevant in numerous scientifically and technologically important areas. High pressure non-equilibrium microdischarge plasmas have applications including excimer radiation sources, sensors, plasma display panels, ozonizers, immersion ion implantation, military and civilian aerospace applications, biomedical and environmental applications [1]– [5]. On the other hand, plasma diagnostics procedures are indispensable for better understanding of microdischarge physics and optimizing device performance. One possibility to achieve high-pressure discharges which are still non-equilibrium is to operate at very small gaps (of the order of a few micrometers) [6]– [8].

In the past few decades, a considerable number of studies on microdischarges have been made [9]– [12]. Fundamental knowledge of the electric breakdown in helium, however, has not kept pace with these increasing interests, mostly due to the complexity of the phenomena related to the plasma breakdown process. At large separations, the breakdown voltage follows the well known Paschen law and dependence on the  $pd$  product (pressure times the electrode separation) [13]. At small gap sizes when a high electric field is generated, however, departures from the Paschen law have been reported indicating that ion-enhanced field emission strongly affects the left hand branch of the Paschen curve [14, 15]. The importance of the role of field emission and vapor arc have been demonstrated for gaps smaller than 10  $\mu\text{m}$ , leading to the description of the "modified" Paschen curve. The general conclusion is that the breakdown voltage decreases rapidly for smaller gaps due to field emission [7, 8, 12, 14].

In spite of a large number of publications devoted to the measurements of breakdown voltages at micro separation there exist only few studies in the literature for separation smaller than 300  $\mu\text{m}$  and in homogeneous electric field [11, 16]. For this reason we built a new system to measure the DC breakdown from 100  $\mu\text{m}$  to 1  $\mu\text{m}$  separations between plane-parallel tungsten and molybdenum electrodes in homogeneous electric field. Tungsten and

\* author. E-mail: marija@ipb.ac.rs

molybdenum materials are used for many years in the field of lighting materials. They have many unique and advantageous properties at an elevated temperature and they are widely used for electric and electronic equipments, electronic devices, medical devices, lighting devices and so on.

In this paper measurements of the breakdown voltage curves for DC discharges in helium over a full range of  $pd$  values are presented. Measurements have been performed for several values of the gas pressure by varying the micrometer gap sizes. The principal problems in obtaining accurate measurements of the electrical breakdown potential are addressed by the electrode preparation and simultaneous measurements of the current-voltage characteristics. Experimental results are supported by the theoretical predictions based on the Fowler-Nordheim theory. The roles of the field emission effect as well as the material and the conditions of the cathode materials are analyzed and discussed.

## 2 Experimental

The discharge system contains two planar electrodes placed in the high vacuum chamber as shown in Fig. 1 [15, 16]. The vacuum chamber itself consists of three parts: positioner for centering the electrode position in three directions (with accuracy about  $1\ \mu\text{m}$ ) and tilting the upper electrode which is located in the upper part. In the middle part there is a glass crux with four fused silica windows. In the bottom part there is also positioning system for tilting electrode as well as improved system for very ultra fine tilting. In this experiment, two different geometries of electrodes were used. Tungsten electrodes were highly polished and their sides were covered by dielectric glass cap in order to prevent discharge to ignite at longer paths. These electrodes allow to study the breakdown voltages in whole range of  $pd$  of Paschen curve. Whereas the molybdenum electrodes with Bruce profile were used to compare measured breakdown voltages on the right side of Paschen curve with tungsten electrodes as well as the influence of long path discharge on the left side of Paschen curves. For both electrodes the same procedures for measurement were applied. One of the electrodes was fixed while the other was moved continuously with micrometer scale linear feed-through. The  $0\ \mu\text{m}$  separation of the electrodes was established by checking the electrical contact between the electrodes and then the movable electrode was pulled away by the means of the micrometer screw at the upper electrode. Both tungsten electrodes were equipped with dielectric caps (immune to vacuum, dielectric breakdown strength  $=13.8\text{kV}/\text{mm}$ ) to prevent the ignition of the discharge at longer path at low pressures. The electrode surface has been polished by the finest diamond paste ( $0.25\ \mu\text{m}$  grain size) in order to achieve the average roughness of the electrode better than  $0.25\ \mu\text{m}$  and measured by using SEM.

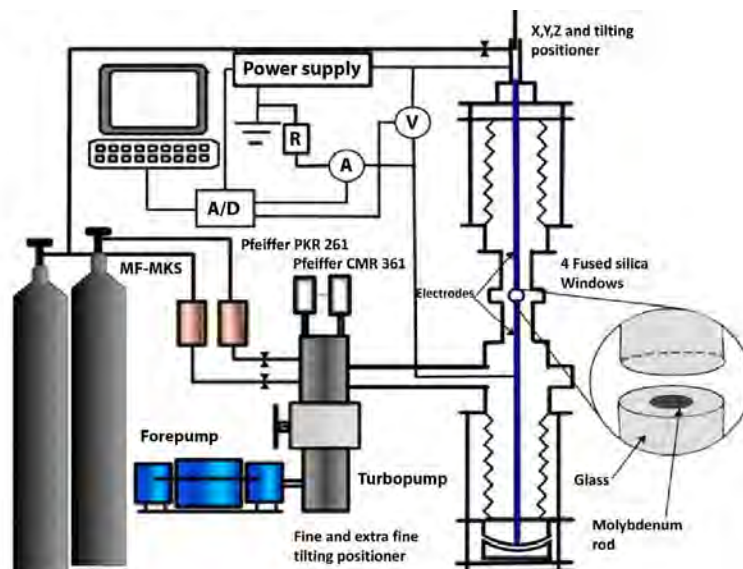


**Fig. 1** Schematic view of the experimental apparatus built for the measurements of the breakdown voltage and volt-ampere characteristics in direct-current discharges in micrometer gaps.

Determination of the breakdown voltages were based on recording the current-voltage characteristics by using a digital oscilloscope and the AD card (National Instruments NI USB-6211). The potential across the discharge tube was increased with rate 0.3 V/s to 20 V/s (depends on the pressure). Faster ramp voltage can be used in the left side of Paschen curve where free electrons are emitted easily from the electrode surface by field emission. The AD card used for the current-voltage measurements has sampling frequency 10 kHz and averages 10 samples. The discharge current was limited to 2 mA for protection of the electrodes. The value of resistor  $R_1$  was in most cases 300 k $\Omega$ , in the case of resistor  $R_2$ , where the current was measured the value was 520  $\Omega$ .

### 3 Theoretical background

Field emission can be described as the extraction of electrons from the surface by the application of very high electric fields. The current density of the emitted electrons is related to the applied electric field by the Fowler-Nordheim (F-N) theory [17]:

$$j_{FE} = \frac{A^2 \beta^2 E^2}{\phi t^2(y)} \exp\left(-\frac{B \phi^{3/2} v(y)}{\beta E}\right) \quad (1)$$

where  $\phi$  is the work function of the metal,  $\beta$  is the field enhancement factor, while  $A$  and  $B$  are constants given by:

$$A = 6.2 \times 10^{-6} \text{ A/eV}$$

$$B = 6.85 \times 10^7 \text{ V/cm/eV}^{3/2}.$$

The terms  $v(y)$  and  $t^2(y)$  represent corrections that were included later in the F-N theory [18]:

$$v(y) \approx 0.95 - y^2$$

$$t^2(y) \approx 1.1,$$

with  $y \approx 3.79 \times 10^{-4} \sqrt{\beta E} / \phi$ . The enhancement factor  $\beta$  strongly depends on the geometrical effects at the surface such as roughness which in turn depend on the technique used to fabricate the devices. Fowler and Nordheim [17] originally have been calculated the current for a cold flat surface, although the current weakly depends on temperature, but it is strongly dependent on emitter shape. To take shape into account, there is a geometric field enhancement parameter  $\beta = E/E_{app}$  which is defined as the ratio of the local emitter field over the applied field. In principle, this factor has a direct physical meaning only for metallic protrusions. If the shape of the protrusion is reasonably simple, the parameter  $\beta$  value can be calculated quite accurately. Experimentally, the numerical value of  $\beta$  can be determined from the F-N plot. At the same time, such plot may allow us to determine if the current flow is due to field-emitted electrons (see, for example, [19]). In general, the F-N equation (1), which are derived from quantum-mechanical considerations, implies that a perfect surface has a  $\beta$  value of unity. However, curve fitting of experimental results requires higher values of  $\beta$  [19]. This is attributed to field gradient enhancements resulting from microscopic surface.

### 4 Results and discussions

The behavior of gases under low pressures and uniform and non-uniform fields, in particular the breakdown characteristics, are covered in details in work by Craggs and Meek [13]. Under low pressures, the gaseous breakdown mechanism is dominated mostly by the electrodes and not affected much by the gases involved. Fig. 2 contains the current-voltage characteristics measured for tungsten electrodes in vacuum at very low pressure of  $1.5 \times 10^{-5}$  Torr. For the 1  $\mu\text{m}$  gap size and voltages greater than 150 V, there is a clear increase in current that grows larger as breakdown is approached. The current starts at around 0.5  $\mu\text{A}$  (resolution of AD card) and increases rapidly. If the electric field generated in micro gaps is sufficiently strong, some of the conduction electrons in the metal lattice are literally pulled into the gap and accelerating toward the electrode. Even if the mean free path is longer than the gap size and electrons could not gain sufficient energy to ionize atoms, a breakdown occurs. With increasing electrode gap, increase of the current appears at higher voltages. From these measurements, determined values of the breakdown voltages for 1  $\mu\text{m}$ , 2.5  $\mu\text{m}$ , 5  $\mu\text{m}$  and 10  $\mu\text{m}$  are 220 V (220 kV/mm) 600 V (240 kV/mm), 1000 V (20 kV/mm) and 1600 V (160 kV/mm). For the 1  $\mu\text{m}$  gap size the voltage is estimated within the accuracy of around 20%, while for the 10  $\mu\text{m}$  within 10 – 15%.

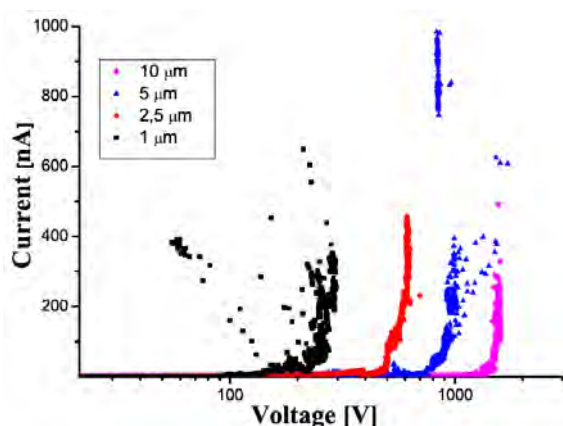


**Fig. 2** Breakdown in vacuum for tungsten electrodes separated by  $1\ \mu\text{m}$  (black symbols),  $2.5\ \mu\text{m}$  (red symbols),  $5\ \mu\text{m}$  (blue symbols) and  $10\ \mu\text{m}$  (pink symbols). The measurements were performed at very low pressure of  $1.5 \times 10^{-5}$  Torr.

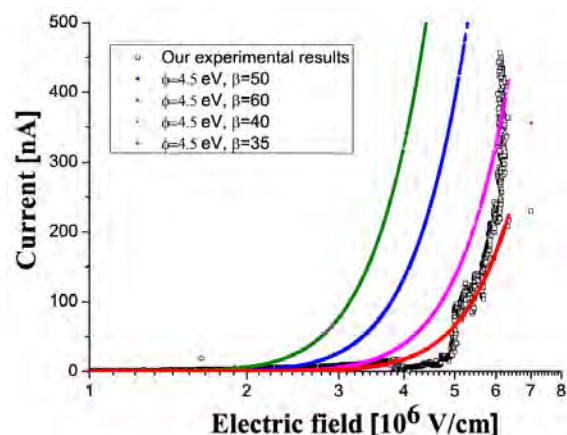


**Fig. 3** Comparison of measured current-voltage characteristics for the  $2.5\ \mu\text{m}$  gap size (black symbols) with corresponding F-N theory curves in accordance with the equation (1) for various values of  $\beta$ .

The influence of the enhancement factor on the current-voltage characteristic is illustrated in Fig. 3. Black symbols represent our experimental results for the tungsten electrodes ( $\phi = 4.5\ \text{eV}$ ) separated by the  $2.5\ \mu\text{m}$ . Calculations were performed in accordance with the F-N equation (1) for the enhancement factor of 35 (red symbols), 40 (pink symbols), 50 (blue symbols) and 60 (green symbols). Since the experimental results agree well with the calculations results obtained with  $\beta = 40$ , we assume such value for the enhancement factor.

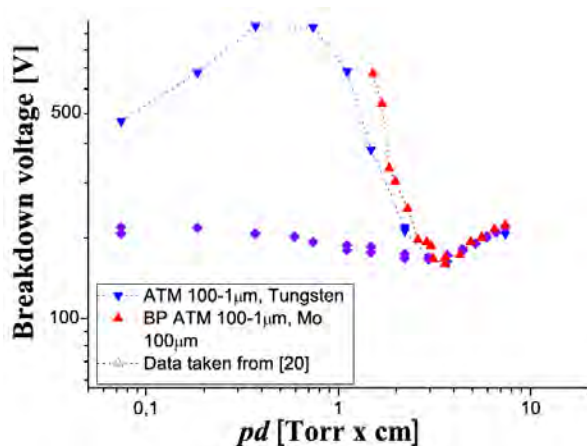


**Fig. 4** The breakdown voltage versus  $pd$  product. Our measurements for tungsten electrodes (blue symbols) and molybdenum electrodes (violet symbols) are compared with the data for copper electrodes (open symbols) and tungsten electrodes (red symbols) taken from [20].

The helium breakdown voltage curves for various gap sizes from  $1\ \mu\text{m}$  to  $100\ \mu\text{m}$  are shown in Fig. 4. Two sets of measurements have been performed: i) with tungsten electrodes with dielectric cap (blue symbols) and ii) with electrodes made of molybdenum with Bruce profile (violet symbols). The results are compared with the Paschen curve obtained at constant electrode separation of  $100\ \mu\text{m}$  for tungsten electrodes (red symbols) and  $10\ \text{mm}$  (open symbols) gap sizes taken from [20]. On the left branch of the breakdown voltage curve, results for the molybdenum electrodes at constant atmospheric pressure and variable electrode distance are much lower and have a different shape than those for tungsten and copper electrodes ref. [20]. However, these results are in agreement with expectations of long path discharge breakdown allowed by construction of electrodes. Thus on the left side of Paschen curve breakdown voltage are more or less equal or slightly higher than minimum breakdown voltage for Helium gas. In contrast to molybdenum electrodes, the results taken for tungsten electrodes do not show long path breakdown at the left side of the Paschen curve due to dielectric cap. For the  $pd$  values greater than  $3\ \text{Torr} \times \text{cm}$ , all results have similar trends indicating that the electrode materials play no significant role



on the right hand branch of the breakdown curve. Our data for tungsten electrodes (blue symbols) satisfactorily agree with data from other electrode materials for the  $pd$  values of  $1.5 \text{ Torr} \times \text{cm}$  and higher. Below this value the effects associated with the high values of the electric field cause departure from the standard Paschen law. In other words, combination of small electrode distance and high reduced electric field leads to decrease of breakdown voltages.

Based on the breakdown voltage curves from Figure 4, the effective yields have been estimated and shown in Figure 5a. It is well known that the effective yield in microgaps depends on the cathode material in accordance with the expression:

$$\gamma_{eff} = Ke^{-D/E}, \quad (2)$$

where  $E$  is the electric field near the cathode and  $K$  and  $B$  are material and gas dependent constants. Although the molybdenum and tungsten have very similar work function (4.2 eV and 4.5 eV, respectively), their current-voltage characteristics determined from expression (2) are different as shown in Figure 5b which could explain the large discrepancies between the yields observed in Figure 5a, especially at large ratios  $E/p$ . On the other hand, different purity of helium also affects the results. Although, we used the same purity of helium, differences can be caused by the evaporation of impurities from electrodes material at low pressures.

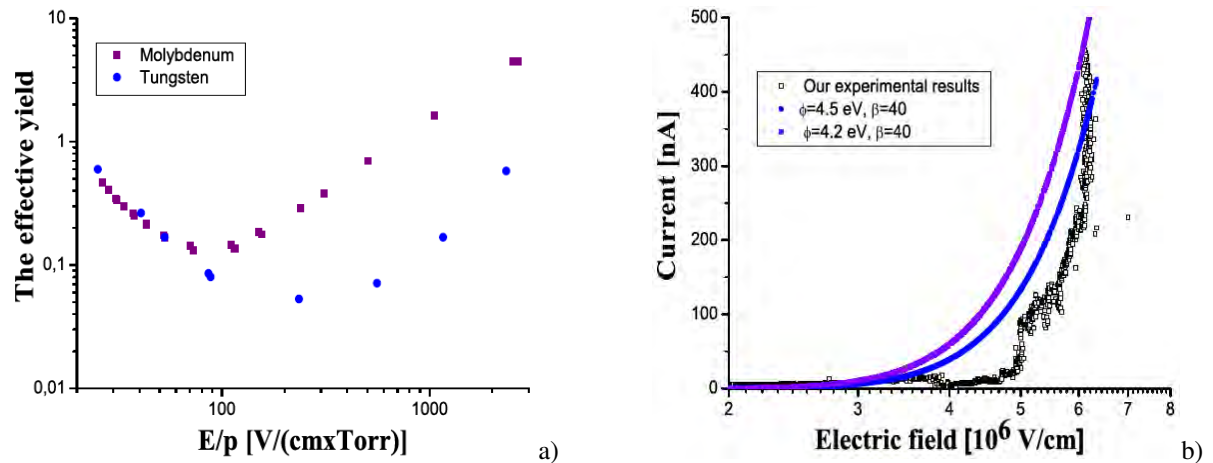


**Fig. 5** The dependence of the effective yield on the  $E/p$  ratio estimated from the breakdown voltage curves and b) current versus the electric field, for two different cathode materials: tungsten (blue symbols) and molybdenum (violet symbols).

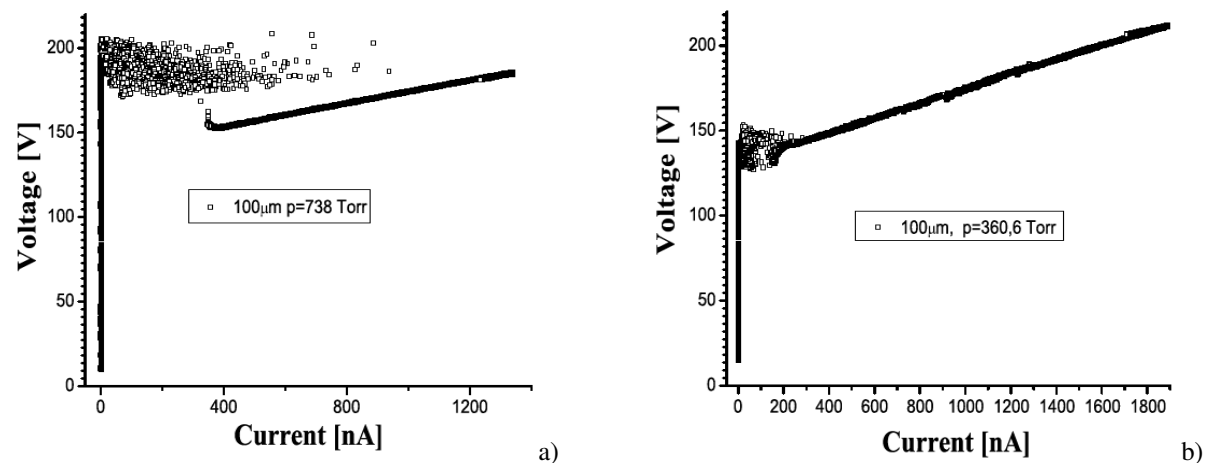


**Fig. 6** Volt-Ampere characteristics for the  $100 \mu\text{m}$  gap size at the  $pd$  of: a)  $7.4 \text{ Torr} \times \text{cm}$  and b)  $3.6 \text{ Torr} \times \text{cm}$ .

The breakdown voltage curve for  $100\ \mu\text{m}$  gap shows no apparent departure from Paschen law and thus we consider it as a normal discharge. This is confirmed by the Volt-ampere characteristics recorded at two different  $pd$  values of:  $7.4\ \text{Torr} \times \text{cm}$  (Figure 6a) and  $3.6\ \text{Torr} \times \text{cm}$  (Figure 6b). The measurements carried out at different pressures have similar tendencies and correspond to the normal discharge characteristics. On the other hand, at  $5\ \mu\text{m}$  electrode separation and the atmospheric pressure the breakdown curve shows departure from Paschen law and thus discharge generated at this electrode separation represents a different type of discharge due to important role of processes associated with high electric field. The Volt-ampere characteristic for this discharge (see Figure 7) clearly demonstrates, that the current is practically limited by the field emission of the electrons from the electrode.

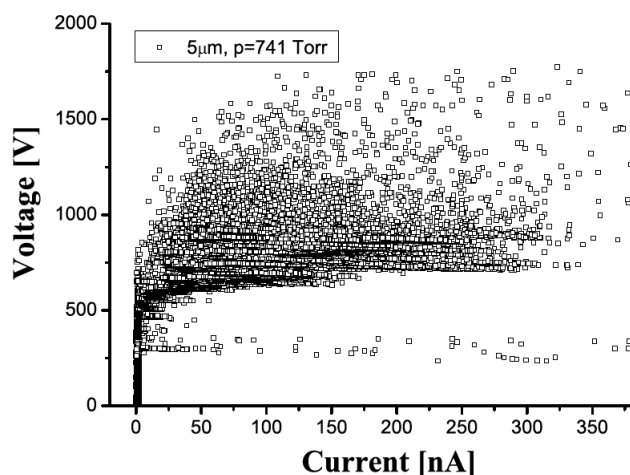


**Fig. 7** Volt-Ampere characteristics for the  $5\ \mu\text{m}$  gap spacing and the  $pd$  value of  $0.37\ \text{Torr} \times \text{cm}$ .

## 5 Conclusions

In this paper novel experimental results for the DC breakdown voltage curves in helium for the gap sizes ranging from  $1\ \mu\text{m}$  to  $100\ \mu\text{m}$  were presented and discussed. Results for the tungsten electrodes are in a good agreement with the previously published data [20]. Results for the molybdenum electrodes (Bruce profile geometry) are systematically lower than results for tungsten and copper electrodes, especially at lower  $pd$  values (left hand branch of the breakdown curve). The results show that the right hand branch, seems to be almost independent of the electrode material.

Based on the measured breakdown voltage curves, the effective yields as a function on the  $E/p$  ratio have been determined. The obtained values clearly illustrated dependence of the yield on the cathode material. Although some materials have a similar work functions, their current-voltage characteristics that correspond to the F-N equation (1) are different. It was also found out that differences between yields for various materials are due to evaporation of impurities from electrodes material at lower pressures.

Besides the electrode materials, the electrode geometry and the electrode separations have important influence on the Paschen curve. With increasing electrode separation, the breakdown voltage increases since the contribution of field emission progressively decreases. Violation of the standard scaling law was observed when the strength of the electric field is high enough to induce the field emission of electrons. Field emission combined with other mechanisms is known to limit usable voltages to values well below those predicted by avalanche breakdown.

**Acknowledgements** The work has been carried out under Ministry of Education and Science Republic of Serbia O171037 and III41011 projects. This work has also been supported by the VEGA grant agency; project VEGA 1/0514/12, the Slovak Research and Development Agency Projects APVV-0733-11 and DO7RP-0025-11, and the Slovak Research and Development Agency under Contract SK-SRB-0026-11. The authors are very grateful to Dr Nikola Škoro and Dr Vladimir Stojanović at the Institute of Physics for very useful comments and suggestions.

## References

- [1] T. Ito, T. Izaki and K. Terashima, *Thin Solid Films* **386**, 300 (2001).
- [2] T. Makabe and Z.Lj. Petrović, *Plasma Electronics: Applications in Microelectronic Device Fabrication* (Taylor & Francis, New York, 2006).
- [3] U. Kogelschatz, *Contribution to Plasma Physics* **47**, 80 (2007).
- [4] S. Adili and C.M. Franck, *IEEE Transaction Dielectrics and Insulation* **19**, 1833 (2012).
- [5] C.M. Du, J. Wang, L. Zhang, H.X. Li, H. Liu, and Y. Xiong, *New Journal of Physics* **14**, 013010 (2012).
- [6] R.S. Dhariwal, *IEE Proceedings - Science, Measurement and Technology* **147**, 261 (2000).
- [7] M. Radmilović-Radjenović, J.K. Lee, F. Iza, and G.Y. Park, *J. Phys. D: Appl. Phys.* **38**, 950 (2005).
- [8] E. Munoz-Serrano, G. Hagelaar, Th. Callegari, J. Boeuf, and L.C. Pitchford, *Plasma Physics and Controlled Fusion* **48**, B391 (2006).
- [9] W.S. Boyle and P. Kisliuk, *Physics Review* **97**, 55 (1955).
- [10] P. Rumbach and D.B. Go, *Journal of Applied Physics* **112**, 103302 (2012).
- [11] Z.Lj. Petrović, N. Škoro, D. Marić, C.M.O. Mahony, P.D. Maguire, M. Radmilović-Radjenović and G. Malović, *J. Phys. D: Appl. Phys.* **41**, 194002 (2008).
- [12] E. Hourdakis, B.J. Simonds, and N.M. Zimmerman, *Review of Scientific Instruments* **77**, 034702 (2006).
- [13] J.M. Meek and J.D. Craggs, *Electrical breakdown of gases* (Oxford University Press, Oxford, 1953).
- [14] M. Radmilović-Radjenović and B. Radjenović, *Contrib. Plasma Phys.* **47**, 165 (2007).
- [15] M. Klas, Š. Matejčik, B. Radjenović, and M. Radmilović-Radjenović, *Physics Letters A* **376**, 1048 (2012).
- [16] M. Radmilović-Radjenović, Š. Matejčik, M. Klas, and B. Radjenović, *J. Phys. D: Appl. Phys.* **46**, 015302 (2013).
- [17] K. Yuasa, A. Shimoi, I. Ohba, and C. Oshima, *Surf. Sci.* **520**, 18 (2002).
- [18] R.E. Burgess and H. Kroemer, *Phys. Review* **90**, 515 (1953).
- [19] M. Radmilović-Radjenović and B. Radjenović, *IEEE Trans. Plasma Science* **35**, 1223 (2007).
- [20] P. Hartmann, Z. Donkó, G. Bánó, L. Szalai, and K. Rózsa, *Plasma Sourc. Sci. Technol.* **9**, 183 (2000).

## The surface charging effects in three-dimensional simulation of the profiles of plasma-etched nanostructures

M. Radmilović-Radjenović<sup>\*,†</sup>, B. Radjenović and M. Savić

*Institute of Physics, University of Belgrade, Pregrevica 118, 11080 Belgrade, Serbia*

### SUMMARY

Particles and fields represent two major modeling paradigms in pure and applied science at all. Particles typically exist in a spatial domain and they may interact with other particles or with field quantities defined on that domain. A field, on the other hand, defines a set of values on a region of space. In this paper, a methodology and some of the results for three-dimensional (3D) simulations that includes both field and particle abstractions are presented. In our studies, charging damage to a semiconductor structure during plasma etching is simulated by using 3D level set profile evolution simulator. The surface potential profiles and electric field for the entire feature were generated by solving the Laplace equation using finite elements method. Calculations were performed in the case of simplified model of Ar<sup>+</sup>/CF<sub>4</sub> non-equilibrium plasma etching of SiO<sub>2</sub>. Copyright © 2010 John Wiley & Sons, Ltd.

Received 15 February 2010; Revised 2 August 2010; Accepted 7 November 2010

KEY WORDS: plasma etching; profile charging; finite elements method; level set method

### 1. INTRODUCTION

Since its introduction in the 1970s, plasma etching has become an integral part of semiconductor integrated circuit (IC) processing, treatment of materials (such as implantation) and especially for achieving massively parallel production of well-organized and designed nanostructures [1–3]. Plasma etching requires a high etching rate, anisotropy, uniformity across the wafer, and process reproducibility [4,5]. Precise monitoring of the etched profile in microelectronic devices during plasma etching process is one of the most important tasks of front-end and back-end microelectronic devices manufacturing technologies. Charging effects during plasma etching of high-aspect ratio structures can cause gate oxide degradation during gate etching and profile deformation issues such as notching or bowing [6–8]. The origin of this phenomenon is due to the difference in directionality between ions and electrons when they cross the plasma sheath and interact with three-dimensional (3D) structures. The potential for using modeling and simulation to benefit industrial users of plasma processes and equipment has never been greater [9,10]. Plasmas are used in about 30% of all semiconductor manufacturing processing steps, and about the same fraction of processing equipment is plasma-based in a typical microelectronics fabrication facility. In the last several years, computational costs continue to decrease steadily and considerable progress has been achieved in establishing the major modeling strategies that are necessary to achieve practical industrial objectives. Nevertheless, low-temperature plasma processing science is a relatively young field, and has not therefore received the in-depth,

---

<sup>\*</sup>Correspondence to: M. Radmilović-Radjenović, Institute of Physics, University of Belgrade, Pregrevica 118, 11080 Belgrade, Serbia.

<sup>†</sup>E-mail: marija@ipb.ac.rs

sustained attention that is required to have a significant, timely impact in industry. This situation is perhaps most evident in the area of the database for physical and chemical processes in plasma materials processing [11]. The profile surface evolution during plasma etching, deposition, and lithography development is a significant challenge for numerical methods for interface tracking itself. Level set methods for evolving interfaces [12,13] are specially designed for profiles, which can develop sharp corners, change topology, and undergo orders of magnitude changes in speed. Additionally, etching submicron features in insulating material such as SiO<sub>2</sub> or materials masked with insulators, e.g. photoresist-masked polysilicon, is accompanied by feature charging effects caused by the differences in electron and ion angular distributions. The plasma charging reported by Yoshida [14] has been studied in recent decades [15,16]. The phenomenon can be described as follows: because of the acceleration in the sheath, the angular distribution is more directional than that of electrons. The difference causes the electron shading effect at the etched feature, thus generating positive potential at the deep trench bottom. This charging effect leads to many serious plasma process induced damage problems such as bowing, trenching, reactive ion etching lag, and notching. The reduction in the device size and multilayer structures requires a high-aspect ratio in the SiO<sub>2</sub> etching. As the aspect ratio increases, the charging effect becomes more observable as reported by Makabe *et al.* [17,18]. The negative charge that might develop on the sidewalls can bend the trajectories of the ions passing close to them. This bending effect may contribute to microtrenching. In addition, etching rate reduction with time and notching of polysilicon sidewalls during the overetching step have been attributed in part to feature charging effects. The main goal of this paper is to include charging effects in our 3D level set etching profile simulator. For that purpose, some basic aspects of the etching profile simulation procedure, the profile surface movement via level set method, particle fluxes calculations using Monte-Carlo method and the electric field (generated by the profile charge) calculations on the basis of the finite elements method will be described. Finally, the obtained simulation results illustrating charging effect will be presented and discussed.

## 2. SIMULATION TECHNIQUE

### 2.1. Sparse field level set method

In the level set method considered surface at a certain time  $t$  is represented by the so-called level set function  $\phi(t, x)$ . The initial surface is given by  $\{x | \phi(0, x) = 0\}$ . The evolution of the surface in time is caused by the surface processes in the case of the etching. The velocity of the point on the surface normal to the surface denoted by  $R(t, x)$  is called velocity function. The velocity function generally depends on the time and space variables and we assume that it is defined on the whole simulation domain. At a later time  $t > 0$ , the surface is as well as the zero level set of the function  $\phi(t, x)$ . Namely, it can be defined as a set of points  $\{x | \phi(t, x) = 0\}$ . This leads to the level set equation in Hamilton–Jacobi form:

$$\frac{\partial \phi}{\partial t} + H(\nabla \phi(t, x)) = 0, \quad (1)$$

in the unknown function  $\phi(t, x)$ , where Hamiltonian function is given by  $H = R(t, x)|\nabla \phi(t, x)|$  and where  $\phi(0, x) = 0$  determines the initial surface. Several approaches for solving level set equations have been developed. Among them, the most important are narrow band level set method, widely used in etching process modeling tools, and recently developed sparse-filed method [19]. The sparse field method uses an approximation to the level set function that makes it feasible to recompute the neighborhood of the zero level set at each time step. As a result, the number of computations increases with the size of the surface, rather than with the resolution of the grid.

It is well known that Hamiltonian function  $H$  is convex if the following condition is fulfilled

$$\frac{\partial^2 H}{\partial \phi_{x_i} \partial \phi_{x_j}} \geq 0, \quad (2)$$



where  $\varphi_{x_i}$  is a partial derivative of  $\varphi(t, \mathbf{x})$  with respect to  $x_i$ . During plasma etching and deposition processes, the etching (deposition) rate, which defines the surface velocity function  $R(t, \mathbf{x})$ , depends on the geometric characteristics of the profile surface itself, or more precisely, on the angle of the incidence of the incoming particles. In our studies, we shall consider an etching beam coming down in the vertical direction, conditions that are characteristic for ion milling technology, but angular dependence of the etching rates appears, more or less, in all etching processes. In these cases, the most useful finite difference scheme that can be applied is the Lax–Friedrichs scheme, one that relies on the central difference approximation to the numerical flux function, and preserves monotonicity through a second-order linear smoothing term. It is shown [20] that it is possible to use the Lax–Friedrichs scheme in conjunction with the sparse field method, and to preserve sharp interfaces and corners by optimizing the amount of smoothing in it. This is of special importance in the simulations of the etching processes in which spatially localized effects appear, such as notching and microtrenching.

## 2.2. Particle fluxes calculations

Particles are usually used in one of the two ways in computer scientific applications: In the first way, the particles known as ‘tracers’ are tracking in order to gather statistics that describe the conditions of a complex physical system. The second way is based on performing direct numerical simulation of systems that contain discrete point-like entities such as ions or molecules. In both cases, there are one or more sets of particles, while each set contains some data associated with it that describes its members’ characteristics, such as charge, mass, or momentum. The state of the physical system is determined by these data.

Simulation of the etch process in details requires knowledge of the etching rates at all the points of the profile surface during the etching process. These rates are directly related to fluxes of the etching species on the profile surface, which are themselves determined by the plasma parameters in the etching device. Electrons do not contribute directly to the material removal, but they are the source, together with positive ions, of the profile charging that has many negative consequences on the final outcome of the process especially in the case of insulating material etching,  $\text{SiO}_2$  for example. As can be observed from Figure 1 that shows the electron energy distribution functions (EEDF) and the energy distribution function for  $\text{Ar}^+$  ions (IEDF), a large number of electrons have low energies while the energy of ions is spread to higher energies. On the other hand, the angular distribution function for electrons (EADF) is different from the angular distribution function for  $\text{Ar}^+$  ions (IADF) indicating that ions are directed toward small angles. These distribution functions obtained by particle-in-cell (PIC) calculations using XPDC1 code [21–23] are used as the boundary conditions for the calculations of ion fluxes incident on the profile surface.

The etching process in medium/high density fluorocarbon plasmas is believed to consist of concurrent etching (of the  $\text{SiO}_2$  substrate in our case) and deposition (of a fluorocarbon polymer layer) phenomena [24]. In this paper, the deposition process is neglected and ion-enhanced etching and physical sputtering and pure chemical etching of  $\text{SiO}_2$  are considered. It is also assumed that the electrons are absorbed at the hitting points, while the neutrals can be absorbed or diffusively reflected, once or many times depending on its sticking coefficient. The positive ions can be absorbed, or specularly reflected, depending on their energy and incident angle. It is assumed that charged particles pass on their charge when they hit the surface, and that this charge does not move after that, what is reasonable for insulating materials. At the boundaries above the profile surface, periodic conditions are assumed. The surface neutrals coverage (i.e. the fraction of surface covered by free radicals)  $\theta_n$  satisfies the balance equation:

$$\frac{d\theta_n}{dt} = J_n S_n (1 - \theta_n) - k_{ni} J_{ion} Y_{ni}^{\text{eff}} \theta_n - k_{ev} J_{ev} \theta_n, \quad (3)$$

where  $J_n$  and  $J_{ion}$  are neutral and ion fluxes,  $S_n$  is the neutral sticking coefficient,  $k_{ni}$  and  $k_{ev}$  are etchant stoichiometry factors, and  $Y_{ni}^{\text{eff}}$  is the effective etching yield for ion-enhanced chemical etching. Here, by the term ‘effective’, we denote a quantity related to the integral flux, not to an individual particle.  $J_{ev}$  is evaporation flux that corresponds to pure chemical etching. It is related

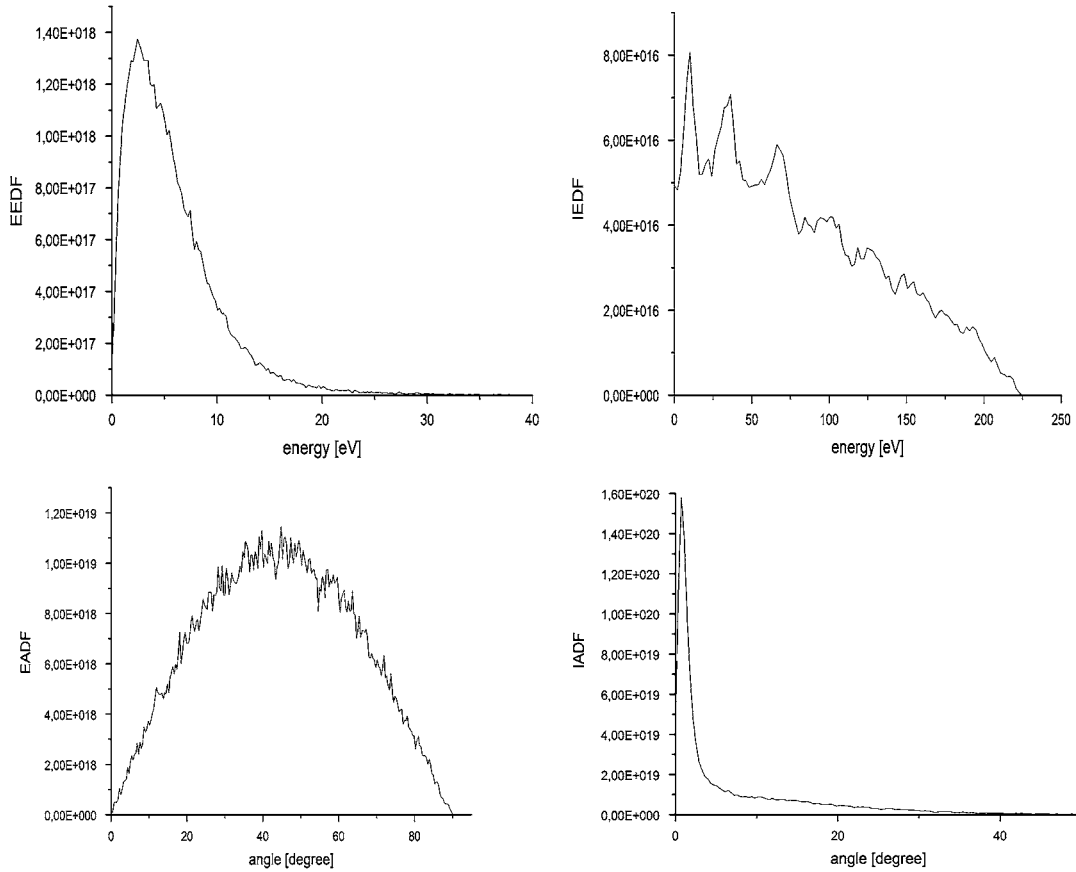


Figure 1. Energy distribution functions of electrons and  $\text{Ar}^+$  ions (EEDF and IEDF, respectively) and angular distribution functions of electrons and  $\text{Ar}^+$  ions (EADF and IADF, respectively) obtained by PIC/MCC simulations.

to the neutrals flux by the Arrhenius law:

$$J_{\text{ev}} = K_{\text{SiO}_2} e^{-\frac{E_{\text{SiO}_2}}{k_b T}} J_n. \quad (4)$$

Balance condition  $d\theta_n/dt = 0$  gives the equilibrium surface coverage:

$$\theta_n = \frac{J_n S_n}{J_n S_n \theta_n + k_{\text{ni}} J_{\text{ion}} Y_{\text{ni}}^{\text{eff}} + k_{\text{ev}} J_{\text{ev}}}. \quad (5)$$

So, now we can write equation defining the etching rate ER in the form

$$\text{ER} = \frac{1}{\rho_{\text{SiO}_2}} [J_{\text{ion}} Y_{\text{ni}}^{\text{eff}} \theta_n + J_{\text{ion}} Y_{\text{ni}}^{\text{eff}} (1 - \theta_n) + J_{\text{ev}} \theta_n], \quad (6)$$

where  $\rho_{\text{SiO}_2}$  is  $\text{SiO}_2$  density and  $Y_{\text{ni}}^{\text{eff}}$  is the effective physical spattering etching yield. The etching rate ER defines the velocity function  $V(t, \mathbf{x})$  at the profile surface. In actual calculation, the feature profile surface is represented by a set of connected triangles, and the above formula should be applied to the every single particular triangle. So, instead of effective etching yields we should define etching yields for every particular ion:

$$Y_{\text{ni}}(E_i, \alpha_i) = A_{\text{ni}} (\sqrt{E_i} - \sqrt{E_{\text{in}}^{\text{th}}}) \cos \alpha_i, \quad (7)$$

and

$$Y_{sp}(E_i, \alpha_i) = A_{sp}(\sqrt{E_i} - \sqrt{E_{sp}^{th}})\cos \alpha_i(1 + B_{sp}\sin^2 \alpha_i), \quad (8)$$

where  $E_i$  is the ion energy and  $\alpha_i$  is the angle between the surface normal and the ion incident direction at the point of incidence. Numerical values of the constants appearing in relations (3), (4), (6), (7), and (8) are taken from the Reference [18]. The triangular representation of the profile surface requires that instead of integral particle fluxes  $J_n$  and  $J_{ion}$ , corresponding summations over every particle incident on the particular triangle

$$J_n = \frac{R_n}{A\Delta t_{etch}} N_n, \quad (9)$$

$$J_{ion} Y_{ni}^{eff} = \frac{R_{ion}}{A\Delta t_{etch}} \sum_i Y_{ni}(E_i, \alpha_i), \quad (10)$$

and

$$j_{ion} Y_{sp}^{eff} = \frac{R_{ion}}{A\Delta t_{etch}} \sum_i Y_{spi}(E_i, \alpha_i), \quad (11)$$

should be used. Here,  $N_n$  denotes the number of neutrals absorbed on the particular triangle,  $R_n$  ( $R_{ion}$ ) is the ratio of actual number of neutrals (ions) passing the upper computational domain boundary during the etching time interval and number of neutrals (ions) used in Monte Carlo calculations,  $A$  is the particular triangle area, and  $\Delta t_{etch}$  is the etching time interval. The ions can be absorbed, or specularly reflected, depending on their energy and incident angle. The probability of specular reflection  $P_d$  is given by [25]:

$$P_d = 1 - C_1 \sqrt{E_i} \left( \frac{\pi}{2} - \alpha_i \right). \quad (12)$$

Neutrals ( $F$  radicals) density is supposed to be  $10^{19} \text{ m}^{-3}$ . The simulation time is 100 s, and it is divided in 100 equal etching intervals (Monte Carlo steps).

### 2.3. Electric fields calculations

In general, electromagnetic field equations were identified with the ‘Maxwell equations’, i.e. with partial differential equations, which are extremely rich in symmetries and (hence) conservation laws. In the continuum, many conservation laws follow directly from invariances of the Lagrangian (Noether symmetries) such as energy or momentum conservation, while others have an inherent topological aspect, such as magnetic charge. When Maxwell’s equations are discretized on a mesh, a number of symmetries of the continuum theory are modified or broken. However, some conservation laws may be preserved on a discrete setting. This is because they often relate a quantity on certain region of space to an associated quantity on the boundary of the region. Because the boundary is a topological invariant, such conservation laws should not depend on the metric of the space. A natural mathematical language that explores this aspect is the calculus of exterior differential forms and associated algebraic topological structures [26]. In this approach, the scalar electrostatic potential is a 0-form, the electric and magnetic fields are 1-forms, the electric and magnetic fluxes are 2-forms, and the scalar charge density is a 3-form. The basic operators are the exterior (or wedge) product, the exterior derivative, and the Hodge star. Precise rules (i.e. a calculus) prescribe how these forms and operators can be combined. In this modern geometrical approach to electromagnetics, the fundamental conservation laws are not obscured by the details of coordinate system-dependent notation. By working within the discrete differential forms framework, we are guaranteed that resulting spatial discretization schemes are fully mimetic. Finite difference method cannot be used when the geometry of the problem is irregular, as it is usual for the etching profiles. Hence, it is naturally to use finite elements method. The calculations of the electric fields in this paper are performed by integrating a general finite element solver GetDP [27] in our simulation framework. GetDP is a thorough implementation of discrete differential forms calculus, and uses mixed finite elements

to discretize de Rham-type complexes in one, two, and three dimensions. Meshing of the computational domain is carried out by TetGen tetrahedral mesh generator [28]. TetGen generates the boundary constrained high-quality (Delaunay) meshes, suitable for numerical simulation using finite element and finite volume methods. As a part of the post-processing procedure, the electric fields, obtained on the unstructured meshes, are recalculated on the Cartesian rectangular domains containing the regions of the particles movement. In this manner, the electric field on the particles could be calculated by simple trilinear interpolation.

### 3. RESULTS AND DISCUSSION

Our simulation results involve the profile charging calculations for the fixed profile surface. All the calculations are performed on  $128 \times 128 \times 384$  rectangular grid. The initial profile surface is a rectangle deep with dimensions  $0.1 \times 0.15 \times 0.1 \mu\text{m}$ . Above the profile surface is the empty space (trench region). The incident particles are generated randomly at the top of the simulation region. In the case of the ion-enhanced chemical etching, the dependence of the surface velocity on the incident angle is simple:  $V = V_0 \cos \theta$  and the evolution of the etching profile is displayed in Figure 2. Although, this is the simplest form of angular dependence, but it describes the ion-enhanced chemical etching process correctly [19]. In this case, we expect that the horizontal surfaces move downward, while the vertical ones stay still. This figure shows that it with optimal amount of smoothing gives minimal rounding of sharp corners, while preserving the numerical stability of the calculations. In order to illustrate the obtained results more clearly, Figure 3 shows the surface mesh of the tetrahedral mesh corresponding to the last profile in Figure 2. This mesh defines the profile surface for the subsequent particle flux and electric field calculations.

The fluxes of different particles are shown in Figure 4. Collisions in the simulation domain are neglected because mean-free path of ions and electrons is much longer than the simulation domain size. Also, the probability that more than two particles exist in the simulation space at the same time is very low because the life time of ions or electrons in the simulation region is much shorter than the incident time interval. The neutral and the electron fluxes distributions are similar: they are concentrated on the top of the wafer and upper portion of the sidewalls, while the ions, due its directionality, are accumulated at the bottom of the profile. Solving the Laplace equation with such a charge distribution as boundary condition leads to the potential distribution on the profile shown in Figure 5. The maximal value of the potential at the bottom



Figure 2. The time evolution of the profile during ion-enhanced chemical etching.

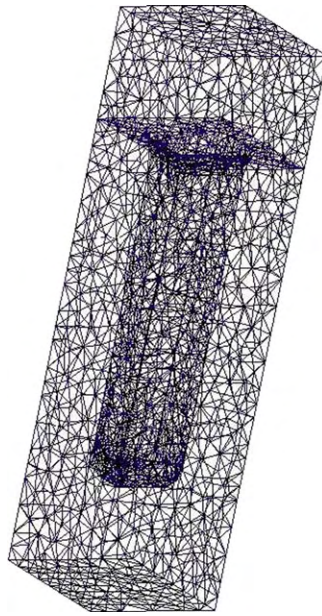


Figure 3. The surface mesh generated by Tetgen related to the last profile.

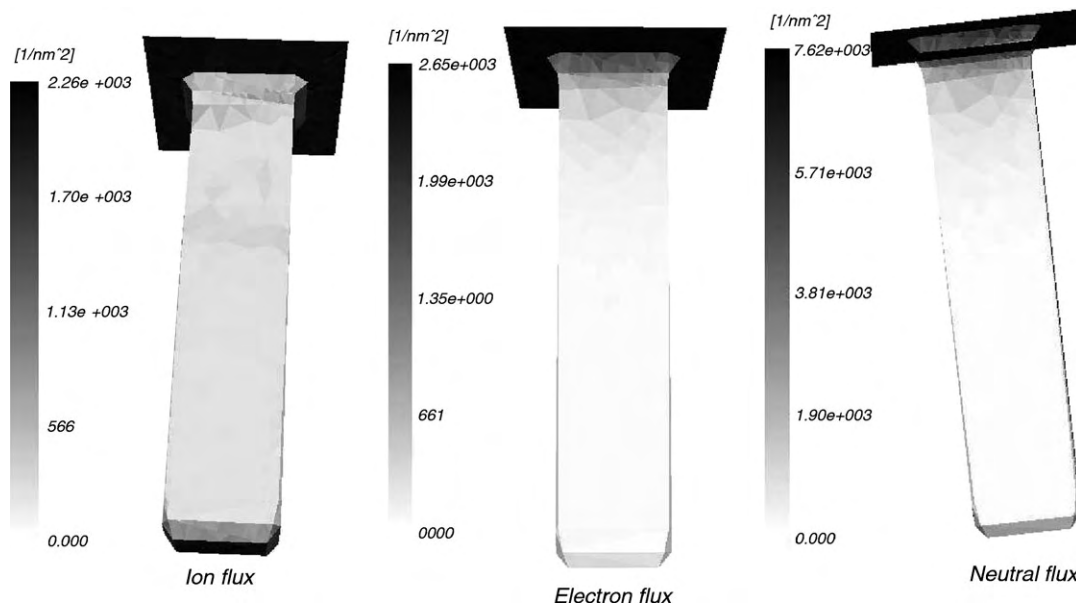


Figure 4. Fluxes of neutrals, electrons, and ions at the profile surface.

of the profile is somewhat bigger than the average ion energy, while the top surface is slightly negatively biased. Since the electrons leave the plasma with relatively high energies, they have very anisotropic distribution as they slow down in the sheath, so they are deposited mainly at the sidewalls and cannot reach the bottom. The deposited electrons at the entrance to the nano trench or nano hole actually also contribute to prevent other electrons from reaching the bottom of the structure and neutralizing the charge. Negative ions from the plasma have low energies so they cannot cross the sheath which was designed to slow down the much more energetic electrons. Similar, Figure 6 illustrates the potential cut. The aspect ratio of a feature typically refers to the ratio of the depth of the feature to its smallest horizontal cross-sectional dimension. It was shown that for the aspect ratios greater than 7 the potential at the bottom of the structure becomes equal to the potential corresponding to the ion energy. On the other hand, the potential



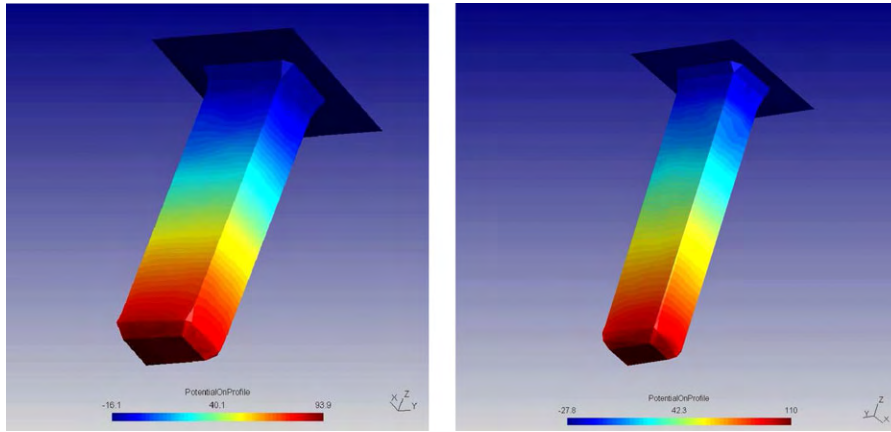


Figure 5. Potential distribution on the profile surface for two different values of the aspect ratio: (a)  $AR = 4.5$  and (b)  $AR = 6$ .

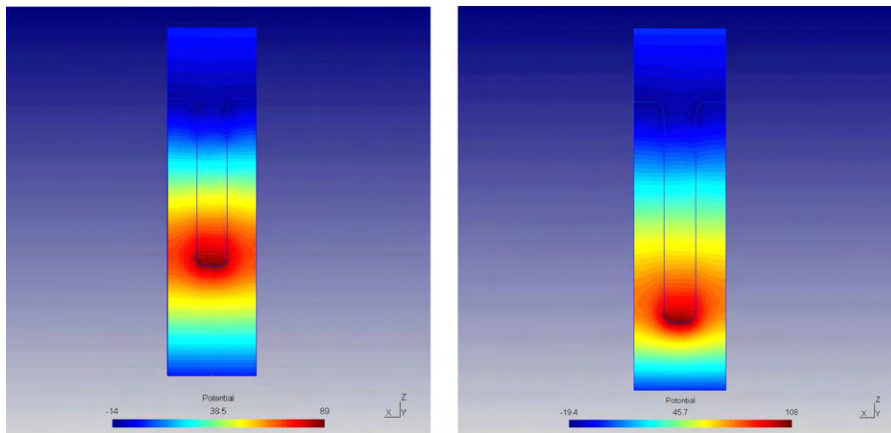


Figure 6. Potential cut in the case of: (a)  $AR = 4.5$  and (b)  $AR = 6$ .

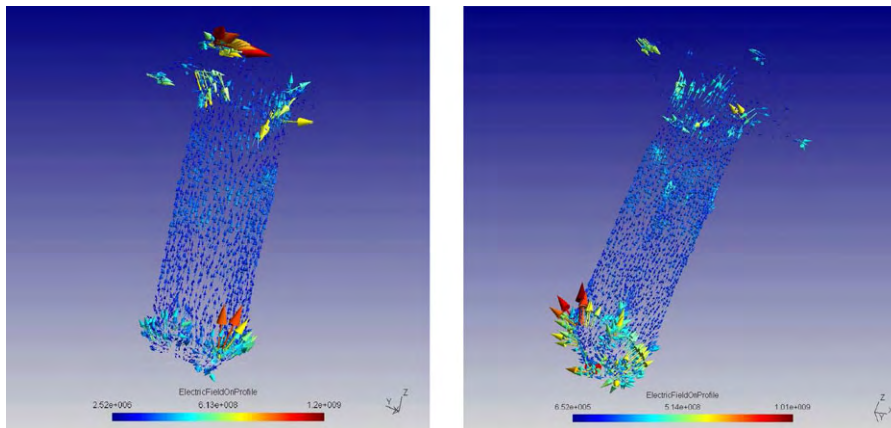


Figure 7. Electric field on the profile surface (expressed in V/m) for: (a)  $AR = 4.5$  and (b)  $AR = 6$ .

at the sidewalls of the structure closer to the top is small as it is defined by the energy of electrons reaching the sidewalls.

The influence of the aspect ratio on the electric field vectors on the profile surface is depicted in Figure 7. It is obvious that the field stimulate notch creation by directing the ions toward sidewalls, as it is explained in Reference [8]. At the very top, the field accelerate the ions

downward, but it quickly changes direction at the lower positions of the profile. The zero field border height is determined by the etching plasma parameters.

#### 4. CONCLUSIONS

As one of the crucial aspect of the modern technologies, plasma processing plays a significant role in fabrication of integrated circuits (IC) and consequently in electronics and consumer goods in general. Damage to ICs during manufacturing as a result of charging of the dielectrics during finalization of interconnects is both reducing the profitability and reducing the ability to reach large sizes of microchips and make complex system integration on a single chip. Therefore, realistic three-dimensional etching profile simulations are needed, although still lacking. It is understandable that realistic calculations should involve complex surface reactions set, the effects of the profile charging, polymer deposition, as well as better statistic (greater number of particles) in the Monte Carlo step of the calculations, which is usually limited by the available computational resources. Emphasis should be placed on etching rates, uniformity, anisotropy, selectivity, and critical dimension control. In this paper, we have presented 3D simulation results for the profile evolution during ion-enhanced etch process as well as potential on profile and the electric fields for different aspect ratio values. The electron shading effect and the resultant charging damage to the structure begin to be significant in etched features having an aspect ratio greater than about 2. The electron shading effect gets worse as the aspect ratio increases, since the electron accumulation near the opening and top sidewalls of the feature makes it increasingly difficult for anything but the positively charged high-energy species to get past that entrance and any distance down into the deepening etched features that arrive at the wafer surface.

#### ACKNOWLEDGEMENTS

The present work has been supported by project 141025 financed by the Ministry of Science and Environmental Protection.

#### REFERENCES

1. Rogers BR, Cale TS. Plasma processes in microelectronic device manufacturing. *Vacuum* 2002; **65**:267–279.
2. Lieberman MA, Lichtenberg AJ. *Principles of Plasma Discharge and Materials Processing*. Wiley: New York, 1994.
3. Makabe T, Petrovic ZLJ. *Plasma Electronics: Applications in Microelectronic Device Fabrication*. Taylor and Francis, CRC Press: New York, 2006.
4. Armstrong NP, Maleham J. A two-stage solution to the anisotropic polysilicon etching problem. *Vacuum* 1983; **33**:291–294.
5. Kassing R, Rangelow IW. Etching processes for High Aspect Ratio Micro Systems Technology (HARMST). *Microsystem Technologies* 1996; **3**:20–27.
6. Hashimoto K. Charge damage caused by electron shading effect. *Japanese Journal of Applied Physics* 1994; **33**:6013–6018.
7. Cismaru C, Shohet JL, McVittie JP. Synchrotron radiation-induced surface-conductivity of SiO<sub>2</sub> for modification of plasma charging. *Applied Physics Letters* 2000; **76**:2191–2193.
8. Radjenović B, Radmilović-Radjenović M, Petrović ZLJ. Dynamic of the profile charging during SiO<sub>2</sub> etching in plasma for high aspect ratios trenches. *IEEE Transactions on Plasma Science* 2008; **36**:874–875.
9. Zhang D, Kushner MJ. Surface kinetics and plasma equipment model for Si etching by fluorocarbon plasmas. *Journal of Applied Physics* 2000; **87**:1060.
10. Radjenovic B, Radmilović-Radjenović M. Level set simulations of 3D etching profile evolution in the anisotropic wet etching of silicon. *Thin Solid Films* 2009; **517**:4233.
11. Petrović ZLJ, Dujko S, Marić D, Malović G, Nikitović Ž, Šašić O, Jovanović J, Stojanović V, Radmilović-Radjenović M. Measurement and interpretation of swarm parameters and their application in plasma modeling. *Journal of Physics D: Applied Physics* 2009; **42**:194002 (33pp).
12. Sethian J. *Level Set Methods and Fast Arching Methods: Evolving Interfaces in Computational Geometry, Fluid Mechanics, Computer Vision and Materials Sciences*. Cambridge University Press: Cambridge, UK, 1998.
13. Osher S, Fedkiw R. *Level Set Method and Dynamic Implicit Surfaces*. Springer: Berlin, 2002.
14. Yoshida Y, Watanabe T. Gate breakdown phenomena during reactive ion etching process. *Proceedings of the Symposium on Dry Process*, Tokyo, 1983; 4.
15. Radjenović B, Radmilović-Radjenović M, Petrović ZLJ. Influence of charging on SiO<sub>2</sub> etching profile evolution etched by fluorocarbon plasmas. *Material Science Forum* 2007; **555**:53–58.

16. Palov AP, Mankelevich YuA, Rakhimova TV, Shamiryan D. Charging and the secondary electron–electron emission on a trench surface: broadening and shift of ion energy spectrum at plasma trench etching. *Journal of Physics D: Applied Physics* 2010; **43**:075203.
17. Matsui J, Maeshige K, Makabe T. Effect of aspect ratio on topographic dependent charging in oxide etching. *Journal of Physics D: Applied Physics* 2001; **34**:2950–2955.
18. Makabe T, Maeshige K. Vertically integrated computer-aided design for device processing. *Applied Surface Science* 2002; 176–200.
19. Whitaker R. A level-set approach to 3D reconstruction from range data. *The International Journal of Computer Vision* 1998; **29**:203–231.
20. Radjenović B, Lee JK, Radmilović-Radjenović M. Sparse field level set method for non-convex Hamiltonians in 3D plasma etching profile simulations. *Computer Physics Communications* 2006; **174**:127–132.
21. Birdsall CK. Particle-in-cell charged-particle simulations, plus Monte Carlo collisions with neutral atoms. *IEEE Transactions on Plasma Science* 1991; **19**:65–85.
22. Verboncoeur JP, Alves MV, Vahedi V, Birdsall CK. Simultaneous potential and circuit solution for 1d bounded plasma particle simulation codes. *Journal of Computational Physics* 1993; **104**:321–328.
23. Kim HC, Iza F, Yang SS, Radmilović-Radjenović M, Lee JK. Particle and fluid simulations of low-temperature plasma discharge: benchmarks and kinetic effects. *Journal of Physics D: Applied Physics* 2005; **38**:R283–R301.
24. La Magna A, Garozzo G. Factors affecting profile evolution in plasma etching of SiO<sub>2</sub>—modeling and experimental verification. *Journal of Electrochemical Society* 2003; **150**:F178–F185.
25. Hwang GS, Anderson C, Gordon M, Moore T, Minton T, Giapis K. Gas-surface dynamics and profile evolution during etching of silicon. *Physical Review Letters* 1996; **77**:3049–3052.
26. Geuzaine C. High order hybrid finite element schemes for Maxwell's equations taking thin structures and global quantities into account. *Ph.D. Thesis*, Universite de Liege, 2001.
27. GetDP. Available from: <http://www.geuz.org/getdp>.
28. TetGen. Available from: <http://tetgen.berlios.de>.

#### AUTHORS' BIOGRAPHIES



**Dr Marija Radmilovic-Radjenovic** obtained her MSc and PhD degrees at the Faculty of Physics, University of Belgrade. Dr Radmilovic-Radjenovic has been employed at the Institute of Physics, University of Belgrade as research professor. She is the leader of the subproject: Physical bases for application of non-equilibrium plasmas in nanotechnology and the treatment of materials. She was a general secretary of the organizing committee of the 5th EU-Japan Workshop on Plasma Processing. She has published more than 50 papers in refereed journals and her interests include plasma etching, nanotechnology, micro discharges, rf plasma modeling and gas breakdown studies. She has been cited more than 200 times in leading international journals.



**Dr Branislav Radjenović** obtained his BEng, MSc and PhD degrees at the Faculty of Electrical Engineering, University of Belgrade (1990). Dr Radjenović has been employed at the Institute of Physics, University of Belgrade as research professor. Dr Radjenović was also elected as associate professor in 2002 at the Military and Technical Academy in Belgrade. He has published more than 40 papers in refereed journals and his interests include plasma etching profile simulation and development of the simulation package for 3D profile evolution based on the level set method.



**Marija Savić** is a PhD student who obtained her BEng and MSc degrees at the Faculty of Electrical Engineering. Marija Savić has been employed at the Institute of Physics, University of Belgrade as research assistant. She has published 3 papers in refereed journals and her interests include rf plasma modeling and gas breakdown studies.

## UTICAJ SEKUNDARNE EMISIJE ELEKTRONA NA KARAKTERISTIKE RADIO-FREKVENTNIH PLAZMI

U ovom radu proučavan je uticaj sekundarne emisije elektrona na karakteristike radio-frekventnih (rf) plazmi. Korišćenjem jednodimenzionalnog PIC/MCC (Particle in Cell with Implemented Monte Carlo Collisions) koda modelovan je kapacitivno spregnuti plazma reaktor, napajan pomoću dva rf generatora na različitim frekvencijama. Sekundarna emisija elektrona je jedan od ključnih procesa, kako sam po sebi tako i zbog uticaja na karakteristike pražnjenja. Sekundarna emisija elektrona sa površina modelovana je pomoću izraza koji su predložili Phelps i Petrović (Plasma Sources Sci. Technol. 8 (1999) R21–R44) za tretirane i netretirane metalne površine. Pokazano je da su karakteristike plazme u velikoj meri zavisne od uslova na površinama elektroda.

Nauka o materijalima nalazi se u žiži savremenog naučno-tehnološkog progressa. U širokom dijapazonu naučnih i inženjerskih disciplina za sintezu novih materijala, nalazi se i upotreba neravnotežne plazme, kao jedan od ključnih postupaka u razvoju široke klase novih materijala. Naročito značajna u razvoju mikro i nano elektronske industrije, upotreba neravnotežnih plazmi predstavlja nezamenljiv tehnološki proces za nagražanje dielektričnih interkonekt slojeva visokog odnosa dubine i širine [1–3]. Uzimajući u obzir da ovi koraci predstavljaju oko 80% aktivnosti u proizvodnji integrisanih kola, neravnotežnim plazmama se posvećuje velika pažnja u istraživanjima koja, u skorije vreme, obuhvataju sve veći broj novih tehnika. Zahvaljujući razvoju brzih računara, računarske simulacije su postale veoma popularna i pouzdana istraživačka tehnika, koja trenutno ima veliki udeo u istraživanju nanotehnologije [4–8].

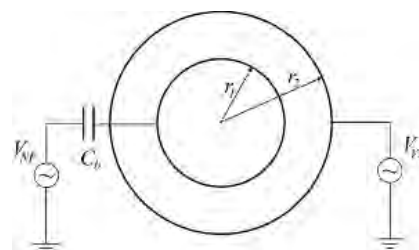
U ovom radu, naročitu pažnju smo posvetili modelovanju procesa sekundarne emisije elektrona kod kapacitivno spregnutog reaktora cilindrične geometrije, korišćenjem jedno-dimenzionalnog PIC/MCC (eng. *Particle in Cell with Implemented Monte Carlo Collisions*) koda [9–11].

Premda je uloga sekundarnih elektrona u procesima električnog proboja u gasovima kod niskostrujnih stacionarnih pražnjenja tematika koja datira još sa početka XX veka, svi njeni aspekti još uvek nisu u potpunosti izučeni. U skorije vreme, uticaj sekundarne emisije elektrona na karakteristike plazmi se ponovo nalazi u žiži interesovanja, pre svega zbog njihove uloge u fundamentalnim istraživanjima i zbog niza industrijskih aplikacija [12–16].

Do sada, modelovanje plazma reaktora je podrazumevalo uključivanje i procesa sekundarne emisije elektrona pretpostavljajući da je prinos sekundarnih elektrona konstantan, što je u velikoj meri prouzrokovalo

značajna odstupanja rezultata modelovanja od eksperimentalno dobijenih podataka. U ovom radu, modelovanje je ostvareno koristeći realne modele za prinos sekundarnih elektrona u argonu, koristeći izraze preuzete iz rada Phelps-a i Petrovića [12].

Simulirani asimetrični dvo-frekventni kapacitivno spregnuti reaktor (slika 1), predstavlja vrstu reaktora koji se najčešće koriste u praksi zbog niza pogodnosti. Povoljna karakteristika dvo-frekventnih reaktora se sastoji u mogućnosti da se proizvodnja plazme i energija jona kontrolišu različitim generatorima. Pod uslovom da je sprega između generatora mala, možemo postići selektivnu kontrolu procesa u plazmi. Za praksu je značajna kontrola jona koji udaraju površinu unutrašnje elektrode, odnosno kontrola onih jona koji se koriste u obradi materijala.



Slika 1. Shematski prikaz asimetričnog kapacitivno spregnutog reaktora sa dve frekvencije.

Figure 1. Schematic representation of the asymmetric dual-frequency capacitively coupled reactor.

U literaturi se može naći detaljno objašnjenje kako dolazi do formiranja napona na unutrašnjoj elektrodi usled ambipolarne difuzije čestica iz plazme. Ovde ćemo reći samo da se prednapon, ili jednosmerna komponenta naizmjeničnog napona, na unutrašnjoj elektrodi formira tako da se izjednače gubici jona i elektrona iz plazme. Prednapon unutrašnje elektrode utiče na srednju vrednost električnog polja u prielektrodnoj oblasti. Zbog brzo-promenljivog električnog polja u plazmi, koje ima srednju vrednost različitu od nule, joni kao znatno inertnije čestice od elektrona kreću se prateći srednju vrednost polja u vremenu. Srednja vrednost električnog polja u prielektrodnoj oblasti je odgovorna za ubrzavanje

Autor za prepisku: A. Bojarov, Institut za fiziku, Centar za neravnotežne procese, Pregrevica 118, 11080 Zemun, Srbija.

E-pošta: bojarov@mail.ipb.ac.rs

Rad primljen: 10. avgust 2010.

Rad prihvaćen: 28. oktobar 2010.

jona, a samim tim utiče i na energiju jona koji bombarduju unutrašnju elektrodu i emituju sekundarne elektrone.

U simulacijama, interesovao nas je, pre svega, uticaj sekundarne emisije na karakteristike plazme. Karakteristike od posebnog interesa su koncentracija plazme, fluks i raspodela energije jona koji dospevaju do elektroda (eng. *Ion Energy Distribution Function*, IEDF), s obzirom da koeficijent sekundarne emisije elektrona zavisi od energije jona koji udaraju u neku od elektroda.

Za metalne elektrode uzeli smo koeficijente sekundarne emisije prema izrazima Phelps-a i Petrovića za nekoliko slučajeva različito tretiranih elektroda. U osnovi su nam dve glavne postavke reaktora: a) kada je unutrašnja elektroda čista i spoljašnja neočišćena (skraćeno čista–neočišćena reaktor) i b) kada je unutrašnja neočišćena i spoljašnja čista elektroda (skraćeno neočišćena–čista reaktor). Pored ove dve postavke, simulirali smo i kombinaciju elektroda kada nema sekundarne emisije na unutrašnjoj, dok je na spoljašnjoj elektrodi koeficijent sekundarne emisije  $\gamma = 0,2$  (skraćeno 0-0.2 reaktor) i kada na obe elektrode nema sekundarne emisije (skraćeno 0-0 reaktor).

Pražnjenje u gasu spada u domen plazme niskog pritiska, neutralni gas je na pritisku od 20 Pa. Unutrašnji poluprečnik reaktora je 0,03 m, dok je spoljašnji poluprečnik 0,0519 m. Generator više frekvencije je na 28 MHz, amplitude 2000 V i vezan je za spoljašnju (veću) elektrodu, dok je generator niže frekvencije na 2 MHz, amplitude 500 V i vezan je za unutrašnju (manju) elektrodu. Kapacitivnost kondenzatora je direktno povezana sa geometrijom reaktora i vrednost od 100 pF je usklađena sa brojem naelektrisanih čestica koji pune kondenzator, odnosno sa padom potencijala u prielektrodnoj oblasti.

### Sekundarna emisija elektrona sa elektroda

Jedna od najznačajnijih pojava koja je ponovo postala aktuelna u poslednje vreme je sekundarna emisija elektrona sa elektroda, koja je posledica udara različitih čestica o površinu elektrode. Za održavanje pražnjenja u gasovima neophodna je proizvodnja sekundarnih elektrona koji treba da zamene elektrone izgubljene na površinama elektroda i na zidovima reaktora. Uslov za sam čin proboja je da sekundarna lavina postane jednaka primarnoj, odnosno da se ukupna proizvodnja elektrona u kružnom toku primarne lavine, povratne sprege i sekundarne lavine izjednači sa gubicima elektrona na anodi. Pod pojmom sekundarne lavine podrazumevamo sve lavine koje nastaju iza prve i to, što posebno ističemo, usled udara jona o površine elektroda.

Procese sekundarne emisije elektrona sa površine izazvane različitim vrstama čestica, opisujemo prinosom sekundarnih elektrona  $\gamma$  koji, u znatnoj meri, zavisi od stanja površine i upadne energije čestica. Kada se joni i atomi sudare sa čistom površinom može se desiti neko-

liko vrsta procesa, ali je najvažniji izbacivanje elektrona sa površine. Ovaj proces direktno utiče na tok električnih pražnjenja obezbeđujući i mehanizam povratne sprege neophodne da se održava pražnjenje u gasovima. Sekundarnu emisiju elektrona uzrokuju četiri osnovna procesa:

- fotoelektronska emisija,
- emisija kao posledica sudara metastabila sa površinom,
- potencijalna emisija u sudarima jona sa površinom i
- kinetička emisija u sudarima jona i atoma sa površinom.

Sva četiri navedena procesa su moguća kod pražnjenja u argonu i međusobno su povezana. Ostali važni procesi na površinama uključuju: sudarno gašenje metastabila (što je povezano sa drugim procesom) i procese refleksije elektrona, jona i neutrala sa površina.

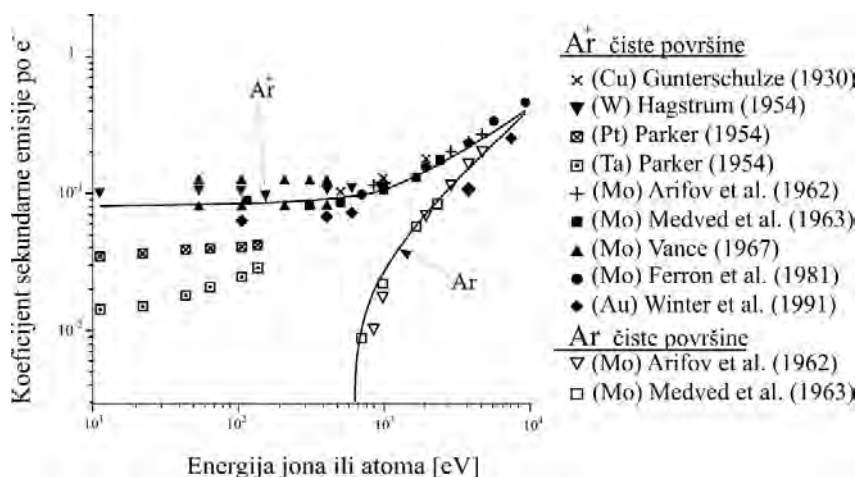
Najpre ćemo dati kratak pregled postojećih rezultata za prinos sekundarnih elektrona izazvanih delovanjem jona na tzv. čiste i neočišćene površine elektroda. Pod pojmom čiste elektrode podrazumeva se elektroda koja je tretirana zagrevanjem njene površine na temperaturi od oko 2000 K u uslovima dobrog vakuuma, dok se sama merenja koeficijenta sekundarne emisije elektrona vrše na sobnoj temperaturi u veoma visokom vakuumu. Ponekad se proces čišćenja katode ostvaruje i skidanjem njenog površinskog sloja jonskim spaterovanjem.

Neočišćene površine elektroda predstavljaju površine obrađene u radionici standardnim mehaničkim i hemijskim tehnikama koje, potom, bivaju izložene atmosferskom gasu što može rezultirati oksidacijom ili nekim drugim kontaminirajućem procesom u procesu pumpanja do relativno niskog vakuuma, kao što je depozicija para iz pumpe. Stabilni oksidni slojevi se na ovaj način ne mogu očistiti, čak ni u slučaju plemenitih metala kao što je zlato.

Na slici 2 prikazani su eksperimentalni rezultati za prinos sekundarnih elektrona za snopove  $\text{Ar}^+$  jona i Ar atoma koji padaju na različite čiste metalne površine u zavisnosti od njihove upadne energije. Slika je preuzeta iz rada Phelps-a i Petrovića [12] i obuhvata sve pronađene podatke za energije ispod 1 keV.

Za većinu katodnih površina koeficijent sekundarne emisije elektrona po jonu gotovo da ne zavisi od upadne energije jona u opsegu jonskih energija ispod 500 eV. Ova nezavisnost od energije se pripisuje Augere-ovom procesu koji se naziva potencijalno izbacivanje elektrona. Oblast zavisnosti koeficijenta sekundarne emisije od upadne energije jona na energijama od nekoliko keV pripisuje se kinetičkom izbacivanju, premda priroda ovog procesa još uvek nije sasvim razjašnjena. Granica na kojoj nastaje kinetičko izbacivanje je određena procesima multielektronske emisije elektrona





Slika 2. Energijska zavisnost prinosa sekundarnih elektrona kada snopovi Ar<sup>+</sup> jona i Ar atoma padaju na različite čiste katodne površine. Puni simboli predstavljaju rezultate različitih autora za Ar<sup>+</sup> jone, dok otvoreni simboli odgovaraju rezultatima za Ar jone. Figure 2. Energy dependence of the secondary electron yield for Ar<sup>+</sup> ions and Ar atoms hitting clean surfaces of different materials. Full symbols represent results from various authors for Ar<sup>+</sup> ions and open symbols correspond to Ar atoms.

sa površine katode. Možemo smatrati da je za većinu metala koeficijent sekundarne emisije elektrona po jonu približno jednak 0,1 za energije ispod 1 keV.

Na slici 3 prikazani su eksperimentalni rezultati za  $\gamma_i$  koeficijente u slučaju Ar<sup>+</sup> jona, kao i za  $\gamma_a$  koeficijente u slučaju Ar atoma koji padaju na metalne površine izložene u različitom stepenu kiseoniku, vodi, okolnom gasu ili koje su na nespecificiran način kontaminirane. Podaci sa slike pokazuju da su na nižim energijama (<150 eV) vrednosti koeficijenta  $\gamma_i$  za Ar veoma rasute (više od jednog reda veličine). Većina ovih podataka za Ar ukazuje na slabu energijsku zavisnost koeficijenta od jonske energije.

U našim PIC/MCC proračunima koristili smo izraze preuzete iz rada Phelps i Petrović [12] za prinos

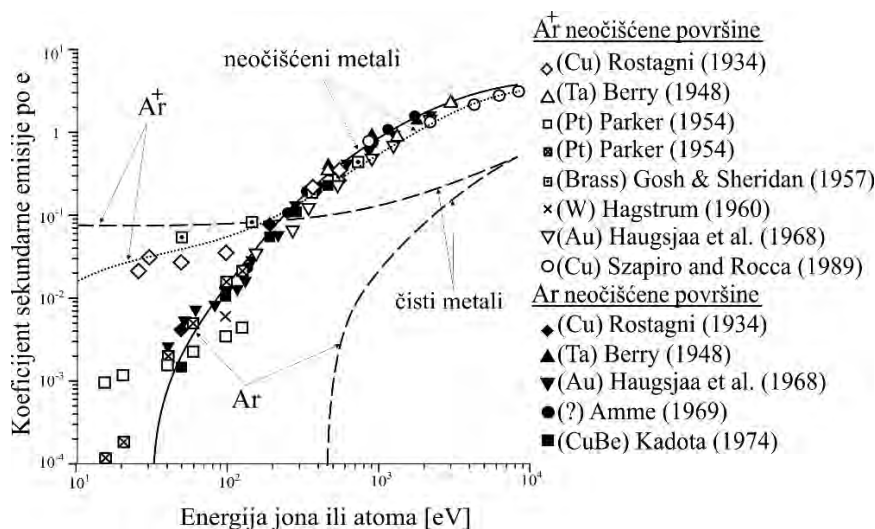
sekundarnih elektrona koje su predstavljene na slici 3. Analitički izrazi za zavisnost koeficijenta sekundarne emisije,  $\gamma_i$ , od energije jona,  $\epsilon_i$ , su:

– Za čiste površine, Phelps i Petrović [12]:

$$\gamma_i^c = 0,07 + \frac{1 \times 10^{-5} (\epsilon_i - 500)^{1,2}}{1 + \left(\frac{\epsilon_i}{7000}\right)^{0,7}} \quad (1)$$

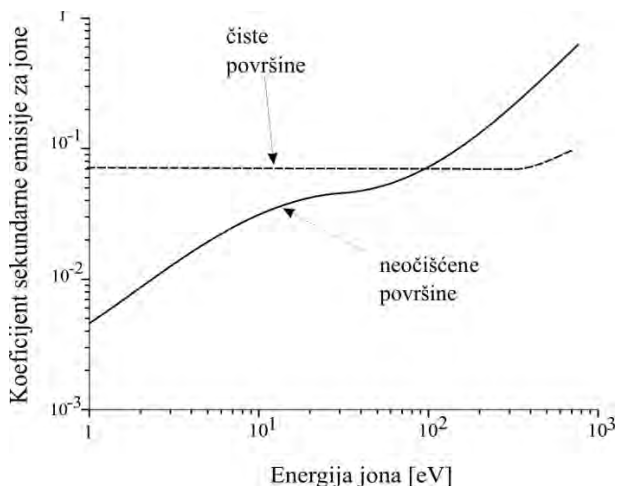
– Za neočišćene površine, Phelps i Petrović [12]:

$$\gamma_i^d = \frac{0,006\epsilon_i}{1 + \left(\frac{\epsilon_i}{10}\right)^{1,5}} + \frac{1,05 \times 10^{-4} (\epsilon_i - 80)}{1 + \left(\frac{\epsilon_i}{8000}\right)^{1,5}} \quad (2)$$



Slika 3. Energijska zavisnost prinosa sekundarnih elektrona kada snopovi Ar<sup>+</sup> jona i Ar atoma padaju na različite neočišćene katodne površine. Puni simboli predstavljaju rezultate različitih autora za Ar<sup>+</sup> jone, dok otvoreni simboli korespondiraju rezultatima za Ar jone. Figure 3. Energy dependence of the secondary electron yield for Ar<sup>+</sup> ions and Ar atoms hitting dirty surfaces of different materials. Full symbols represent results from various authors for Ar<sup>+</sup> ions and open symbols correspond to Ar atoms.

Prinos drugog sabirka u svakom od izraza (1) i (2) jednak je nuli za energije incidentnih jona ispod 500 eV i 80 eV, za čiste i neočišćene površine redom. Na slici 4 date su krive koje odgovaraju izrazima za koeficijent sekundarne emisije.



Slika 4. Koeficijent sekundarne emisije elektrona u zavisnosti od energije čestice za snopove  $Ar^+$  jona koji padaju na različito tretirane površine. Obe krive su nacrtane koristeći izraze (1) i (2).

Figure 4. Coefficient of secondary electron emission induced by  $Ar^+$  ions hitting differently treated surfaces. Curves represent graphs of the relations (1) and (2).

### Opravdanost rezultata simulacije

Pre pretstavljanja samih rezultata simulacije, dajemo kratak kvantitativni uvid u same parametre simulacije kako bi utvrdili da ne postoje velika odstupanja koja bi eventualno mogao da unese sam PIC/MCC kod. Osnovni zahtev koji treba da zadovolji PIC tehnika jeste dobra prostorna rezolucija pojedinih ćelija, kako bi se razlučile sve karakteristične dužine koje se javljaju u gasnim pražnjenjima. Jedna od najmanjih karakterističnih dužina je svakako Debay-eva dužina termalnih elektrona u središnjem delu pražnjenja (balku), koja je u rf gasnim pražnjenjima reda  $\lambda_D \approx 10^{-4}$  m. Prostor pražnjenja izdvojen je na 2000 ćelija, odnosno ćelijama dužine  $\Delta x = 1,095 \times 10^{-5}$  m, što omogućava dobro razlaganje dužine  $\lambda_D$ . Ovim se minimizuje odstupanje izazvano aproksimacijom konačnih elemenata s obzirom da je zadovoljen uslov:

$$\frac{\Delta x}{\lambda_D} \approx 0,11 < 1 \quad (3)$$

Takođe, vrlo važan parametar simulacije je vremenski korak,  $\Delta t$ , za koji je uzeto da je 1/5000 periode generatora od 28 MHz, odnosno  $\Delta t = 7,142857 \times 10^{-12}$  s. Time je postignuto razlučivanje brzine čestica do:

$$\Delta x / \Delta t \approx 1,533 \times 10^{11} \text{ m/s} \quad (4)$$

što u potpunosti pokriva, čak i za više redova veličine, opseg energija svih čestica koje se javljaju u simulaciji.

Potrebno je da vremenski korak razluči i maksimalnu kolizionu frekvenciju na osnovu korišćenih preseka sudara [17]. Uzima se u obzir najgori slučaj, odnosno maksimalna vrednost totalnog preseka sudara, iz domena od važnosti, za jone  $\sigma_{i_{\max}} \approx 1,80 \times 10^{-18} \text{ m}^2$  i elektrone  $\sigma_{e_{\max}} \approx 1,25 \times 10^{-19} \text{ m}^2$ , zatim energije jona na kojima je presek maksimalan (uzimamo što veće vrednosti) za jone  $E_{i_{\max}} \approx 1000 \text{ eV}$  i za elektrone  $E_{e_{\max}} \approx 100 \text{ eV}$ . Pritisak neutralnog gasa argona je 20 Pa na temperaturi od 300 K. Izraz za kolizionu frekvenciju je:

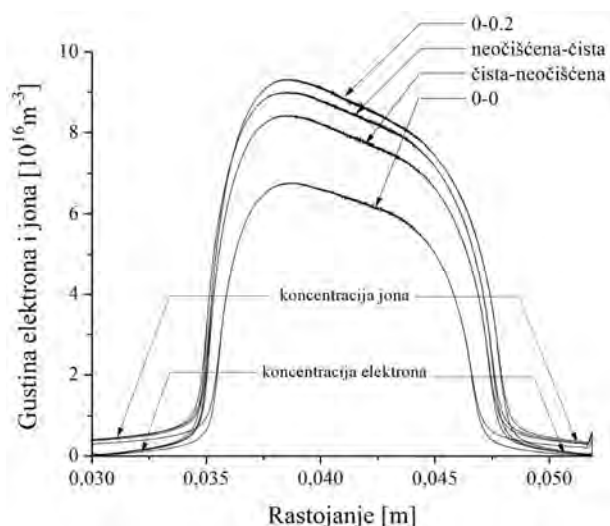
$$f = n_n \sigma \sqrt{\frac{2E}{m}} \quad (5)$$

gde se gustina neutralnog (pozadinskog) gasa,  $n_n$ , dobija iz zakona o gustini idealnog gasa,  $m$  je masa elektrona ili jona,  $\sigma$  i  $E$  su gore definisani totalni presek i energija čestice, redom. Ovim je frekvencija sudara za jone i elektrone  $f_i \approx 1,91 \times 10^7 \text{ Hz}$  i  $f_e \approx 3,58 \times 10^9 \text{ Hz}$ , što opravdava korišćenje Monte Carlo tehnike sudara za dati vremenski korak, s obzirom da je frekvencija sudara u najgorem slučaju nekoliko redova veličine niža od vrednosti  $1/\Delta t$ .

### Koncentracija plazme

Jedna od osnovnih karakteristika svakog pražnjenja jeste koncentracija naelektrisanih čestica u gasu, odnosno njihova raspodela u prostoru pražnjenja. Središnji deo pražnjenja sadrži većinu naelektrisanih čestica koje su kvazineutralnoj ravnoteži, odnosno koncentracije jona i elektrona su skoro identične, kao što se može videti sa slike 5. Prielektrodne oblasti sadrže vrlo mali broj naelektrisanih čestica, međutim, zbog toga što postoji neravnoteža u koncentraciji jona i elektrona (slika 5), one utiču gradijentom polja na ubrzanje jona ka elektrodama i time direktno utiču i na procese na površinama. Profil plazme dostiže svoj ustaljeni oblik nakon samo nekoliko mikrosekundi, a zatim se koncentracija čestica samo povećava, bez velikih odstupanja od uspostavljenog profila.

Na slici 5, na kojoj su date usrednjene vrednosti koncentracija čestica u vremenu, može se primetiti uticaj koji sekundarna emisija ima na apsolutnu koncentraciju elektrona i jona u plazmi. Najuočljivija je razlika između krive dobijene za sistem bez sekundarne emisije (0-0) i krivih za sistem sa sekundarnom emisijom. Osnovan zaključak je da se za precizan opis profila plazme mora u model pražnjenja uključiti sekundarna emisija elektrona od strane jona. Međutim, kao što se može zaključiti sa slike 5, odnosno iz razlike krivih za  $\gamma = 0,2$  i  $\gamma = \gamma(\varepsilon)$  ( $\gamma(\varepsilon)$  odgovara slučajevima čista-neočišćena i neočišćena-čista), nije dovoljno samo da postoji koeficijent sekundarne emisije za jone, već on mora da bude konzistentan sa realnim fizičkim procesima.



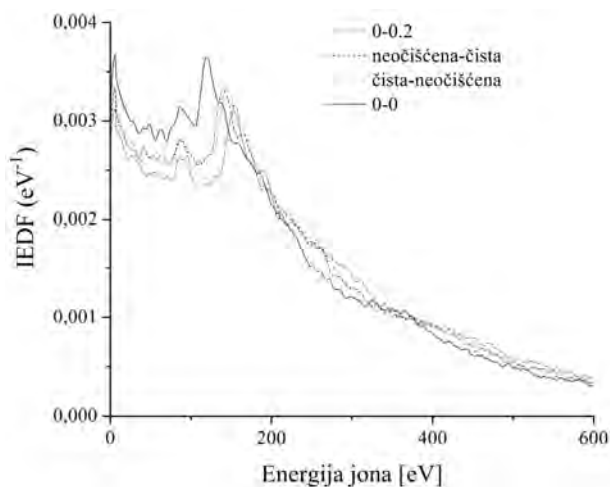
Slika 5. Koncentracija jona i elektrona za četiri konstrukcije reaktora sa različito tretiranim elektrodama, nakon proteklih 5  $\mu$ s simulacionog vremena.

Figure 5. Ion and electron concentrations for four reactor constructions with differently treated electrodes, after 5  $\mu$ s of simulated time.

### Raspodela energije jona na elektrodama

Sledeća važna karakteristika plazme, naročito za praksu, jeste raspodela energije jona (IEDF) na unutrašnjoj elektrodi. Uzimajući u obzir da se dvo-frekventni kapacitivno spregnuti reaktori najčešće koriste zapravo zbog energetskih jona koji padaju na unutrašnjoj elektrodi, vrlo je važno precizno poznavanje raspodele energije jona u blizini elektroda.

Na slici 6 prikazane su krive raspodele za četiri ispitivana slučaja, gde se vidi razlika za različite koeficijente sekundarne emisije. Zavisnost IEDF-a od sekundarne emisije je složena, zbog toga što veza između ova dva parametra ima oblik povratne sprege. Pored ovoga,



Slika 6. Raspodela jona po energijama koji padaju na unutrašnju elektrodu.

Figure 6. Ion energy distributions on the inner electrode.

koncentracija plazme koja je takođe zavisna od sekundarne emisije, utiče na profil IEDF na unutrašnju elektrodu.

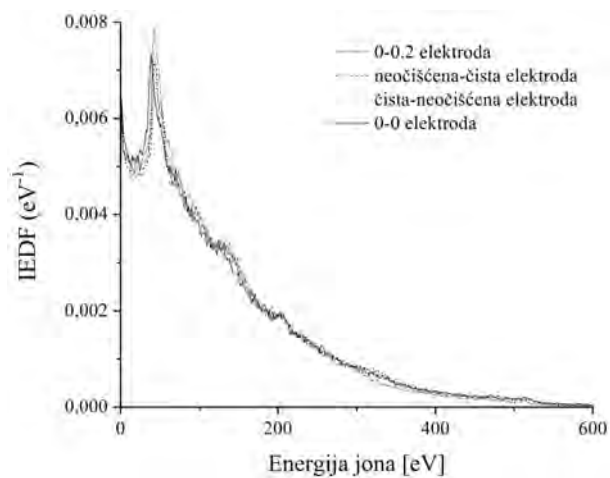
Sa slike 7 vidi se da je uticaj sekundarne emisije na raspodelu energije jona koji dospevaju na spoljašnju elektrodu, relativno mali. Relativno velike razlike u koeficijentu za spoljašnju elektrodu (od 0 do 0,2) ne unose bitne promene u raspodeli energije jona, što znači da će pri istim uslovima više elektrona nastati iz površine sa većim koeficijentom sekundarne emisije.

Dosadašnji rezultati nas mogu dovesti do zaključka da zbog razlike u gustini plazme i IEDF-a na unutrašnju elektrodu (slika 6) sekundarna emisija sa elektroda ima veliki uticaj na raspodelu energije jona na unutrašnju elektrodu, što je vrlo važan parametar kada se govori o primeni rf plazme u obradi materijala.

### Potencijal plazme

Potencijal plazme ima ulogu da zadrži elektrone u plazmi i da izazove da što veći broj jona napusti plazmu. S obzirom na to, potencijal plazme je uvek na većoj vrednosti od potencijala elektroda. U toku vremena potencijal plazme se menja, prateći uglavnom oscilacije nisko-frekventnog izvora, pri ovome dolazi i do promene pada potencijala u prielektrodnoj oblasti. Na slici 8 primećuje se da za realne postavke reaktora (čiste i neočišćene elektrode) nema razlike u prostornom potencijalu plazme. Drugim rečima, joni u reaktorima konfiguracije čista-neočišćena i neočišćena-čista elektroda padaju na unutrašnju i spoljašnju elektrodu pod istim uslovima. Naravno, ovo još više dovodi u prvi plan uticaj sekundarne emisije, jer i pri istim uslovima u plazmi promena koeficijenta sekundarne emisije dovodi do drastičnih promena karakteristike plazme (slike 5 i 6).

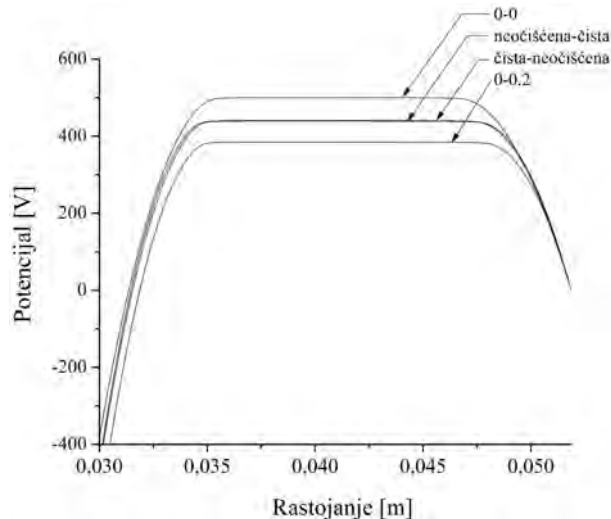
Napomena je da ovi zaključci važe u slučaju realnog modelovanja sekundarne emisije prema izrazima Phelps-a i Petrovića, gde koeficijent sekundarne emisije



Slika 7. Raspodela jona po energijama koji dospevaju na spoljašnju elektrodu.

Figure 7. Ion energy distributions on the outer electrode.

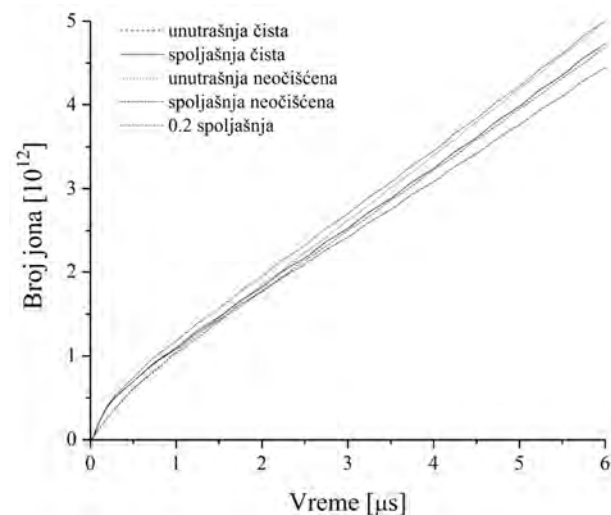
zavisi od energije jona. Sa slike 8 može se zaključiti da nerealni modeli sekundarne emisije drastično menjaju sliku procesa u pražnjenju, što se vidi iz razlike prostornog potencijala za elektrode sa konstantnom sekundarnom emisijom.



Slika 8. Prostorni potencijal u plazmi usrednjen po vremenu.  
Figure 8. Time averaged plasma potential.

### Efektivni $\gamma$ koeficijenti

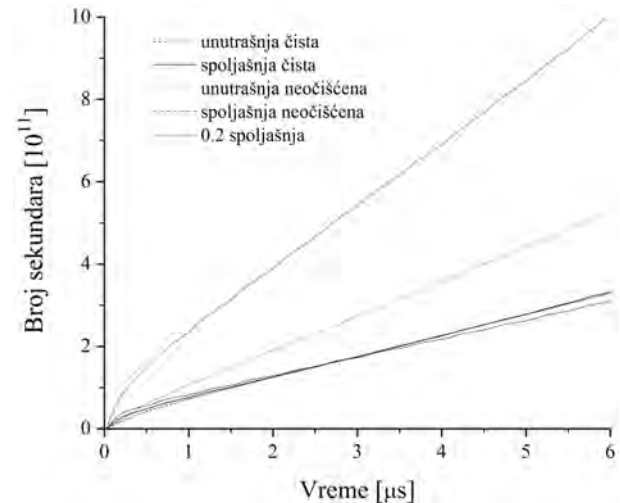
U ovom odeljku, cilj je da se pokaže kako može da se predstavi koeficijent sekundarne emisije njegovom efektivnom vrednošću, na osnovu simulacionih rezultata za fluks jona (slika 9) i fluks sekundarnih elektrona (slika 10).



Slika 9. Broj jona koji je pao na nekoj od elektroda u toku vremena.  
Figure 9. Number of ions that have fallen on the electrodes.

Po definiciji, koeficijent sekundarne emisije predstavlja verovatnoća da jon proizvede sekundarni elektron. Drugim rečima, odnos između broja sekundarnih

elektrona koji nastaje na elektrodi i broja jona koji nestane na njoj jednak je koeficijentu sekundarne emisije. Koristeći ovu činjenicu, možemo na osnovu flukseva jona i sekundarnih elektrona da izračunamo efektivni  $\gamma$  koeficijent, odnosno vrednost konstantnog  $\gamma$  koeficijenta koji bi u toku vremena dao isti broj sekundarnih jona kao i sekundarna emisija zavisna od energije.



Slika 10. Broj sekundarnih elektrona emitovanih sa nekoj od elektroda u toku vremena.  
Figure 10. Number of secondary electrons that have been emitted from the electrodes.

Na osnovu koeficijenata pravih, odnosno flukseva jona i sekundarnih elektrona (slike 9 i 10), možemo napisati izraz iz kojeg se može naći efektivna vrednost sekundarne emisije:

$$\gamma_{\text{eff}} = \frac{\alpha_s}{\alpha_i} \quad (6)$$

gde su  $\alpha_s$  fluks sekundarnih elektrona sa površine,  $\alpha_i$  fluks jona na površini i  $\gamma_{\text{eff}}$  efektivni koeficijent sekundarne emisije. Za različite slučajeve imamo:

$$\text{- spoljašnja 0,2: } \gamma_{\text{eff}} = \frac{1,111 \times 10^6}{5,556 \times 10^6} \approx 0,2$$

$$\text{- spoljašnja neočišćena: } \gamma_{\text{eff}} = \frac{3,310 \times 10^5}{4,882 \times 10^6} \approx 0,0678$$

$$\text{- unutrašnja neočišćena: } \gamma_{\text{eff}} = \frac{6,077 \times 10^5}{5,700 \times 10^6} = 0,1066$$

$$\text{- spoljašnja čista: } \gamma_{\text{eff}} = \frac{3,692 \times 10^5}{3,250 \times 10^6} \approx 0,1136$$

$$\text{- unutrašnja čista: } \gamma_{\text{eff}} = \frac{3,731 \times 10^5}{5,306 \times 10^6} \approx 0,0703$$

Iz dobijenih rezultata možemo izvesti zaključak koja je površina elektroda najefikasnija u proizvodnji sekundarnih elektrona, pored konstantne 0,2 površine,

koju smo uzeli kao primer. Najveći koeficijent sekundarne emisije imaju unutrašnja neočišćena i spoljašnja čista elektroda, što znači da će ova konstrukcija reaktora biti najefikasnija u proizvodnju sekundarnih elektrona, kao što smo već i utvrdili (slika 5).

Važno je napomenuti da date efektivne sekundarne emisije važe samo za dati reaktor, sa parametrima koje smo naveli na početku. Za svaku drugu simulacionu postavku, menjaće se i efektivne sekundarne emisije. Odatle se može videti značaj ove simulacije, kao i računarskih simulacija uopšte, s obzirom da smo uspeli da dobijemo vrednosti efektivne sekundarne emisije na osnovu preciznih fizičkih modela koji se mogu koristiti u praksi.

## ZAKLJUČAK

Istraživali smo uticaj sekundarne emisije elektrona različito tretiranih površina na karakteristike dvo-frekventnih kapacitivno spregnutih pražnjenja. Osnovni motiv ovog istraživanja je velika praktična primena dvo-frekventnih plazmi u industriji, kao i potreba preciznog opisivanja sekundarne emisije sa površina, uzimajući u obzir da se upravo u praksi ovaj tip plazmi najčešće koriste za plazma-nagrizanje dielektrika.

Rezultate do kojih smo došli govore nam da za precizan opis plazme moramo da uzmemo u obzir sekundarnu emisiju elektrona koja zavisi od energije jona koji vrše jonizaciju. Precizan model sekundarne emisije su dali Phelps i Petrović, na osnovu kojeg smo u ovom radu modelovali interakciju jona sa površinama elektroda na kojima dolazi do sekundarne emisije. Pokazali smo na osnovu rezultata simulacije da gustina plazme zavisi od sekundarne emisije i to tako što se njena vrednost u centru pražnjenja drastično povećava sa porastom  $\gamma$  koeficijentata. Raspodela energija jona na unutrašnjoj elektrodi je, takođe, pokazala zavisnost od koeficijenta sekundarne emisije, dok smo sa druge strane pokazali da to ne važi za raspodelu energije jona na spoljašnjoj elektrodi. Zaključili smo da potencijal plazme zavisi od sekundarne emisije sa obe elektrode, tako što je za realne površine pokazivao male razlike ukazujući na to da postoje procesi koji dovode do kompenzacije efekata sekundarne emisije za različite konfiguracije reaktora.

Svakako, najvažnije je to što smo uspeli da pomoću simulacije dobijemo efektivne koeficijente sekundarne

emisije, koji se mogu koristiti u praksi za jednostavnije opisivanje simuliranih plazma-reaktora, pri tom zadržavajući precizni model sekundarne emisije. Značaj dobijenih rezultata opravdava korišćenje simulacionih modela za dobijanje podataka, koji su korisni u praksi i koji smanjuju vremenske i materijalne troškove eksperimentalnih postupaka.

## LITERATURA

- [1] J.M.A. Liberman, A.J. Lichtenberg, Plasma Discharges and Materials Processing, Wiley, New York, 1994.
- [2] T. Makabe, Z.Lj. Petrović, Plasma Electronics: Applications in Microelectronic Device Fabrication, Taylor & Francis, New York, 2006.
- [3] Z.Lj. Petrović, B. Radjenović, M. Radmilović-Radjenović, Proceedings of 26<sup>th</sup> International Conference on Microelectronics, MIEL, Niš, Serbia, 2008, p. 19.
- [4] M. Radmilović-Radjenović, J.K. Lee, Phys. Plasmas **12** (2005) 063501–063508.
- [5] A. Bojarov, M. Radmilović-Radjenović Z.Lj. Petrović, 24<sup>th</sup> Summer School and International SPIG, Contributed Papers, p. 387.
- [6] M. Radmilović-Radjenović, B. Radjenović, Plasma Sources Sci. Technol. **15** (2006) 1–7.
- [7] A. Bojarov, M. Radmilović-Radjenović, Z.Lj. Petrović, Hem. Ind. **63** (2009) 233–238.
- [8] M. Radmilović-Radjenović B. Radjenović, Contrib. Plasm. Phys. **47** (2007) 165–172.
- [9] V. Vahedi M. Surendra, Comput. Phys. Commun. **87** (1995) 179–168.
- [10] C.K. Birdsall, IEEE Trans. Plasm. Sci. **19** (1991) 65–85.
- [11] J.P. Verboncoeur, Plasma Phys. Control. Fusion **47** (2005) A231–A260.
- [12] A.V. Phelps, Z.Lj. Petrović, Plasma Sources Sci. Technol. **8** (1999) 445–449.
- [13] J.K. Lee, N.Yu. Babaeva, H.C. Kim, O.V. Manuilenko, J.W. Shon, IEEE Trans. Plasma Sci. **32** (2004) 47–53.
- [14] M. Radmilović-Radjenović, Z.Lj. Petrović, Europ. J. Phys. D **54** (2009) 445–449.
- [15] M. Radmilović-Radjenović, Z.Lj. Petrović, B. Radjenović, J. Phys. Conf. Ser. **71** (2007) 012007, p. 19.
- [16] M. Radmilović-Radjenović, Z. Lj. Petrović, G.N. Malović, D. Marić, B. Radjenović, C. J. Phys. **56** (2006) B996–B1001.
- [17] A.V. Phelps, J. Phys. Chem. Ref. Data **20** (3) (1991) p. 557.



**SUMMARY****INFLUENCE OF THE SECONDARY ELECTRON EMISSION ON THE CHARACTERISTICS OF RADIO FREQUENCY PLASMAS**

Aleksandar Bojarov, Marija Radmilović-Radjenović, Marija Savić

Institute of Physics, Belgrade, Serbia

(Scientific paper)

In this paper the influence of secondary emission on the characteristics of rf plasmas has been studied. An asymmetrical dual-frequency capacitively coupled plasma reactor has been modeled with one dimensional PIC/MCC (Particle in Cell with Implemented Monte Carlo Collisions) code. The main feature of the modeling code represents the realistic model of the ion-induced secondary electron emission. Secondary emission of electrons is one of the important processes that effects the characteristics of rf plasmas. For modeling the secondary yield per ion, we have used equations proposed by Phelps and Petrović (Plasma Sources Sci. Technol. **8** (1999) R21–R44) for differently treated metal surfaces. In the model, the energy dependence of the yields per ion for differently treated metal surfaces has been implemented. Results are compared for yields for the so called “dirty” and “clean” surfaces, and the spatial profiles of charged particles and ion energy distributions were observed. The simulation results indicate that the plasma characteristics are greatly affected by the ion-induced secondary emission, changing the overall parameters of dual-frequency capacitively coupled plasma reactors especially in applications as etching devices. Conclusion is that an exact model of the secondary electron emission should be included, as to ensure better agreement between simulation and experiment.

Ključne reči: Radio-frekventna pražnjenja • Računarske simulacije pražnjenja u gasovima • Sekundarna emisija

Key words: Radio frequency discharges • Computer simulations of gas discharges • Secondary emission of electrons

MARIJA B. SAVIĆ  
MARIJA  
RADMILOVIĆ-RAĐENOVIĆ

Institut za fiziku, Beograd, Srbija

NAUČNI RAD

UDK 537.565:621.3.032.21

DOI: 10.2298/HEMIND091221022S

## MODELOVANJE PROBOJA U GASOVIMA NA NISKIM PRITISCIMA MONTE KARLO TEHNIKOM\*

*Osnovna pretpostavka Townsend-ove teorije da joni prouzrokuju emisiju sekundarnih elektrona sa katode važi u veoma uskom opsegu vrednosti redukovanog električnog polja  $E/N$ . U skladu sa revidiranim Townsend-ovom teorijom koju su koncipirali Phelps i Petrović, sekundarni elektroni nastaju usled udara jona, brzih neutrala, metastabila i fotona o katodu, ili jonizacijom atoma gasa brzim neutralima. U ovom radu smo pokušali da izgradimo model koji će omogućiti određivanje vrednosti za prinos sekundarnih elektrona za različite tipove čestica, korišćenjem Monte Karlo tehnike. Dobijeni rezultati su u saglasnosti sa analitičkim rezultatima Phelpsa i Petrovića (Plasma Sources Sci. Technol. 8 (1999) R1).*

Pod terminom gasno pražnjenje podrazumevamo proticanje struje kroz gas. Gas, sam po sebi, predstavlja neprovodnu sredinu. Međutim, ukoliko u gasu postoje naelektrisane čestice, pod uticajem dovoljno jakog električnog polja, može doći do slabe provodnosti, ili čak do proboja u gasu. Gas se tada ponaša kao provodnik, koji omogućava proticanje električne struje uz malu otpornost.

Uticaj lavina sekundarnih elektrona u procesima električnog proboja u gasovima, kod niskostrujnih stacionarnih pražnjenja, dobro je izučen u velikom broju radova i udžbenika [1–3]. Uslov za sam čin proboja podrazumeva da sekundarna lavina elektrona postane jednaka primarnoj. Preciznije rečeno, proboj nastaje kada se ukupna proizvodnja elektrona u kružnom toku primarne lavine, povratne sprege i sekundarne lavine izjednači sa gubicima elektrona na anodi. Mi ćemo pod pojmom sekundarne lavine podrazumevati sve elektrone koji nastaju nakon primarne. Elektronska emisija sa površine katode indukovana pozitivnim jonima, brzim atomima, fotonima i metastabilnim atomima, sudarna jonizacija brzim jonima i atomima proizvedenim u ranijim lavinama, sudarna jonizacija elektronima koji su reflektovani sa anode i fotojonizacija gasa fotonima nastalim u ranijim lavinama predstavljaju osnovne procese nastajanja sekundarnih elektrona [4].

Osnovu modela koji su razvili Phelps i Petrović [4] čini uključivanje dodatnih mogućih izvora sekundarne emisije elektrona, kao i emisije nastale usled dejstva fotona, metastabila na katodu. Sekundarna emisija elektrona može nastati i usled jonizacije izazvane dejstvom neutrala u gasnoj fazi i dejstvom elektrona reflektovanih sa anode. Pored toga, razmatran je i efekat povratne difuzije elektrona na katodu. Samim tim, ovaj jedinstveni model, osim što predstavlja reviziju Townsend-ove teo-

rije, pruža detaljan opis procesa koji dovode do sekundarne emisije elektrona.

Jedna od egzaktnih tehnika koja se može koristiti za proučavanje sekundarne emisije elektrona sa katode je, svakako, Monte Karlo tehnika [5]. Za dobijanje rezultata, predstavljenih u ovom radu, korišćen je kompjuterski kod baziran na Monte Karlo metodu, razvijen u Institutu za fiziku [6]. Simulacije su izvršene, najpre za pražnjenje u argonu, koristeći dobro definisan set efektivnih preseka detaljnije opisanih u radu [5].

### MODEL PHELPS–PETROVIĆ

Predstavljeni model je analitički aproksimativni model pomoću koga se mogu izvršiti proračuni stacionarnih flukseva različitih vrsta čestica: elektrona,  $Ar^+$ , brzih  $Ar$  atoma, metastabila i rezonantnih fotona u prostorno uniformnom električnom polju.

Analizom do sada objavljenih rezultata, Phelps i Petrović su pokazali da prinos sekundarnih elektrona značajno zavisi od stanja površine katode. U tom smislu, razlikujemo površine koje su na neki način tretirane (recimo za materijale sa visokom tačkom ključanja zagrejane na 2000 K u vakuumu, dok se eksperimenti vrše na sobnoj temperaturi) i njih nazivamo čistim površinama. Osim njih, postoje i netretirane ili neočišćene površine, kod kojih je izvršen neki postupak čišćenja, ali ne zagrevanjem do visokih temperatura kao kod čistih površina.

Ovaj model nam omogućava da odredimo vrednosti prinosa sekundarnih elektrona sa katode indukovane jonima, brzim atomima, metastabilima ili fotonima, u zavisnosti od uslova na metalnoj površini, kao i od vrednosti redukovanog električnog polja. Parcijalni doprinos pojedinih čestica (fotona, jona, metastabila i atoma) sekundarnoj emisiji elektrona [4], prikazan je na slikama 1 i 2.

U ovom radu smo koristili izraze koje su predložili Phelps i Petrović [4], za koeficijente sekundarne emisije elektrona sa katode pri udaru atoma, jona i fotona o površinu katode za čiste (*eng. clean*), odnosno neočišćene (*eng. dirty*) površine, jednačine (1)–(6):

\*Rad saopšten na skupu „Osma konferencija mladih istraživača“, Beograd, 21–23. decembar 2009.

Autor za prepisku: M.B. Savić, Institut za fiziku, Pregrevica 118, 11080 Beograd, Srbija.

E-pošta: smarija@ipb.ac.rs

Rad primljen: 21. decembar 2009.

Rad prihvaćen: 29. decembar 2009.

$$\gamma_a^c = 1 \times 10^{-5} (\epsilon_a - 500)^{1.2} / [1 + (\epsilon_a / 70000)^{0.7}] \quad (1)$$

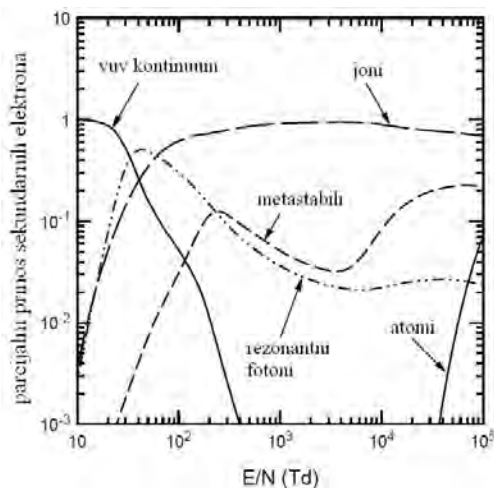
$$\gamma_a^d = 1 \times 10^{-4} (\epsilon_a - 90)^{1.2} / [1 + (\epsilon_a / 8000)^{1.5}] + 7.0 \times 10^{-5} (\epsilon_a - 32)^{1.2} / [1 + (\epsilon_a / 2800)^{1.5}] \quad (2)$$

$$\gamma_i^c = 0.07 + 1 \times 10^{-5} (\epsilon_i - 500)^{1.2} / [1 + (\epsilon_i / 70000)^{0.7}] \quad (3)$$

$$\gamma_i^d = 0.006 \epsilon_i / [1 + (\epsilon_i / 10)^{1.5}] + 1.05 \times 10^{-4} (\epsilon_i - 80)^{1.2} / [1 + (\epsilon_i / 8000)^{1.5}] \quad (4)$$

$$\gamma_{ph}^c = \frac{0.0015(360/\lambda - 1)^4}{[1 + (110/\lambda)^{5.5}]} \quad (5)$$

$$\gamma_{ph}^d = \frac{0.13}{[1 + (\lambda/110)^{1.3}][35/\lambda)^{3.3} + 1]} \quad (6)$$



Slika 1. Parcijalni prinos različitih procesa produkciji sekundarnih elektrona na katodi za pražnjenje u Ar za čiste površine, prema modelu Phelps-Petrović [4].

Figure 1. Fractional contributions of various processes to electron production at the cathode for Ar at breakdown for clean surfaces, Phelps-Petrović model [4].

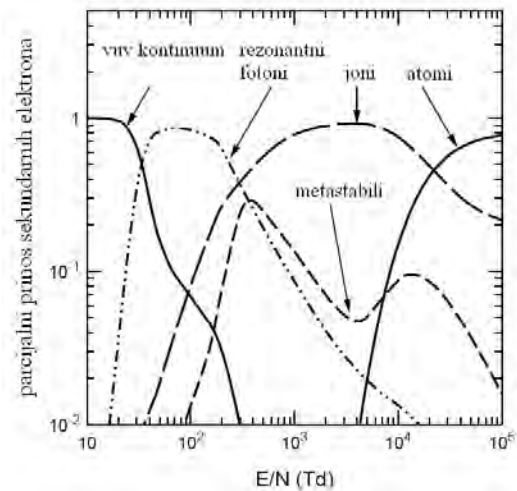
### Monte Karlo tehnika

Naše proračune smo izvršili koristeći Monte Karlo kod [6], sa preseccima za sudare elektrona [5], atoma [7], jona [8] i metastabilnih atoma [9] sa pozadinskim gasom. Na slici 3 prikazani su presecci za sudare elektrona i pozadinskog gasa.

### DISKUSIJA REZULTATA

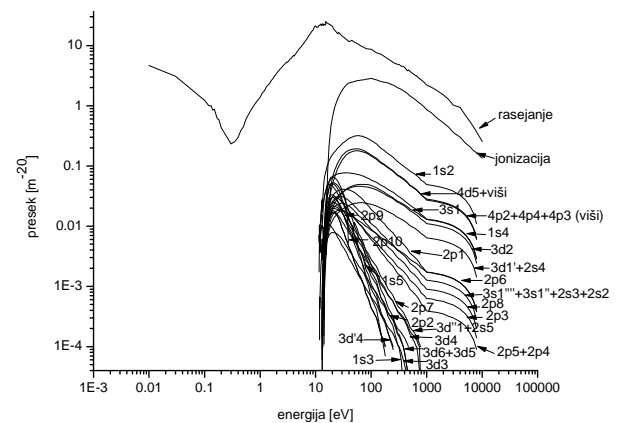
Prvi model prati jone u Monte Karlo kodu, iz koga se izračunava njihov prinos sekundarnih elektrona. Fotoni su, kao što je ranije pomenuto, praćeni u posebnom kodu. Što se tiče metastabila, u ovom modelu je uzet najjednostavniji slučaj. Ukupan broj nastalih metastabila, uključujući i deeksitaciju sa viših stanja na metasta-

bilno, podeljen je tako da je verovatnoća da dođu na katodu 50%, kao u slučaju dve beskonačne planparalelne elektrode gde polovina čestica dospe na jednu, a polovina na drugu elektrodu. Grafici koji ovo ilustruju dati su na slikama 4 i 5 za očišćene i neočišćene površine, redom.



Slika 2. Parcijalni prinos različitih procesa produkciji sekundarnih elektrona na katodi kod probuja u Ar za neočišćene površine, prema modelu Phelps-Petrović [4].

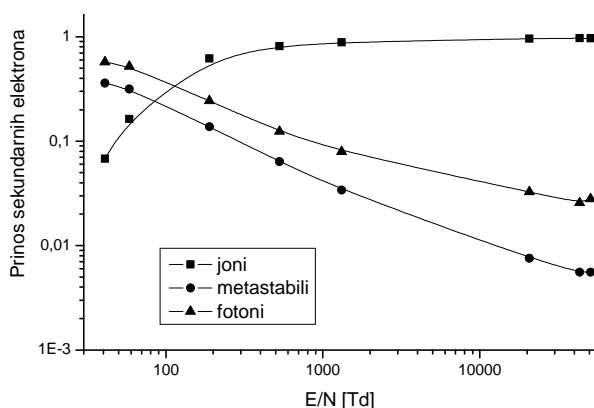
Figure 2. Fractional contributions of various processes to electron production at the cathode for Ar at breakdown for dirty surfaces, Phelps-Petrović model [4].



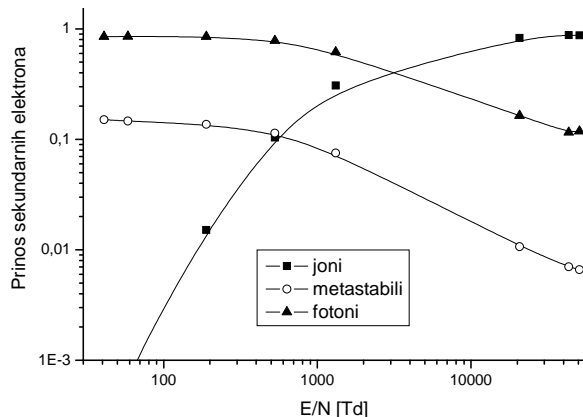
Slika 3. Grafički prikaz presecca za sudare elektrona i čestica pozadinskog gasa [5].

Figure 3. Cross sections for electron-atom collision [5].

Drugi model prati jone i neutrane u Monte Karlo kodu i direktno izračunava njihov prinos sekundarnih elektrona. Fotoni su odrađeni na isti način kao i u prethodnom slučaju. Metastabili su ovog puta takođe uključeni u Monte Karlo kod koji ih prati kao i druge čestice. Produkcija metastabila je jedino iz direktnog pobuđivanja na jedno od dva metastabilna stanja.



Slika 4. Prinos sekundarnih elektrona u funkciji  $E/N$  za različite tipove čestica, za čiste površine.  
Figure 4. Secondary electron yield as a function of  $E/N$  for different types of particles, clean surfaces.

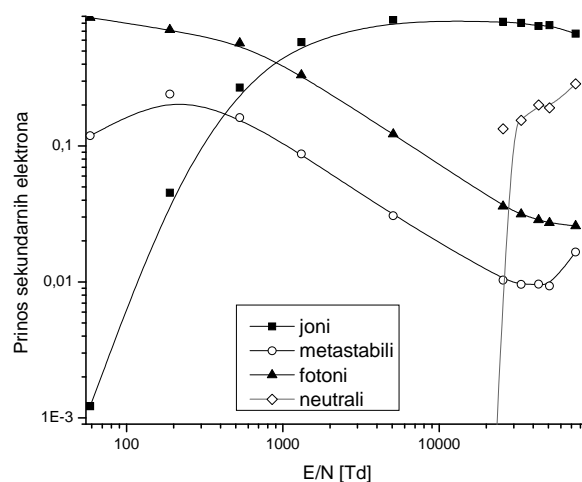


Slika 5. Prinos sekundarnih elektrona u funkciji  $E/N$  za različite tipove čestica, za neočišćene površine.  
Figure 5. Secondary electron yield as a function of  $E/N$  for different types of particles, dirty surfaces.

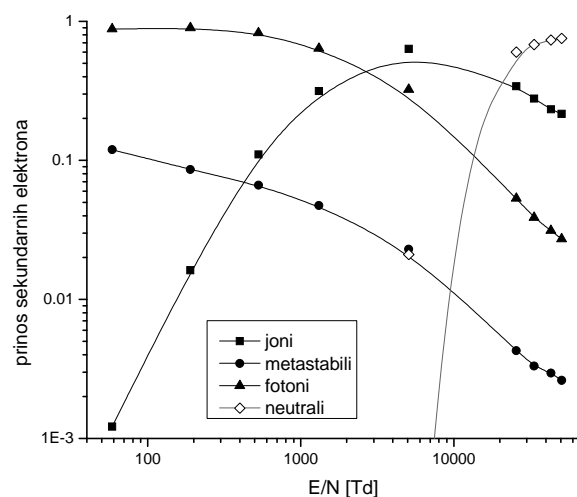
Nestajanje metastabila je usled „kaljenja“ (*quenching-a*) i pri prenosu količine kretanja (*momentum transfer-a*). Iz koda beležimo broj metastabila koji su udarili u katodu. Konačan prinos sekundarnih elektrona od metastabila dobijamo množenjem broja metastabila koji su došli do katode sa koeficijentom  $\gamma = 0,02$ . Grafici su dati na slikama 6 i 7 za očišćene i neočišćene površine, redom.

U narednom koraku uključili smo i refleksiju jona od katode i anode. Koeficijent refleksije iznosi  $R = 0,5$ . Rezultati dobijeni na ovaj način prikazani su na slikama 8 i 9 za čiste i neočišćene površine, redom. Uključivanjem refleksije jona od katode i anode očekivano je da se poveća uticaj jona na produkciju sekundarnih elektrona. Upoređivanjem slika 6 i 8 možemo zaključiti da na većim  $E/N$ , tj. manjim pritiscima, postoji blagi porast prinosa sekundarnih elektrona od strane jona. Slično razmatranje važi i u slučaju neočišćenih površina, što se ponovo zaključuje posmatranjem slika 7 i 9. Što se tiče metastabila, možemo primetiti da je prinos sekundarnih

elektrona od ovog tipa čestica nešto manji nego u slučaju kada nema refleksije. Ovo možemo objasniti na sledeći način: refleksija dovodi do povećanja broja sudara i samim tim povećanja broja jona. Samim tim imamo više elektron-jon sudara, tj. joni „troše“ elektrone. Kako znamo da metastabili nastaju direktnim pobuđivanjem elektrona na metastabilno stanje u sudarima elektron-atom pozadinskog gasa, to i prethodno razmatranje povlači manji broj metastabila.



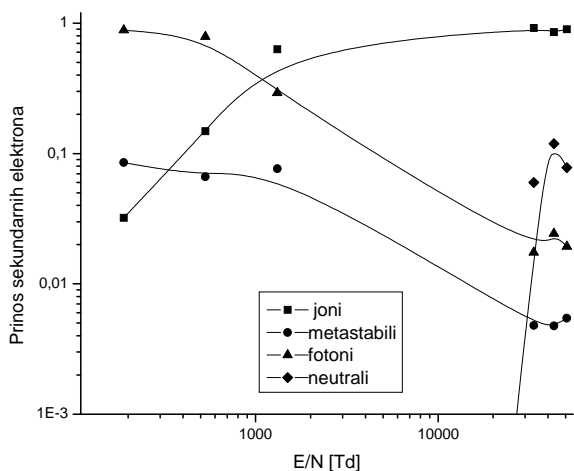
Slika 6. Prinos sekundarnih elektrona u funkciji  $E/N$  za različite tipove čestica, za čiste površine.  
Figure 6. Secondary electron yield as a function of  $E/N$  for different types of particles, clean surfaces.



Slika 7. Prinos sekundarnih elektrona u funkciji  $E/N$  za različite tipove čestica, za neočišćene površine.  
Figure 7. Secondary electron yield as a function of  $E/N$  for different types of particles, dirty surfaces.

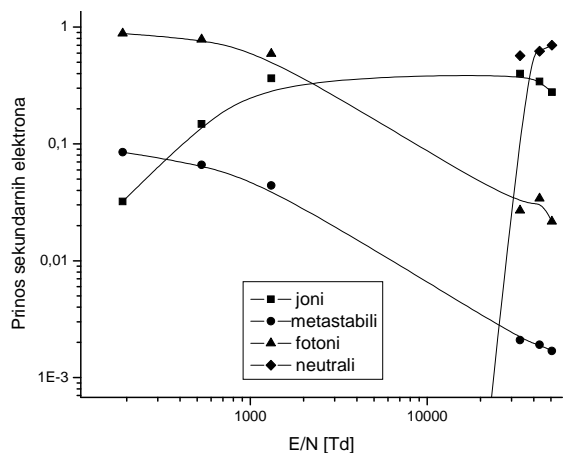
Ukoliko uporedimo prikazane rezultate sa graficima koje su dali Phelps i Petrović [4] možemo doći do određenih zaključaka. Prvi model je (gde je preraspodela metastabila na katodama 50%), kao što se očekivalo, dao rezultate koji dosta odstupaju od analitički

predviđenog rešenja u pomenutom radu. Međutim, može se ipak uočiti očekivani oblik krivih prinosa sekundarnih elektrona.



Slika 8. Prinos sekundarnih elektrona u funkciji  $E/N$  za različite tipove čestica, za čiste površine.

Figure 8. Secondary electron yield as a function of  $E/N$  for different types of particles, clean surfaces.



Slika 9. Prinos sekundarnih elektrona u funkciji  $E/N$  za različite tipove čestica, za neočišćene površine.

Figure 9. Secondary electron yield as a function of  $E/N$  for different types of particles, dirty surfaces.

Drugi model (metastabili su uključeni u Monte Karlo kod) značajno je bolji. Samim uključivanjem metastabila u Monte Karlo kod očekivali smo bolje slaganje, što se i pokazalo opravdanim. Konkretno, kriva koja predstavlja prinos sekundarnih elektrona od metastabila pokazuje dobro poklapanje u regionu srednjih  $E/N$ . Na manjim  $E/N$ , tj. većim pritiscima, model još uvek nije dobar, mada za očišćene površine postoji određen pad koji se i očekuje.

Kao dodatak, prikazan je i slučaj kada je uključena refleksija jona od elektroda. Dobijeni su rezultati koji su i očekivani u slučaju povećanja broja jona u pražnjenju.

Na osnovu prikazanih rezultata možemo uočiti, u skladu sa očekivanjima, da na malim vrednostima  $E/N$

fotoni dominiraju u proizvodnji sekundarnih elektrona, dok je, na visokim vrednostima  $E/N$ , najveći doprinos neutrala. Za srednje vrednosti redukovano električnog polja, ne sme se zanemariti doprinos jona i metastabila u generisanju sekundarnih elektrona.

Uspeli smo da dobijemo zadovoljavajuće slaganje sa analitičkim rezultatima iz rada Phelps i Petrović [4]. Bez obzira na prikazane rezultate, postoji još dosta prostora za usavršavanje modela. Ono na čemu treba raditi je pre svega model metastabila. U sadašnji model uključena je samo produkcija metastabila direktnim pobuđivanjem na metastabilno stanje i u sudarima brzi neutral-pozadinski gas. Neophodno je uključiti u Monte Karlo kod još i kaskade, tj. relaksiranje pobuđenih stanja argona na metastabilna stanja kao još jedan proces produkcije metastabila.

Na čemu još treba raditi jeste i model fotona. Ideja je da se i fotoni uključe u Monte Karlo kod kao zaseban tip čestica i da se kao takvi prate tokom pražnjenja.

## ZAKLJUČAK

U ovom radu učinjeni su početni koraci ka dobijanju modela koji će omogućiti izračunavanje parcijalnih prinosa sekundarnih elektrona za pojedinačne tipove čestica, korišćenjem Monte Karlo koda, koji je razvijen u Laboratoriji za gasnu elektroniku Instituta za fiziku u Zemunu. Ovaj model je dovoljan za više vrednosti  $E/N$  dok se za niže vrednosti mora još razviti model transporta fotona i formiranja molekularne emisije, a generalno se model tretiranja metastabila mora donekle poboljšati.

## Zahvalnica

Ovaj rad je omogućen sredstvima Ministarstva za nauku i tehnološki razvoj, broj projekta: 141025. Autori duguju veliku zahvalnost Prof. dr Zoranu Lj. Petroviću na koncipiranju ideje i korisnim sugestijama tokom izrade ovog rada.

## LITERATURA

- [1] Y.P. Raizer, Gas Discharges Physics, Springer, Berlin, 1991.
- [2] T. Makabe, Z.Lj. Petrović, Plasma Electronics: Applications in Microelectronic Device Fabrication, Taylor & Francis, New York, 2006.
- [3] M.A. Liberman, A.J. Lichtenberg, Plasma Discharges and Materials Processing, Wiley, New York, 1994.
- [4] A.V. Phelps, Z.Lj. Petrović, Plasma Sourc. Sci. Technol. **8** (1999) R21–R44.
- [5] Z.Lj. Petrović, V.D. Stojanović, J. Vac. Sci. Technol. A **16** (1998) 329–336.
- [6] Z.Lj. Petrović, Z. Ristivojević (to be submitted).
- [7] A.V. Phelps, Phys. Chem. Ref. Data **20** (1991) 557.
- [8] A.V. Phelps, J. Appl. Phys. **76** (1994) 747–753.
- [9] B.M. Smirnov, Physics Of Weakly Ionized Gases, Mir Publishers, Moscow, 1981.



**SUMMARY****GAS DISCHARGES MODELING BY MONTE CARLO TECHNIQUE**

Marija Savić, Marija Radmilović-Rađenović

Institute of Physics Belgrade, Pregrevica 118, 11080 Belgrade, Serbia

(Scientific paper)

The basic assumption of the Townsend theory – that ions produce secondary electrons – is valid only in a very narrow range of the reduced electric field  $E/N$ . In accordance with the revised Townsend theory that was suggested by Phelps and Petrović, secondary electrons are produced in collisions of ions, fast neutrals, metastable atoms or photons with the cathode, or in gas phase ionizations by fast neutrals. In this paper we tried to build up a Monte Carlo code that can be used to calculate secondary electron yields for different types of particles. The obtained results are in good agreement with the analytical results of Phelps and Petrović (*Plasma Sources Sci. Technol.* **8** (1999) R1).

Ključne reči: Sekundarna emisija elektrona • Model Phelps–Petrović • Monte Karlo kod

Key words: Secondary electron emission • Phelps–Petrović model • Monte Carlo code

# Breakdown Phenomena in Water Vapor Microdischarges

M. RADMILOVIĆ-RADJENOVIĆ, B. RADJENOVIĆ\* AND M. SAVIĆ

Institute of Physics, Pregrevica 118, 11080 Belgrade, Serbia

The gas breakdown at the large gap sizes is reasonably well understood. However, the breakdown phenomenon in microgaps is still not sufficiently explored. The high electric fields realized in small gaps combined with the lowering of the potential barrier, seen by the electrons in the cathode as ion approaches lead to ion-enhanced field emission leading to deviations from the standard Paschen law. In this paper, semi-empirical expressions for the breakdown voltage based on the fitting of numerical solutions of the DC breakdown criteria in microdischarges have been derived. In the standard breakdown criteria the secondary emission coefficient that incorporates the enhancement of the secondary electron emission has been included. The obtained expressions can be used for determination the pressure and the gap dependence of the breakdown field strength in the water vapor, separately.

PACS numbers: 52.50.Qt, 52.65.Rr, 52.80.Pi

## 1. Introduction

In the past few decades the field of microdischarges have become more common in everyday life. Microplasmas encompass the advantages of low-pressure plasmas with the advantages of being micro [1–4]. Due to their portability and the non-equilibrium character of the discharges, microplasmas are finding application in many research disciplines, from the optimizing the plasma screens [5], localized silicon etching [6], tunable UV source [7], gas spectroscopy [8, 9], spectroscopy of water impurities [10], up to localized treatment of materials and assembly of nanostructures [11]. On the other hand, plasma-based microsystems can find application in bio microelectromechanical system (bio-MEMS) sterilization, small-scale materials processing and microchemical analysis systems [12]. However, integrability requires not only a reduction in size, but also an understanding of the physics governing the new small-scale discharges.

Making the gap small is the easiest way to obtain a big force, which is restricted by the electric field of breakdown [13, 14]. It is necessary to be aware of the breakdown voltage in microgaps. When changing the size of plasmas, there are scaling laws that are helpful in determining the operating parameters of various sizes of plasmas. The fact that microdischarges operate under conditions, where boundary effects dominate, indicates the importance of establishing scaling laws in a such small gaps. The best way is perhaps to start from the low pressure discharges and to employ the standard scaling laws [15]. The motivation for our studies, resulting from the fact that the electrical breakdown in microgaps occurs at voltages far below the pure Paschen curve mini-

mum and that the modified Paschen curve should be used instead for micron and sub-micron gaps [16]. Electrons from the field emission are one of the possible reasons why the breakdown and sparks occur in a vacuum, which of course is not possible if one only considers the Townsend avalanche mechanisms for the gas phase and the surface ionization that are normally used to generate the Paschen curve [17].

Microplasma can be generated in a wide range of the pressure. In the large scale systems, the experimentally observed Paschen law has been successfully explained by the Townsend theory [18]. The Paschen's law is based on the observation that, over a large range of the pressures and electrode separations, the probability of the ionization per collision in the gas and the probability of the production of electrons by ions by a secondary process are both dependent on the average kinetic energy of the electrons and ions and therefore on the reduced electric field  $E/N$  (the electric field  $E$  to the gas number ratio  $N$ ) [19]. The Townsend mechanism by which successive ionizations of the gas molecules induce the gas breakdown describes the process satisfactorily at large separations [20]. The significant parameter is  $pd$  (the product of the gap distance and the pressure  $P$ ). Typically, the Townsend's mechanism (and by extension Paschen's law) applies at  $pd$  products less than 1000 Torr cm, or gaps around a 1 cm at 1 atm [21].

The mechanism of the electrical breakdown is, however, completely different in microgaps [2, 3, 4, 14, 15]. A rapid fall of the breakdown voltage with decreasing the gap size may be attributed to the onset of the ion-enhanced field emission in microgaps. Violations of the similarity law take place for the left hand branch of the curve, for such  $pd$  values where the electron mean free path is comparable with the gap. When the electron mean free path is comparable with the electrode separa-

\* corresponding author; e-mail: bradjeno@ipb.ac.rs

ration the electrical breakdown is based on the cathode-induced breakdown model.

Water vapour in the atmosphere is the key trace gas controlling weather and climate. It also plays a central role in atmospheric chemistry, influencing the heterogeneous chemical reactions that destroy stratospheric ozone. The effects of water vapour are large in the upper troposphere and lower stratosphere, but there are few measurements of water vapour concentrations and its long-term variation in this altitude only region. The influence of water vapour on the breakdown voltage of uniform field gaps has been investigated by Ritzl [22], who was found that the breakdown voltage in air increases by 2% for a change in the partial pressure of water vapour. Later on, some results indicated that the presence of water vapour raised the breakdown voltage by 2.7% above that of dry air [23]. Allen and Phillips [24] investigated the effect of humidity on the spark breakdown voltage. Recently, measurements have been performed for low-pressure breakdown in water vapor [25].

In this paper, high-pressure breakdown field strength in water vapor has been theoretically studied [26]. The expressions for the DC breakdown criteria including the ion-enhanced secondary emission coefficient has been numerically solved for water vapor in order to determine the breakdown voltage versus the gap spacing and the pressure, respectively. The results of this research can be applied in the construction of compact pulse power generators for bioelectric applications.

## 2. Semi-empirical expressions

Combining the expressions for the electron yield [13]:

$$\gamma = K e^{-D/E}, \quad (1)$$

and for the ionization coefficient [27]:

$$\alpha/p = A e^{-Bp/E}, \quad (2)$$

with the expression for the DC breakdown criteria:

$$\gamma (e^{\alpha d} - 1) = 1, \quad (3)$$

we obtain the transcendental equation [28]:

$$K e^{-D/E} \left( e^{A p d e^{-B p/E}} - 1 \right) = 1, \quad (4)$$

where the material dependent constant  $D$  can be calculated using the expression:

$$D = 6.85 \times 10^7 \phi^{3/2} / \beta, \quad (5)$$

knowing a field enhancement factor  $\beta$  and the work function of the metal  $\phi$  expressed in eV. On the other hand, from the experimental values of the slope of the  $\log \gamma$  versus  $1/E$ , the values of  $D$  were also determined for some materials, for example, aluminum, stainless steel and conventional steel (as can be seen, from Table I in Ref. [13]). In this paper we have used the value of  $9.3 \times 10^8$  V/m that corresponds to the aluminum. Contrary, determination of the constant  $K$  that appears in Eqs. (1) and (4) may be quite difficult, especially if there are additional complications due to electron attachment, ionization by metastables, ect. [14]. In practice, the constant  $K$  can be found from the ratio of the field emis-

sion current density to the positive ion current density onto the cathode.  $A$  and  $B$  are gas dependent constants that can be found elsewhere [27]. The expressions for the breakdown field strength will be determined by solving transcendental Eq. (4) numerically by using the package Mathematica and then by fitting these solutions.

## 3. Results and discussion

For a fixed pressure, the transcendental Eq. (4) has been numerically solved by varying the interelectrode distance  $d$ . The obtained numerical solutions for the breakdown field strength  $E$  against the gap size  $d$  are shown in Fig. 1. These values can be fitted by a simple formula:

$$E = a d^{-1} + b \times d^c, \quad (6)$$

where the fitting coefficients  $a$ ,  $b$  and  $c$ , for the a few pressures are listed in Table I.

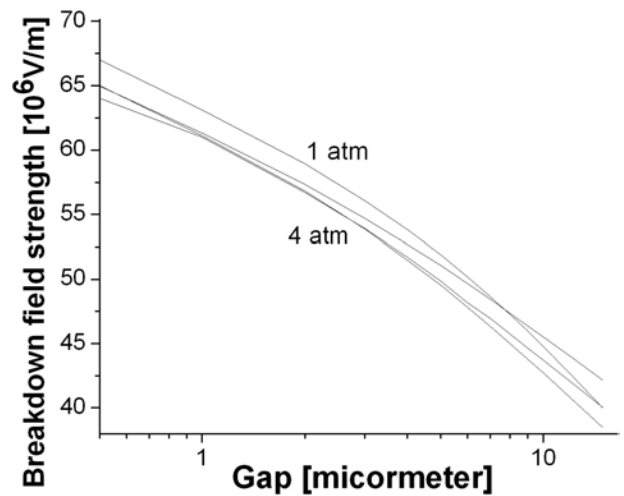


Fig. 1. The breakdown field strength versus the gap spacing for pressure in the range from 1 atm up to 4 atm. The gap was varied between  $0.5 \mu\text{m}$  up to  $15 \mu\text{m}$ .

TABLE I

Fitting coefficients for the Eq. (6) for various values of the pressure.

Pressure [atm]	$a$	$b$	$c$
1	-26.122	90.012	-0.281
2	-20.662	82.597	-0.267
3	-14.906	76.304	-0.228
4	-11.456	73.16	-0.196

As can be seen from Fig. 1, the breakdown field strength defined as the ration of the breakdown voltage and the gap size strongly depends on the interelectrode separation. For gaps less than  $5 \mu\text{m}$ , the breakdown phenomena are attributed to the ion-enhanced field emission [14]. At large separations, however, processes in

TABLE II  
The Values of the fitting coefficients  $m$  and  $n$ , for a few gap sizes, in Eq. (7).

Gap [ $\mu\text{m}$ ]	$m$	$n$
0.5	90.188	-0.0442
1	85.898	-0.0456
2	83.266	-0.052
4	82.527	0.0574

the gas cause breakdown rather than secondary electron emission.

In a similar way, for a fixed gap sizes, the transcendental Eq. (4) has also been solved by varying the gas pressure, in order to obtain the pressure dependence of the electric field strength. Numerical solutions are presented in Fig. 2 and fitted by using expression:

$$E = m \cdot p^n, \quad (7)$$

with fitting coefficient  $m$  and  $n$  given in Table II.

Figure 2 clearly illustrates the weak dependence of the breakdown field strength on the pressure, even for the gaps of the order of a few micrometers. Such trend in the curves presented in Fig. 2 can be explained by the exponential dependence of the ion-enhanced field emission on the electric field and not on the pressure.

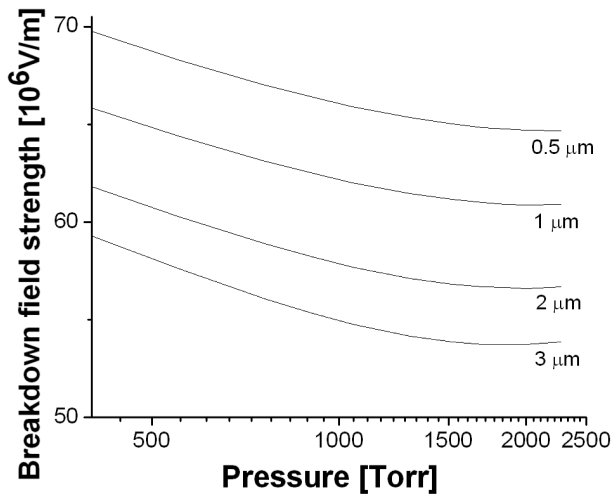


Fig. 2. The breakdown field strength as a function of the gas pressure for the gaps from 0.5 to 3  $\mu\text{m}$ .

#### 4. Conclusion

This paper contains theoretical studies of the breakdown field strength in the microgaps. Departures from the large scale similarity laws are expected with the onset of field emission on such small gaps indicating that Townsend mechanism is not sufficient to explain the breakdown mechanism. The semi-empirical expressions

for the breakdown field strength suggested here are based on the fit of the numerical solutions of the breakdown criteria including field emission effects in microgaps. The new breakdown field curve obtained, when the field emissions are accounted for, retains the right branch of the conventional Paschen curve, i.e. field emissions can be neglected in large gaps. The left branch, however, is substituted by a rapid decrease of the breakdown voltage and increases in the breakdown field strength below the minimum of the conventional Paschen curve. This reduction in the breakdown voltage is observed for gap sizes smaller than 5  $\mu\text{m}$  and is a direct consequence of the onset of field emissions.

The results of our studies should be useful for determining minimum ignition voltages in microplasma sources as well as the maximum safe operating voltage and critical dimensions in other microdevices.

#### Acknowledgments

The authors acknowledge financial support of the Ministry of Science of the Republic of Serbia 141025.

#### References

- [1] J.M. Thores, R.S. Dhariwal, *Nanotechnology* **10**, 102 (1999).
- [2] M. Radmilović-Radjenović, J.K. Lee, F. Iza, G.Y. Park, *J. Phys. D, Appl. Phys.* **38**, 950 (2005).
- [3] M. Radmilović-Radjenović, B. Radjenović, *Contrib. Plasma Phys.* **47**, 165 (2007).
- [4] M. Radmilović-Radjenović, B. Radjenović, *Plasma Sources Sci. Technol.* **16**, 337 (2007).
- [5] S.S. Yang, J.K. Lee, S.W. Ko, H.C. Kim, J.W. Shon, *Contrib. Plasma Phys.* **44**, 536 (2004).
- [6] H. Wang, G. Li, L. Jia, L. Li, G. Wang, *Chem. Commun. (Camb)* **7**, 3786 (2009).
- [7] P. Kurunczi, J. Lopez, H. Shah, K. Becker, *International Journal of Mass Spectroscopy* **205**, 277 (2001).
- [8] T. Svensson, M. Andersson, L. Rippe, J. Johansson, S. Folestad, S. Andersson-Engels, *Opt. Lett.* **33**, 80 (2008).
- [9] M. Saito, T. Hiraga, M. Hattori, S. Murakami, T. Nakai, *Magn. Reson. Imaging* **23**, 607 (2005).
- [10] L. Que, C.G. Wilson, Y.B. Gianchandani, *J. Microelectromech. Syst.* **14**, 185 (2005).
- [11] A.K. Chakraborty, A.J. Golumbskie, *Annual Review of Physical Chemistry* **52**, 537 (2001).
- [12] W.K.T. Coltro, *Química Nova* **30**, 1986 (2007).
- [13] W.S. Boyle, P. Kisliuk, *Phys. Rev.* **97**, 255 (1955).
- [14] M. Radmilović-Radjenović, B. Radjenović, *Plasma Sources Sci. Technol.* **17**, 024005 (2008).
- [15] Z.Lj. Petrović, N. Škoro, D. Marić, C.M.O. Mahony, P.D. Maguire, M. Radmilović-Radenović, G. Malović, *J. Phys. D, Appl. Phys.* **41**, 194002 (2008).
- [16] L.H. Germer, *J. Appl. Phys.* **30**, 46 (1959).
- [17] P. Kisliuk, *J. Appl. Phys.* **30**, 51 (1959).
- [18] F. Paschen, *Wied. Ann.* **37**, 69 (1889).

- [19] L.B. Loeb, *Fundamental Processes of Electrical Discharges in Gases*, J. Wiley and Sons, Inc., New York (1939).
- [20] J.M. Meek, J.D. Craggs, *Electrical breakdown of gases*, Oxford University Press, (1953).
- [21] M.A. Lieberman, A.J. Lichtenberg, *Principles of Plasma Discharges and Materials Processing* 2nd ed. Wiley Interscience, Hoboken, NJ: Wiley, (2005).
- [22] H. Ritz, *Archiv fur Elektrotechnik* **26**, 219 (1932).
- [23] W. Kohrman, *Ann. d. Phys.* **18**, 379 (1956).
- [24] K.R. Allen, K. Phillips, *Nature* **183**, 174 (1959).
- [25] D. Marić, N. Škoro, G. Malović, Z.Lj. Petrović, Proceedings of the 29th ICPIG, Cancun Mexico, (12–17 July 2009), PA8-5 (2009).
- [26] M. Radmilović-Radjenović, B. Radjenović, Contributed papers of 24th Summer School and International Symposium on the Physics of Ionized Gases, Novi Sad, Serbia (25–29 August 2008) 379 (2008).
- [27] D. Marić, M. Radmilović-Radjenović, Z.Lj. Petrović, *EPJ D* **35**, 313 (2005).
- [28] M. Radmilović-Radjenović, B. Radjenović, *Europhys. Lett.* **83**, 25001 (2008).



Република Србија  
Универзитет у Београду  
Електротехнички факултет  
Д.Бр.2009/5048  
Датум: 16.01.2019. године

На основу члана 29. Закона о општем управном поступку („Сл. гласник РС”, бр.18/2016) и службене евиденције издаје се

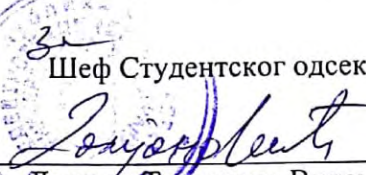
### УВЕРЕЊЕ

**Пуач (Бојан) Марија**, бр. индекса 2009/5048, рођена 10.06.1985. године, Параћин, Република Србија, уписана школске 2018/2019. године, у статусу: самофинансирање; тип студија: докторске академске студије; студијски програм: Електротехника и рачунарство, модул Наноелектроника и фотоника.

Према Статуту факултета студије трају (број година): три студијске године и има најмање 180 ЕСПБ бодова.

Рок за завршетак студија: у двоструком трајању студија.

Ово се уверење може употребити за регулисање војне обавезе, издавање визе, права на дечији додатак, породичне пензије, инвалидског додатка, добијања здравствене књижице, легитимације за повлашћену вожњу и стипендије.

  
Шеф Студентског одсека  
Драгана Трневски Виденов



Република Србија  
Универзитет у Београду  
Електротехнички факултет  
Д.Бр.2009/5048  
Датум: 16.01.2019. године

На основу члана 29. Закона о општем управном поступку („Сл. гласник РС”, бр.18/2016) и службене евиденције издаје се

### УВЕРЕЊЕ

**Пуач (Бојан) Марија**, бр. индекса 2009/5048, рођена 10.06.1985. године, Параћин, Република Србија, уписана школске 2018/2019. године, у статусу: самофинансирање; тип студија: докторске академске студије; студијски програм: Електротехника и рачунарство, модул Наноелектроника и фотоника.

Према Статуту факултета студије трају (број година): три студијске године и има најмање 180 ЕСПБ бодова.

Рок за завршетак студија: у двоструком трајању студија.

Ово се уверење може употребити за регулисање војне обавезе, издавање визе, права на дечији додатак, породичне пензије, инвалидског додатка, добијања здравствене књижице, легитимације за повлашћену вожњу и стипендије.

  
Шеф Студентског одсека  
Драгана Трневски Виденов



РЕПУБЛИКА СРБИЈА

УНИВЕРЗИТЕТ У БЕОГРАДУ  
ЕЛЕКТРОТЕХНИЧКИ ФАКУЛТЕТ

# ДИПЛОМА

О СТЕЧЕНОМ ВИСОКОМ ОБРАЗОВАЊУ

## САВИЋ БОЈАН МАРИЈА

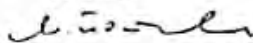
РОЂЕН-А 10. 6. 1985. ГОДИНЕ У ПАРАЋИНУ, РЕПУБЛИКА СРБИЈА,  
УПИСАН-А 2004/05. ГОДИНЕ, А ДАНА 28.10. 2008. ГОДИНЕ ЗАВРШИО-ЛА ЈЕ СТУДИЈЕ  
НА ЕЛЕКТРОТЕХНИЧКОМ ФАКУЛТЕТУ НА ОДСЕКУ ЗА ФИЗИЧКУ ЕЛЕКТРОНИКУ-СМЕР  
НАНОЕЛЕКТРОНИКА, ОПТОЕЛЕКТРОНИКА И ЛАСЕРСКА ТЕХНИКА, СА ОПШТИМ УСПЕХОМ  
8,89 (ОСАМ 89/100) У ТОКУ СТУДИЈА И ОЦЕНОМ 10 ( ДЕСЕТ ) НА ДИПЛОМСКОМ  
ИСПИТУ.

НА ОСНОВУ ТОГА ИЗДАЈЕ МУ-ЈОЈ СЕ ОВА ДИПЛОМА О СТЕЧЕНОМ ВИСОКОМ  
ОБРАЗОВАЊУ И СТРУЧНОМ НАЗИВУ ДИПЛОМИРАНИ ИНЖЕЊЕР ЕЛЕКТРОТЕХНИКЕ.

РЕДНИ БРОЈ ИЗ ЕВИДЕНЦИЈЕ О ИЗДАТИМ ДИПЛОМАМА 17148.

У БЕОГРАДУ, 28. 10. 2008. ГОДИНЕ.

ДЕКАН

  
Проф. др Миодраг Поповић

РЕКТОР

  
Проф. др Бранко Ковачевић



УНИВЕРЗИТЕТ У БЕОГРАДУ  
Електротехнички факултет



ДОДАТАК ДИПЛОМИ  
диплома број 17148

**1. Информације које идентификују имаоца квалификације**

- |   |   |
|---|---|
| 1.1 Презиме: Савић                          | 1.6 Држава рођења: Република Србија   |
| 1.2 Име: Марија                             | 1.7 Идентификациони број (ЈМБГ): 1006985728226                                    |
| 1.3 Име једног од родитеља: Бојан           | 1.8 Шифра (Број индекса): 2004/0128   |
| 1.4 Датум рођења (дд.мм.гггг.): 10.06.1985. | 1.9 На овај факултет је први пут уписана школске 2004/05, на прву годину студија. |
| 1.5 Место рођења: Параћин                   |   |

**2. Информације које идентификују квалификацију**

- 2.1 Счени стручни назив квалификације: **Дипломирани инжењер електротехнике**
- 2.2 Главне области студирања за квалификацију: **Техничко-технолошке науке**
- 2.3 Назив установе која даје квалификацију: **Универзитет у Београду**
- 2.4 Врста установе која даје квалификацију: **Универзитет**
- 2.5 Оснивач установе која даје квалификацију: **Република Србија**
- 2.6 Назив институције која управља студијама: **Електротехнички факултет Универзитета у Београду**
- 2.7 Оснивач установе која управља студијама: **Република Србија**
- 2.8 Језик студија: **српски**

**3. Информације о нивоу квалификације**

- 3.1 Ниво квалификације: Основне студије - VII/1 степен
- 3.2 Званична дужина трајања студија: 4 године
- 3.3 **Услови уписа:** У 1. годину основних студија на Електротехничком факултету може се уписати лице које има средње образовање у четворогодишњем трајању
  - А: Упис после завршене средње школе**
    - 3.3.1а Назив и седиште школе: Гимназија, Параћин  
Завршила 2004. године.
    - Б: Прелаз са другог факултета**
    - 3.3.1б Назив и седиште факултета: --
    - В: Упис после завршене више школе**
      - 3.3.1в Назив и седиште више школе: --  
Завршила -- године.



#### 4. Информације о садржајима и постигнутим резултатима

4.1 Начин студирања: редован студент (са пуним обимом ангажовања)

4.2 Захтев програма: Студент који положи све испите утврђене наставним планом основних студија и одбрани дипломски рад стиче високо образовање и стручни назив дипломирани инжењер електротехнике одговарајућег усмерења (Одсек за физичку електронику - смер Наноелектроника, оптоелектроника и ласерска техника).

4.3 Појединости оствареног програма:

Шифра	Предмет	Укупан фонд часова			Испит Оцена	Наставник
		Предавања	Вежбе	Остало		
ОО1ЛОЕ	Лабораторијске вежбе из Основа електротехнике	0	0	30	9 (девет)	Ђорђевић Антоније
ОО1ЛФ	Лабораторијске вежбе из Физике	0	0	30	8 (осам)	Осмокровић Предраг
ОО1ММ1	Математика 1	45	45	0	6 (шест)	Радосављевић Зоран
ОО1ММ2	Математика 2	45	45	0	9 (девет)	Лацковић Иван
ОО1ОЕ1	Основи електротехнике 1	45	45	0	7 (седам)	Петровић Владимир
ОО1ОЕ2	Основи електротехнике 2	45	45	0	6 (шест)	Петровић Владимир
ОО1П1	Програмирање 1	45	30	0	6 (шест)	Протић Јелица
ОО1П2	Програмирање 2	45	30	0	9 (девет)	Протић Јелица
ОО1ПКР	Практикум из коришћења рачунара	15	0	15	8 (осам)	Милићев Драган
ОО1ПМА	Практикум из Математике 1 - а	15	15	0	9 (девет)	Цветковић Драгош
ОО1ПФ2	Практикум из Физике 2	0	0	30	10 (десет)	Срећковић Милеса
ОО1УЕ	Увод у електронику	15	0	15	7 (седам)	Поповић Миодраг
ОО1Ф1	Физика 1	45	30	0	10 (десет)	Елазар Јован
ОО1Ф2	Физика 2	45	30	0	10 (десет)	Елазар Јован
ОФ2Е	Електромагнетика	45	30	0	8 (осам)	Петровић Владимир
ОФ2ЕЈ3	Енглески језик 3	30	0	0	10 (десет)	Ђурић Милош
ОФ2ЕЈ4	Енглески језик 4	30	0	0	10 (десет)	Ђурић Милош
ОФ2ЕЕ	Елементи електронике	45	30	15	7 (седам)	Дрндаревић Вујо
ОФ2КМ	Квантна механика	45	30	0	8 (осам)	Тадић Милан
ОФ2М3	Математика 3	45	30	0	8 (осам)	Цакић Ненад
ОФ2М4	Математика 4	30	30	15	10 (десет)	Цакић Ненад
ОФ2ОФЕ	Основи физичке електронике	45	30	0	7 (седам)	Гвоздић Дејан
ОФ2ПКЕ	Практикум из конструисања електронских уређаја	15	0	22,5	10 (десет)	Милановић Витомир
ОФ2ПРК	Практикум из рачунарске анализе кола	15	0	22,5	10 (десет)	Рељин Бранимир
ОФ2СИС	Сигнали и системи	45	15	15	9 (девет)	Турајлић Србијанка
ОФ2ТЕК	Теорија електричних кола	45	30	0	8 (осам)	Рељин Бранимир
ОФ3ДОС	Дигитална обрада сигнала	45	15	15	10 (десет)	Станковић Срђан
ОФ3КЕ	Квантна електроника	45	30	0	10 (десет)	Милановић Витомир
ОФ3МИН	Микроелектроника и наноелектроника	45	30	0	9 (девет)	Рамовић Рифат
ОФ3О	Оптоелектроника	45	15	15	10 (десет)	Матавуљ Петар
ОФ3ОТ	Основи телекомуникација	45	15	15	9 (девет)	Петровић Зоран
ОФ3ПОТ	Простирање оптичких таласа	45	30	0	10 (десет)	Цветић Јован
ОФ3СП	Сензори и претварачи	45	0	30	10 (десет)	Златановић Миодраг
ОФ3СФ	Статистичка физика	45	30	0	8 (осам)	Радуновић Јован
ОФ3ФЕЧ	Физичка електроника чврстог тела	45	30	0	8 (осам)	Милановић Витомир
ОФ3ФТМ	Физичко техничка мерења	45	0	30	9 (девет)	Станковић Драган
ОФ4ЛТ	Ласерска техника	45	30	0	10 (десет)	Елазар Јован
ОФ4ОЛС	Оптоелектронски и ласерски мерни системи	45	0	30	10 (десет)	Матавуљ Петар
ОФ4ОМ	Оптичке мреже	45	30	0	8 (осам)	Матавуљ Петар
ОФ4ОТ	Оптичке телекомуникације	45	30	0	10 (десет)	Гвоздић Дејан
ОФ4ПKN	Полупроводничке квантне наноструктуре	45	30	0	10 (десет)	Милановић Витомир
ОФ4ТП	Техника плазме	45	30	0	10 (десет)	Златановић Миодраг
ОФ4ФЕГ	Физичка електроника гасова и плазме	45	30	0	10 (десет)	Цветић Јован
ОФ4ФС	Фиброоптички сензори	45	15	15	10 (десет)	Матавуљ Петар
ОФ3О	Дипломски испит (Дипломски рад)	225	225	--	10 (десет)	Матавуљ Петар

Тема дипломског рада:

**Анализа интергисаних таласовода специфичне геометрије са шупљим језгром**

Наставник - ментор дипломског рада: Матавуљ Петар, ванредни професор

Датум одбране дипломског рада (дд.мм.гггг.): 28.10.2008.



#### 4.4 Шема оцењивања:

Оцена	Значење оцене	Процент од укупног броја поена (%)
10	Изузетан	91 - 100
9	Одличан	81 - 90
8	Врло добар	71 - 80
7	Добар	61 - 70
6	Довољан	51 - 60
5	Недовољан	≤ 50

#### 4.5 Укупна оцена квалификације:

Просечна оцена: **одличан: 8.89** (осам, 89/100)

### 5. Информације о функцији квалификације

#### 5.1 Приступ даљем студирању:

Ималац дипломе има право да настави даље образовање и усавршавање у складу са Законом о високом образовању

### 6. Додатне информације

6.1а Положила следеће предмете који нису предвиђени наставним планом и програмом за стицање дипломе: —

6.1б Похађала следеће ваннаставне курсеве: —

6.1в Постигла успех на студентским такмичењима у знању: —

6.1г Остале активности: —

6.2 Извори о додатним информацијама:

О институцији: [www.etf.bg.ac.yu](http://www.etf.bg.ac.yu); [www.mps.sr.gov.yu](http://www.mps.sr.gov.yu)

О програму: Студентски одсек ЕТФ-а

7. Оверавање додатка:

7.1 Овај додатак дипломи односи се на следећа оригинална документа:

Диплома факултета број: 17148 издата дана (дд.мм.гггг.): 28.10.2008.

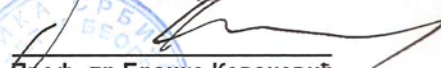


Декан:

  
Проф. др Миодраг Поповић



Ректор:

  
Проф. др Бранко Ковачевић



Република Србија

УУБ

Универзитет у Београду  
Електротехнички факултет, Београд



Оснивач Република Србија

Дозволу за рад - уверење број 612-00-791/2008-01 од 31. јануара 2009. године  
издала је Комисија за акредитацију и проверу квалитета Републике Србије

*Диплома*

Марија, Бојан, Савић

рођена 10. јуна 1985. године у Параћину, Република Србија, уписана школске  
2008/2009. године, а дана 22. децембра 2009. године завршила је мастер академске  
студије другог степена на студијском програму Електротехника и рачунарство,  
обима 60 (шездесет) бодова ЕСПБ са просечном оценом 10,00 (десет и 0/100).

На основу тога издаје јој се ова диплома о стеченом високом образовању и академском називу  
мастер инжењер електротехнике и рачунарства

Број: 6900

У Београду, 2. фебруара 2011. године

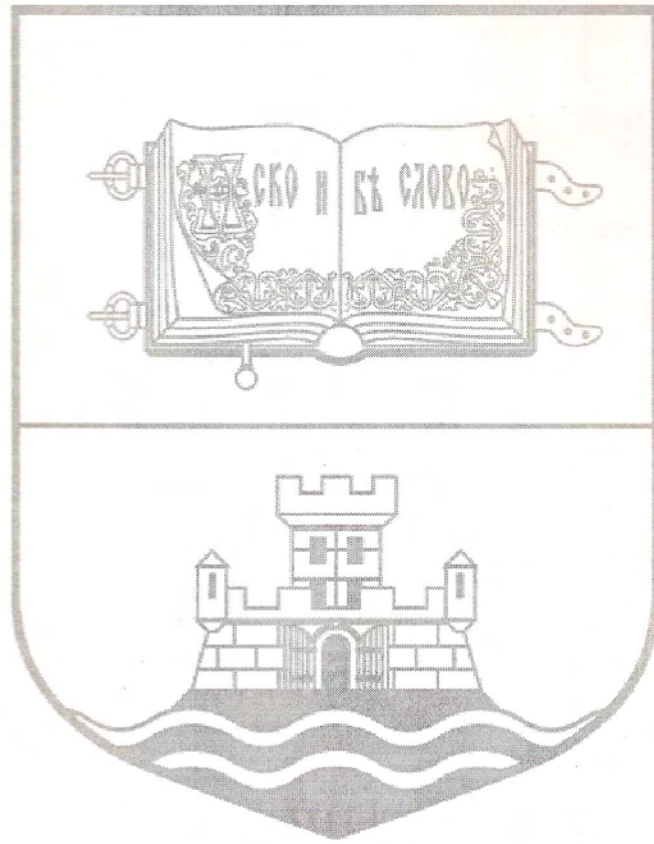
Декан  
проф. др Миодраг Појовић

Ректор  
проф. др Бранико Ковачевић



*Република Србија*

*Универзитет у Београду*



ДОДАТАК ДИПЛОМИ



**1. Подаци о имаоцу дипломе**

- 1.1 Име: *Марија*  
 1.2 Презиме: *Савић*  
 1.3 Датум рођења: *10. јун 1985. године*  
 1.4 Број индекса студента: *2008/3158*  
 ЈМБГ: *1006985728226*

**2. Подаци о стеченој дипломи**

- 2.1 Стечени академски назив: *мастер инжењер електротехнике и рачунарства*  
 2.2 Научна/уметничка/стручна област (или области) студија: *електротехничко и рачунарско инжењерство*  
 2.3 Назив и статус високошколске установе која издаје диплому:  
*Универзитет у Београду, државна самостална високошколска установа*  
 2.4 Назив и статус високошколске установе која организује студије (уколико се разликује од 2.3):  
*Универзитет у Београду - Електротехнички факултет, државна високошколска установа*  
 2.5 Језик на коме се одржава настава: *српски језик*

**3. Подаци о врсти и нивоу студија**

- 3.1 Врста и степен студија: *мастер академске студије првог степена*  
 3.2 Дужина трајања студија: *1 година (60 ЕСПБ)*  
 3.3 Услови уписа:  
*Остварен обим основних академских студија од 240 ЕСПБ бодова и посебни услови прописани одговарајућим актом факултета.*

**4. Подаци о садржају и постигнутим резултатима**

- 4.1 Начин студирања: *студије у седмичној установи*  
 4.2 Назив студијског програма:  
*Електротехника и рачунарство*  
*Модул: Наноелектроника, оптичката електроника и ласерска техника*  
 4.3 Циљеви студијског програма:
  - *Образовање високо квалификованих инжењера за анализу, развој и пројектовање делова система и сложених система,*
  - *Оспособљавање за рад на истраживачким пројектима у областима електротехнике и рачунарства,*
  - *Оспособљавање за самостални и тимски рад и презентовање резултата,*
  - *Обезбеђивање додатних знања неопходних за праћење брзој технолошкој развоја у областима електротехнике и рачунарства,*
  - *Стецање високих компетенција и академских и практичних вештина из области електротехнике и рачунарства,*
  - *Развој креативних способности размишљања проблема и способности критичкој мишљења,*
  - *Оспособљавање за праћење наставе на докторским студијама,*
  - *Овладавање специфичним практичним вештинама потребним за успешно бављење научноистраживачким радом,*
  - *Стецање навика за перманентно образовање и напредовање у области електротехнике и рачунарства.*
 4.4 Појединости студијског програма и постигнуте оцене:

ред. бр.	шифра	Наставни предмети		ста-тус	ЕСПБ	укупан број часова			год. оцена	наставник
		назив	ЕСПБ			пред.	веж.	ост.		
1	МС1ЛИП	Ласери и њихова примена	и.	6	60	0	0	1	10	Јован Елазар
2	МС1СТП	Судари и транспортни процеси у јонизованим гасовима	и.	6	45	15	0	1	10	Зоран Петровић
3	МС1ФП	Физика плазме	и.	6	45	15	0	1	10	Јован Цветић



ред. бр.	шифра	Наставни предмети назив	ста-тус	ЕСПБ	укупан број часова			год. студ. прог.	оце-на	наставник
					пред.	веж.	ост.			
4	MC10MM	Оптичке мреже са мултиплексирањем по таласним дужинама DWDM	и.	6	45	15	0	1	10	Петар Матавуљ
5	MC1ENH	Елементи нанооптике и нанофотоники	и.	6	45	15	0	1	10	Милан Тадић
6	-	Завршни рад	о.	30	-	-	-	1	10	

Наслов завршног рада: *Мониторинг Карло симулација њоробоја у часовима*

Комисија за одбрану завршног рада: *Миодраг Злајановић (ментор), Зоран Пејировић, Дејан Раковић*

#### 4.5 Начин оцењивања на предметима:

Оцена	Значење оцене	Број поена	
		од	до
10	одличан	91	100
9	изузетно добар	81	90
8	врло добар	71	80
7	добар	61	70
6	довољан	51	60
5	није положио	0	50

4.6 Просечна оцена и општи успех: *10,00 (десет и 0/100) - одличан*

## 5. Подаци о намени стеченог назива

### 5.1 Приступ даљим студијама:

*Ималац дипломе се може уписаати на специјалистичке академске студије или докторске студије. За упис на докторске студије њојредна је њишња просечна оцена од најмање 8 на основним академским студијама и мастер академским студијама.*

### 5.2 Професионални статус:

*Мастер инжењер електротехнике и рачунарства.*

*Студенти који су успешно завршили овај студијски њорограм, су у стању да у областима електротехнике и рачунарства:*

- Примене фундаментална знања из електротехнике, рачунарства и информатике у моделовању њроблема, њројектовању и научним истраживањима,*
- Раде самостално или у њиму састављеном од стључњака различитих њрофила и ефикасно комуницирају,*
- Пројектују сисџеме, компоненте и њроцесе на основу задатих спецификација,*
- Планирају и изводе инжењерске експерименте, анализирају и интерпретирају добијене резултате и на основу њих стљварају нова њтехничка решења,*
- Користе њтехнике, вешџине и савремене софџверске алате у инжењерској њпракси и откривају њихову нову њримену,*
- Уочавају, формулишу и решавају нове инжењерске њроблеме,*
- Имају професионалну и еџичку одговорност мастер инжењера електротехнике и рачунарства,*
- Разумеју уџицај инжењерских решења и нових њтехнолоџа на друшџтво и околину,*
- Унаџређују своје знање и њраџте развој науке и њтехнолоџе њоком целоџ живџта.*

## 6. Додатне информације

### 6.1 Додатне информације о студенту:

*Нема додатних информација*

### 6.2 Извори додатних информација о установи:

*Законом о универзитету из 1905. њодине њроглашена је Висока школа у Београду за Универзитет, а чланом 116.*

*Закона о високом образовању из 2005. њодине дефинисан је даљи рад Универзитета.*

<http://www.bg.ac.rs>

<http://www.etf.bg.ac.rs>



## 7. Овера додатка дипломи

7.1 Број: 6901 Датум: 2 фебруар 2011. године

7.2 Одговорно лице

Декан, проф. др Миодраг Појковић

Одговорно лице

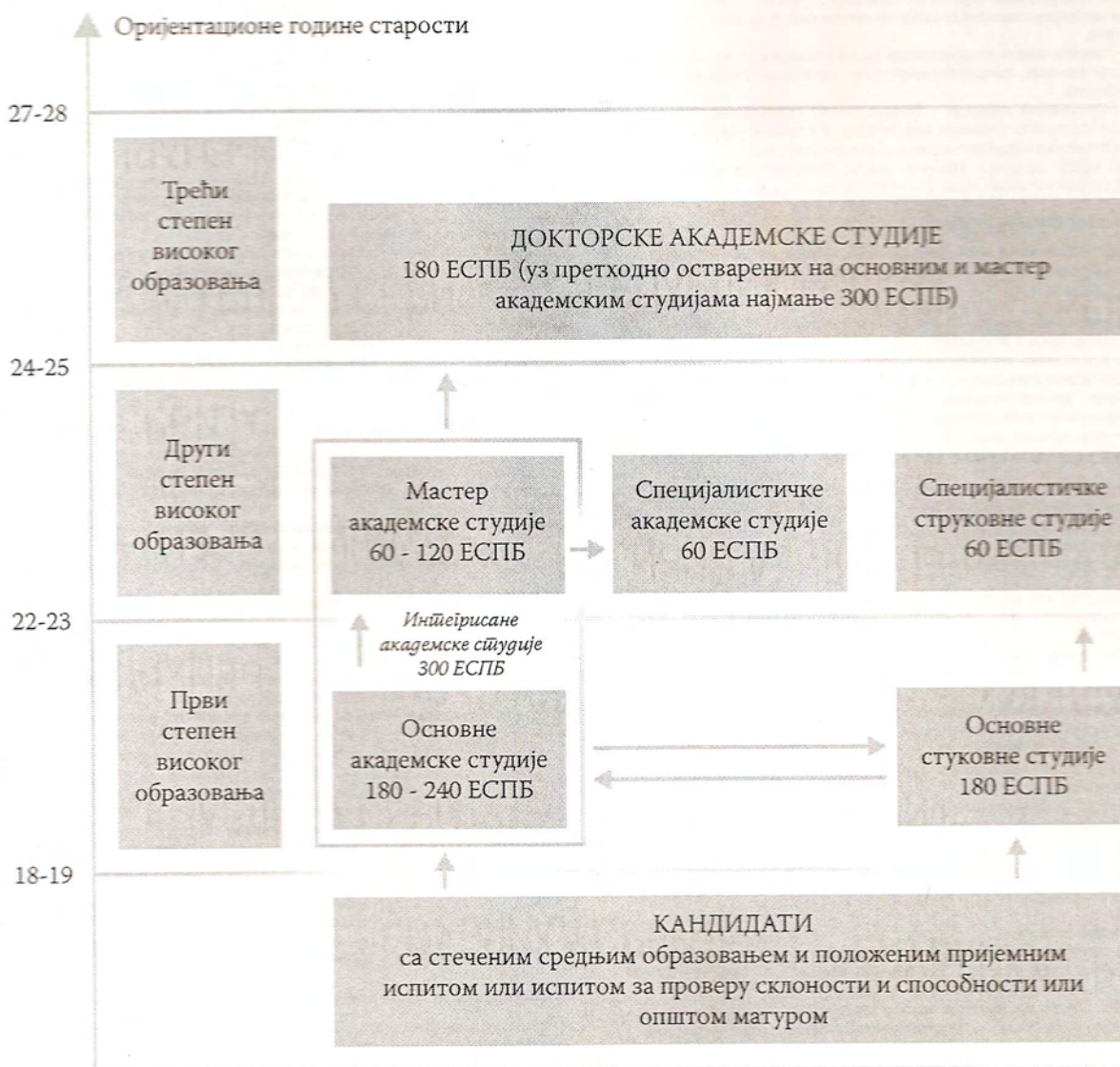
Ректор, проф. др Бранко Ковачевић

7.3 Печат и потпис

Печат и потпис



## 8. Подаци о систему високог образовања у Републици Србији





Република Србија  
Универзитет у Београду  
Електротехнички факултет  
Број индекса: 2009/5048  
Датум: 19.04.2018.

На основу члана 29. Закона о општем управном поступку и службене евиденције издаје се

## УВЕРЕЊЕ О ПОЛОЖЕНИМ ИСПИТИМА

Марија Пуач, име једног родитеља Бојан, рођена 10.06.1985.године, Параћин, Република Србија, уписана школске 2009/2010. године на докторске академске студије, школске 2017/2018. године уписана на статус самофинансирање, студијски програм Електротехника и рачунарство, модул Наноелектроника и фотоника, током студија положила је испите из следећих предмета:

Р.бр.	Шифра	Назив предмета	Оцена	ЕСПБ	Фонд часова**	Датум
1.	13Д061ТПНФ	Транспортни процеси у наноелектроници и фотоници	10 (десет)	9	I:(90+0+0)	15.09.2011.
2.	13Д061МФКС	Модерне фотонске компоненте и системи	10 (десет)	9	I:(90+0+0)	01.09.2017.
3.	13Д061ППСТ	Примена плазме у савременим технологијама електроници и науци о материјалима	10 (десет)	9	I:(90+0+0)	13.02.2011.
4.	13Д061СЧМ	Спектроскопија чврстих материјала	10 (десет)	9	I:(90+0+0)	25.09.2011.
5.	13Д061ПОТС	Простирање оптичких таласа у комплексним срединама	10 (десет)	9	I:(90+0+0)	19.06.2017.
6.	13Д091ЕЈ	Енглески језик	8 (осам)	6	III:(90+0+0)	22.06.2017.
7.	ДС06НР3	Научни рад 3	10 (десет)	9	III:(90+0+0)	29.06.2017.
8.	13Д061НО	Нелинеарна оптика	10 (десет)	9	III:(90+0+0)	20.06.2017.
9.	13Д061СМНН	Скенирајућа микроскопија у нанонауци и нанотехнологији	10 (десет)	9	III:(90+0+0)	19.09.2014.
10.	ДС06НР4	Научни рад 4	10 (десет)	9		05.07.2017.

\* - еквивалентан/признат испит.

\*\* - Фонд часова је у формату (предавања+вежбе+остало).

Начин оцењивања на предметима:

Оцена	Значење оцене	Број поена	
		од	до
10	одличан	91	100
9	изузетно добар	81	90
8	врло добар	71	80
7	добар	61	70
6	довољан	51	60

Одрађене обавезе:

Р.бр.	Назив обавезе	ЕСПБ
1.	Научно стручни рад	3
2.	Студијски истраживачки рад I	15
3.	Студијски истраживачки рад II	15

Укупно остварено 120 ЕСПБ.

Општи успех: 9,80 (девет и 80/100), по годинама студија (10,00, 9,60, /).



Датум: 19.04.2018. године  
Место: Београд, Катедра за Електротехнику

Др Драган Милошевић Виденов



**УНИВЕРЗИТЕТ У БЕОГРАДУ**  
**ЕЛЕКТРОТЕХНИЧКИ ФАКУЛТЕТ**

Булевар краља Александра 73, П.Ф. 35-54, 11120 Београд, Србија

Тел: +381 11 3248464, Факс: +381 11 3248681

Република Србија  
Универзитет у Београду  
Електротехнички факултет  
Број: 2009/5048  
Датум: 16.1.2019. године

**ПОТВРДА**

**Пуач (Бојан) Марија**, мастер инж.електротехнике и рачунарства, рођена 10.6.1985. године, у Параћину, Република Србија, пријавила је тему за израду докторске дисертације на Електротехничком факултету у Београду, под насловом: **“Моделовање пробоја у гасовима Монте Карло техником”**.

Наставно-научно веће Електротехничког факултета на седници одржаној 11.9.2018. године размотрило је предложену тему и закључило да је тема подобна за израду докторске дисертације.

Универзитет у Београду, Веће научних области техничких наука дало је сагласност на предлог теме докторске дисертације Марије Пуач, на седници одржаној 24.9.2018. године.

Шеф Студентског одсека  
  
